Evolution and distribution of pore pressure across the Taranaki Basin, New Zealand

SEAN RICHARD O'NEILL

Mount Taranaki from Lake Mangamahoe (June 2018)

Evolution and distribution of pore pressure across the Taranaki Basin, New Zealand

Sean R. O'Neill

This thesis is submitted in partial fulfilment of the requirements for the degree of Doctor of Philosophy at Durham University

Department of Earth Sciences

University of Durham

2018

ABSTRACT

The Taranaki Basin lies onshore and offshore in the central-west of New Zealand's North Island. The polyphase nature of the basin has led to a complex pore pressure history, generating significant variations in the present-day vertical and lateral distribution of overpressures. Investigating pore pressure distributions at a basin scale can mask key details, so in this study eight new sub-basin areas and structural zones are designated, each displaying individual pore pressure trends defined by their stratigraphic architecture and structural development. Variations in the thickness and facies of Eocene-Oligocene stratigraphy both within and between sub-basins are shown to provide a first-order control on the magnitude, distribution and maintenance of overpressure across the Taranaki Basin. Fluid pressure compartmentalisation through sealing faults and stratigraphic architecture has been identified across the basin. Deep pore pressure transitions within Taranaki Basin are shown to be sealed by diagenetic, structural and stratigraphic mechanisms and generated by an increase in mudrock volume (reduced permeability) or gas generation.

A series of one-dimensional basin models are used to investigate the phases of overpressure generation by disequilibrium compaction across the Taranaki Basin: initially driven by the formation and early filling of a foreland basin in the eastern basin margin from ~22 Ma, and subsequently by loading due to the progradation of a succession of sedimentary wedges across the continental shelf from ~10 Ma to the present day. The plotting of vertical effective stress against porosity from reservoirs across each stratigraphic interval and depositional facies within the Taranaki Basin, identifies no clear relationships, primarily due to the late and deep onset of abnormal pressures.

Analyses focused on Palaeocene Farewell Formation and the F-Sands reservoirs, demonstrates that mechanical compaction is the principle porosity reducing mechanism during the first 3000m of burial. Dissolved CO_2 in the pore fluids of the F-Sands and Farewell Formation are likely to have driven the dissolution of detrital grains, generating secondary porosity and enhancing permeability. Continued compaction of secondary porosity in the Farewell Formation has further reduced porosity towards maximum burial. The F-Sands and Farewell Formation can be characterised as geochemically closed systems, where dissolved solutes are being preferentially precipitated in fine-grained heterolithic siltstone beds.

This research presents the pore pressure evolution and distribution of the Taranaki Basin within a tectonostratigraphic context, demonstrating how multiphase overpressure generation and subsequent maintenance are controlled by a combination of sediment loading, uplift, lithofacies variations, fault zone permeability and mechanical compaction. This research has important implications for both hydrocarbon exploration in tectonostratigraphically diverse regions and research into the evolution of polyphase sedimentary basins worldwide.

TABLE OF CONTENTS

DECLARATION

I declare that this thesis, which I submit for the degree of Doctor of Philosophy at Durham University, is my own work, except where acknowledgement is made in the text, and not substantially the same as any work which has previously been submitted at this or any other university for any degree, diploma or other qualification.

December 2018

ACKNOWLEDGEMENTS

Firstly to my supervisor, Stuart Jones, a huge vote of thanks for giving me the freedom to take the project in the directions that interested me, for providing timely feedback, having an open door policy and for generally being a chilled out guy. Huge thanks must also go to Peter and Betty-Ann Kamp for hosting me twice in Hamilton and making me so welcome in their home. Peter again, for his excellent contributions on the regional geology and for invaluable advice and feedback during the later stages of my work. Thanks also to Stefan Stricker for numerous stimulating discussions which helped me greatly throughout my PhD. I am also very grateful to my undergraduate and masters supervisors, Nick Kamenos and Oliver Kuhn, who both were instrumental in persuading me to go down the PhD road.

The project would not have been possible without support from Robert Crookbain of Shell New Zealand, who hosted me twice in New Plymouth and provided both data and specialist knowledge of the region. Further thanks must also go to all the staff in Shell New Zealand exploration team, especially Ted Bates, for providing samples and geomatics support. I must acknowledge Richard Swarbrick, for initially introducing me to geopressure research by offering me my first job in the oil industry, and for always being willing to answer some of the more difficult questions during my studies. I must also thank the staff at IKON Science who provided me with numerous RokDoc licenses over the years, and always offered support during my PhD journey.

Furthermore, I would like to thank Iain Chaplin and Sophie Edwards for the preparation of petrographic samples; James Utley for QEMSCAN analyses; Rob Funnel for bottom hole temperature data; Leon Bowen for advice on the scanning electron microscopy and Norman Oxtoby for the analysis of fluid inclusions.

I am very grateful to Anna Clark, Lorna Morrow and John Underhill at Herriot-Watt University for all of the hard work they did in facilitating the CDT and making it run like clockwork throughout my four years. I am grateful for all of the friends I have made in 2014 NERC CDT in Oil and Gas cohort, especially my great friends Nathaniel, Scott and Nic ('John Webb'). I would like to thank Stefan and Nuala who were always willing to go out to dinner and pay most of the time, and Liz for making me numerous meals over the years, and being my travelling partner during our many CDT trips.

Shout outs must go to all my friends who hosted me while couching surfing: Nic and Hayley in Perth; Tas in Sydney; Charlotte and Callum in Melbourne; Matt in New Plymouth; Lucy & Mark in Auckland, Stefan & Nuala in San Francisco; Claire in Portland and Kate & Rob in Reykjavik. During my numerous trips to London I was hosted by Seb & Sophie, Nicola & Cam and more recently Anji & Olivia, so I thank you, people, for that.

I have been blessed by being part of a very sociable department, so a very big thank you must go to all the friends and acquaintances I have a made over the years in Durham Earth Sciences: Sarah, Erin (writing up buddy), Jamie, Chris, Olly, Emma, Mathieu, Katy, Nuno, Juan, Dimitrios, George, Mark, Jack, Jordan, Tom, Matt, Adam, Kate, Ilaria and many more. Special thanks must go to Chris Harbord for always being around for a pint whenever I suggested one! Being the 'live in landlord' at number 41 Hallgarth Street over the past four years has been a great privilege, and I would like to thank Anji for placing me in charge and for all of my housemates who have enriched my life while in Durham and for never caring what I was doing at work: Claire, Christoph, Malin, Arianne, Sabrina, Fillipo, Hannah, Ted, Erin, Will, Guilia, Costanza, Joshua and Luis.

Extra special thanks for my mum and dad, Lynn and Richard, for always being around to provide logistical support, many meals out and contributions to motoring costs during my numerous issues! For my girlfriend Elöise who has been a welcome distraction from work during the final months of writing. I am also grateful for the help and support provided by Luke and Harriet throughout my PhD. Finally, and potentially most importantly, I would like to thank all the volunteers at Yad Moss ski area, who gave me a welcome break from work during the winter months during my days off with 'powderea', and for Michael and all the staff at the Victoria Inn for consistently providing a great location for drinking quality beer, while enjoying excellent chat.

CHAPTER I:

INTRODUCTION

Large scale copies of the Figures 1.1 & 1.2 can be found in Enclosures 1 & 2, which can be used for reference throughout the thesis.

1.1. PROJECT RATIONALE

The pore pressure distribution within the Taranaki Basin, as in most polyphase or composite sedimentary basins, is the product of several distinct phases of basin evolution and development (Chen et al., 2010; King and Thrasher, 1996), but these phases are poorly understood. The pore pressure distribution within the basin has previously been defined using a discrete depth-based pressure interval approach (Webster et al., 2011), which is tested here through the addition of extensive well data and refined division of the tectonostratigraphy. The maintenance or drainage of abnormal pressures, and thus migration of formation fluids (both hydrocarbons and pore waters) within a sedimentary basin is dependent on pore pressure variations (Yu and Lerche, 1996) and the presence of pathways or alternatively barriers to fluid flow. Analysis of abundant pore pressure data will aid in the understanding of the processes controlling the magnitude and distribution of overpressure across the Taranaki Basin and highlight broader implications for the fluid flow and porosity distribution within sedimentary basins. Furthermore, the accurate spatial definition of overpressure is crucial to prospect risking and ranking, implementing effective well design, drilling safety, determining hydrocarbon column heights, field development strategies and potential prediction of reservoir quality across a basin (Kukla et al., 2011; O'Neill et al., 2018b; Webster et al., 2011).

Hydrocarbon producing basins that display shallow onset and the geological maintenance of high pore fluid pressure (i.e. low vertical effective stress (VES)) have been shown to preserve anomalously high porosity (>30%) at significant depth (>5000 m) by lessening the impact of mechanical compaction (Grant et al., 2014; Nguyen et al., 2013; Oye et al., 2018; Sathar and Jones, 2016; Stricker et al., 2016). The distinct tectonic regimes present within the Taranaki Basin have generated huge variations in the onset and subsequent evolution of pore pressures and thus reservoir stress histories. This knowledge will enable the determination of the role played by VES in potentially arresting porosity loss in reservoirs across the Taranaki Basin.

1.1.1. AIMS OF RESEARCH

- To redefine the pore pressure distribution within the Taranaki Basin, New Zealand, through the addition of new pore pressure data, and implementation of a sub-basin approach defined by shared stratigraphy, tectonic evolution and pore pressure distribution.
- To investigate the onset and subsequent evolution of pore fluid overpressures across the separate tectonic regimes within the Taranaki Basin, New Zealand.
- To investigate whether vertical effective stress is acting to arrest primary porosity loss in sandstone reservoirs across the Taranaki Basin, New Zealand.

- To identify the controlling factors upon the reservoir quality of sandstones from differing burial depths and tectonic histories within the Palaeocene of Taranaki Basin, New Zealand.

1.2. Regional geology of the Taranaki Basin

1.2.1. Basin evolution

The Taranaki Basin covers approximately 100,000 km^2 underlying the shelf and continental slope of central-western North Island (Fig. 1.1). It contains an Upper Cretaceous to Quaternary sedimentary fill up to 8 km thick, as described by King and Thrasher (1996). The basin comprises a relatively undeformed block (the Western Platform) and a heavily deformed area termed the Eastern Mobile Belt (King and Thrasher, 1996). The Eastern Mobile Belt contains significant compressional structures such as Taranaki Fault, where basement overthrusts Neogene and older formations and the Manaia Anticline. Both of these structures may have formed during the Late Eocene (Stagpoole and Nicol, 2008) and certainly by the Early Miocene (e.g. Kamp et al., 2014; King and Thrasher, 1996; Nelson et al., 1994).

The sedimentary fill of the Taranaki Basin records an early (84-57 Ma) phase of extension, concurrent with sea floor spreading in the Tasman Sea to the west. This extension has been attributed either to an intracontinental manifestation of a transform fault offsetting the spreading centre or to a failed rift system (Strogen et al., 2017). The extension controlled the formation of normal fault-bounded grabens and half-grabens, filled by fluvial sandstones and interbedded coal measures of the Late Cretaceous Rakopi and North Cape formations (Fig. 1.2; Enclosure 2). The basin transitioned into a passive margin during the Paleocene, characterised by regional subsidence and the formation of a large embayment, where the Eocene Kapuni Group sandstones and laterally equivalent shelfal Turi mudrocks accumulated (Fig. 1.2; King and Thrasher, 1996). The Kapuni Group (Fig. 1.2) comprises a transgressive sequence of alternating sandstone, shale and coal beds, deposited in a fluvial to fluvio-estuarine depositional environment (Voggenreiter, 1993).

From 52 Ma to ~40 Ma the basin was tectonically quiescent and passively subsiding, before the first manifestations of overprinting arising during the development of the Australia-Pacific plate boundary through New Zealand (Furlong and Kamp, 2013), which may date from the Late Eocene (e.g. King and Thrasher, 1996). A rapid deepening of the basin occurred in the Early Oligocene, associated with a limiting of terrigenous sediment supply, leading to deposition of basinal limestones and mudrocks of the Tikorangi and Otaraoa formations (Fig. 1.2). Uplift and inversion displacement initiated on the Taranaki Fault in the Late Oligocene (~29 Ma) (Kamp et al., 2014), and basement overthrusting on the Taranaki Fault created a prominent eastern basin boundary with an adjacent north-trending foredeep (Holt and Stern, 1994; Stern and Davey, 1990). Continued overthrusting during the Late Oligocene-Early

Miocene, led to the foredeep deepening to bathyal depths, which was infilled by re-deposited shelf carbonates of the Tikorangi Formation and the basin floor fans of the Tariki Formation (de Bock et al., 1990).

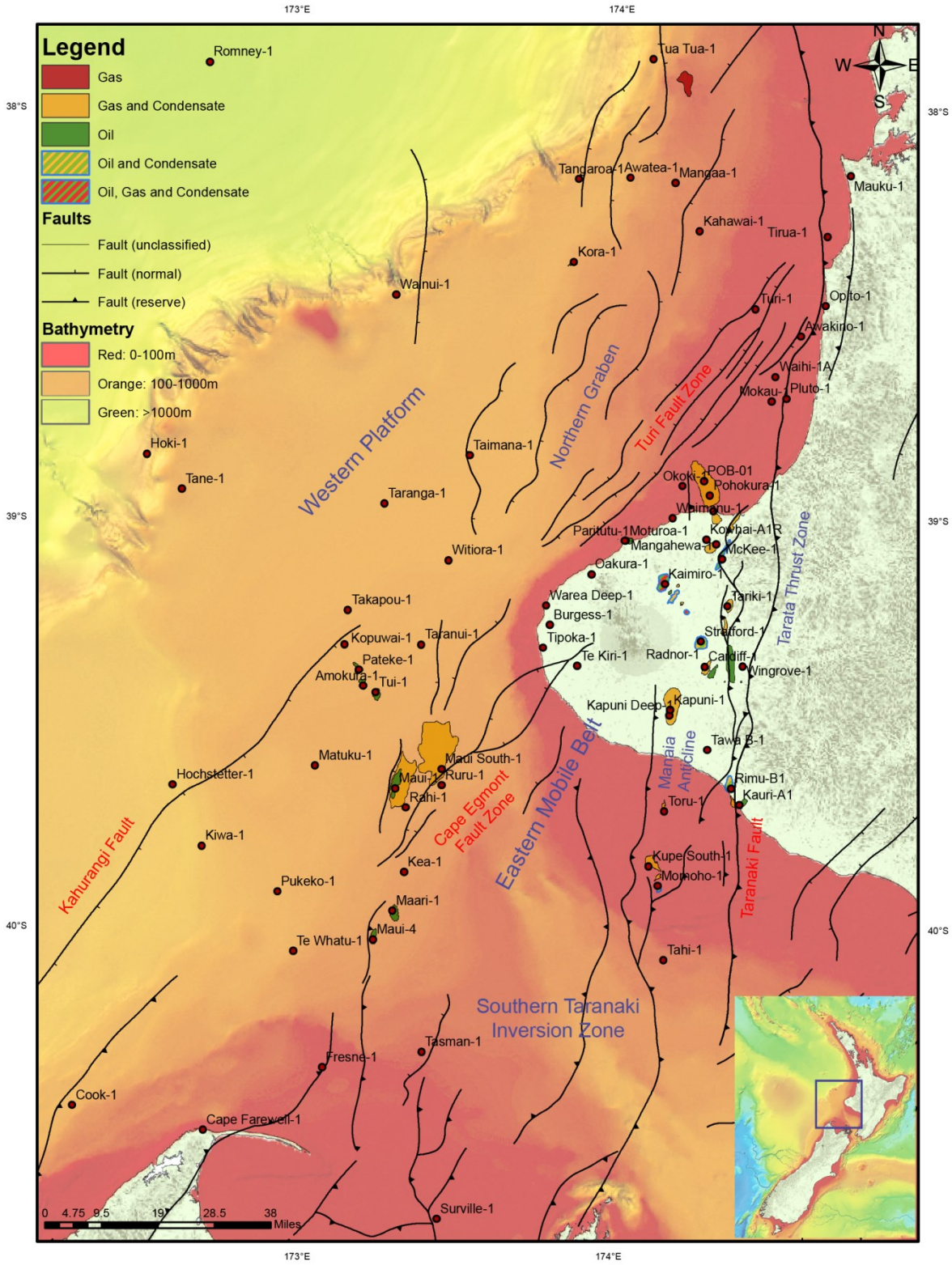

Figure 1.1. Map of Taranaki Basin displaying key wells, producing fields, structure and bathymetry (bathymetry after Mitchell et al., 2012).

A shelf-slope system was established in the Late Oligocene pinned to the top of the Taranaki Fault (Hood et al., 2003a). An increase in terrigenous sediment input during the Early-Mid Miocene overwhelmed carbonate sedimentation, leading to the deposition of a thick

continental wedge comprised of the bathyal Manganui Formation mudrocks and associated interbedded basin floor fans (Moki, Mohakatino, & Mount Messenger formations; Fig. 1.2) (Kamp et al., 2004; Lodwick, 2018; Masalimova et al., 2016; Sharman et al., 2015).

Late Miocene inversion structures formed parallel to the major basin bounding Taranaki Fault, producing several anticlines that trap hydrocarbons in the Eocene Kapuni Group. Thickening of strata against the Manaia fault identified by Stagpoole & Nicol (2008) suggests that displacement may have started during the Late Eocene. These structures contain the bulk of the proven hydrocarbon reserves in the Kapuni, Maui, Pohokura and Kupe South producing fields. These inversion structures, which plunge to the north, formed through reactivation of Late Cretaceous-Palaeocene normal faults (Crowhurst et al., 2002).

Crustal shortening ended at ~5 Ma, due to the formation of the Alpine Fault, which enabled basement in southern North Island to be dexturally offset from similar basement terranes in northern South Island (Furlong and Kamp, 2013), followed by the progressive emplacement of the Pacific plate beneath southern parts of the Taranaki Basin. This led to change in the stress regime to mid-crustal extension, resulting in subsidence during the Plio-Pleistocene (Kamp et al., 2004), and the progradation of a second continental slope and shelf wedge system, known at the Giant Foresets (Fig. 1.2), towards the northwest (Hansen and Kamp, 2004; King and Thrasher, 1992; Mattos et al., 2018; Salazar et al., 2018).

The eastern margin of North Taranaki Basin has been uplifted and eroded since the Early Pliocene as a result of doming of central North Island, preceding the 1.6 Ma outbreak of andesitic and silicic volcanism in Taupo Volcanic Zone (Armstrong and Chapman, 1999; Kamp et al., 2004). Turi-1 well (Fig. 1.1) lies 20 km West of the present day coast on the edge of this zone of uplift and experienced very little uplift and erosion, whereas ~1200 m of section has been eroded off lower parts of Mt Messenger Formation along the modern coast in North Taranaki Bight (Kamp et al., 2004).

1.2.2. Stratigraphy and petroleum system of the Taranaki Basin

The Taranaki Basin has an established stratigraphy, outlined in the New Zealand Stratigraphic lexicon (https://data.gns.cri.nz/stratlex/), which is used wherever possible throughout this study (Fig. 1.2). Laterally time equivalent formations in different parts of the basin are sometimes given alternative names, often defined by operating companies who first intersected the formations during initial basin exploration. Lateral time equivalents are always quoted alongside alternative formation names when appropriate (Fig. 1.2).

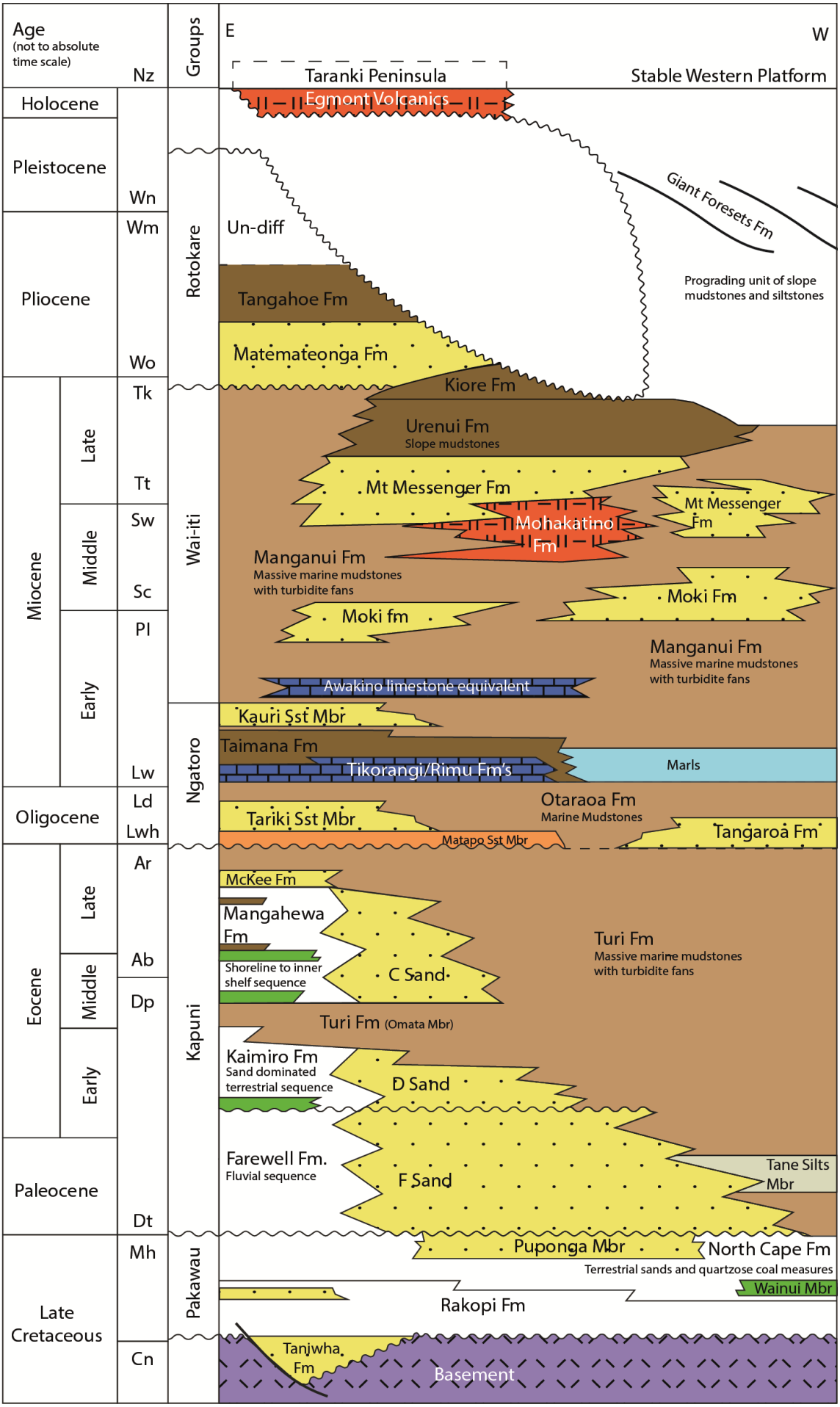

Figure 1.2. Subsurface stratigraphy of Taranaki Basin from the Taranaki Peninsula across the Western Platform (modified from King and Thrasher, 1996).

The Taranaki Basin is currently the only hydrocarbon producing basin in New Zealand, with oil, gas and condensate being produced from Palaeocene-Pliocene reservoirs. The majority of the producing fields contain mainly gas, but nearly all produce a proportion of oil and/or condensate. CO_2 is produced alongside hydrocarbons in many fields and contributes an average of 43% in the Kapuni Field (Higgs et al., 2013). Palaeocene to Eocene hydrocarbon reservoirs are stacked in the major fields (Fig. 1.2; Maui, Pohokura & Kapuni), with some smaller fields producing from both Eocene and Miocene stratigraphic levels (Fig. 1.2; Kaimiro & Waihapa).

1.2.2.1. RESERVOIRS

The Cretaceous Rakopi and North Cape formations were deposited as a series of fluvial floodplains, transgressed periodically by marine incursions (Browne et al., 2008). Core data has only been collected in four wells, reservoir quality is variable, but can be excellent with permeabilities >100 mD and porosities up to 16% (Higgs et al., 2010). Hydrocarbon shows have been identified, but no commercial discoveries have to been made to date in the Cretaceous. The Palaeocene fluvial to shallow marine sandstones of the Farewell Formation act as reservoirs in the Kupe South and Maui fields (Killops et al., 2009; Martin et al., 1994), and will be further discussed in Chapters IV and V. The majority of the petroleum reserves within the Taranaki Basin are contained in single or stacked shoreline and coastal plain sandstone reservoirs of Eocene age (McKee, Mangahewa, Kaimiro formations), which were deposited on a mature continental margin, and sealed by numerous transgressive marine mudrocks (Higgs et al., 2012b; King and Thrasher, 1996; Strogen, 2011). Laterally equivalent shoreface facies of the Kapuni Group reservoirs (C, D & F-Sands) are present on the Western Platform (Fig. 1.2).

Oligocene clastic reservoirs consist of a series of interbedded fine to very fine-grained sandstones within thick packages of mudrocks. They were deposited as a series of turbidites and outer shelf fans that are confined to the eastern basin margin (Higgs and King, 2018; King and Thrasher, 1996). The bathyal Tariki Sandstones Member (Fig. 1.2) forms the major reservoir in a number of fields across the Tarata Thrust Zone (Fig. 1.1), displaying porosities of up to 24% (de Bock et al., 1990). The Oligocene Tikorangi Formation (Fig. 1.2) was deposited across the basin and is characterised by three contrasting megafacies: pelagic basinal deposits, mixed siliciclastic-carbonate foredeep deposits and shallow-shelfal limestones (Hood et al., 2004, 2003a, 2003b). The Tikorangi Formation displays an open fracture system, in the foredeep facies, formed during early Miocene thrusting at subsurface depths of 3 km, which produce mainly oil in the Waihapa Field (Fig. 1.1; Hood et al., 2003c).

The Late Miocene Kauri Sandstones, which act as hydrocarbon reservoir on the Southern Taranaki Peninsula, display similar geometries to the Tariki Sandstones but were deposited in shelfal conditions (Higgs and King, 2018). The Middle-Late Miocene reservoirs of the

Taranaki Basin belong to a regressive sedimentary system, characterised by low stand deep-water sandstone turbidites (King and Thrasher, 1996). The Middle Miocene Moki Formation sandstones are described as a submarine slope channel facies, while the Early Miocene Mount Messenger sandstones were deposited as more distal basin floor fans (Higgs and King, 2018). Hydrocarbons are produced from Miocene reservoirs in the Maari (offshore), Kaimiro, Ngatoro, Goldie, and Cheal fields in the Taranaki Basin (Fig 1.1; Higgs et al., 2015), from amalgamated very-fine to fine-grained sandstone packages of up to 20 m thick (King and Thrasher, 1996).

Latest Miocene-Early Pliocene shoreface to mid-shelfal sandstones of the Matemateaonga Formation (Fig. 1.2) were deposited on a broad, extensive continental shelf with a shoreline to the south and a wide progradational front to the north-northwest (King and Thrasher, 1996; Vonk and Kamp, 2004). The Matemateaonga reservoirs are the youngest to have produced hydrocarbons in the Taranaki Basin at the Moturua Field (King and Thrasher, 1996), which began production in 1911 (Townsend et al., 2008).

1.2.2.2. SEALS

Mudrocks are widespread in the Taranaki Basin, making up 70% of the stratigraphy (Darby and Funnell, 2001), forming top seals or internal seals to all hydrocarbon-bearing clastic reservoirs. The carbonates of the Oligocene Tikorangi Formation are inherently low permeability and thus can act as seals away from areas of intense deformation, like on the Western Platform (King and Thrasher, 1996). Eocene Kapuni Group reservoirs are sealed by Eocene to Oligocene and lower Miocene maximum flooding derived siltstones and marls (Fig. 1.2; Turi, Otaraoa, and Taimana formations), while the deep-water sandstones of the Moki and Mount Messenger formations are sealed by mudrocks of the mid Early Miocene Manganui Formation (Ilg et al., 2012; King and Thrasher, 1996).

1.2.2.3. SOURCE ROCKS

Hydrocarbons (oil, gas and condensate) are sourced primarily from coaly organic matter within terrestrial formations of the Pakawau (Late Cretaceous) and Kapuni (Palaeocene-Eocene) groups (Fig. 1.2; Killops et al., 1996, 1994; Sykes, 2001). Key source rock units are found in the relatively coal-rich Rakopi (Late Cretaceous), Farewell (Palaeocene), Kaimiro and Mangahewa (Eocene) formations. The Taniwha Formation (mid-Cretaceous) and Wainui Member of North Cape Formation (Late Cretaceous) may be locally important towards the north of the basin (Fig. 1.2) (Sykes, 2001).

1.3. OVERPRESSURE GENERATION– AN OUTLINE

Pressure is the measurement of the amount of force exerted on a unit area, as such, various pressure attributes (hydrostatic pressure, lithostatic pressure, pore pressure and effective stress) are used in conjunction to define the geopressure regime in a sedimentary basin (Schofield, 2016). Hydrostatic pressure is defined as the amount of force exerted by the weight of a static column of fluid in equilibrium with the surface pressure, which is a function of the density of the water and, as such, defines the gradient on a pressure depth plot (Fig. 1.3). The lithostatic pressure refers to the stress of the overlying sediments and pore fluids acting upon a rock at a given depth in a vertical direction (Schofield, 2016). Pore pressure is defined as the pressure of the fluids within the pores of a rock matrix, while the effective stress can be described as the pressure exerted at a certain depth borne purely by the rock matrix grain to grain contacts (Schofield, 2016).

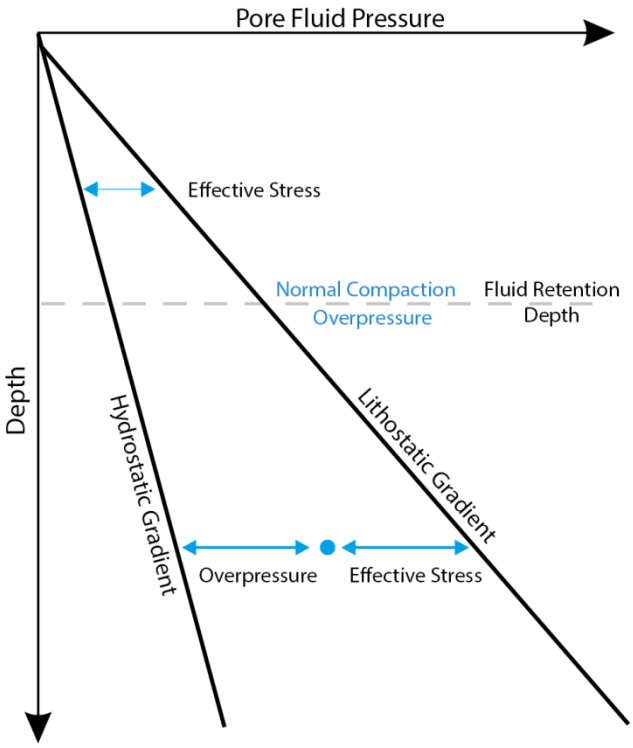

Figure 1.3. Schematic pressure depth plot displaying hydrostatic and lithostatic gradients, and observed overpressure and effective stress for specific pore pressure (modified from Webster et al., 2011).

Abnormal pore pressure is defined as a pore pressure that lies either above or below (overpressure or underpressure respectively) the hydrostatic pressure (Fig. 1.3). Overpressure is caused by the inability of fluids within a rock matrix to escape, and occurs below the fluid retention depth (Fig. 1.3; Swarbrick et al., 2002). Overpressure in clastic sedimentary basins is created by two main groups of mechanisms: (1) stress applied to a compressible rock (disequilibrium compaction, lateral compression); and (2) fluid expansion and/or increase in fluid volume (through hydrocarbon cracking, gas generation and load transfer) (Lahann and Swarbrick, 2011; Swarbrick et al., 2002).

1.3.1. STRESS RELATED MECHANISMS

1.3.1.1. DISEQUILIBRIUM COMPACTION

Disequilibrium compaction is considered to be the principle mechanism contributing to overpressure in sedimentary basins, occurring when burial rates and increases in load stress outpace the rate at which connate fluids can dissipate (Chapman, 1980; Dickey, 1976; Hubbert and Rubey, 1959; Secor, 1965; Swarbrick and Osborne, 1998). During burial, fluids are expelled from the pore spaces within granular rocks, increasing the vertical effective stress, and reducing the porosity and permeability. If a balance between additional load stress and compaction and/or loss of fluid is achieved, then hydrostatic conditions prevail. When out of equilibrium, permeability has reduced to a point where fluids cannot be sufficiently expelled or dewatered and assumes some of the load normally burdened by the grain contacts (Schofield, 2016).

1.3.1.2. HORIZONTAL STRESS

Laterally compressive stresses, often in combination with vertical stress, can lead to limited dewatering and the maintenance of overpressure. This phenomenon has been identified in New Zealand's East Coast basin, associated with plate convergence at the Hikurangi Margin (Burgreen-Chan et al., 2016; Darby and Funnell, 2001)

1.3.2. OTHER MECHANISMS

Other overpressure generating mechanisms are summarised in Table 1.1 and fully explained in Osborne and Swarbrick (1997). Hydrocarbon generation, lateral drainage and lateral transfer are discussed in the following sections as they also contribute to overpressures in the Taranaki Basin.

Table: 1.1. Summary of overpressure generating mechanism (after Osborne and Swarbrick, 1997; modified from Schofield, 2016)

1) Stress-related mechanisms	Disequilibrium compaction (vertical loading)
	Tectonic stress (lateral compressive stress)
2) Fluid volume increases mechanisms	Temperature increase/aquathermal
	Mineral transformation
	Hydrocarbon generation & cracking
3) Load transfer mechanisms	Kerogen to oil conversion
	Clay mineral transformations
4) Chemical compaction	
5) Other generation mechanisms	Hydraulic head
	Excess density contrast buoyancy
	Osmosis

1.3.2.1. HYDROCARBON GENERATION

The transformation of kerogen into hydrocarbons (oil, gas or both) increases the fluid volume within pores, leading to the generation of overpressure (Osborne and Swarbrick, 1997), though oil generation volume changes are thought to be negligible (England et al., 1987). In contrast, gas generation has the potential to significantly increase the pore volume. Swarbrick et al. (2002) suggest that late-stage oil to gas cracking has the potential to increase pore volumes by up to 140%, contributing to overpressures increases in excess of 6000 psi.

1.3.2.2. LATERAL TRANSFER & DRAINAGE

Lateral transfer only involves the redistribution of pore fluid pressure, therefore cannot be strictly classified as a generating mechanism. Yardley and Swarbrick (2000) first defined lateral transfer as the internal redistribution of fluid pressure in a confined and tilted reservoir. This process produces elevated crestal pore pressures and lower than would be expected pressures downdip (Fig. 1.4), with an equilibrium point in the centre called the centroid where the reservoir and shale pressures are, in theory, equal (Bowers, 2001; Dickinson, 1953; Traugott, 1997).

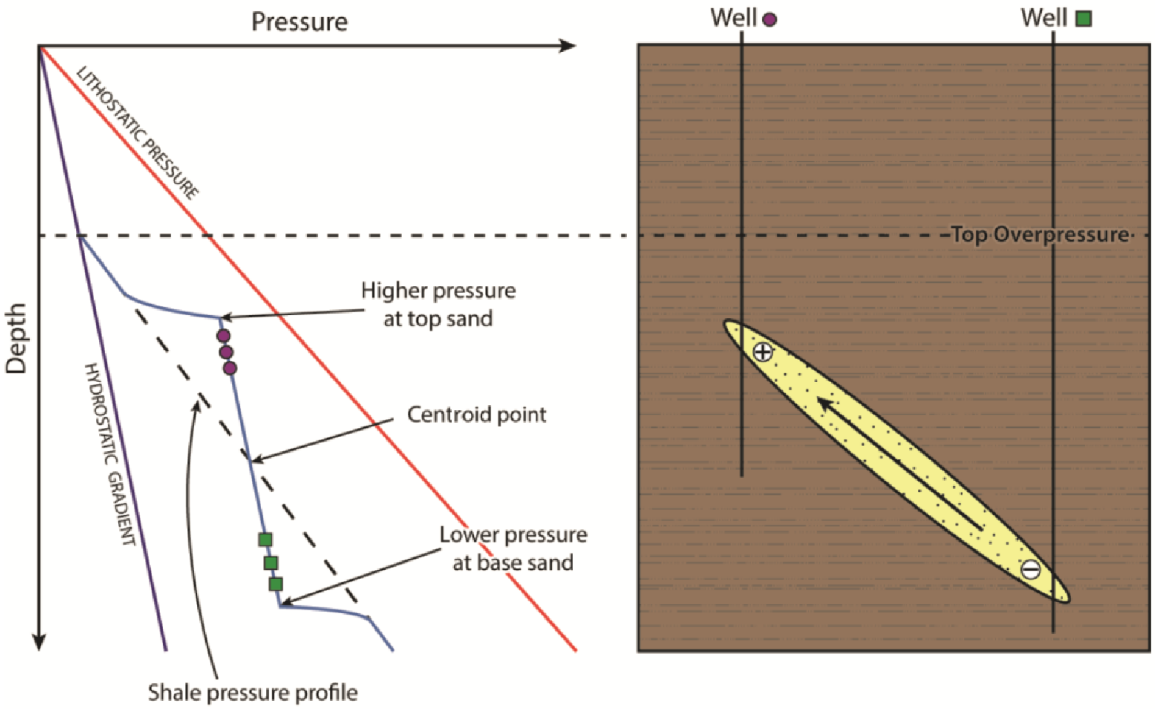

Figure 1.4. Schematic illustration and pressure-depth plot showing how lateral transfer may enhance and lessen overpressures at the structural crest and base of a tilted sandstone body respectively when compared to pore pressures within the surrounding mudrock. The depth at which overpressure within the sand and surrounding mud is equal is termed the 'centroid' (from Robertson, 2013).

Lateral drainage occurs when permeable formations are hydraulically connected updip, allowing excess fluid pressure to escape to the surface, or too stratigraphically higher formations, via either continuous reservoirs or fault linkage (O'Connor and Swarbrick, 2008). Lateral drainage is identified in pressure depth space by pressure reversals, where sandstone

overpressure is lower than in the surrounding mudrock. Shoulder effects may occur where fluids drain out from the surrounding mudrock (Fig. 1.5; Robertson, 2013).

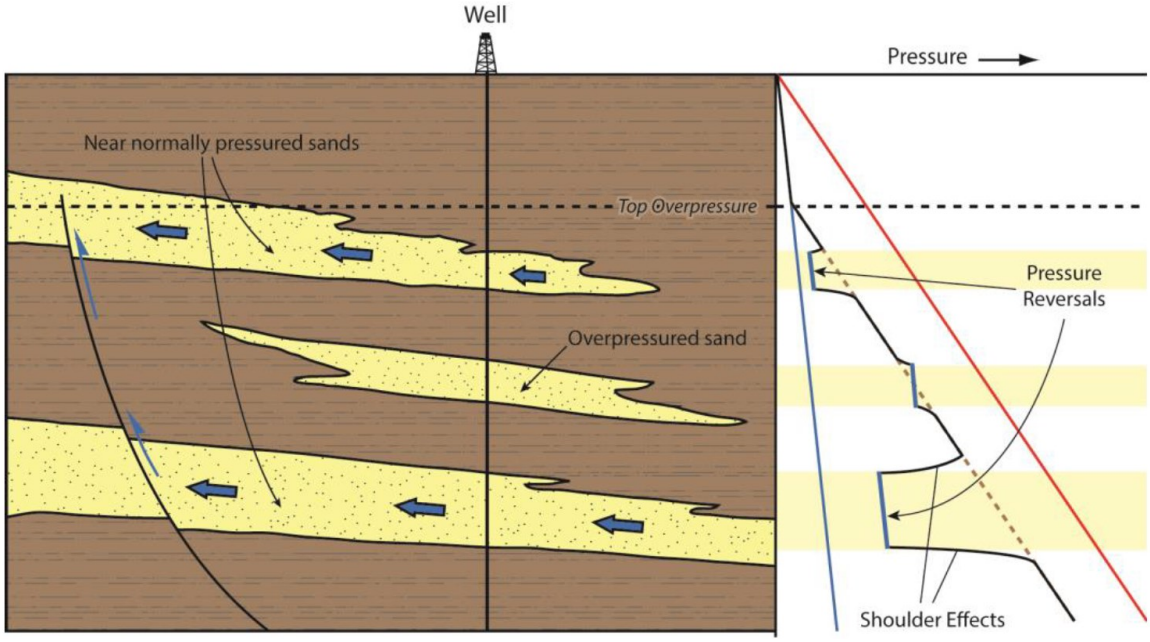

Figure 1.5. Schematic block diagram and pressure-depth plot illustrating lateral drainage. Fluids flow preferentially along higher permeability pathways from regions of higher to lower overpressure. Pathways for fluid flow may include higher permeability sandstones or nonsealing faults (as above) (from Robertson, 2013).

1.3.3. Taranaki Basin mechanisms

Analysis of wireline velocity cross plots by Webster et al., (2011) identified the primary cause of overpressure in the Taranaki Basin as disequilibrium compaction preserved in upper Eocene, Oligocene and early Miocene marine shales (Turi, Otaraoa and Manganui formations). In parts of the basin, hydrocarbon generation (and in particular cracking to gas at high maturities) is interpreted to contribute to the overpressures encountered in deeper portions of the basin (Webster et al., 2011; Webster and Adams, 1996). Furthermore, the presence of lateral drainage has been demonstrated across the Western Platform, Manaia Anticline and Southern Taranaki Inversion Zone (O'Neill et al., 2018b; Webster et al., 2011), while lateral transfer is suggested to be occurring in the Tarata Thrust Zone (O'Neill et al., 2018a).

1.4. Thesis Outline

The full outlines of Chapters II-VI are described individually below. The main data sections, chapters II-V, have been written as standalone manuscripts and have/will be submitted for publication in peer-reviewed international journals. As such, each chapter contains a specific introduction, methods (when not repeated), results, discussion and conclusions. The thesis only contains manuscripts for which I am the first author, and I have been responsible for more than 50% of the primary data collection, and over 90% of the interpretation and research manuscript writing.

1.4.1. Chapter II: Evaluation of pore pressure distribution in the Taranaki Basin

Direct pressure data from 129 wells are used to redefine the pore pressure distribution within the Taranaki Basin using a new sub-basin approach. Facies variations across the basin and compartmentalisation (structural and stratigraphic) are described and discussed in the context of the distribution and differing magnitudes of overpressure.

1.4.2. Chapter III: Pore pressure evolution and its relationship to reservoir quality in the Taranaki Basin

One-dimensional basin modelling is used to investigate how the initiation and evolution of overpressure varies across the Taranaki Basin. Measured core porosity data compiled from reservoirs ranging from the Palaeocene to early Miocene are used to investigate whether vertical effective stress is acting to preserve primary porosity at depth.

1.4.3. Chapter IV: Pore pressure and reservoir quality evolution in the deep Taranaki Basin

Chapter IV expands on work done in Chapter III, using various petrographic techniques and basin modelling to investigate the diagenetic paragenesis and reservoir quality evolution of the overpressured Palaeocene Farewell Formation at Kapuni Deep-1 well. The role of continued high VES and secondary compaction is discussed in the context of the very low measured porosity and intergranular volumes. This chapter has been published in the journal *Marine and Petroleum geology*, DOI: 10.1016/J.MARPETGEO.2018.08.038.

1.4.4. Chapter V: Controls on reservoir quality in the shallow Palaeocene stratigraphy of the Taranaki Basin

This chapter investigates the diagenetic paragenesis and reservoir quality evolution of the hydrostatically pressured Palaeocene F-Sands reservoir of the hydrocarbon producing Maui Field. The development and preservation of significant secondary porosity is outlined, along with a discussion on whether the F-Sands are a geochemically open or closed system.

1.4.5. Discussion, conclusion, and future work

This chapter elaborates on the discussion sections from the preceding chapters while using an integrated approach to summarise and discuss the wider implications of: overpressure and facies distributions; basin modelling approaches and sandstone reservoir quality. Conclusions drawn throughout the body of the thesis are summarised. This chapter also reveals areas of future research that might develop the themes covered in this thesis.

CHAPTER II:

EVALUATION OF PORE PRESSURE DISTRIBUTION WITHIN THE TARANAKI BASIN, NEW ZEALAND

2.1. INTRODUCTION

Pore pressure distribution is an essential component of the petroleum system in a sedimentary basin and hence of significant importance for exploration, appraisal and production of hydrocarbons (Lindberg et al., 1980; Verweij, 1999). Accurate prediction of the magnitude and depth of overpressure is crucial for safe and efficient drilling (Law and Spencer, 1998) and for the prevention of blowouts such as the one involving McKee-13 in Taranaki Basin (discussed in section 2.4.3.2; O'Neill et al., 2018a). In addition, knowledge about the distribution of pore pressure within permeable formations together with their interaction with overpressure maintaining facies (mudrocks) forms a powerful tool for investigating lateral fluid flow and regional migration pathways (Iliffe et al., 1999; Javanshir et al., 2015; O'Connor and Swarbrick, 2008; Robertson et al., 2013).

Overpressure is not static; rather, it is a transient phenomenon (Tingay et al., 2009), which has a tendency to dissipate over time unless renewed by active generation mechanisms (Robertson, 2013). Excess pressure is predisposed to re-equilibrate to hydrostatic pressure within inclined reservoirs or into shallower reservoirs by fluid migration through faults or fractures (Tingay et al., 2007; Yardley and Swarbrick, 2000). The polyphase evolution of the Taranaki Basin has led to a complex pore pressure history, producing a significant variation in present day vertical and lateral distribution of overpressure. Overpressures within the Taranaki Basin has been maintained through sealing faults, stratigraphic pinch out and dissipated via large scale lateral migration pathways (Webster et al., 2011). This chapter presents the spatial variations of overpressure within a tectonostratigraphic context, in order to help constrain the dynamic features of the present-day distribution (Chen et al., 2010).

2.1.1. CURRENT UNDERSTANDING OF PORE PRESSURE DISTRIBUTION

Initial research into geopressure systems of New Zealand basins (Darby, 2002; Darby and Ellis, 2003; Darby and Funnell, 2001) showed that although the Taranaki and East Coast basins display similar stratigraphy, their pore pressure histories are significantly different. Excessively high pore pressures intercepted in the East Coast Basin, are produced by lateral shortening driven by subduction accretion and associated processes. Exploration wells drilled in East Coast basins have encountered fluid pressures of 1856 psi at 600 m depth, which equates to 90% of lithostatic pressure; mudweights of 19.56 ppg were required to control formation fluids at only 1400 m (Darby and Funnell, 2001). By contrast, in Taranaki Basin, which lies in a foreland position with respect to the subduction zone, subsidence rates are 500-1000 Ma/yr and fluid pressures equal to about ~60% of lithostatic pressure below 3 km in the basin (Darby and Ellis, 2003).

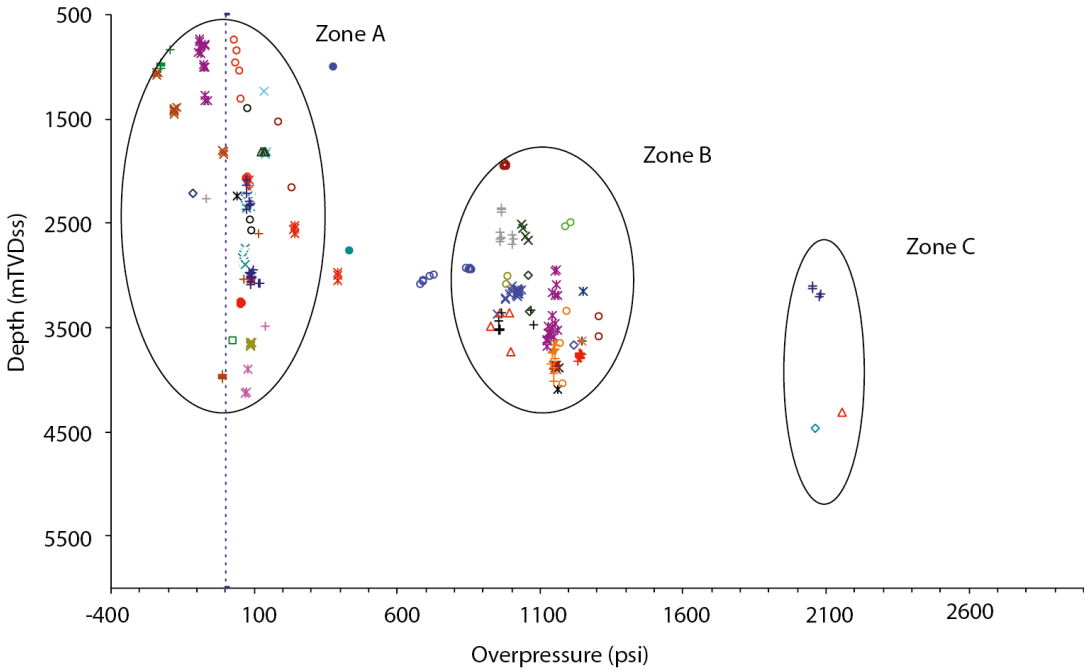

Figure 2.1. Overpressure-depth plot for Taranaki Basin, displaying three discrete overpressure zones A-C (after Webster et al., 2011)

Webster et al. (2011) identified both the pore pressure distribution with depth across the Taranaki Basin and potential overpressure generating mechanisms. They designated three semi-stratigraphically separated overpressure zones in the basin (Fig. 2.1): a near-hydrostatic interval (Zone A), which extends from surface to varying depths in different parts of the basin; a generally underlying overpressured interval (Zone B) of ~1200 psi, which extends from ~1900 m to ~4000 m; and a third interval (Zone C) of >2000 psi, which directly underlays zones A & B in different parts of the basin. The Oligocene Otaraoa Formation (Fig. 1.2), a bathyal calcareous mudrocks, acts as the principal top seal between hydrostatic Zone A and deeper variably overpressured zones. The Otaraoa Formation and underlying massive marine mudrocks of the Turi Formation are considered to be the formations where overpressure (low vertical effective stress) is maintained in the basin through the mechanism of disequilibrium compaction (Webster et al., 2011).

2.1.2. Sub-basin model

This chapter tests the Webster et al. (2011) model of discrete depth-based pressure intervals through the analysis of a more comprehensive set of pressure data for wells that are now open file (Fig. 2.5b & 2.6a). A key outcome of this study is the introduction of a novel sub-basin approach to the analysis and interpretation of pore pressure data available for the basin. This approach is considered to have applicability to other basins globally exhibiting fluid overpressure and having a polyphase tectonostratigraphic history.

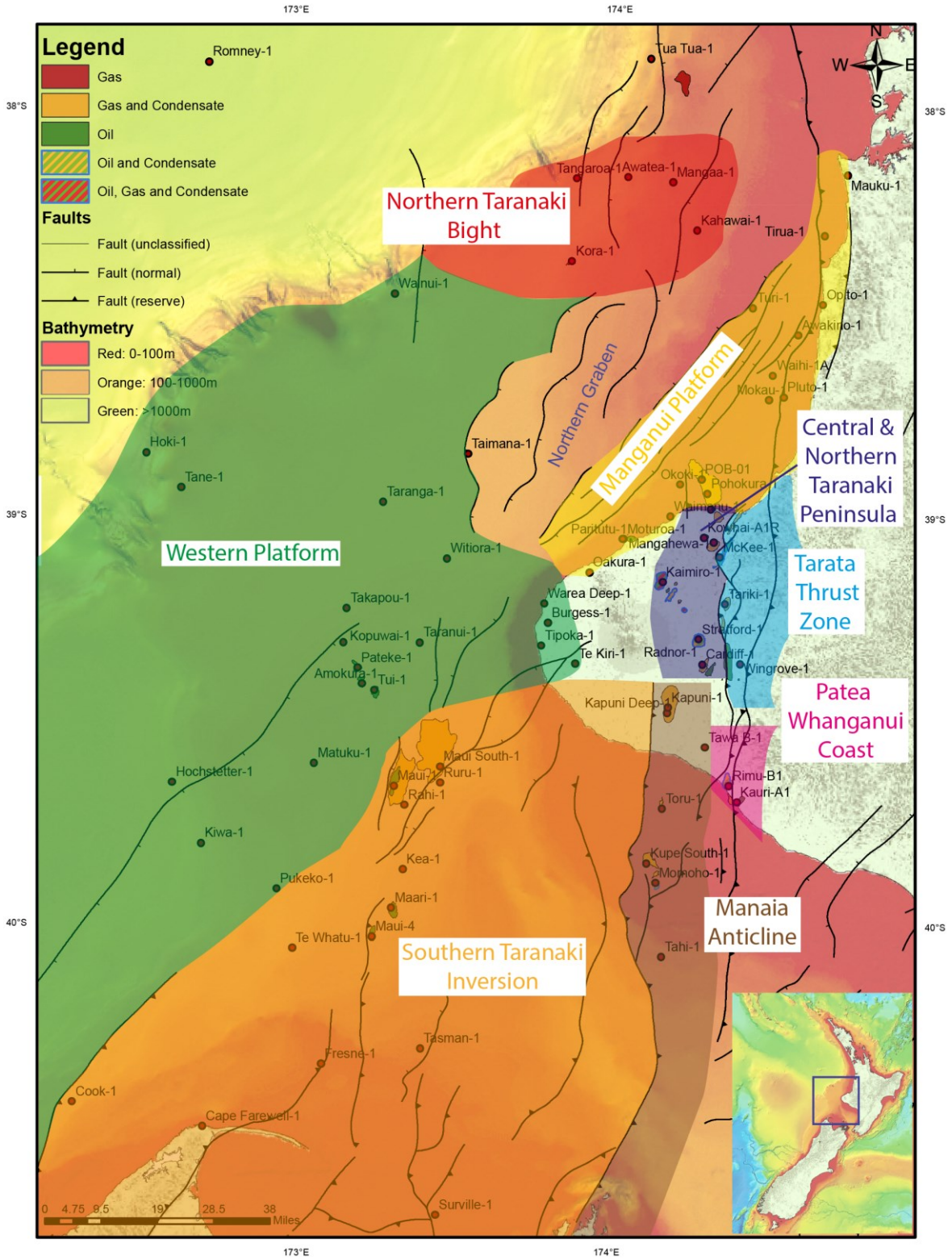

Figure 2.2. Map of Taranaki Basin with sub-basin overlays of the Southern Taranaki Inversion Zone (orange), Manaia Anticline (brown), central and northern Taranaki Peninsula (blue), Tarata Thrust Zone (turquoise), Patea Whanganui Coast (purple), Western Platform (green), Northern Taranaki Bight (red) and Manganui Platform (yellow). Wells for basin modelling in Chapter III are also displayed.

Eight sub-basin areas and structural zones (Fig. 2.2; Southern Taranaki Inversion Zone, Manaia Anticline, Central and Northern Taranaki Peninsula, Tarata Thrust Zone, Patea Whanganui Coast, Western Platform, Northern Taranaki Bight, and Manganui Platform) are defined through shared stratigraphy, tectonic evolution and pore pressure distribution. Interpretation of regional seismic lines (Fig 2.4) enables the identification of facies variations

between the subareas and structural zones, which are shown to have first order control on overpressure maintenance, regional fluid flow and reservoir quality in the basin. Additional pore pressure and mudweight data from recent deep wells are used to investigate pressure transition below 4000 mTVD (see Chapter IV, section 4.4.5 for further discussion). The compilation and calculation of kick pressures ranging from the Palaeocene to Oligocene provide important information on geopressure hazards, which are crucial for pore pressure prediction and well engineering. Compartmentalisation and maintenance of excess pressure due to sealing faults is discussed using recent well data from northern Taranaki Peninsula.

2.2. METHODOLOGY

In this study, single well pressure depth plots were analysed for 129 wells in Taranaki Basin, of which 99 contained direct wireline formation tester (WFT) data (RFT, MDT, XPT, FIT & RCI), 22 contained Drill Stem Tests (DST) and 21 contained well bore kicks. Values of overpressure were calculated using IKON Sciences RokDoc software (v.6.3.0.272) and these values were assigned to the correct reservoir unit by referring to composite logs, biostratigraphy and wireline data, resulting in a final database comprised of 242 formation overpressure values. Quality control was applied to reject any pressure values that might have been affected by production in nearby fields, as depletion during production can lead to pore pressure drawdown. This was achieved through the visualisation of data from the same field or sub-basin on a multi-well plot and comparing the overpressure values, which would indicate whether those pressures represent virgin pressure or whether production related depletion has caused an alteration of the pressure regime.

All of the WFT and kick data were collected from well completion reports and their associated enclosures, supplied in the 2015 & 2016 New Zealand Petroleum Exploration Data Pack (NZP&M, 2018)(https://data.nzpam.govt.nz/GOLD/system/mainframe.asp). DST data were collected from Leap Energy's New Zealand ArcGIS Geodatabase (Leap Energy, 2014).

As is the convention with operating companies in Taranaki Basin, pressure values will be quoted in psi and depth in metres throughout this study.

2.2.1. DIRECT PRESSURE MEASUREMENTS: ACQUISITION AND QUALITY CONTROL

2.2.1.1. WIRELINE FORMATION TESTERS QUALITY CONTROL

Wireline Formation Test (WFT) tools are the most reliable and efficient method for the acquisition of multiple pressure measurements in open-hole conditions (Gunter and Moore, 1987). The selected tool is lowered down an uncased well and then jacked and sealed against the borehole wall. A small probe, extending from the tool, is inserted into the formation wall and the rate at which pressure builds up within the tool is recorded using a pressure gauge (Robertson, 2013).

Obtaining high quality interpretations for pressure data requires particular attention to data acquisition procedures as well as interpretation techniques (Gunter and Moore, 1987). Wireline formation tests can be assigned a measure of quality based on their build-up plots, depending on whether the tests have reached equilibrium or full build-up with respect to the formation pore fluid pressure. In this study over 2000 build-up plots have been analysed and quality values applied to each of the pressure points. An example MDT build-up plot, in Figure 2.3, displays a formation pressure reading which stabilised to within 0.01psi over a 45 second interval, so is designated as 'good' quality. The quality values and full criteria are explained below:

Good - the test has either completely stabilised to 2nd decimal point over at least 45 seconds, or is changing by only 0.01 psia over 45 seconds.

Fair - the test has stabilised to 1st decimal point over 1-2 minutes, but the 2nd decimal point is fluctuating or rising by 0.02-0.09 psi/min.

Poor – the test has failed to stabilise on the 1st decimal point over a minute and is either still building, falling or fluctuating by 0.1 psi/min.

Unknown - pressure data provided with no build up plots. These data can still be used to define overpressure and contacts if points lie on a solid water gradient.

Invalid - supercharged, seal failure, no flow, tight etc.

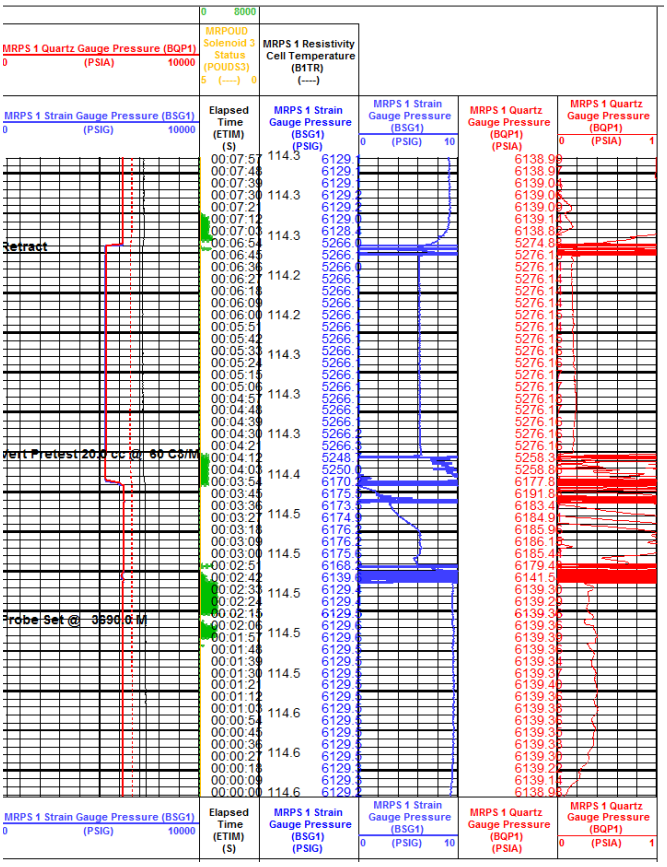

Figure 2.3. Wireline Pressure (MDT) Plot for well Mangahewa-3 (Quality: Good)

If the pressure point has been designated as invalid, then the wireline tool has encountered problems and failed to acquire a representative reading of the formation pressure. The two most commonly encountered problems are a 'tight' formation and 'seal failure'. In a tight test, the formation usually has low permeability and is abandoned if it cannot be conducted in a 15-20 min interval. Seal failures occur when the packer fails to provide isolation of the probe from borehole mud, which results in a rapid pressure build-up to the static mud pressure. Also, in low permeability formations drilling mud can invade the formation and retain some of the excess pressure, which is called 'supercharging'. This is observed when the formation pressure is higher than the static mud pressure. The formation pressures must also be plotted as absolute pressure values and adjusted if they are recorded in gauge pressure.

2.2.1.2. Drill stem tests

Drill stem tests are typically carried out during drilling when zones containing hydrocarbon fluids have been identified using perforated drill pipe and packers (Robertson, 2013), which isolate formations to determine the fluids present and potential production rates. WFT data are generally more reliable because of greater sampling capabilities and more reliable vertical pressure profiles. Also, WFT pressures are measured at specific depths in the reservoir, whereas DST gauges are usually positioned in the test tool string above the reservoir being tested (Gunter and Moore, 1987). In this study, all DST pressures are plotted at the mid perforation depth for consistency. Only DST measurements that have been designated as 'final build-ups' are used in the database, as these provide the best representation of true formation pressure.

2.2.1.3. Kicks

A kick is defined as any unplanned influx or intrusion of formation fluids into the wellbore, which results in an unexpected gain of fluid into the mud pits, indicative of a formation fluid in excess of the weight of the mud column (Lee et al., in press). Quality control methodologies from Lee et al. (in press) were applied to any well bore influxes, where shut-in drill pipe pressures (SIDPP), were recorded, by removing any erroneous data due to swabbing or well bore breathing. Kick pressures were calculated using the 'u-tube model', which uses the sum of the estimated downhole pressure exerted by the column of mud in the drill pipe and the shut-in drill pipe pressure (SIDPP) (from a surface gauge) to calculate the kick pressure:

Kick pressure (psi) = (Drilling fluid gradient in ppg/19.25 x TVD (ft)) + SIDPP (psi)

2.2.2. Indirect pressure measurements

2.2.2.1. Mudweight

In the absence of direct pressure measurements, mudweight can be used as a proxy for pore pressure, using the assumption that mudweights are kept in balance or at slightly greater

pressures than the formation pressure (e.g. Webster et al., 2011). Mudweight cannot be used in fine-grained facies (mudrocks) as their inherent low permeabilities mean that these intervals can often be drilled underbalanced or overbalanced, which may go undetected. In this study, mudweight increases in wells due to underbalanced drilling where influxes occurred are used as a proxy for formation pressure.

2.2.2.2. WIRELINE LOG DATA

Pore pressure in fine-grained sediments can be estimated using wireline log data, which exploit the deviation of mudrock properties (e.g., sonic velocities, density, and resistivity data) relative to those values typical of a normally compacted sequence at the depth of interest (Webster et al., 2011). Overpressures generated by disequilibrium compaction, as in Taranaki Basin, are associated with anomalously high sediment porosities (undercompaction) and are thus more readily detectable in wireline data (Sayers et al., 2002). Deviation in the log data can be used qualitatively to predict where porosity anomalies and therefore overpressure may be present within fine-grained facies.

2.2.3. OVERPRESSURE DETERMINATION

A constant unique hydrostatic gradient of 1.4235 psi/m was assumed for the entire Taranaki Basin, to calculate overpressure from direct pore pressure measurements (Robertson et al., 2013). This hydrostatic gradient was calculated using the average value from 21 category 4 aquifer gradients (see section 2.5) from various reservoirs in wells across the basin. Applying best fit straight lines to possible fluid gradients in each well enabled the identification the most likely type of pore fluid present within the reservoir (i.e. gas, condensate, oil or water), and these were cross-checked where possible against known hydrocarbon accumulations, wireline data and well completion reports (e.g. Robertson et al., 2013). Where possible, water, oil and gas columns were defined, along with calculated depths to associated oil-water, gas-water and gas-oil contacts.

In all reservoirs that contain a water leg, a value of overpressure representative of the entire reservoir unit was calculated using the shallowest pore pressure measurement interpreted to lie directly on the water gradient. If only hydrocarbons are present, the deepest direct pore pressure measurement interpreted to lie on the hydrocarbon gradient was used to calculate the overpressure. Hydrocarbon buoyancy affects cause overpressure values calculated in the oil or gas leg to be an over overestimation of pressure in the water column (Robertson et al., 2013).

2.2.3.1. ERRORS ASSOCIATED WITH USING A CONSTANT REGIONAL HYDROSTATIC GRADIENT

The use of a constant hydrostatic gradient of 1.4235 psi/m for the entire Taranaki Basin, implies the absence of salinity variation and hence pore water density across the region, which is an unrealistic assumption, and introduces errors into overpressure calculations

(Robertson et al., 2013). The gradient across both the Southern Taranaki Inversion Zone and the Western Platform display a slightly shallower gradient of 1.4268 psi/m, implying that the aquifer is more saline. The depositional pore waters of the reservoirs in these two sub-basins will have been saline, owing to their deposition in shelfal to shoreface settings. The Eocene to Cretaceous reservoirs in Central and Northern Taranaki Peninsula and Manaia Anticline were deposited in coastal plain and marginal marine settings (Higgs et al., 2012b; Strogen, 2011), which had fresh water input. Therefore, reservoirs across the Southern Taranaki Inversion Zone and the Western Platform that are slightly overpressured (~100 psi) are actually hydrostatically pressured.

2.2.3.2. Overpressure category system

A modified version of the Ikon Geopressure category system (Robertson et al., 2013; Swarbrick et al., 2004) has been used in this study to classify the pressure data per well from which overpressure values were calculated. The classification system comprises four categories:

Category 1: not used in practice because no direct pressure readings were taken; pressure readings are depleted or mudweights are not representative of pore pressure.

Category 2: gradients, in general, are not well established, with a few sporadically placed 'poor' points. Also includes gradients with only two points and where hydrocarbons are present that are not complemented with an associated aquifer gradient. Gradients are then divided into sub-categories based on fluid type:

2A: fluid type is known to be water;
2B: fluid type is known to be a hydrocarbon;
2U: fluid type is unknown.

Category 3: 'Fair' and 'good' pressure points are used to generate a reasonable water gradient with some minor scattering in the slope.

Category 4: 'Good' pressure data generates a very clear water gradient with very little or no scatter in the data.

2.2.4. Wireline time-depth conversion

RokDoc (v.6.3.0.272) was used to calculate depth to time conversion for wireline sonic logs from selected wells for plotting on Figure 2.4. Check shot data were compiled from well completion reports.

2.2.5. Sub-basin determination

Wells from regions of the basin with shared tectonostratigraphic history were grouped and analysed using multi-well pressure depth plots to identify shared trends. Sub-basins were then defined through shared structural architecture, stratigraphic stacking and pore pressure

trends. Large uncertainty can placed on the boundaries between certain sub-basins, which is chiefly dependant on the well density. Well density on the Taranaki Peninsula and nearshore areas is significantly greater than in the deep water, towards the west and north-west, due to higher number of hydrocarbon fields and associated near fields exploration.

For example, the distinction between the Western Platform and Northern Taranaki Bight is unclear as it is solely defined by the presence of the Oligocene Tangaroa Formation Sandstones, which has limited well penetrations and thus a large uncertainty on the dimensions of the geobody. In this situation the most accurate estimation of the boundary is defined using information from published literature and New Zealand petroleum reports. The boundaries between the sub-basins within the Eastern Mobile Belt are defined by major faults which often offset the stratigraphy and act as barriers to fluid flow. The Specific structural styles and stratigraphic stacking of each sub-basin is described in sections 2.3.2.1 to 2.3.2.8.

2.3. RESULTS

The Taranaki Basin does not display excessively high overpressure values, as seen in other rapidly subsiding basins such as the Central North Sea and the South Caspian, where reservoirs exhibit overpressures in excess of 8000 and 9000 psi, respectively (Gilham and Hercus, 2005; Javanshir et al., 2015). The maximum overpressure intercepted in the Taranaki Basin is 4149 psi (3321 mTVDss), but the basin does display significant variation with depth, as hydrostatically pressured reservoirs are also found at this depth (Fig. 2.5b & 2.6). As previously discussed, the interpretation of pressure data within the Taranaki Basin at basin scale quickly breaks down due to its complex tectonostratigraphic evolution, which is demonstrated in the following section.

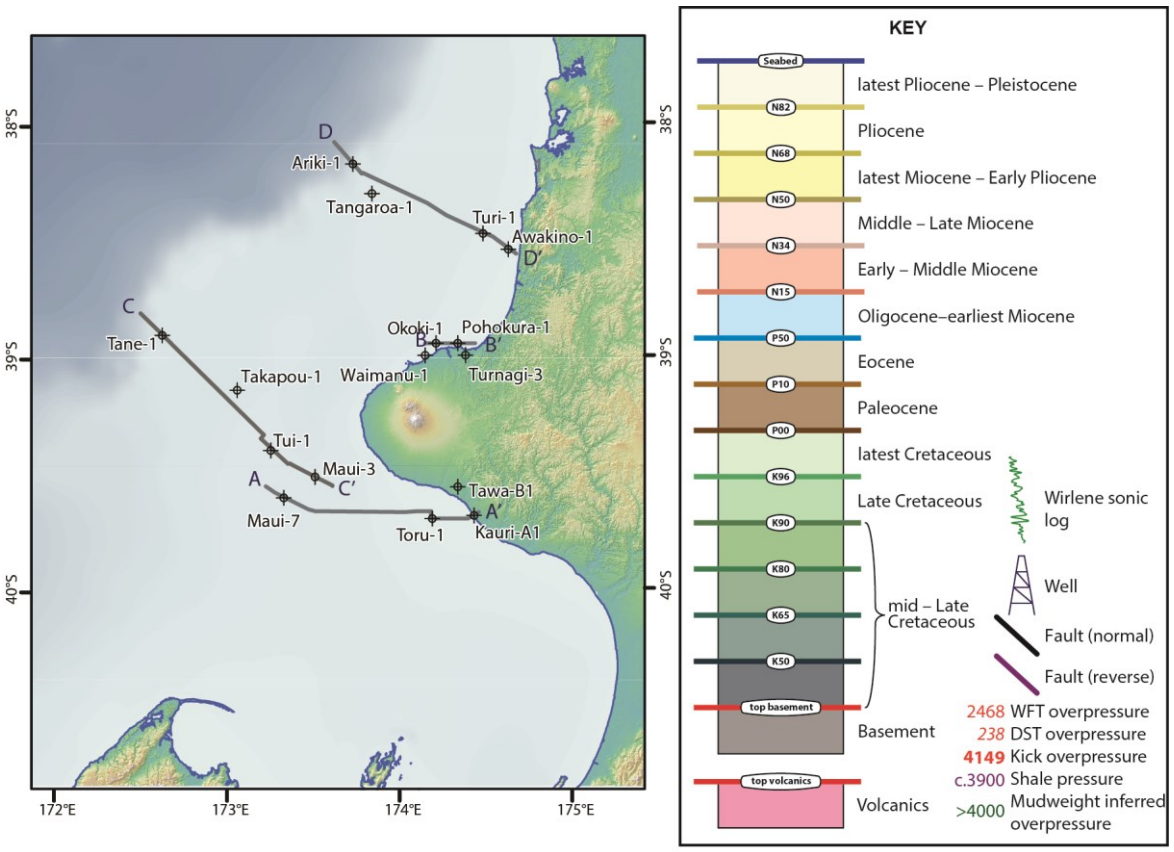

Figure 2.4. Map of Taranaki Basin displaying four cross section lines from parts a-c of this figure and associated legend. a) Interpreted cross section through southern Taranaki Basin from the Patea-Whanganui Coast to the Maui High, displaying thrusted 'sled runners' on the eastern basin margin and variations in the thickness of the Oligocene. b) Interpreted cross section through northern Taranaki Peninsula, displaying both stratigraphic and structural pressure compartmentalisation. c) Interpreted cross section from the Maui High across the Western Platform to the present day shelf edge, displaying the variation in net-to-gross of the Eocene stratigraphy and associated changes in shale pressures. d) Interpreted cross section through the Manganui Platform, Northern Graben and Northern Taranaki Bight, displaying very high overpressures in isolated sandstones within the Kapuni Group in the Turi Fault Zone and Oligocene Tangaroa Sandstones in the Northern Taranaki Bight. Sections a,c & d modified from Strogen et al., (2014a), and section B modified from (Murray, 2000)

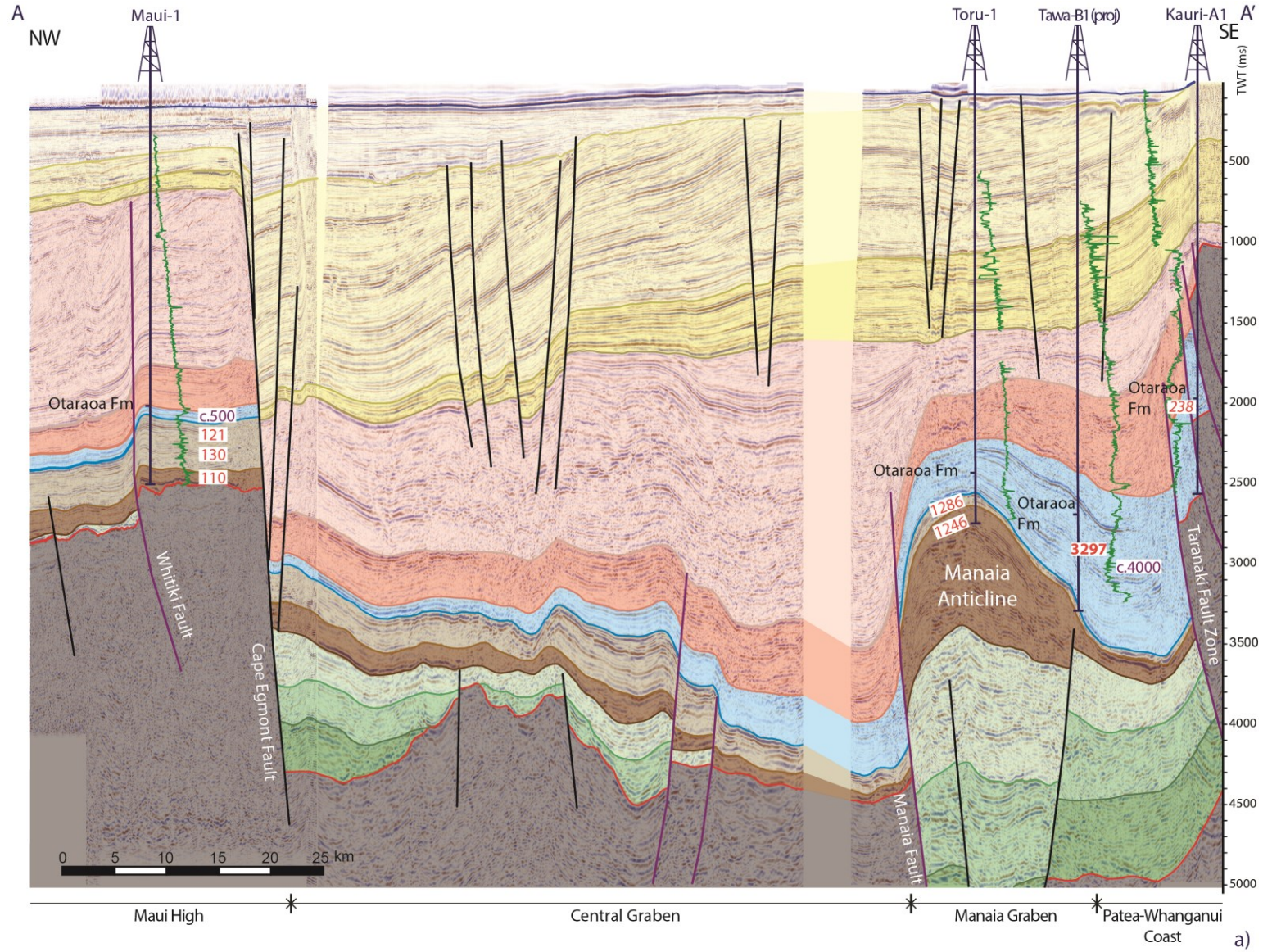
A
NW
Maui-1
Toru-1
Tawa-B1(proj)
Kauri-A1
A'
SE
TWT (ms)
500
1000
1500
2000
2500
3000
3500
4000
4500
5000
Otaraoa Fm
c.500
121
130
110
Whitiki Fault
Cape Egmont Fault
Otaraoa Fm
1286
1246
Otaraoa Fm
238
Otaraoa Fm
3297
c.4000
Manaia Anticline
Taranaki Fault Zone
Manaia Fault
0 5 10 15 20 25 km
Maui High
Central Graben
Manaia Graben
Patea-Whanganui Coast
a)

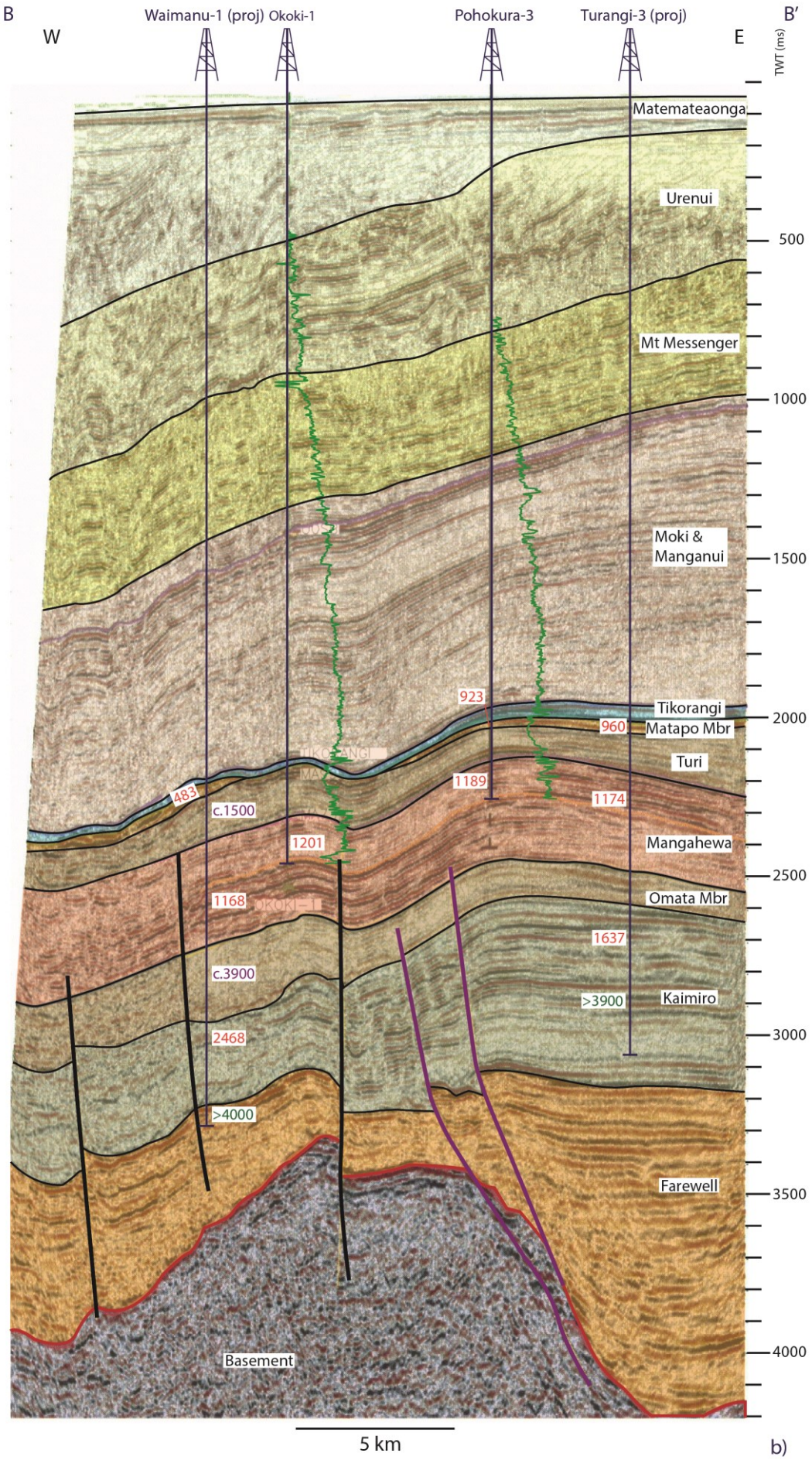
B
W
Waimanu-1 (proj)
Okoki-1
Pohokura-3
Turangi-3 (proj)
E
B'
TWT (ms)
Matemateaonga
Urenui
Mt Messenger
Moki &
Manganui
Tikorangi
Matapo Mbr
Turi
Mangahewa
Omata Mbr
Kaimiro
Farewell
Basement
923
960
1189
1174
1637
>3900
483
c.1500
1201
1168
c.3900
2468
>4000
500
1000
1500
2000
2500
3000
3500
4000
5 km
b)

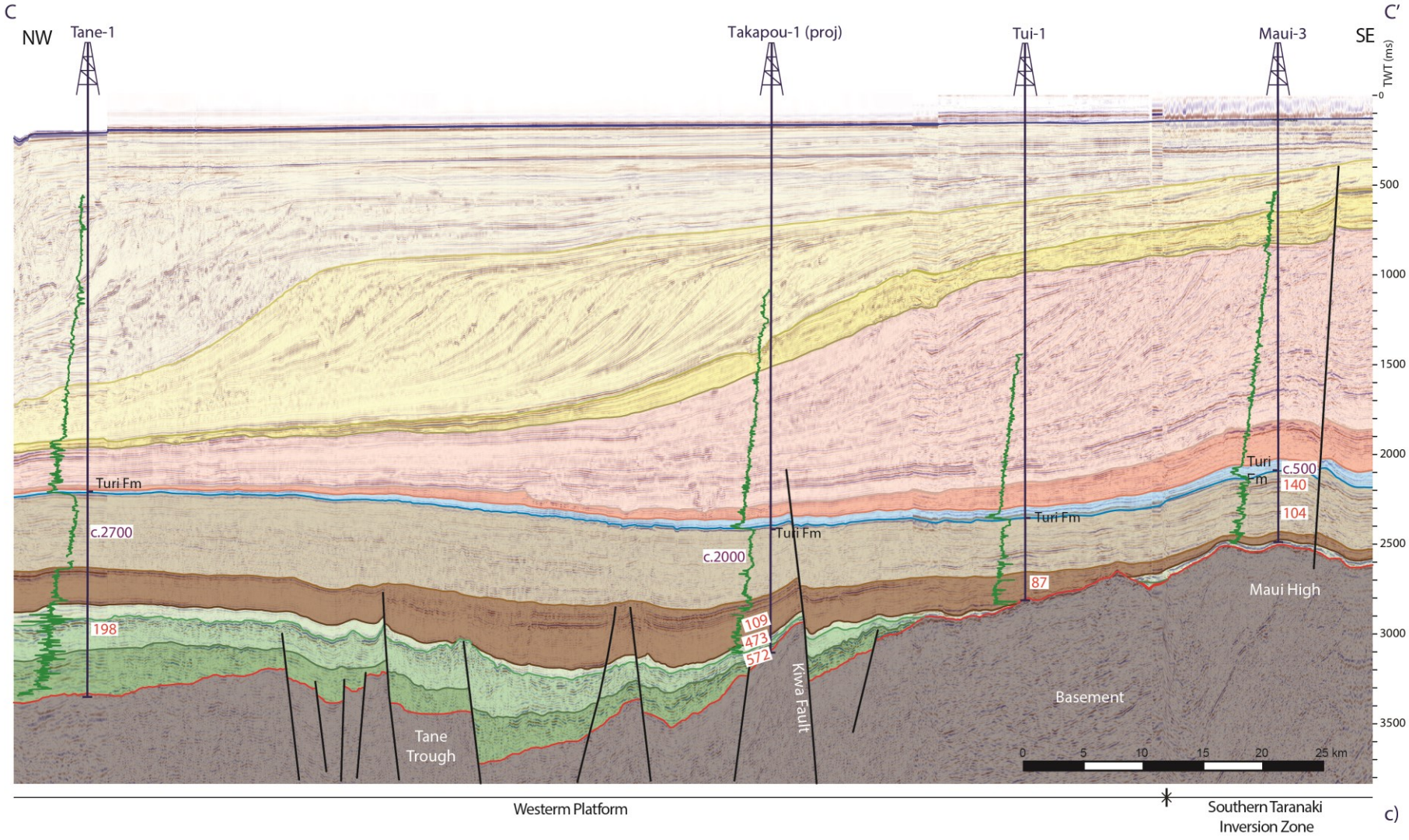
C
NW
Tane-1
Takapou-1 (proj)
Tui-1
Maui-3
SE
C′
TWT (ms)
0
500
1000
1500
2000
2500
3000
3500
Turi Fm
c.2700
198
Turi Fm
c.2000
109
473
572
Kiwa Fault
Turi Fm
87
Turi Fm
c.500
140
104
Maui High
Basement
Tane Trough
0 5 10 15 20 25 km
Westerm Platform
Southern Taranaki Inversion Zone
c)

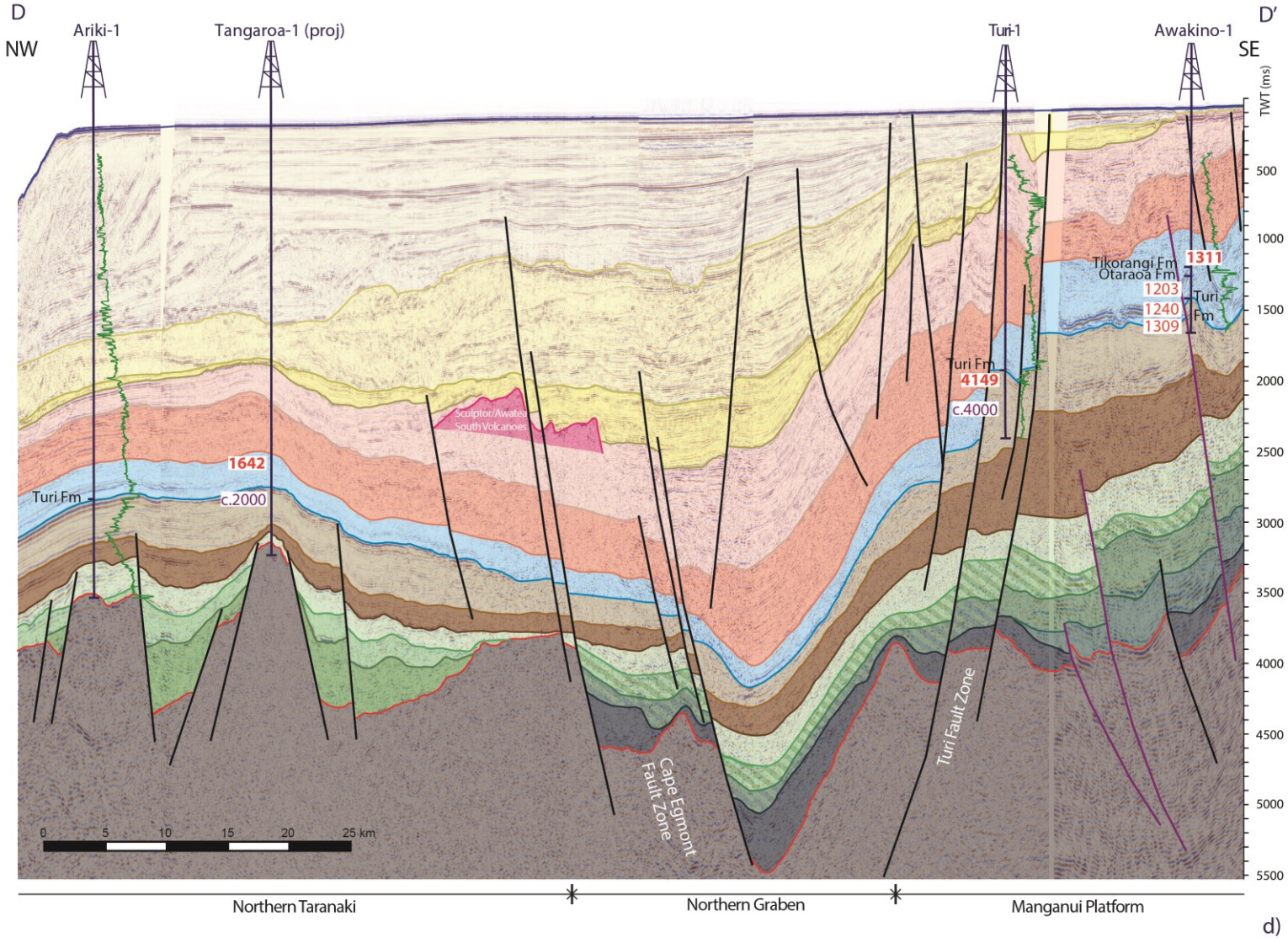
D
NW
Ariki-1
Tangaroa-1 (proj)
Turi-1
Awakino-1
D'
SE
TWT (ms)
500
1000
1500
2000
2500
3000
3500
4000
4500
5000
5500
Tikorangi Fm
Otaraoa Fm
1311
1203
1240
1309
Turi Fm
Turi Fm
4149
c.4000
Sculptor/Awatea
South Volcanoes
1642
Turi Fm
c.2000
Cape Egmont
Fault Zone
Turi Fault Zone
0 5 10 15 20 25 km
Northern Taranaki
Northern Graben
Manganui Platform
d)

2.3.1. BASIN WIDE PRESSURE DISTRIBUTION

Distribution of pore pressure across the Taranaki Basin has been appraised and illustrated in Figure 2.5. Extracting any clear relationship with depth without any quality control is very difficult (Fig. 2.5a). While many of the relationships outlined by Webster et al. (2011), alongside some clear deviations, can be identified in Fig. 2.5b.

The Miocene to Recent section for the most part is normally pressured. Wells drilled on the foothills of Mt. Egmont/Mt Taranaki, have highlighted the occurrence of underpressure in the Plio-Pleistocene section (Fig. 2.5), even with a sea level correction applied. The geological mechanisms for underpressure were outlined by Swarbrick and Osborne (1998) as: a) differential recharge/discharge of reservoirs, b) deflationary pressures during elastic rebound on uplift, c) thermal contraction of fluid, and d) location of a well at a site where the water table is substantially below the Earth's surface. Central Taranaki Peninsula and the area to the east have experienced Quaternary (2 Ma) uplift of ~2 km due to doming of the North Island (Kamp et al., 2004) and have large variations in water table elevation, due to seasonal discharge variations. Mount Taranaki, in addition, is a large semi-circular volcano with an elevated water table and radial drainage pattern.

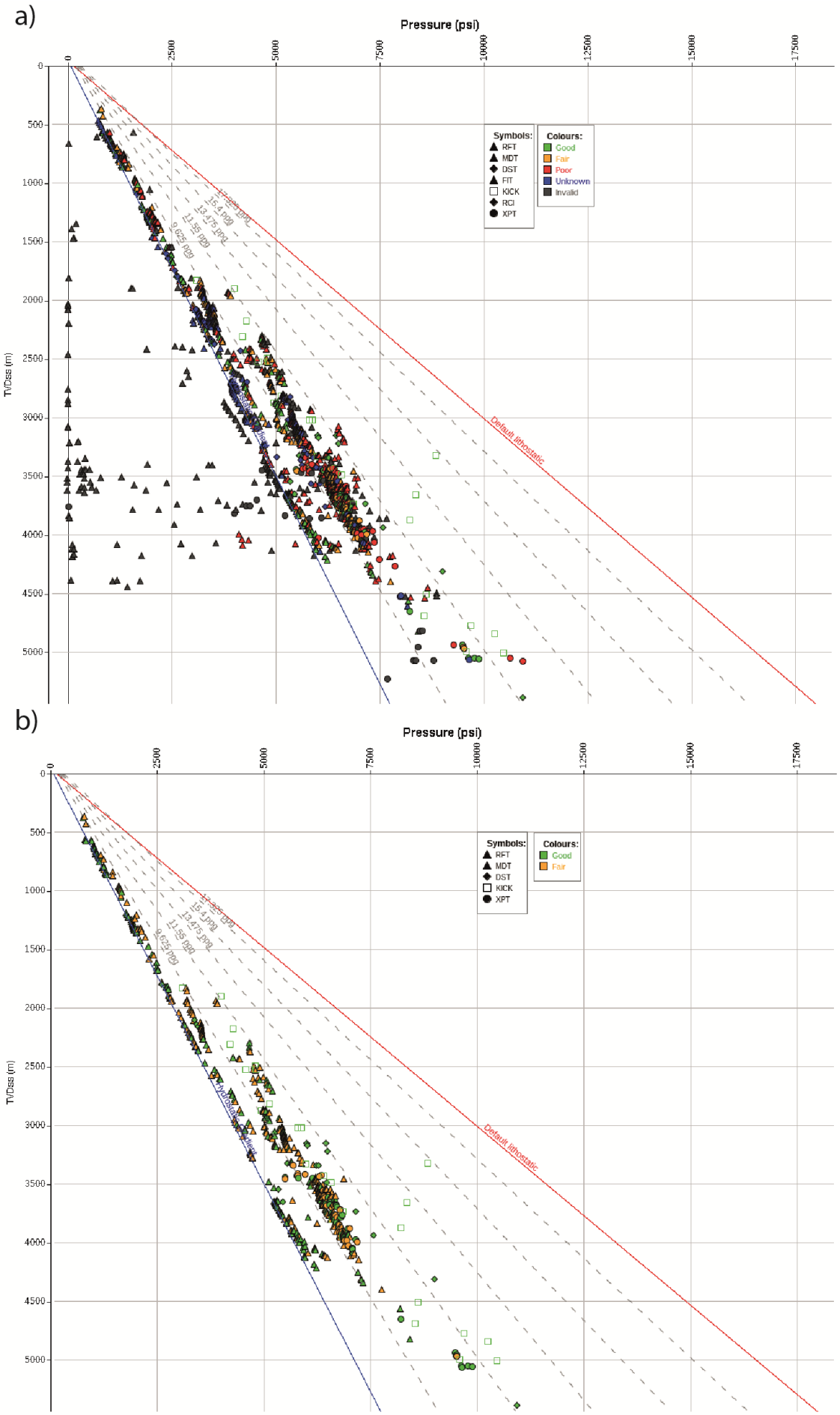

Figure 2.5. Basin wide plots of pore pressure against depth: a) all data with no quality control applied; b) all WFT data are designated as either good or fair (stabilises to 0.1 psi over the last 45 sec of the test), DST and Kick data included but no quality designation given.

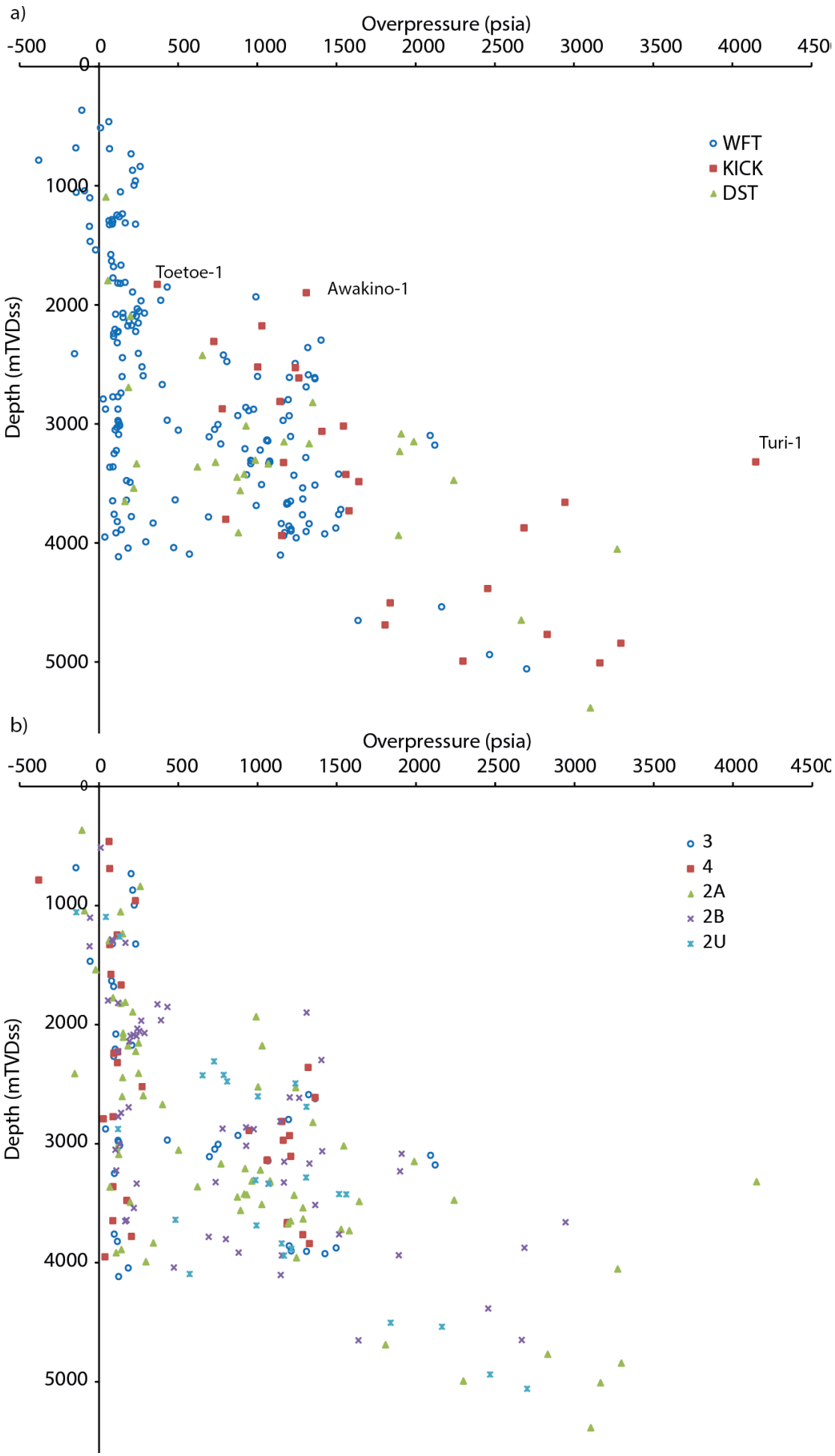

Figure 2.6. Basin wide plots of overpressure against true vertical depth: a) labelled for data type; b) labelled for data quality

A new basin-wide top of overpressure was recorded in a 370 psi kick at 1830 mTVDss in the McKee Sandstone in Toetoe-1 in the greater McKee Field (Enclosure 1). A second significantly larger kick (1310 psi) was taken at the top of the fractured Tikorangi Limestone in Awakino-1 on the Manganui Platform, which marks the top of the pressure transition into significant (>1000 psi) overpressure. Although Zone B from Webster et al. (2011)(Fig2.1) shows a spread of overpressure data between 1900-4000 mTVD, the additional data has highlighted the presence of outliers of both higher and lower pressure, which is discussed in the course of this chapter.

The highest (10934 psi) and deepest pore pressure (5388 mTVDss) measurements were recorded in a DST test in Kapuni Deep-1, which is discussed at length in Chapter IV. The maximum overpressure was recorded in a kick (4149 psi) taken at the top of the Kapuni Group (Fig. 1.2) sandstone beds in Turi-1 well on the Manganui Platform. The vast majority of overpressures in excess of 2000 psi are recorded in kicks and drill stem tests, as wireline formation test measurements are notoriously hard to take in high pressure zones due to differential sticking. The addition of recent deep well data to the dataset highlights the rapid increase in pore pressure below 4000 m, and the mechanisms behind this transition are discussed in section 2.4.4 and Chapter IV.

The quality category applied to highest pore pressure values are usually “low”, as they are not associated with the aquifer gradients and often the pore fluid type is not known (Fig. 2.6b).

2.3.2. Sub-basin evolution and pore pressure distribution

The location of wells is illustrated in Enclosure 1. Figure 2.2 details the locations and names of sub-basins used here for the Taranaki Basin.

2.3.2.1. Southern Taranaki Inversion Zone

The Southern Taranaki Inversion Zone is characterised by a series of inverted Late Cretaceous to Palaeocene grabens and half-grabens, forming a series of positive structures (antiforms) along a sequence of north/northeast striking, re-activated reverse faults. The structures are antiformal pop-ups that plunge northward, many of which emerge onshore on the northern South Island where shortening and inversion has continued into the Pleistocene (Bloch, 1991; Bull et al., 2018; King and Thrasher, 1996; Reilly et al., 2015; Vonk and Kamp, 2008). The inversion phase began in the late Mid-Miocene and propagated west and north through the basin, reaching its maximum in the latest Miocene to Early Pliocene, extending west to the Kahurangi Fault, northwest to the Maui region and across the central Taranaki Peninsula region (King and Thrasher, 1996; Strogen, 2011; Vonk and Kamp, 2008). The seismic section in Figure 2.4a displays one of these pop-up structures, the Maui High, which formed through reactivation of the Whitiki Fault, creating the structure that traps hydrocarbons in the Maui Field (Reilly et al., 2016). The Cape Egmont Fault, upthrown on its

south-eastern side, is considered to be a normal fault that reversed its sense of displacement during the Late Miocene (King and Thrasher, 1996).

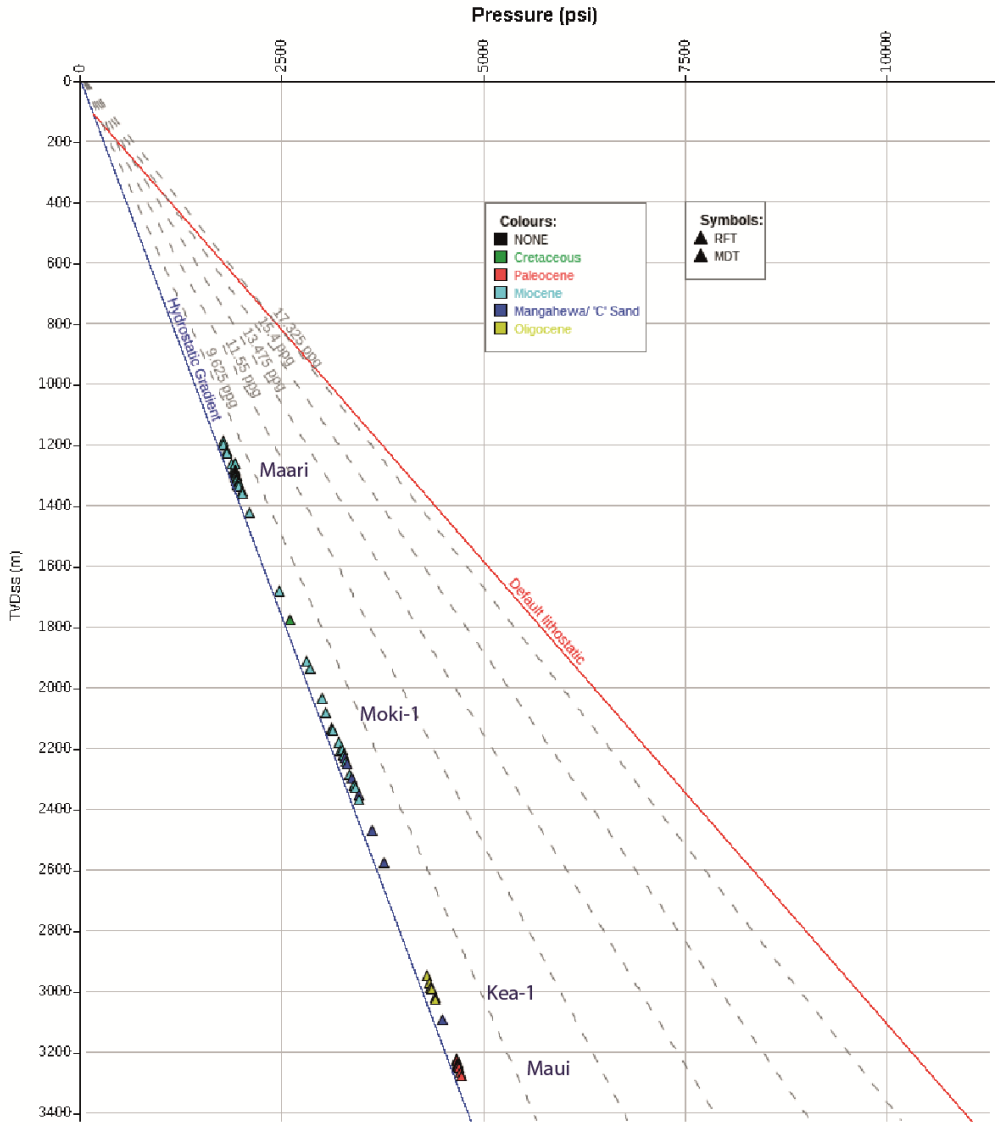

Figure 2.7. Multi-well pressure depth plot from the Southern Taranaki Inversion Zone (displaying only fair and good data)

In contrast to every other sub-basin, the Southern Taranaki Inversion Zone does not contain thick sequences of undercompacted Eocene or Oligocene mudrocks, which are the primary location for the maintenance of excess pressure in the basin (Webster et al., 2011). The sub-basin displays hydrostatic (or near to) pressures, across the entire region, from the Cretaceous to Pliocene-Pleistocene section (Fig. 2.7). As previously discussed, the hydrostatic pressure gradient across both the Southern Inversion Zone and Western Platform is slightly shallower than the basin scale gradient, implying that the reservoirs are normally pressured, not slightly overpressured as shown in Figure 2.7. As highlighted in Figures 2.4a and 5.7, the mudrock sections in the Maui Field, albeit thin, act as barriers to vertical flow demonstrated by the differential pressure between the stacked reservoirs. The mudrock barriers also act over large distances, shown by the lack of depletion in F-sands in Rahi-1 (Enclosure 1), even

after significant production (17 years) from the overlying Early Eocene Kaimiro Formation in the Maui Field.

2.3.2.2. MANAIA ANTICLINE

The previously discussed late Mid-Miocene start of inversion in Southern Taranaki Basin also led to reverse displacement on the Manaia Fault (Fig. 2.4a), forming the Manaia anticlinal ridge, which incorporates three separate structural closures forming the Kapuni, Toru, and Kupe South Fields (Ilg et al., 2012; King and Thrasher, 1996; Voggenreiter, 1993). Figure 2.4a shows a seismic section through the Manaia Anticline that displays the inversion and significant thickness of Cretaceous to Palaeocene stratigraphy beneath the producing field, which are thin or absent in the foot-wall block. In the Kupe South area, the Palaeocene Farewell Formation is unconformably overlain by the Oligocene Otaraoa Formation (Martin et al., 1994) and this unconformity cuts down through the stratigraphy in Southern Taranaki Basin. The Otaraoa Formation is undercompacted, and so preserves overpressure across the Manaia Anticline.

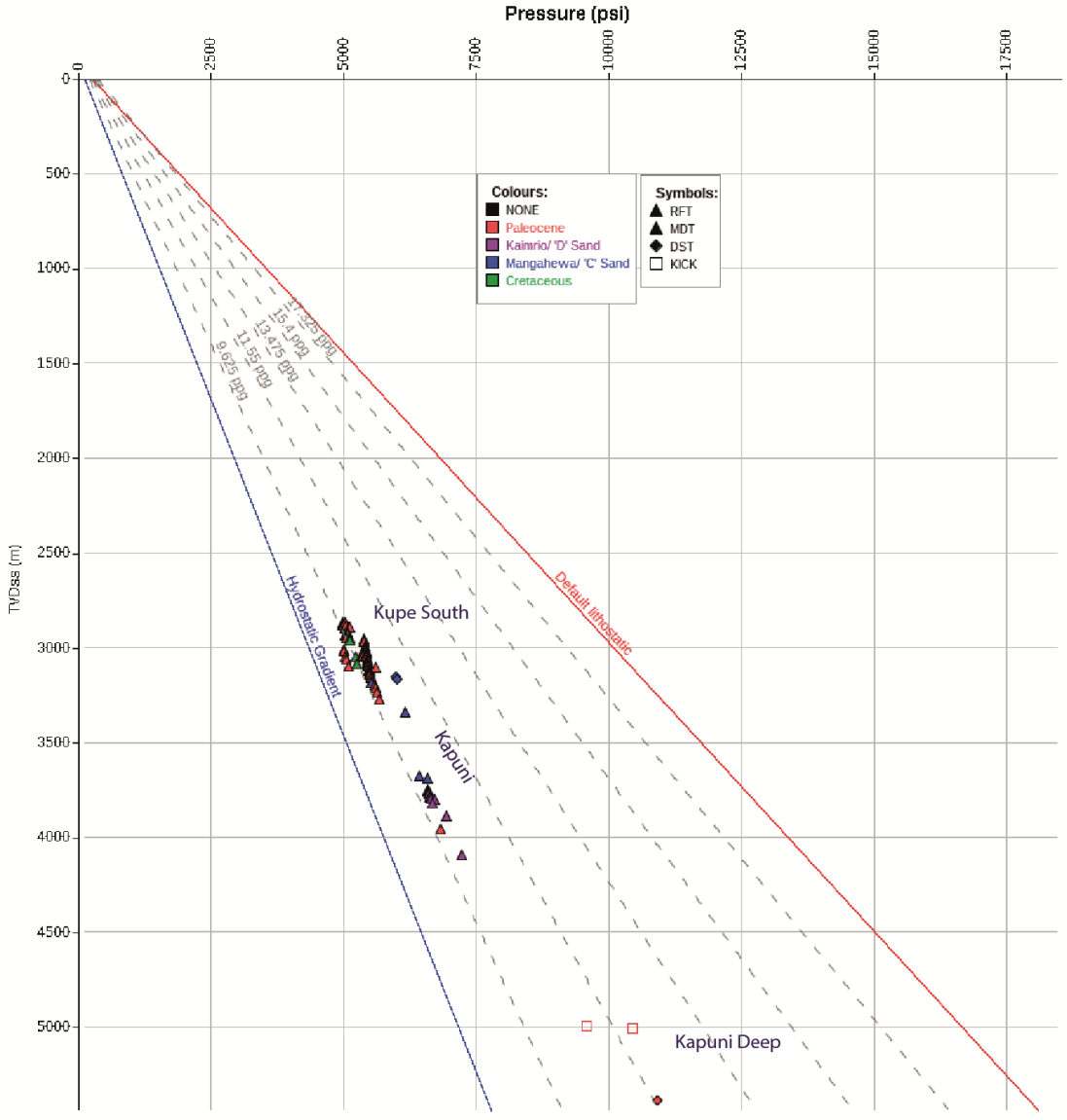

Figure 2.8. Multi-well pressure depth plot from the Manaia Anticline (displaying only fair and good data)

Hydrostatic conditions prevail through the Neogene until the Eocene section where facies variations and depth of burial play a crucial role in defining the overpressure (Fig. 2.8). The nature of the unconformity in the region means that the top of overpressure across the sub-basin occurs in the Palaeocene Farewell Formation at Momoho-1 (2878 mTVDss, 976 psi), south of the Kupe South Field. Overpressure increases to ~1300 psi with increasing depth of burial to the north in the Kaimiro Formation at Toru-1 (Enclosure 1). The pore pressure distribution and pressure transitions within the Kapuni Field are discussed in section 4.2, but both DST and Kick pressures increase to >3000 psi above hydrostatic in the Farewell Formation.

2.3.2.3. Central & Northern Taranaki Peninsula

The Central and Northern Taranaki Peninsula contains one major hydrocarbon play type which occurs as a series of structures of the same origin to previously mentioned reactivated grabens and half-grabens from the Southern Inversion Zone (King et al., 2009; King and Thrasher, 1996). In the northern part of the Peninsula, numerous gas condensate fields (Pohokura, Mangahewa, Turangi and Kowhai) occur in small traps on the same large inversion, and an example of one of these structures is highlighted in Fig. 2.4b (Townsend et al., 2008).

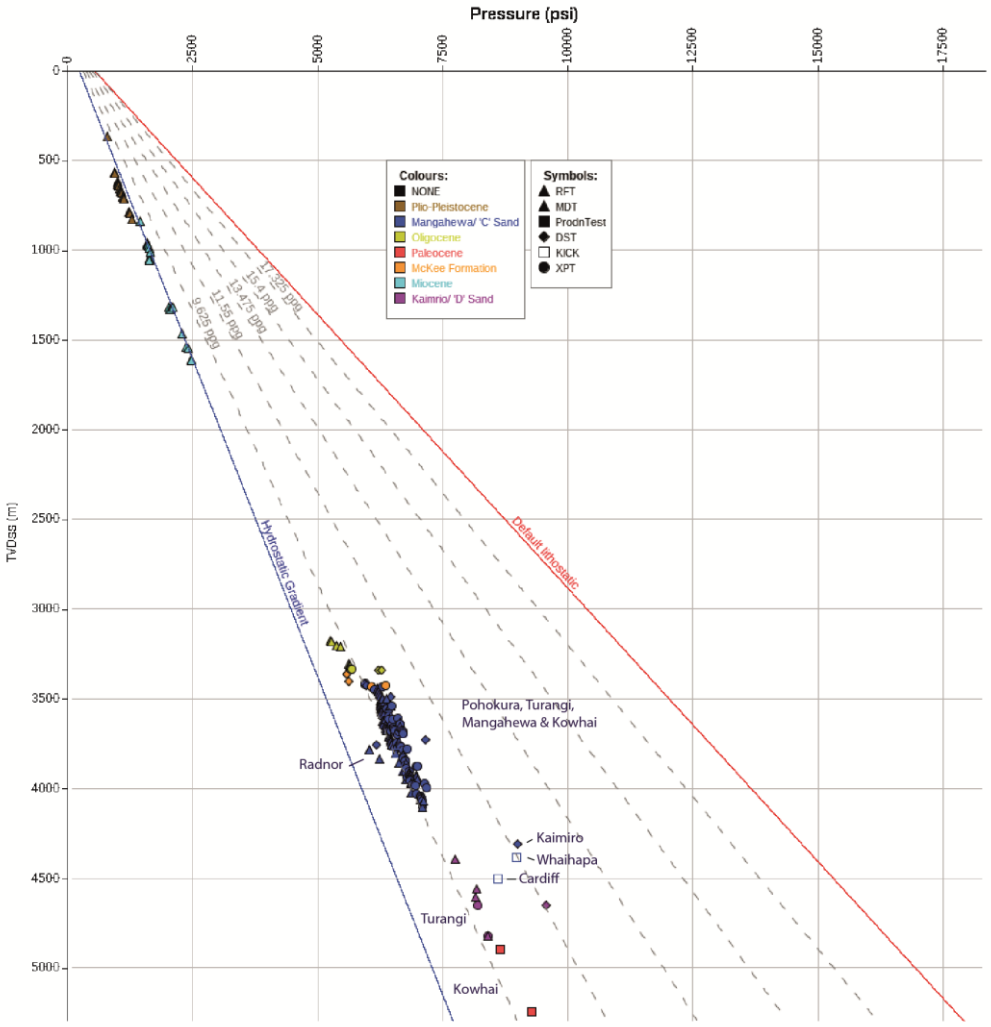

Figure 2.9. Multi well pressure depth plot from the Central Taranaki Peninsula (displaying only fair and good data)

The top of overpressure (771 psi, 3169 mTVDss) in the sub-basin occurs in isolated Late Oligocene to Early Eocene intra-Turi sands in Pohokura-3 well, which become better developed to the north on the Manganui Platform (Fig 1.2; Enclosure II). The pressure transition between the Mangahewa Formation and McKee Formation/Matapo varies across the region, both in depth and magnitude (Fig. 2.9). In Waitui-1 and in the Mangahewa Field, the McKee and Mangahewa formations are in pressure communication, while to the north there is a ~250 psi differential in the Pohokura and Turangi fields.

Overpressure in the Mangahewa Formation in the greater inversion structure (Pohokura, Mangahewa, Turangi and Kowhai fields) ranges from ~1000-1250 psi, suggesting an element of pressure communication across the structure. The Omata Member (Turi Formation) is present in the region and acts as a vertical pressure barrier, as shown by the 200 psi differential in the Turangi Field (Fig. 2.9 & 2.4b). The Radnor Field situated towards the south in the very centre of the Peninsula displays three pressure transitions through the Mangahewa Formation, sealed by thick coal and fine-grained floodplain sequences. Wireline signatures, mudweight and mud log profiles form three outliers (Cardiff, Waihapa & Kaimiro Fields) again suggest numerous pressure transitions through the Mangahewa Formation due to sealing interbedded fine-grained horizons.

Production tests completed over the Palaeocene Farewell Formation in Kowhai-A1R suggest pressure communication with overlying Kaimiro Formation, which may be the case, but influxes and associated increases in mud weight at depth suggest formation pressure in excess of 4000 psi above hydrostatic, which is further discussed in section 2.4.4.

2.3.2.4. TARATA THRUST ZONE

The Tarata Thrust Zone is located along the basin's eastern margin onshore on Taranaki Peninsula (Fig. 2.2), with an overall north striking fault trend, west of and sub-parallel to the basin-bounding Taranaki Fault (King and Thrasher, 1996; Stagpoole et al., 2004). The Taranaki Fault comprises multiple laterally and vertically discontinuous and anastomosing slip surfaces that define a series of fault-bound slivers or horse structures, which act as traps to hydrocarbons (Stagpoole et al., 2004). Slip surfaces often interconnect at depth and may splay from the main fault. Thrusted blocks can be entirely confined within Tertiary strata or inter-fingering with basement and Cretaceous-Tertiary strata in mixed stratigraphic order (Stagpoole and Nicol, 2008).

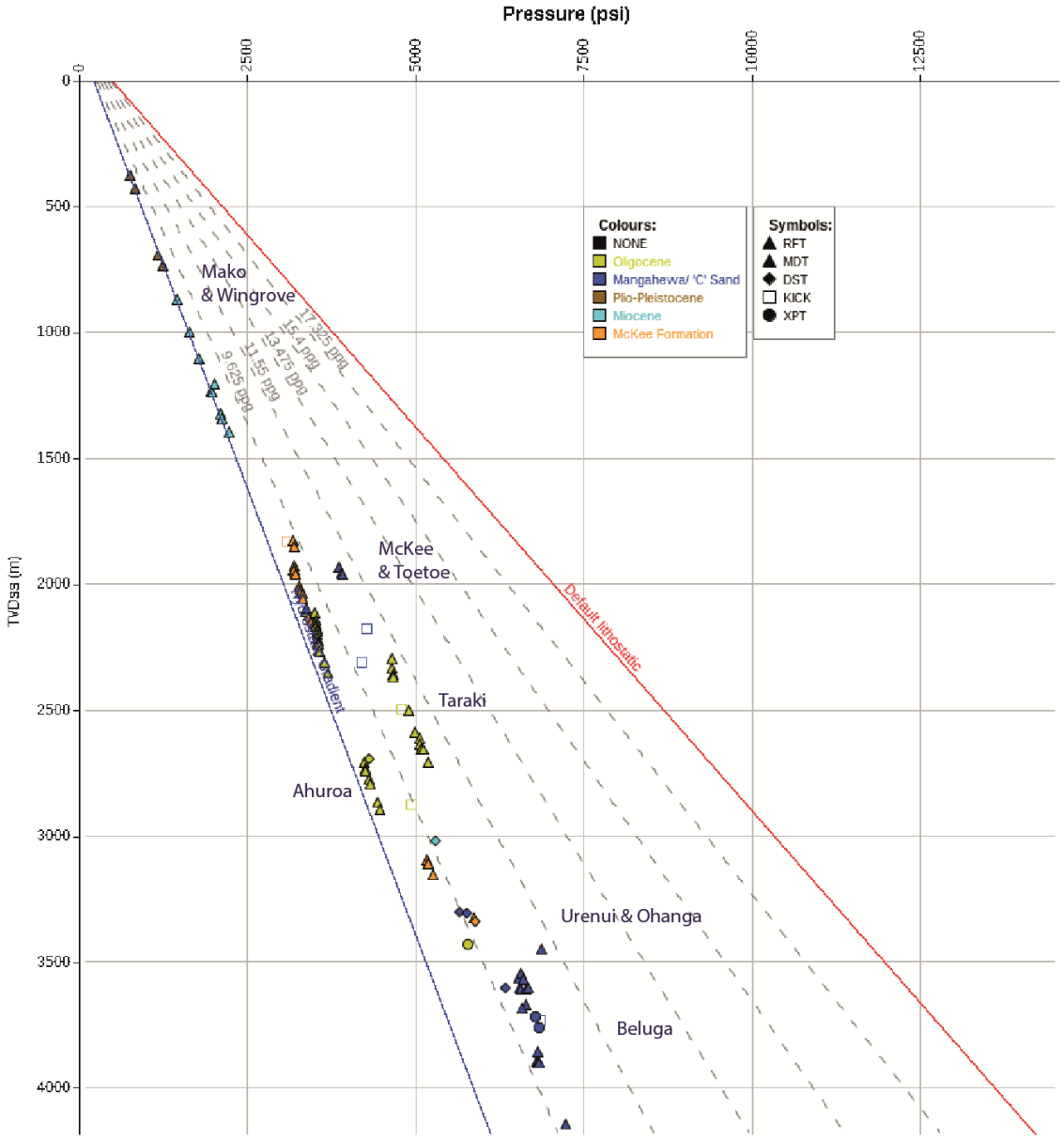

Figure 2.10. Multi well pressure depth plot from the Tarata Thrust Zone (displaying only fair and good data)

The timing of Miocene displacement along the length of the fault changes from mainly Early Miocene displacement north of the peninsula to Late Miocene and Early Pliocene movement south of the peninsula (Giba et al., 2010; Stagpoole and Nicol, 2008). Fields to the north of the Peninsula have been buried deeper than the McKee trend in the central East, but the depth of burial is not a good proxy for overpressure magnitude in the sub-basin. Fault duplexing and the irregular nature of the hanging-wall means that hydrocarbon traps are formed at multiple levels (Stagpoole et al., 2004).

Hydrocarbons are trapped in most of the overthrust structures, which include the major McKee, Tariki, Ahuroa and Ohanga Fields. The top overpressure (1830 mTVDss, 370 psi) occurs in a kick from Toetoe-2 well in the Maui Field in the Late Eocene McKee Formation. The McKee Field is a good example for displaying the complexity of the sub-basin, exemplified by uncertainty around the depth and magnitude of the pressure transition zone

between the Mangahewa and McKee formations (Enclosure 1 & 2). The Mangahewa Formation can be found both hydrostatically pressured and significantly overpressured (1030 psi) at the same depth in different parts of the field (Fig. 2.10).

The Ohanga Field has the deepest reservoirs (~3500 mTVDss) in the thrust zone with overpressure values of ~1300 psi in Mangahewa Formation. McKee-1 drilled past the deepest thrust and Beluga-1 (Fig. 2.15) was drilled down-dip of the McKee Field, and pressures recorded on those two wells are in line at the same depth. Although Figure 2.10 does highlight some of the pressure distribution trends within the region, the tectonostratigraphic complexity requires analysis on an induvial well to field scale.

2.3.2.5. PATEA WHANGANUI COAST

The Patea Whanganui Coast is situated towards the south of the Taranaki Peninsula (Fig. 2.2), differing from the Tarata Thrust Zone, because its overthrust morphologies are directly related to the Taranaki Fault (Fig. 2.4a). Basement and Cenozoic cover rocks are up-thrown immediately west of the Taranaki Fault forming a series of stacked overthrusts and imbricate wedges and allochthonous slivers of basement, all controlled by west-verging thrust faults (King and Thrasher, 1996). Both the recently discovered Rimu and Kauri fields are located across a number of these stacked imbricate wedges and produce oil, gas and condensate from Oligocene submarine fans (Bull et al., 2018; Higgs and King, 2018) (Enclosure 1 & 2).

An example of the stratigraphic stacking in the region is shown in Figure 2.4a, where Kauri-A1 well intersects three stacked thrust sheets of basement rocks. A drill stem test taken in the Tariki Sandstone in Kauri-1 was only slightly overpressured. However, other wells at the same depth are significantly overpressured (>1000 psi) (Fig. 2.11). As in the Tarata Thrust Zone, the stacked thrust sheets have created traps at multiple levels, acting as independent pressure cells and compartments.

Wells in both the Kauri and Rimu fields experienced kicks and influxes at multiple levels while drilling proceeded, associated with uncertainty in the depth to and number of thrust sheets encountered. Kauri-A4 ST1 experienced two successive kicks of 1545 psi and 2685 psi, 855 mTVD apart, at the top of two thrust sheets both in the fractured Rimu Limestone.

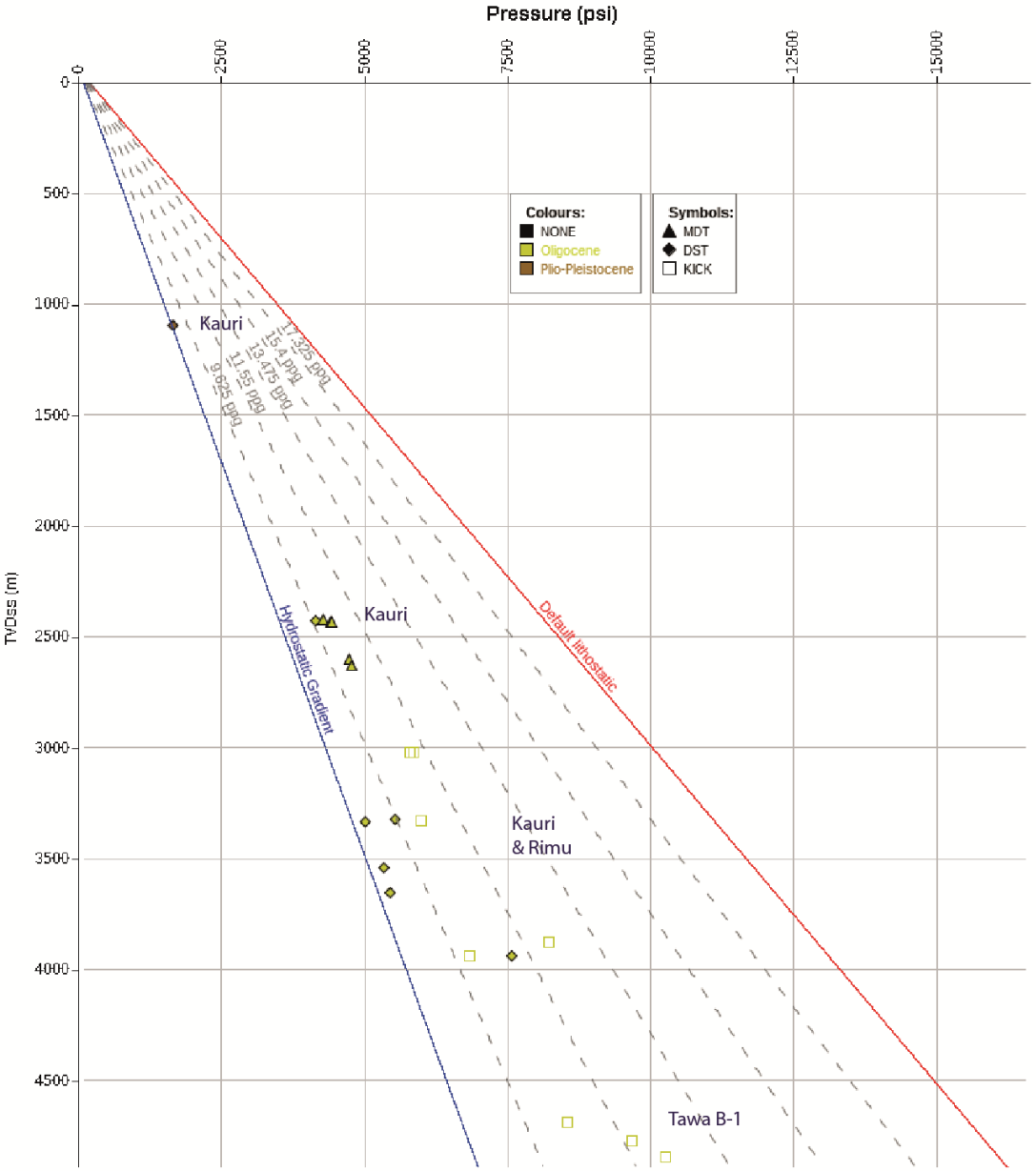

Figure 2.11. Multi well pressure depth plot from the Patea Whanganui Coast (displaying only fair and good data)

Tawa-B1, although placed within this sub-basin, displays a relatively unique stratigraphy, due to its location in the deepest part of the Oligocene foredeep in the footwall of the Taranaki Fault (Strogen et al., 2014b)(Fig. 2.4a). As shown in the lithology log from the single well plot in Appendix I.4, the Oligocene basin floor fan reservoirs of the Kauri and Rimu fields are poorly developed leaving a stratigraphy almost entirely comprised of mudrocks. The Otaraoa Formation is >800 mTVD in thickness in the well, meaning it has greater potential for overpressure maintenance, as demonstrated by overpressures in excess of 3000 psi (Fig. 2.4a & section 2.4.5).

2.3.2.6. Western Platform

The Western Platform (Fig. 2.2) has remained relatively quiescent since the Late Cretaceous and is characterised by progradational deposition on a structurally undisturbed, regionally subsiding sea floor (Baur et al., 2014; Holt and Stern, 1991; King and Thrasher, 1996). The

seismic line in Figure 2.4c shows a transect across the western platform, displaying progradation of the Miocene and Plio-Pleistocene continental wedges across the platform (Kamp et al., 2004; Scott et al., 2004) which are over 2500 mTVD thick at Tane-1 close to present day shelf edge break (Fig. 2.4c). The Eocene strata grade from predominantly sand grain sizes in the Maui Field to largely silt-mud at Tane-1 and the sonic wireline signature suggests severe undercompaction driven by loading of Neogene stratigraphy (Hansen and Kamp, 2004; Kamp et al., 2004)

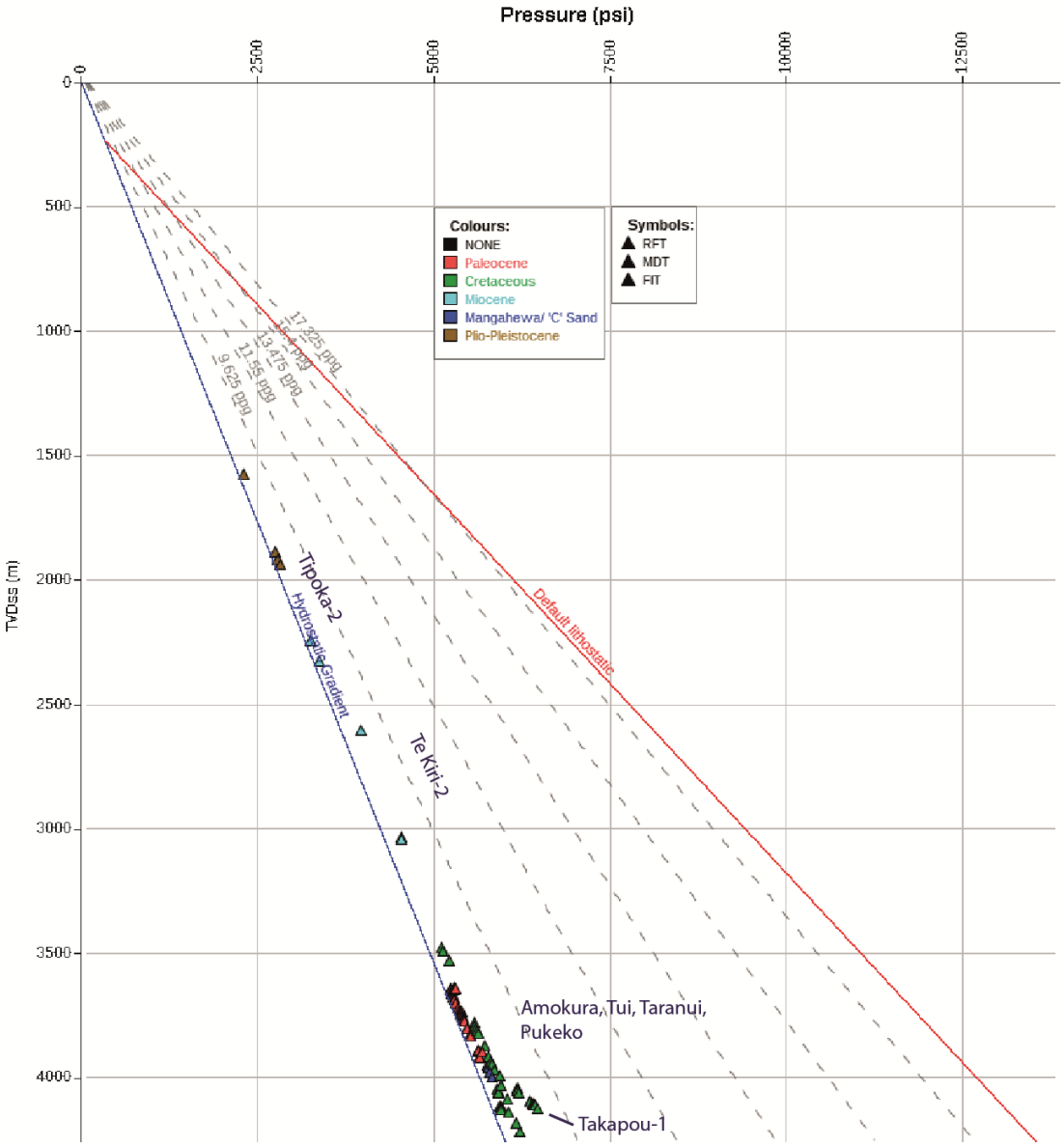

Figure 2.12. Multi well pressure depth plot from the Western Platform (displaying only fair and good data)

Almost the entire stratigraphy of the Western Platform is hydrostatically pressured, with the exception of Takapou-1, which displays a maximum overpressure of 572 psi in the Late Cretaceous section (Fig 2.12). Undercompaction and overpressure maintenance in the Turi Formation has been identified on the Western Platform by Webster et al. (2011), but they suggest any excess pressure is transferred into adjacent permeable beds and laterally drained.

2.3.2.7. NORTHERN TARANAKI BIGHT

The Northern Taranaki Bight displays a similar morphology to the Western Platform, differing due to the presence of the Early Oligocene Tangaroa Formation, comprised of a sequence of fine to medium-grained sandstones deposited as a submarine fan between bathyal mudrocks of the Turi Formation (Bloch, 1994; Gresko et al., 1990). Based on facies composition, fan lobe geometry and internal channelling, the formation has been interpreted as a progradational wedge of slope to basin-floor fans, which are draped across basement highs (Gresko et al., 1990), as seen in the seismic sections across Ariki-1 and Tangaroa-1 wells (Fig. 2.4d).

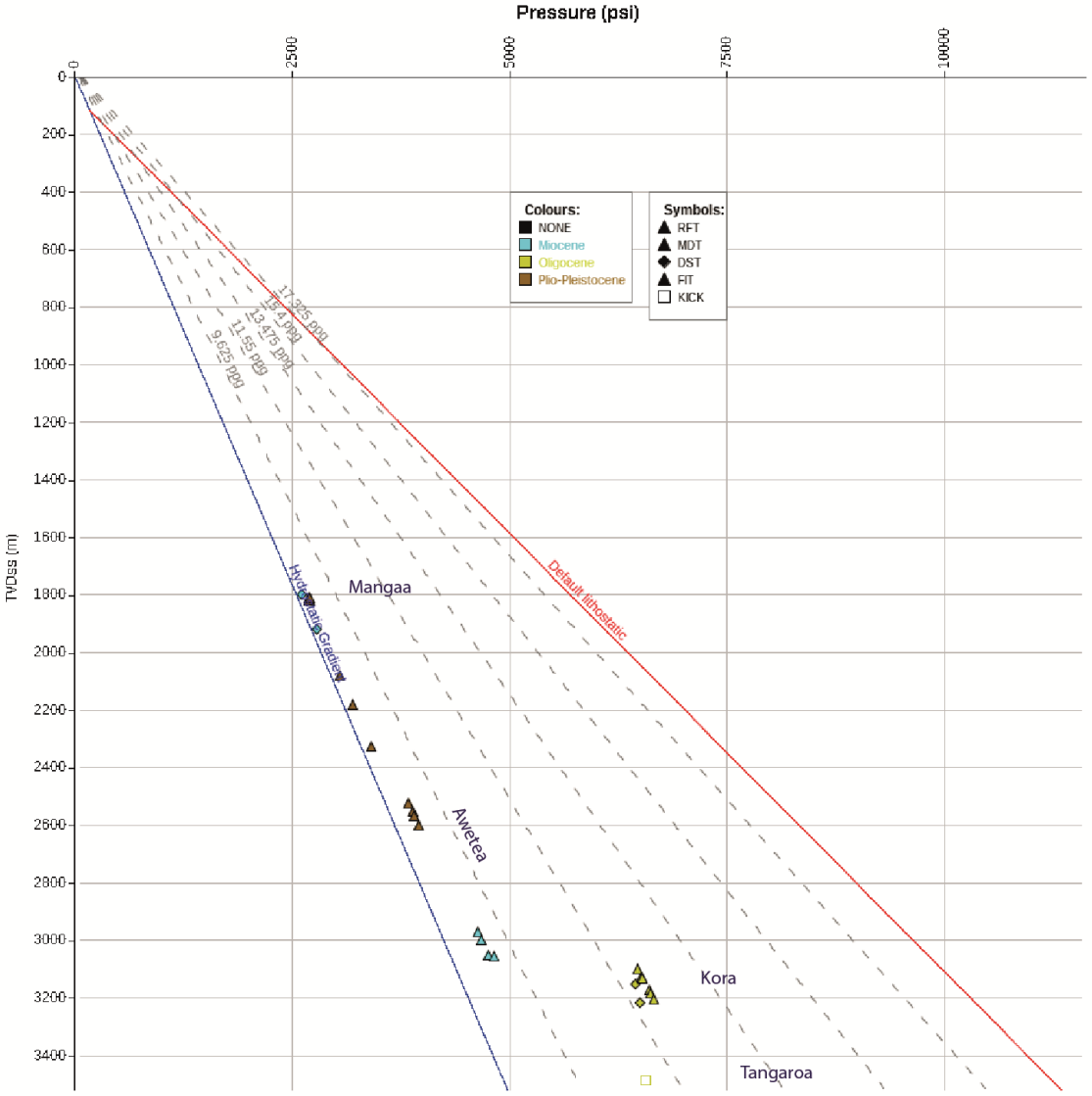

Figure 2.13. Multi well pressure depth plot from the Northern Taranaki Bight (displaying only fair and good data)

The isolated nature of the Oligocene Tangaroa Sandstone has enabled it to maintain excess pressures of up to 2122 psi above hydrostatic (O'Neill et al., 2018b). All wells that have penetrated the Tangaroa Sandstone have shown overpressure either through direct pressure data (Kora-4 & Tangaroa-1 [Figure 2.13]) or wireline signatures (Ariki-1, Fig. 2.4d). After the sizeable kick in the discovery well (Tangaroa-1) and high overpressures in the Kora well cluster, subsequent wells like Moana-1 were drilled significantly overbalanced (840 psi).

Awatea-1 is a notable exception to the trend of hydrostatic pressures in the Plio-Pleistocene section, as it displays steadily increasing overpressure in three separate isolated fan deposits (107-273-432 psi) of the Pliocene Mangaa Formation (Webster et al., 2011).

2.3.2.8. MANGANUI PLATFORM

The Manganui Platform is a tectonostratigraphically diverse sub-basin, incorporating elements from the Tarata Thrust Zone, Central & Northern Taranaki Peninsula and Western Platform, creating an assortment of pore pressure regimes and associated drilling hazards. The Awakino anticline, drilled by Awakin-1 well, offshore and east of Taranaki Fault lies above a thrust zone routed in the Taranaki Fault, which deformed the Late Oligocene Tikorangi Limestone and underlying beds. This structure can be regarded as genetically similar to the Tarata Thrust Zone but disconnected from it (King and Thrasher, 1996; Stagpoole and Nicol, 2008). To the south, the controlling thrust fault on its western margin gradually dies out, and the structure appears as an anticline to the west of the Taranaki Fault, which was drilled by Mokau-1 well (King and Thrasher, 1996). Mauku-1 well was drilled through a basement overthrust and took a kick on entering the Mangahewa Formation.

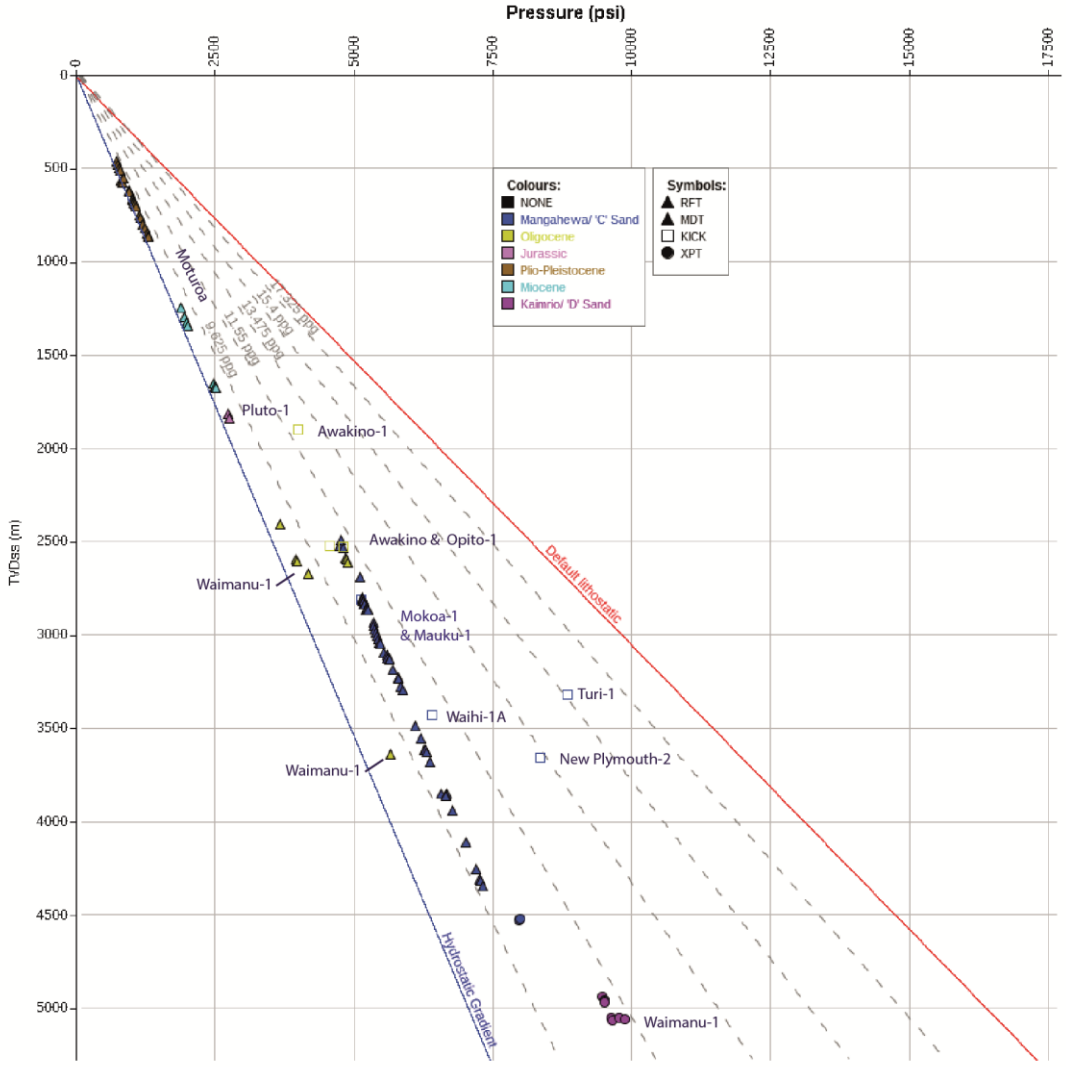

Figure 2.14. Multi well pressure depth plot from the Manganui Platform (displaying only fair and good data)

An interpreted seismic section across the Manganui Platform from East to West (Fig. 2.4d) displays both the location and stratigraphy of Awakino-1 and Turi-1 wells, which experienced the shallowest and highest overpressures in the basin, respectively. The top of overpressure (1311 psi, 1899 mTVDss) was recorded in a previously mentioned kick in the fractured Tikorangi Limestone at the crest of the Awakino structure (Fig. 2.14 & 2.4d). Successions of isolated turbidites within the Otaraoa Formation were intercepted in most wells, which have varying magnitudes of overpressure and are often hydrocarbon bearing, and led to a kick in Opito-1. The Mangahewa Formation in Mokoa-1, Mauku-1, Awakino-1 and Waimanu-1 sit on a clear water gradient with the same overpressure.

Waimanu-1 and Okoki-1 (Fig. 2.4b) share some characteristics with wells on Central and Northern Taranaki Peninsula, but the top Eocene is not intercepted until ~3900 mTVDss. Waimanu-1 acts as an outlier, due to its depth and complex stratigraphy, and does not fit into the trend of the Central and Northern Taranaki Peninsula or the Manganui Platform, displaying five separate pressure transitions (Fig. 2.4b & Appendix 2). Also, as for Kowhai-A1R, influxes and associated increases in mudweight below 4500 mTVDgl suggest formation pressure in excess of 4000 psi above hydrostatic.

The three kicks taken in Waihi-1A, New Plymouth-2 and Turi-1, are associated with a rapid stratigraphic change into predominant fine-grained facies due to wells being drilled close to the maximum extent of reservoir facies (Fig 2.17) and are further discussed in section 2.4.4.

2.4. DISCUSSION

Each sub-basin in Taranaki Basin displays its own pore pressure regime, nevertheless linked through a shared stratigraphy and regional fluid flow pathways. Facies differences between stratigraphic intervals provide a first-order control on the maintenance and distribution of overpressure, both vertically and spatially across the basin.

2.4.1. FACIES VARIATION AS A CONTROL ON OVERPRESSURE MAINTENANCE AND DISTRIBUTION

The stratigraphy of Taranaki Basin is dominated by the occurrence of mud-silt grade facies (~70% by volume). While these facies are low risk from a drilling perspective, they are the main producer of overpressure and thus cannot be ignored (Darby, 2002). Overpressure has a tendency to increase basinward from coarse grained basin margins into deep-water environments dominated by mudrocks (Harrison and Summa, 1991; Javanshir et al., 2015). Hence, a better understanding of the distribution of mudrocks within a basin aids prediction of the likely magnitude of overpressure. Harrison and Summa (1991) used well data from the Gulf of Mexico to define a cut-off of less than 30% sand, after which hydraulic conductivity between stacked permeable sandstone beds is limited enough to maintain excess pressure.

This understanding, coupled with an appreciation of the connectivity of permeable units within the Taranaki Basin, can lead to the identification of regional fluid flow pathways. In other foreland basin settings such as the South Junggar Depression (Western China) and the Bavarian Molasse Basin, the magnitude of overpressure has been shown to be associated with depositional environment, and in particular the thickness of mudrocks in the basin fill (Drews et al., 2018; Yan et al., 2002).

Facies content and formation thicknesses vary significantly across the Taranaki Basin, which can be directly correlated to the presence and magnitude of preserved overpressure. The variation in net-to-gross of Eocene sandstone beds in the Mangahewa and Kaimiro formations and their associated laterally equivalent mudrocks (Omata Member of the Turi Formation) plays a first-order control on overpressure maintenance. The transect across the Manganui Platform (Fig. 2.4c) displays an increase in pore pressure from Awakino-1 to Turi-1 in the Eocene Mangahewa Formation (Mokau-1 displays an intermediary pore pressure), which is correlated to a significant increase in mudrock volume as the facies grade from a palaeo-shoreline in the east to shelfal-bathyal conditions to the northwest (Fig. 2.17) (Higgs et al., 2012b). Wireline sonic values plotted against well trajectories in Figure 2.4, display porosity anomalies below the Tikorangi Limestone (Sayers et al., 2002), which are pronounced at Turi-1 (Fig. 3.6). The isolated nature of these sandstone beds in Mangahewa Formation has allowed them to maintain excess pressure, as shown by good correlation to shale pressure in Turi-1 (Fig. 2.4d).

The transect from the Maui High (at the northern end of the Southern Taranaki Inversion Zone) across the Western Platform to the present shelf edge break (Fig. 2.4c), displays a gradation within the Eocene from ~90% coarse sanstone facies at the Maui Field to essentially 100% silt-mud grade facies at Tane-1. The east-west change in seismic amplitude from high to low impedance is consistent with a gradation from sandstone dominated stratigraphy with interbedded mudrocks, to 100% mudrock facies at the shelf edge break. The calculated shale pressures within the Eocene section range from ~500 psi at Maui to ~2700 psi at Tane-1, which can be directly correlated to mudrock volume. Pressure data from Takapou-1 well, which is positioned towards the middle of the present day shelf shows that Cretaceous reservoirs are maintaining excess pressure at depth, suggesting that net sand in the half grabens containing the Cretaceous reservoirs is less than 30% of the sediment volume (Harrison and Summa, 1991).

The Oligocene Otaraoa Formation not only acts as the primary seal to hydrocarbons in the basin but also maintains overpressure, often in tandem with the Turi Formation. The facies within the Otaraoa Formation do not change significantly, apart from the occurrence of thin turbidites as noted earlier, but thickness variations (increasing eastward toward Taranaki Fault) are considerable and directly link to shale pressure. The most dramatic thinning of the

Otaraoa Formation can be seen in Figure 2.4a, where the thickness ranges from ~800 m at Tawa-B1 in the deepest section of the foredeep, westward to ~200 m at Toru-1 on the Manaia Anticline, to only ~30 m farther west in the Maui Field, which at that time lay near the forebulge position of the foreland basin (King and Thrasher, 1996). Again, this thickness variation can be directly correlated to increasing shale pressure eastward toward Taranaki Fault. In the Bavarian Molasse Basin, lateral distribution of overpressure correlates to an increase in mudrock volume and deepening and thickening of the wedge-shaped basin from north to south, generating high pore pressures in a similar foredeep position to that of Tawa-B1 (Drews et al., 2018).

The Palaeocene palaeogeography and associated facies variations in Taranaki Basin also drive the pore pressure regime in the deep section of the Taranaki Peninsula. Overpressures within the Palaeocene play fairway show an increase from the Kupe South Field to Kapuni Deep-1 and then a subsequent increase based on mudweight at Kowhai-A1R, which will be discussed in section 2.4.4. Pore pressure distribution and the occurrence of petroleum accumulations across the palaeo basin margin (shoreline), are defined by the development of sequences and their systems tracts, and associated facies variations within the Eocene Kaimiro and Mangahewa formations. Eocene shoreline to coastal plain sandstone reservoirs (in McKee, Mangahewa and Kaimiro formations) are overlain by a series of transgressive marine mudrock beds which act as pressure seals across tens of kilometres perpendicular to the palaeoshoreline (Higgs et al., 2012b; King and Thrasher, 1996; Strogen, 2011).

More subtle facies changes within reservoir units in the Central and Northern Taranaki Peninsula bring a further level of complexity to the pore pressure system. Radnor-1 well in the Stratford Field (Enclosure I) produces from the Eocene Mangahewa Formation, which at that location was deposited in a terrestrial coastal plain setting (Higgs et al., 2012b; Strogen, 2011), exemplified by the presence of numerous stacked coal sequences. The maximum overpressure encountered in the field (943 psi) is lower than in Mangahewa reservoirs at a similar depth to the north, mainly due to the limited marine influence and thus lack of thick overpressured Oligocene and Eocene mudrocks (20 m in Radnor-1). Two pressure transitions are present within Radnor-1, both sealed by inter-bedded coal and mudrock-rich intervals, and similar relationships have been identified within the Cardiff area. The pressure at depth may have been driven from deeper sources of overpressure or from gas expansion from interbedded coal sequences (e.g. Kapuni Deep, Farewell Formation: Chapter IV).

2.4.2. COMPARTMENTALISATION

Compartmentalisation occurs when flow is prevented across ‘sealed’ boundaries that produce a segregation of pore fluids into separate fluid/pressure compartments (Jolley et al., 2010). Fault controlled fluid overpressure compartmentalisation has been identified in sedimentary basins worldwide, through cataclasis, shale gouge or diagenetic alteration

(Darby et al., 1996; Prada et al., 2018; Richards et al., 2010; Wonham et al., 2010). Faults have been shown to act as barriers to lateral and vertical fluid flow in thrusted sections on the Tarata Thrust Zone and in the Patea-Whanganui Coast area within the Taranaki Fault Zone, and in the Turi Fault Zone, and can also define barriers between sub-basins (Fig. 2.4b).

Stratigraphic architecture can also affect hydraulic connectivity through compartmentalisation of parallel geobodies by continuous mudrocks (Hovadik and Larue, 2010). Figure 2.4b shows a section through Central and Northern Taranaki Peninsula onto the Manganui Platform, which highlights the varying connectivity of reservoirs across the region. Pressure data from the Eocene Mangahewa Formation shows hydraulic connectivity between two structures from Okoki-1/Waimanu-1 to Pohokura/Turangi, which does not hold true for other reservoirs. The Matapo Sandstone Member is in pressure communication across the Central Taranaki Peninsula structure, but is not present in the syncline or at Okoki-1. The Matapo Sandstone Member is present in Waimanu-1, but at a lower pressure, suggesting that it is a separate geobody.

The Early to Mid-Eocene Omata Member (Turi Formation) acts as a seal on both sides of the basement high, but the pore pressure values are 831 psi higher In Waimanu-1, which suggest that the intervening faults are acting as barriers to horizontal fluid flow. The proximity of these wells to the maximum extend of coarse-grained facies at the palaeoshoreline, suggests that reverse faults on the eastern side of the structure have entrained fine grained material from depth decreasing the permeability of the fault zone.

2.4.3. Regional migration pathways

Shale pressures can provide an excellent proxy for reservoir pressures, assuming that the adjacent permeable beds have the potential to maintain excess pressure transferred from surrounding mudrocks. As highlighted in the seismic section in Figure 2.4d, in parts of the basin such as the Western Platform, shale pressures are not in equilibrium with reservoirs, indicating lateral and vertical fluid flow through permeable beds.

2.4.3.1. Lateral drainage

Lateral drainage has been identified by Webster et al. (2011) in the Western Platform in Tane-1 well (Fig. 2.4c) and a similar trend has been observed in Takapou-1 and in the Maui Field (Fig. 2.4d). It is assumed that any excess pressure transferred into permeable beds from the Eocene and Oligocene mudrocks in the Southern Taranaki Inversion Zone and in the Western Platform has laterally drained through connected Palaeocene and Cretaceous reservoirs, as observed in palaeogeographic maps (Strogen, 2011). The Cretaceous and Palaeocene sections represent a continuously connected pathway for pressure dissipation until they are exposed on the seafloor and on the South Island (Fig 3.12). Stacked fluvial systems in Cretaceous sequences on the north coast of the South Island (south of Farewell

Spit) have excellent connectivity and a high percentage of net sand (Browne et al., 2008), which would allow pressures to dissipate rapidly up dip (Harrison and Summa, 1991).

The potential for lateral fluid flow across large distances is highlighted through reservoir depletion in the Kaimiro Formation in the Tui Field, where pressure data plots as underpressured, due to 20 years of production at the Maui Field 20 km away. This large scale flow suggests the absence of significant compartmentalisation in the Western Platform, which could be expected given its relatively quiescent history in comparison with the Eastern Mobile Belt (Enclosure I).

Recent rapid loading of the basin by thick Miocene to Pleistocene deposits has led to the formation of fluid escape features. Pockmarks highlight the presence of active or palaeo fluid flow that would aide in lateral drainage of pressure (Chenrai and Huuse, 2017). Ilg et al. (2012) have identified the presence of gas chimneys associated with predominantly late stage (~3.6 Ma) normal faults acting as conduits to flow in southern parts of Taranaki Basin, which again could act as conduits for lateral drainage.

2.4.3.2. LATERAL TRANSFER

This work received the Outstanding Presentation Award at the AAPG Geoscience Technical Workshop, Pore Pressure and Geomechanics: From Exploration to Abandonment in Perth, Australia (06/06/18)

Lateral fluid flow by the centroid effect can produce elevated crestal pore pressure (Bowers, 2001; Dickinson, 1953; Traugott, 1997). The term lateral transfer was defined by Yardley and Swarbrick (2000) as the internal redistribution of fluid pressure in a confined and tilted reservoir. This phenonmon can cause challenges in pore pressure prediction, especially in complex environments such as fold and thrust belts and can become a drilling hazard if not properly predicted (Flemings and Lupa, 2004; Kaeng et al., 2014). The McKee Field in the Tarata Thrust Zone is comprised of a number of adjoining fault blocks that produce oil, gas and condensate from a steep south-easterly dipping (up to 60°) sandstone reservoir sequence truncated against a deep thrust (Fig. 2.15) (King and Thrasher, 1996).

McKee-13 was the 35th well to be drilled on the McKee structure, some 11 years after production started, with the aim of improving drainage through the McKee Formation and testing the deeper Eocene Mangahewa Formation. The well experienced a pressure kick on entering the Eocene Mangahewa Formation, culminating in an underground blow out, which resulted in hydrocarbons breaching the surface and eventually a total loss of the well.

An offset well along the structure, Toe Toe-2, experienced a pressure kick in the Mangahewa Formation at a similar depth to McKee-13. The calculated formation pressure from this kick plots anomalously high for the depth when compared with offset wells, requiring a mechanism to transfer this pressure into the shallower stratigraphy. A recent well drilled in

2010, Beluga-1 (Fig. 2.15) down dip of the McKee Field encountered overpressures of 1512 psi in the Mangahewa Formation. If we assume that the Mangahewa Formation is confined and in lateral continuity, then that pressure is transferring up dip via the process of lateral transfer.

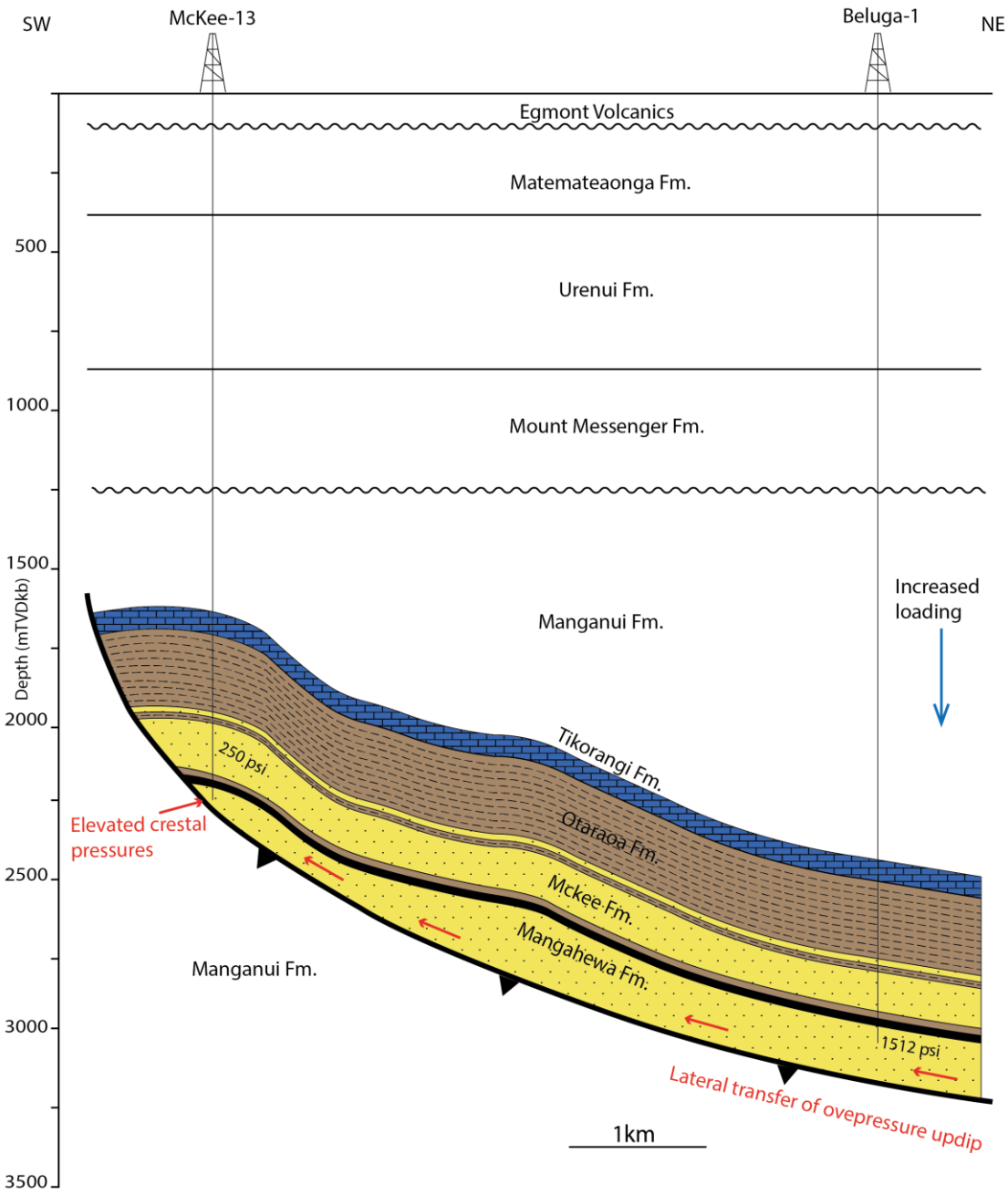

Figure 2.15. Schematic Cross section showing lateral transfer of formation pressure in the Tarata Thrust Zone (modified from Adams et al., 1989)

A mudweight of 12.3 ppg would be required to contain the pressure, which would easily breach the fracture pressure below the 9 5/8" casing set at 595 mTVDgl when transferred up-dip and into the borehole, which was left uncased for 1678 mTVD. The dipping nature of many of the thrusted reservoir sequences across the Tarata Thrust Zone and Patea Whanganui Coast implies lateral transfer may be occurring across the eastern basin margin.

As movement on the Taranaki Fault in the south of the Taranaki Peninsula ceased ~6 Ma ago (Stagpoole and Nicol, 2008), there is a greater likelihood that young fractures may still be

open (Stagpoole et al., 2004), increasing the probability of pressure transfer. The significant overpressure intercepted at depth in Kauri-A1 ST1 could be explained through the lateral transfer of excess pressure from deeply buried underlying Palaeogene and Cretaceous rocks (Fig 2.4a). Also, considering the recent cessation of thrusting and proximity to the axis of movement, the reservoirs in the Patea Whanganui Coast, may still maintain any excess pressure generated through horizontal stresses.

2.4.4. DEEP PRESSURE TRANSITIONS

Well penetration below 4500 mTVD in the basin are very rare, and direct pressure data have only been acquired in two wells that reached those depths (Wamainu-1 & Kapuni-Deep-1). Figure 2.16 displays mudweight depth profiles for five of the deepest wells, all on the Taranaki Peninsula, and two wells on the Manganui Platform, which intercepted very high pressures at ~3500 mTVDss. Mudweight can be used as a proxy for formation pressure, especially when increases are due to well bore kicks or dynamic fluid influx, as was the case with all these wells.

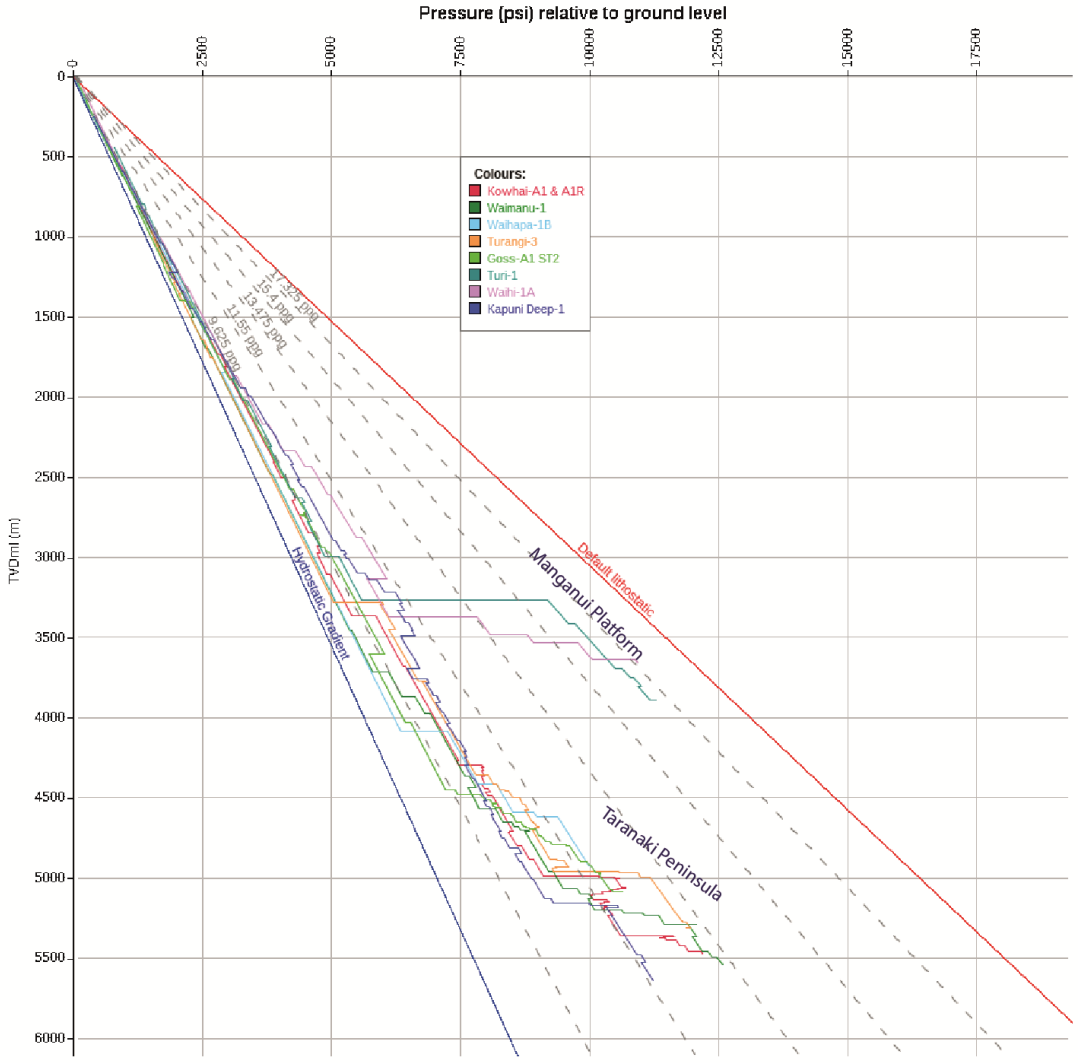

Figure 2.16. Mudweight depth profiles for specific wells in the Central Taranaki Peninsula and on the Manganui Platform

Pressure transition zones, defined by Swarbrick and Osborne (1996), occur where the rate of increase in pressure with depth exceeds the increase attributable to the density of the formation fluids. The depth of transition occurs as a function of the mechanism that is causing the overpressure and the evolution of excess pressure through time. Hydrocarbon generation, specially kerogen to gas maturation, has been attributed as the principal overpressure generating mechanism in certain basins (Amazon Fan, Kutai Basin & Malay Basin), which are associated with significant transition zones of up to 0.676 psi/ft (Cobbold et al., 2004; Ramdhan and Goulty, 2010; Tingay et al., 2013). Disequilibrium compaction induced transition zones are characterised by relatively abrupt deviations from hydrostatic gradient, below which almost all pore fluids are retained (Swarbrick and Osborne, 1996), highlighted in numerous rapidly subsiding Tertiary Basins (Nile Delta, Niger Delta, Gulf of Mexico & Taranaki Basin) (Badri et al., 2000; Bilotti and Shaw, 2005; Dickinson, 1953; Webster et al., 2011).

A number of mechanisms could be contributing to pressure transitions in the Taranaki Basin, and, due to the complex tectonostratigraphic evolution of the basin, each well must be analysed on a case-by-case basis. The previously mentioned Kowhai-A1R well, reached a total depth of 5459 mTVDgl, experiencing two drilling breaks and associated minor influxes within the Palaeocene Farewell Formation, the lower at 5354 mTVDgl recording an 88% gas cut. No shut-in pressures were recorded at these incidents, but the kill mudweight used in the lower break equates to an overpressure of ~4000 psi. The well penetrated the Farewell Formation at the distal end of the Palaeocene coastal plain sequence, which is exemplified by a substantial increase in mudrock volume in the mud log and wireline signatures. The increase in mud-silt grade facies suggests great potential for overpressure maintenance, which could be providing the excess pressure. Also, the presence of a significant gas cut in the lower influx hints at the possibility of gas expansion and kerogen cracking as a further overpressure generating mechanism.

The mud log implies that the drilling break occurred in soft, friable, very fine-grained and weakly calcareous sandstone, which is overlain by a hard calcareous concretionary layer. This hints at the presence of a vertical pressure barrier of diagenetic origin, which will be further discussed in a case study from Kapuni Deep-1 well in section 4.5.1.

As discussed in section 2.4.1, thick sequences of interbedded coal and mudrocks act as pressure seals in Radnor-1 well, and this is also the case to the west in the deeper Waihapa-1B and its re-drill Goss-A1 ST2. Successive mudrock sequences within the Mangahewa Formation at Waihapa-1B maintain a pressure differential of ~2000 psi across 532 mTVD, supported by a kick at the base of the Mangahewa Formation and a subsequent DST at the top of the Kaimiro Formation.

2.4.4.1. SAND DISTRIBUTION

Figure 2.17 displays the maximum extent of shoreline facies (reservoir sandstones) for the major reservoir intervals within the Taranaki Basin, and associated wells that were drilled close to these boundaries. Kowhai-A1R was drilled close to the north-west extent of shoreline facies of the Early Eocene Kaimiro Formation, and as discussed in the previous section, terminated in a thick sequence of undercompacted mudrocks, which are suggested to be contributing to the preservation of overpressure at depth (>4500 mTVD). Similarly, Waimanu-1 and New Plymouth-2 were drilled close to the maximum extent of the shoreline facies for the Farewell and Mangahewa formations, and again both terminated in thick packages of undercompacted mudrocks. Turi-1 was drilled past the north-eastern extent of reservoir facies in the Mangahewa Formation. In all of these wells, mudrock volume increases dramatically towards total depth, associated with an increase in the formation pressure of adjacent sandstone beds. The rapid decrease in net sand leads to a reduction in hydraulic connectivity thereby limiting the permeability to a point where the majority of the excess pressure is maintained, producing the relatively abrupt pressure transitions indicative of disequilibrium compaction (Swarbrick and Osborne, 1996). Porosity anomalies and associated significant deviation of wireline sonic data below the Tikorangi Limestone support this hypothesis (Sayers et al., 2002) (Fig. 2.4d).

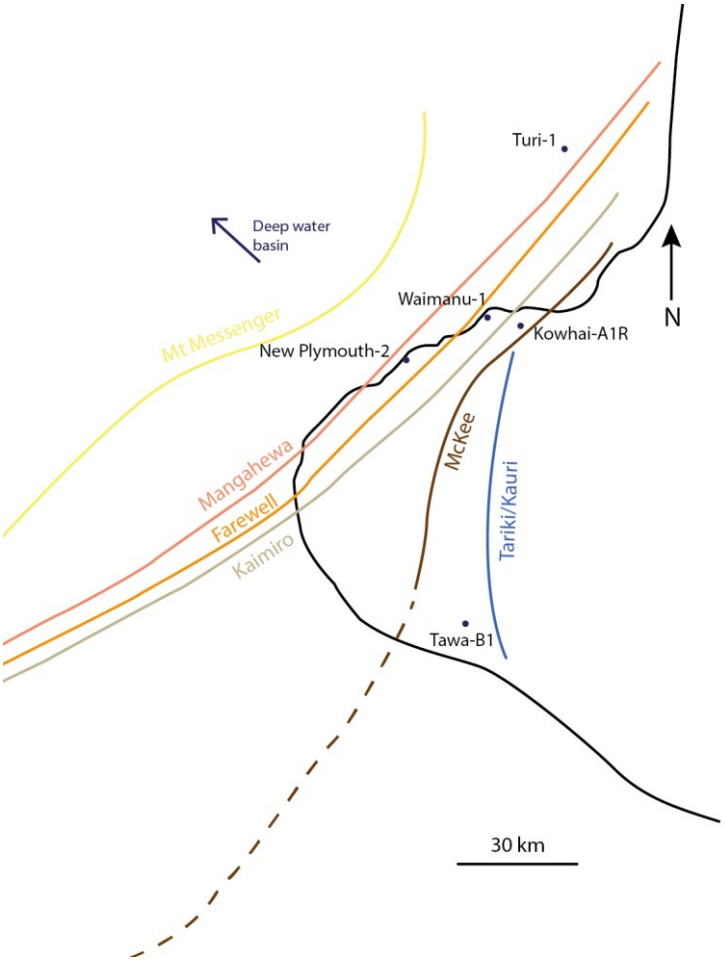

Figure 2.17. The outer, north-western extents of sandstone distribution in the main reservoir formations (modified from King and Thrasher, 1996)

The presence of various types of vertical pressure seal have been identified (mudrock & diagenetic), but to maintain any excess pressure, competent lateral seals must be present. Laterally sealing faults have been identified on the Central Taranaki Peninsula and Manganui Platform and associated stratigraphic pinch-outs involving Oligocene turbidites (Tangaroa Formation).

2.4.5 Pore pressure related drilling hazards

Taranaki Basin's first deep (>3000 mTVD) well, Kapuni-1, drilled in 1959 experienced a kick on entering the Mangahewa Formation; a trend which has continued to the present day in both exploration and appraisal wells that have penetrated permeable formations ranging from the Palaeocene to Oligocene (Fig. 2.18). Kicks are especially useful pore pressure measurements, as they occur outside of conventional reservoirs with WFT and DST data, so can significantly improve the quality of pore pressure prediction.

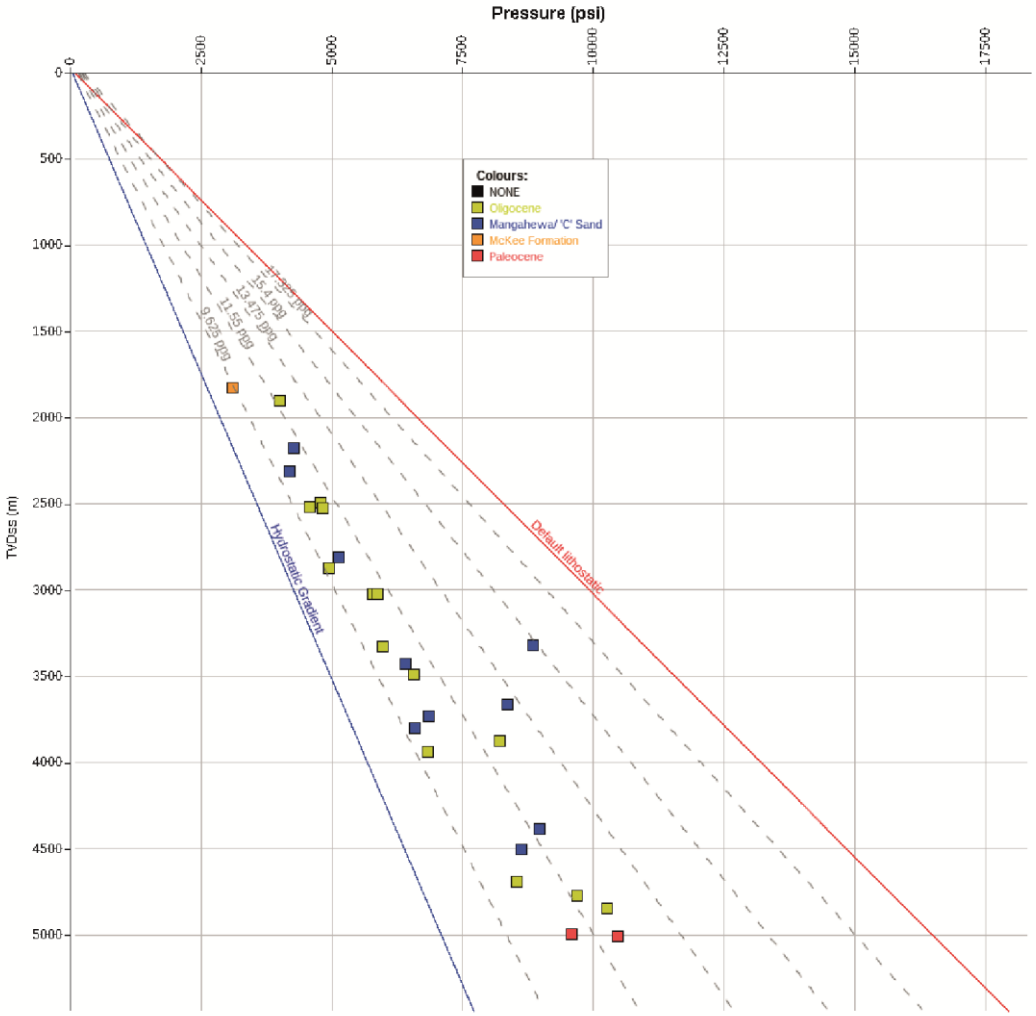

Figure 2.18. Pressure depth plot displaying 40 separate well bore pressure kicks from 20 wells across the Taranaki Basin

Thin (<30 m) stratigraphically isolated deep-water sandstone beds within the Otaraoa and Turi formations have been intercepted in numerous wells (Armstrong et al., 1996), but are very difficult to recognise while drilling or to predict in the pre-drill phase. Notable examples

come from the Manganui Platform where Awakino-1 and Opito-1, both took kicks in thin sandstone stringers. A further example comes from the Patea Whanganui Coast where Tawa-B1 experienced three successive kicks in 150 mTVD, which display a pressure increase of 1500 psi. These highly permeable intervals act as pressure valves and can be catastrophic if not managed effectively.

Kicks are often easy to handle as drill mudweights are already matched to the underlying predicted overpressure, but this may not be the case in regions like the Western Platform where lateral drainage is prevalent. Thick packages (>500 mTVD) of overpressure undercompacted mudrocks of the Turi Formation occur across the Western Platform and Northern Taranaki Bight, which are underlain by hydrostatic (or close to) reservoirs. Although the associated laterally connected reservoirs are draining, mudrocks may still encase isolated sandstone beds at virgin pore pressure, which could pose a major problem when drilling with a hydrostatic mud weight.

Repeated stratigraphic slices due to thrust faulting along the eastern basin margin place major uncertainty on the prediction of the stratigraphy and associated facies, resulting in numerous wells experiencing kicks in permeable formations within stacked thrust sheets. Wellbore mud losses do not often develop into serious issues, but they can if not controlled, especially in tectonostratigraphically complex basins such as the Taranaki Basin. Tirua-1 (Enclosure I) well was drilled on the basin margin through a thick overthursted fractured basement section and experienced total mud losses in fractures, leaving the kick tolerance at essentially zero. Reservoir depletion and the subsequent lowering of mudweight for infill wells can significantly reduce the kick tolerance, but this can be avoided through careful casing designs.

Although shallow gas has not been identified as a significant drilling issue within Taranaki Basin, the previously mentioned pockmarks and gas chimneys could have, or be aiding, in the transfer of high pressure formation fluids, which could pool at anomalously shallow depths.

2.5. CONCLUSIONS

1) The interpretation of pore pressure data at basin scale within the Taranaki Basin has been shown to be best explained by consideration of the basin as eight sub-basins, each having its own distinctive pore pressure trends defined by their stratigraphic architecture and structural development.
2) The prior interpretation of a constant hydrostatic gradient by Webster et al. (2011) for the whole of Taranaki Basin is unrealistic because of regional variation in aquifer salinity.
3) New definitions have been made in this chapter of the highest pore pressure value (in Kapuni Deep-1), the occurrence of shallowest overpressure (in Awakino-1) and the highest overpressure value (in Turi-1).
4) Facies variations across stratigraphic intervals provide a first-order control on hydraulic conductivity within interbedded sand and mudrock sequences, which in turn, define the level of overpressure maintenance and distribution across the basin.
5) Faults have been shown to act as barriers to lateral and vertical fluid flow in the thrusted sections on the Tarata Thrust Zone and Patea Whanganui Coast area, and in the Turi Fault Zone, but they can also define barriers between sub-basins.
6) Deep pressure transitions in the basin have been shown to occur across sealing horizons caused by diagenetic, structural and stratigraphic mechanisms and generated by an increase in mudrock volume or gas generation.

CHAPTER III:

PORE PRESSURE EVOLUTION AND ITS RELATIONSHIP TO RESERVOIR QUALITY IN THE TARANAKI BASIN, NEW ZEALAND

3.1. INTRODUCTION

In this chapter a series of one-dimensional basin models for Taranaki Basin hydrocarbon wells have been constructed to investigate the onset and subsequent evolution of overpressure across the basin and within the discrete tectonic sub-basins identified in Chapter II.

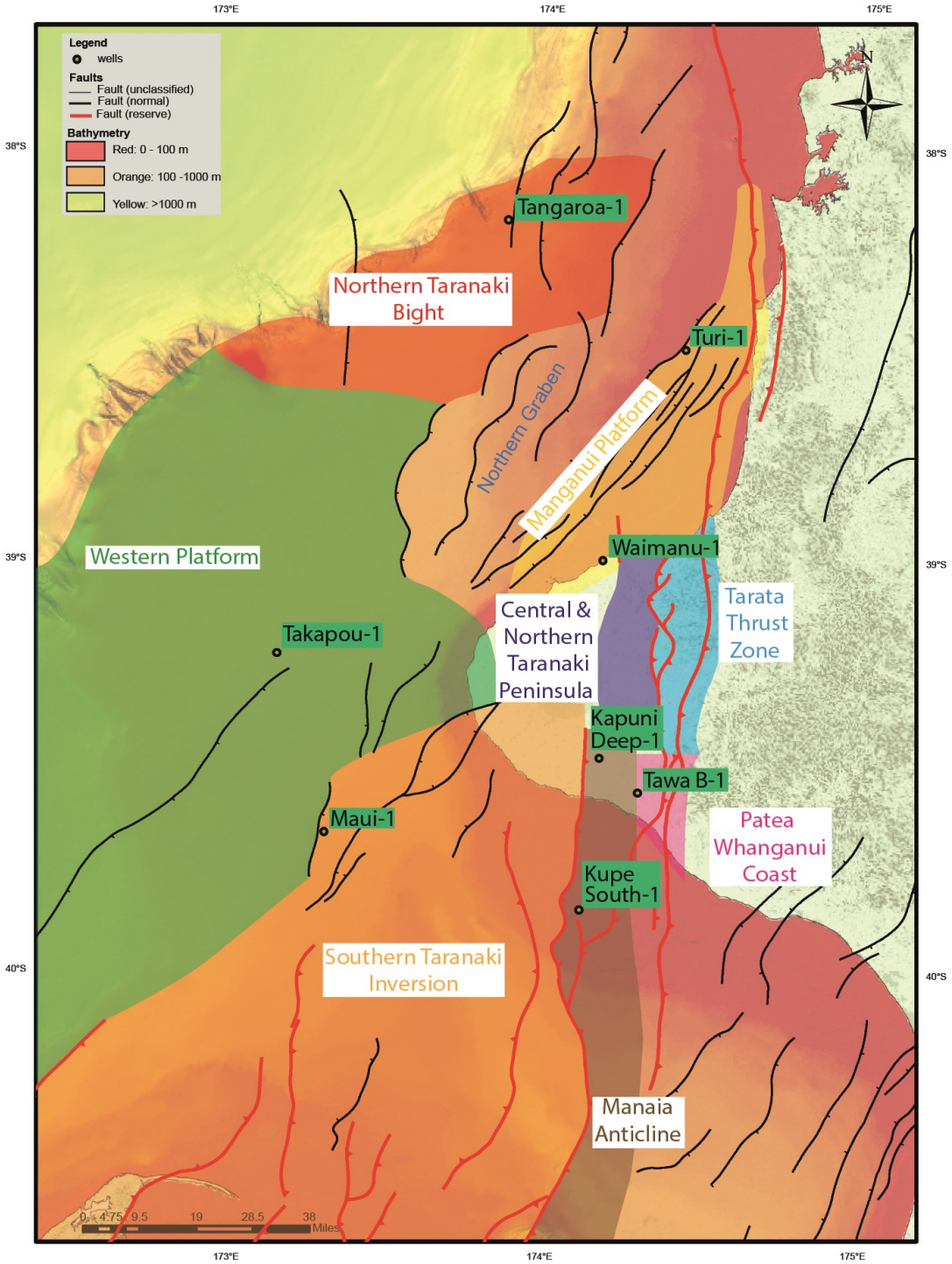

Figure 3.1. Map of the Taranaki Basin area with sub-basins identified in Chapter II highlighted, generalised bathymetry and the hydrocarbon wells that have been modelled in this chapter.

The one-dimensional models have been calibrated against measured pressure data (WFT or kicks) for the wells shown in Figure 3.1 and calculated shale pressures in laterally draining reservoirs. Traditionally, directly measured pore pressure data and one-dimensional

modelling has been used for drilling and well appraisal, but here we present a new methodology for investigating the timing of pore pressure evolution and the calibration of pore pressure models for different tectonostratigraphic parts of a basin.

3.1.1. FORELAND BASIN FORMATION

The initial onset of overpressure in Taranaki Basin occurred relatively recently in its history (~22 Ma), driven by regional tectonic forcing. The modern Australia-Pacific plate boundary in the North Island region is expressed as under-thrusting of Pacific oceanic lithosphere beneath eastern North Island, this lithosphere is turning down at the Hikurangi Trough, which is the southern continuation of the Tonga-Kermadec Trench (van de Lagemaat et al., 2018). This conventional ocean-continent convergent margin passes southward into a continent-continent convergent zone that previously involved Australia plate of North Island against continental lithosphere of eastern South Island (Canterbury). The subduction started east of northern North Island at ~28 Ma (van der Lagemart et al., 2018). Through the Late Oligocene and Neogene, this plate boundary system shifted south-westward, including the transition from ocean-continent convergence to continent-continent convergence, which currently lies at Kaikoura.

Crustal shortening within the Australia plate along the eastern margin of Taranaki basin, probably as a result of continent-continent convergence, was expressed at ~27 Ma. This is shown by reverse displacement on Manganui and Taranaki faults (King and Thrasher 1996; Kamp et al., 2006). In the Taranaki Peninsula area, reverse displacement on Taranaki Fault during the Late Oligocene and Early Miocene formed the distinctive foreland basin wedge geometry associated with thick accumulation of Late Oligocene Otaraoa Formation and lower parts of the Manganui Formation (Fig. 3.2) (King and Thrasher 1996; Holt and Stern, 1994; Stern and Davey, 1990).

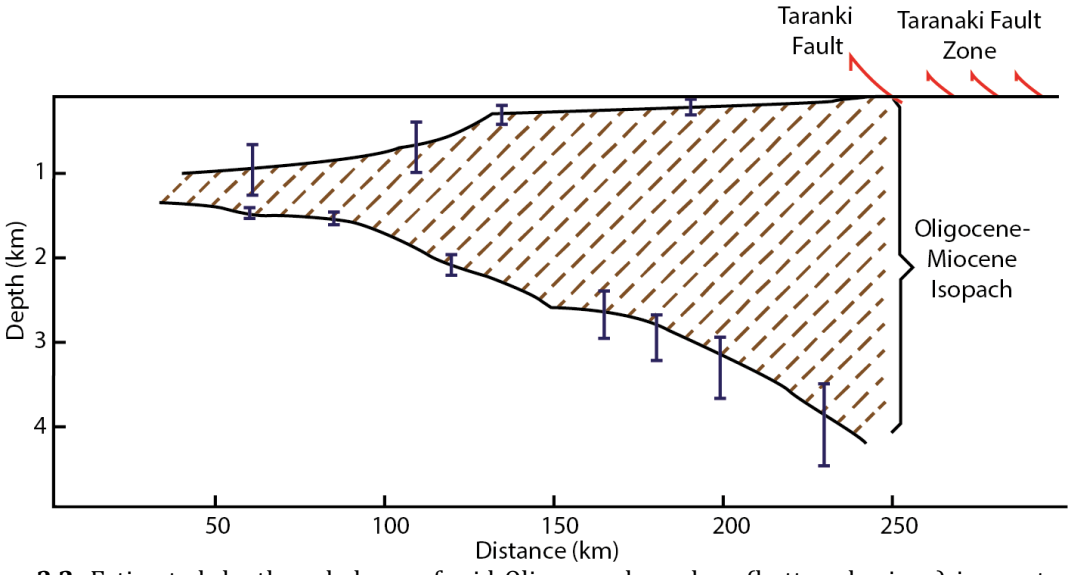

Figure 3.2. Estimated depth and shape of mid-Oligocene boundary (bottom horizon) is constrained from paleobathymetry and sediment thickness at the end of the Miocene (top horizon). Depth uncertainties from scatter in sonic velocity in 19 exploration wells (Thrasher and Cahill, 1990) are approximately ±100 m (modified from Holt and Stern, 1994).

At this time the Taranaki Fault developed as a complex series of thrusts displacing wedges of Murihiku basement terrane over and within the Cenozoic basin fill, including "sled-runners" that detached sediment fill beneath eastern Taranaki Peninsula and displaced them into parts of the basin fill farther westward, forming the Tarata Thrust Zone. The sum of displacements on the Taranaki Fault Zone led to the uplift of hinterland, which augmented sediment input derived from the south. A thick wedge of sediment filled the foredeep during the Miocene (Holt and Stern, 1994; King and Thrasher, 1992), particularly in the peninsula area and south of the peninsula where displacement on Taranaki Fault continued until approximately the end of the Miocene.

From the Late Miocene (beginning of the Tongaporutuan Stage; 11-7.2 Ma) and through the Pliocene a shelf-slope sedimentary system prograded to the northwest beyond the Maui Field (Enclosure 1) onto the Western Platform and northward into the North Taranaki Graben, which formed through extension during the latest Miocene (Kapitean Stage; 7.2 to 5.3 Ma) (Kamp et al., 2004). Latest Miocene extension in North Taranaki Graben was possible because through the Neogene the continent-continent convergent part of the plate boundary zone shifted to the southwest and into South Island, leaving the Taranaki Basin in a back-arc position. Currently the whole of the Taranaki Basin is outside of the zone of continent-continent convergence and this developed southwards starting around 19 Ma in the Awakino area of North Taranaki and ending during the Pleistocene north of Nelson in southern Taranaki Basin (King and Thrasher, 1996). The development of abnormal pressures across the basin (Section 3.4.1) is correlated with this record of tectonic development of Taranaki Basin and its various subareas.

3.1.2. Effective stress and reservoir quality

Timing and depth of onset and potential maintenance of overpressure in sedimentary basins is of importance when predicting reservoir quality, as it can aid in preserving porosity to significant depth (Lander and Walderhaug, 1999; Paxton et al., 2002). Hydrocarbon producing basins that display shallow onset and the maintenance of high pore fluid pressure (i.e. low vertical effective stress [VES]) have been shown to preserve anomalously high porosity (>30%) at significant depth (>5000 m) by lessening the impact of mechanical compaction (Grant et al., 2014; Nguyen et al., 2013; Oye et al., 2018; Sathar and Jones, 2016; Stricker et al., 2016).

Processes leading to porosity loss in sediments may be divided into mechanical compaction, which is a function of increasing effective stress, and chemical compaction, which is controlled by the thermodynamics and kinetics of fluid-rock interaction. Increasing effective stress caused by sediment loading is the major physical force driving the reduction in porosity of sandstone beds by compaction. Mechanical compaction is the dominant process by which sand porosity is reduced from surface depositional values of 40-45% to typical

values of 25-35% prior to lithification (e.g. Paxton et al., 2002). The development of fluid overpressures has been shown to lessen VES, thereby reducing the load borne by intergranular and cement-grain contacts within buried sand and sandstone. Overpressure can slow the rate of compaction but does not result in a bulk-rock volume (i.e., porosity) increase. The compaction of sand is an irreversible process and can only be stalled by the formation of an early grain framework or by shallow onset of high pore fluid pressure and its maintenance (e.g. Stricker et al., 2016). High pore fluid pressure limits and helps to prevent significant quartz cementation by forestalling the onset of intergranular pressure solution, thereby reducing the effects of a primary source of silica (e.g. Osborne and Swarbrick, 1997; Oye et al., 2018).

Differing levels of compaction and cementation produced variable reservoir quality across the Taranaki Basin, but reservoir porosity can be as high as 26% at >3000 mTVDss (Table: 3.1; Killops et al., 2009). The potential influence of VES on porosity in Taranaki Basin is investigated by calculating VES at maximum burial depth for 45 wells (Table 3.1) and plotting these values against measured helium porosity data from conventional cores compiled by Higgs et al. (2012b). One-dimensional basin modelling results are used to investigate whether there is appropriate stratigraphic stacking and pore pressure history to facilitate porosity preservation. Where well control or core analysis data are limited, basin modelling and regional geology are used here to predict the potential for enhanced porosity preservation. This approach is used to enable the prediction of where shallow anomalously high overpressures may be present in the basin and crucially where low VES has allowed the preservation of excellent reservoir quality to significant (>3500 m) depth (see section 3.4.3).

3.2. METHODOLOGY:

3.2.1. ONE-DIMENSIONAL BURIAL HISTORY MODELLING

Pore pressure and temperature evolution within the stratigraphy intersected by eight wells in the Taranaki Basin were modelled in one dimension using Schlumberger's PetroMod software (V. 2015). One-dimensional modelling provides insight to overpressure build-up by disequilibrium compaction that is considered to be the primary cause of overpressure in Taranaki Basin (Webster et al., 2011). However, in some parts of the basin, hydrocarbon generation (and in particular cracking to gas at high maturities) is interpreted to contribute to overpressures. PetroMod is based on a forward modelling approach to calculate the geological evolution of a basin from its burial history (Hantschel and Kauerauf, 2009). However, these models do not include other mechanisms for generating excess pore pressure, such as hydrocarbon cracking, gas generation or load transfer (Lahann and Swarbrick, 2011) and are only able to account for vertical stress. One-dimensional modelling will also not show the potential discrepancies in overpressure between reservoirs and mudrocks caused by lateral fluid flow, but this can be calibrated using measured reservoir

pressure data where available. The generation and dissipation of pore pressure is a 3D process, which cannot be captured by a 1D system.

Shale pressures were calculated using the equivalent depth method (Hottmann and Johnson, 1965), to calibrate modelling derived pressures. Shale and basin modeling derived pressures were then compared with measured formation pressure data (WFT, DST and Kicks), to investigate lateral fluid flow. Fluid flow in the form of lateral drainage, lateral transfer and fault-related flow have been identified in the Taranaki (O'Neill et al., 2018a; Webster et al., 2011) and must be taken into consideration when interpreting model results.

The Taranaki Basin wells shown in Figure 3.1 were selected for pore pressure analysis on the basis of differing tectonostratigraphic histories of the stratigraphic successions encountered within them, and are considered to be representative of the surrounding areas (Sub-basins-Chapter II; Fig. 2.1). The burial models use well stratigraphy and lithologies from mud log cuttings data in respective well completion reports. Heat flow has been estimated after Funnell et al. (1996), uplift where appropriate from Armstrong et al. (1998) and palaeo-water depths were extracted from biostratigraphy reports within well completion reports. The models were calibrated against corrected bottom hole temperate well data (Rob Funnel pers. comm. 2018), measured formation pressures and, where available, fluid inclusion data. The lithological units used in these models are mainly PetroMod (V. 2015) default lithologies, which have been mixed based on well log descriptions, mud log cuttings and core analysis reports for the respective wells (Fig 3.1).

Athy's (1930) law for porosity loss with depth was used for all models, as it utilises effective stress rather than total depth and is applicable for a wide range of rock types (Hantschel and Kauerauf, 2009). To calibrate overpressure values, a permeability adjustment must be made for layers in which overpressure builds up (Hantschel and Kauerauf, 2009). Calibrating to overpressure values in permeable formations is not useful as they may have experienced pressure changes due to fluid in or outflow (Hantschel and Kauerauf, 2009), which is why shale pressures are used as an alternative. Yang and Aplin (2007) measured vertical permeabilities for 30 deeply buried mudrock sequences, producing a range from 0.16 μD to 0.2 nD, which were used as a guideline for permeability ranges in the Taranaki Basin models. Permeabilities used for sealing lithologies range from 0.11μD to 0.1nD.

3.2.2. SHALE PRESSURE CALCULATIONS

Shale pressure calculations were performed using the equivalent depth method (Fig. 3.3; Hottmann and Johnson, 1965) on data for each of the previously mentioned eight wells to calibrate modelling derived formation pressures. Pore pressure prediction methods exploit the deviation of mudrock properties in wireline log data relative to the typical values of a normally compacting sequence at the depth of interest (Sayers et al., 2002). Overpressures

generated by disequilibrium compaction (undercompaction), as observed in the Taranaki Basin (Webster et al., 2011) are associated with anomalously high sediment porosities (Hubbert and Rubey, 1959). In rapidly subsiding basins with low-permeability sediments (mudrocks), fluid is unable to escape, leading to the progressive development of overpressure as a part of the total vertical stress is transferred to enclosed fluids. Porosity is a direct measure of compaction, and anomalously high porosity for depth of burial by undercompaction can be used to assess pressure in these mudrocks (Webster et al., 2011). Porosity is being used as a proxy for VES such that pore pressure can be estimated from the equation (below) of Terzaghi (1943) if the vertical stress is known:

$S_v = \sigma' + P_p$

Rearranged to give pore pressure:

$P_p = S_v - \sigma'$

where P_p = pore pressure (psi); S_v = overburden pressure or vertical stress (psi); σ' = vertical effective stress (psi)

Velocity is one of the responses to pressure that is measured routinely both in wells and in seismic data, both of which have been previously applied successfully in the Taranaki Basin to predict overpressure (Humphris and Ravens, 2000; Webster et al., 2011). The eight selected wells (Fig. 3.1) have a combination of high-quality wireline suites, direct pressure data and mud-weight data, all acquired during drilling. Supplementary data, such as temperature, stratigraphic information, composite logs and drilling reports were also analysed to calibrate the shale pressure profiles as produced in this study.

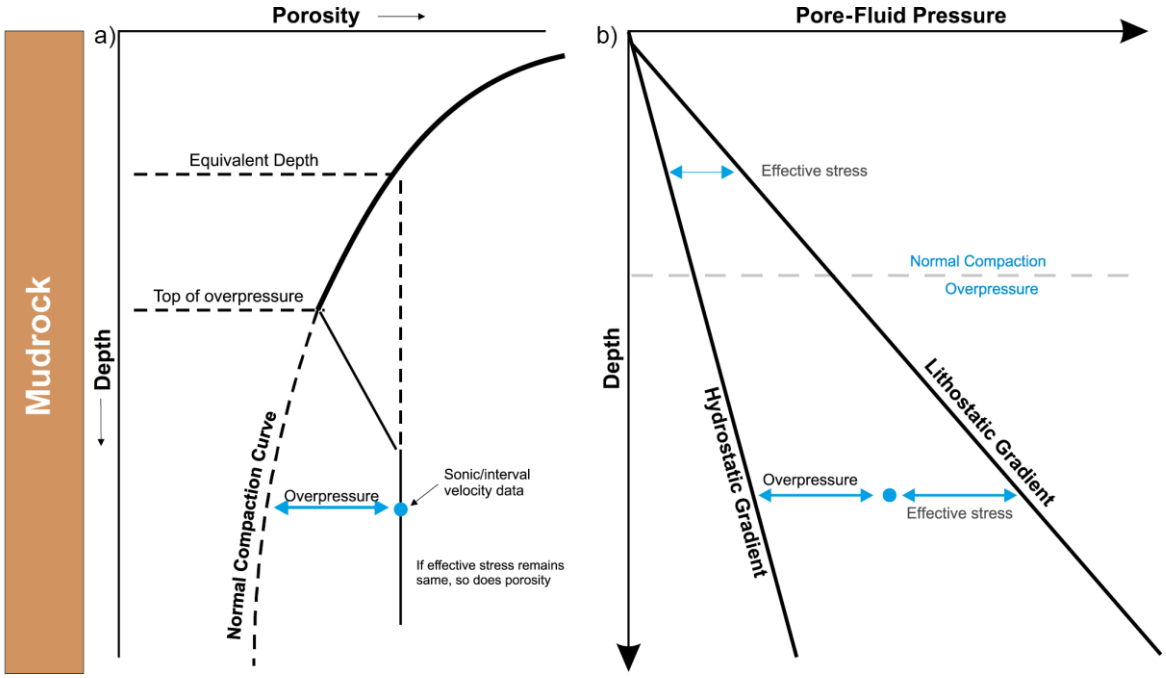

Figure 3.3. Disequilibrium profiles showing normal and anomalous compaction curves diverging below top of overpressure. A: Effective stress remains constant in the situation where porosity loss is completely inhibited, typically producing pore pressure profiles that are parallel to the lithostatic gradient in shales. B: Overpressure also increases with increasing depth (after Hottmann and Johnson, 1965; modified from Webster et al., 2011).

The equivalent depth method (Hottmann and Johnson, 1965) assumes that porosity relates directly to vertical effective stress, meaning that for any value of velocity that does not plot on the normal compaction trend (NCT), the pressure can be estimated by projecting the value vertically onto the NCT (in the normally pressured section) on a velocity versus depth plot (Fig 3.3). The method is not valid within sandstone beds, but when combined with direct measured pressure from adjacent permeable formations an assessment of whether they are in equilibrium can be made. Hydraulic conductivity of reservoirs can lead to lateral fluid flow, which produces discrepancies between measured reservoir pressure and calculated shale pressures through mechanisms such as lateral drainage (Bredehoeft et al., 1988; O'Connor and Swarbrick, 2008) and lateral transfer (Yardley and Swarbrick, 2000). Therefore, knowledge of the tectonic setting, stratigraphy, regional fluid flow and basin plumbing must be applied when calibrating shale pressure estimates.

The equivalent depth method assumes that overpressure is generated by disequilibrium compaction, that the rocks are at their maximum effective stress, and that the basin is extensional. Harrold et al. (1999) highlighted the potential importance of examining the mean stress instead of simply the vertical stress, and indeed, the eastern mobile belt contains compressional structures (King and Thrasher, 1996). However, the sole use of vertical stress is widely accepted particularly because of generally poor constraint on measurement of the magnitude of horizontal stress. By the Pliocene, movement on the Taranaki Fault had ceased, meaning any excess pore pressure generated by horizontal stress would have started to dissipate, particularly during the extensional phase of the Taranaki Basin dating from the mid-Pliocene (Rajabi et al., 2016).

As previously mentioned, to produce pore pressure profiles using the equivalent depth method, one needs to establish (1) vertical stress (here the commonly used 3.281 psi/m was applied) and (2) NCTs based on sonic data. Taranaki Basin has several distinct structural provinces with contrasting burial, uplift, inversion and erosion patterns (Western Platform, Southern Taranaki Inversion Zone, Manaia Anticline etc.), so a series of different models for compaction were derived by using sonic data for a number of wells within the same structural province to define a series separate NCTs.

3.2.3. VERTICAL EFFECTIVE STRESS & POROSITY

To investigate the potential influence of VES on porosity in Taranaki Basin, VES was calculated at maximum burial depth for forty-five wells (Table 3.1). VES was then plotted against measured helium porosity data from conventional cores compiled by Higgs et al., (2012b). These forty-five well records were selected because their cored reservoirs cover all of the depositional environments, depth ranges (~1900-5500 m) and sub-basins within Taranaki Basin (Table 3.1). Also, only reservoirs that had greater than twenty separate samples were chosen to ensure the calculated mean was representative. Any porosity data

collected from side-wall core was omitted as these data are not as reliable as conventional core analysis results.

Table 3.1: 45 wells (48 separate cores) used to investigate the relationship between VES and porosity (Higgs et al., 2012b)

Well Name	Formation	Mid core depth max. burial (mTVDss)	VES (psi)	Depositional Environment	No. of Samples	Helium Porosity (%)		
						Min	Max	Mean
Ahuroa-1	Tariki Sandstone	3524	6180	Outer shelf	154	2.2	18.8	13.8
Amokura-1	Farewell	3596	6400	Shoreline	63	2.8	21.5	18.3
Awakino-1	Mangahewa	2500	3422	Shoreline	61	1.2	15.4	10.1
Cardiff-1	Mangahewa	4790	6207	Estuarine/coastal plain	63	6.6	14.2	10.9
Cheal-2	Mt Messenger	2111	3843	Basin floor/slope	82	15.9	25.6	21.5
Kaimiro-16	Mt Messenger	1937	3526	Basin floor/slope	46	22.5	30.5	27.8
Kaimiro-18	Mt Messenger	1916	3488	Basin floor/slope	90	11.1	28.6	24.5
Kapuni Deep-1	Farewell	5292	6956	Shoreline	37	1.1	4.4	3
Kapuni-14	Mangahewa	3805	5772	Estuarine/coastal plain	267	2	24.3	15
Kapuni-15	Mangahewa	3953	6339	Estuarine/coastal plain	38	2.9	14.2	11
Kora-4	Tangaroa	3112	3471	Basin floor	26	4.6	23.3	17.7
Kupe South-1	Farewell	3126	4692	Coastal plain	230	1.1	26.2	19.2
Kupe South-2	Farewell	3105	4631	Coastal plain	243	2.3	24.8	16
Kupe South-4	Farewell	3053	4584	Coastal plain	143	4.1	22.5	14.1
Kupe South-5	Farewell	2872	4358	Coastal plain	52	6.2	24.6	21
Maui A-1G	Mangahewa	3044	5541	Shoreline	279	2.5	25.7	17.5
Maui A-1G	Kaimiro	3331	6064	Shoreline	161	1.9	23.4	14.4
Maui-5	Mangahewa	3057	5565	Shoreline	298	0.8	26.4	17.2
Maui-6	Mangahewa	3083	5612	Shoreline	226	0.7	24.9	15.8
Maui-7	Mangahewa	2933	5339	Shoreline	354	1.7	25.4	17.2
Maui-7	Kaimiro	3182	5793	Shoreline	185	2	25.5	17.6
MB-P8	Kaimiro	3217	5856	Shoreline	150	2.5	22.3	13.6
MB-R(1)	Farewell	3407	6005	Shoreline	141	2.5	20	15.6
MB-W(2)	Farewell	3412	6015	Shoreline	82	3.4	22.1	17.3
Mokau-1	Mangahewa	3290	4938	Shoreline	119	2.2	14.2	10.6
Moki-1	Mangahewa	3351	6100	Estuarine/coastal plain	115	1.2	19.3	13.4
Moki-2, 2A	Moki	2842	5547	Basin floor	112	7.1	24.5	13.5
Ngatoro-1	McKee	3641	5721	Inner shelf/shoreline	62	0.3	10.9	6.1
Ngatoro-11	Mt Messenger	2029	3694	Basin floor/slope	32	22.9	27.2	25.7
Ngatoro-2	Mt Messenger	2085	3796	Basin floor/slope	89	11.1	29.7	25.3
Ngatoro-3	Mt Messenger	2071	3770	Basin floor/slope	49	15.5	28.9	24.6
Ngatoro-4	Mt Messenger	1952	3553	Basin floor/slope	61	0.5	29.9	19
Ngatoro-5	Mt Messenger	2071	3770	Basin floor/slope	130	3.6	32.6	20.3
Ngatoro-7	Mt Messenger	2101	3825	Basin floor/slope	111	15.6	26.7	22.9
Ohanga-2	McKee	3401	4650	Inner shelf/shoreline	92	2.2	11.5	8
Ohanga-2	Mangahewa	3732	5628	Estuarine/coastal plain	205	0.9	12.4	8.9
Okoki-1	Mangahewa	3769	5687	Shoreline	22	1.7	9.7	6.9
Pohokura South-1	Mangahewa	3630	5257	Shoreline	215	0.8	12.7	7.8
Pohokura South-1B	Mangahewa	3523	5298	Shoreline	198	0.9	11.7	8
Pohokura-1	Mangahewa	3521	5250	Shoreline	83	1.4	11.2	7.5
Pohokura-2	Mangahewa	3564	5403	Shoreline	179	3.8	12.7	9.5
Pohokura-3	Mangahewa	3564	5402	Shoreline	323	1.6	16.5	9.9
Tangaroa-1	Tangaroa	3584	4771	Basin floor	22	17	21.6	19.6
Tariki North-1A	Tariki Sandstone	2608	3677	Outer shelf	61	3.8	16.6	13.2
Tariki-1	Tariki Sandstone	2938	4448	Outer shelf	31	3	18.6	13.7
Tariki-4/4A	Tariki Sandstone	2574	3778	Outer shelf	594	1.3	20.2	15.1
Toru-1	Kaimiro	3829	5924	Coastal plain	211	2.4	22.2	14.8
Waihi-1	Mangahewa	2897	3091	Shoreline	57	2	13.5	7.8

The vertical effective stress of the 48 separate reservoirs (from 45 wells) was calculated by subtracting the lithostatic pressure from the measured pore pressure, as shown in Figure 3.3. A basin-wide lithostatic gradient of 3.281 psi/m was used and offset wells have been used to calculate a basin-wide hydrostatic gradient of 1.424 psi/m (section 2.2.4.1).

3.3. RESULTS

3.3.1. ONSET AND EVOLUTION OF OVERPRESSURE

The earliest phase of overpressure generation is directly linked to formation of a foreland basin in eastern Taranaki Basin from the late Oligocene to Early Miocene (Fig. 3.2). Subsequent phases of uplift, erosion and subsidence lead to the episodic generation of accommodation space through sub-basin formation along the basin margin in a southward direction. These sub-basins were then filled by the progradation of a number of continental sedimentary wedges (Bull et al., 2018; Kamp et al., 2004; King and Thrasher, 1996), which loaded the underlying strata generating overpressure through disequilibrium compaction (from 22-10 Ma, see Fig. 3.4). The development of the plate boundary during the Early Miocene to the Pleistocene, involved the episodic north-westward progression of a further series sedimentary sequences, sourced from the South Island, across the continental shelf. This resulted in continued phases of overpressure generation from 10 Ma to the present day as demonstrated in Figure 3.4.

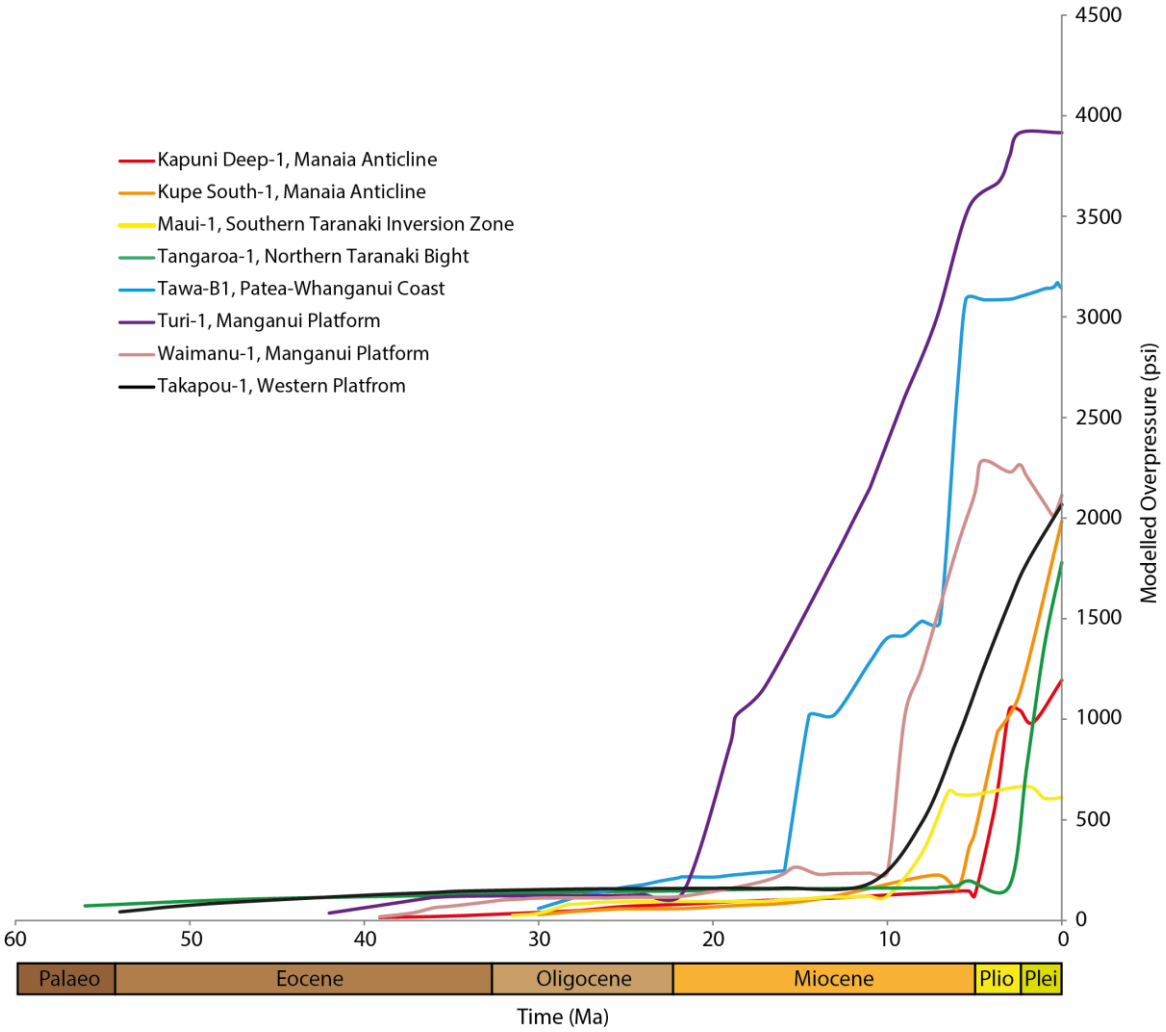

Figure 3.4. Overpressure histories for the base of overpressure generating mudrock formations (Turi, Otaraoa or Manganui) against time in eight wells (locations found in Fig 3.1)

The Oligocene to Miocene section is primarily comprised of fine-grained calcareous mudrocks with an upward increasing content of terrigenous siltstone facies. The first

occurrence of sandstone transported as gravity flow deposits occur in the late-Early Miocene Moki Formation followed by the Late Miocene Mount Messenger Formation (Baur et al., 2014). The Plio-Pleistocene section is a slope to shelf mud-dominated succession in North Taranaki Basin and across parts of the Western Platform (Giant Foresets Formation; Enclosure II) or an onlapping shelfal succession in Southern Taranaki Basin (King and Thrasher, 1996; Kamp et al., 2004).

Well locations for the following sections can be found in Figure 3.1 and Enclosures 1. Extra burial history plots and single well plots are located in Appendix I. Compiled overpressure histories can be found in Figure 3.4.

3.3.1.1. EARLY MIOCENE (TURI-1 & WAIMANU-1)

Turi-1 well on the Manganui Platform drilled into an isolated fault compartment and intercepted overpressures of 4149 psi in a well bore kick take in thin Late Eocene sandstone beds of the Kapuni Group (Fig. 2.4d & 3.6). The well penetrated over 800 m of Turi Formation marine mudrock, which are overlain by a thin (~3 m) sandstone and sealed by the Oligocene Otaraoa Formation and Tikorangi Limestone (Enclosure II). The Turi Formation underwent limited initial compaction due to slow rates of accumulation during the Late Eocene and Early Oligocene, but was subsequently rapidly buried during the deposition of early Miocene (Fig. 3.5a) bathyal mudrocks of the Manganui Formation (Enclosure 2). This allowed for limited dewatering, leading to the onset of overpressure through disequilibrium compaction during the Early Miocene (from ~22 Ma) at a depth of ~2 km (Fig 3.5b).

Shale pressures calculated using the equivalent depth method are consistent with the measured pore pressure from the kick and mudweight (Fig. 3.6), which support the hypothesis that the sandstones beds at the top of the Turi Formation are isolated and do not laterally drain pore pressure. Both the resistivity and sonic velocity logs from Turi-1 display very significant reversals below the Tikorangi Limestone, which is indicative of a porosity anomaly and the presence of overpressure (Sayers et al., 2002). The overpressure is generated through disequilibrium compaction and maintained through the presence of laterally sealing faults and a thick competent top seal, which inhibits lateral and vertical drainage. The calculated pore pressure is only 730 psi (5 MPa) below leak-off (Fig. 3.6).

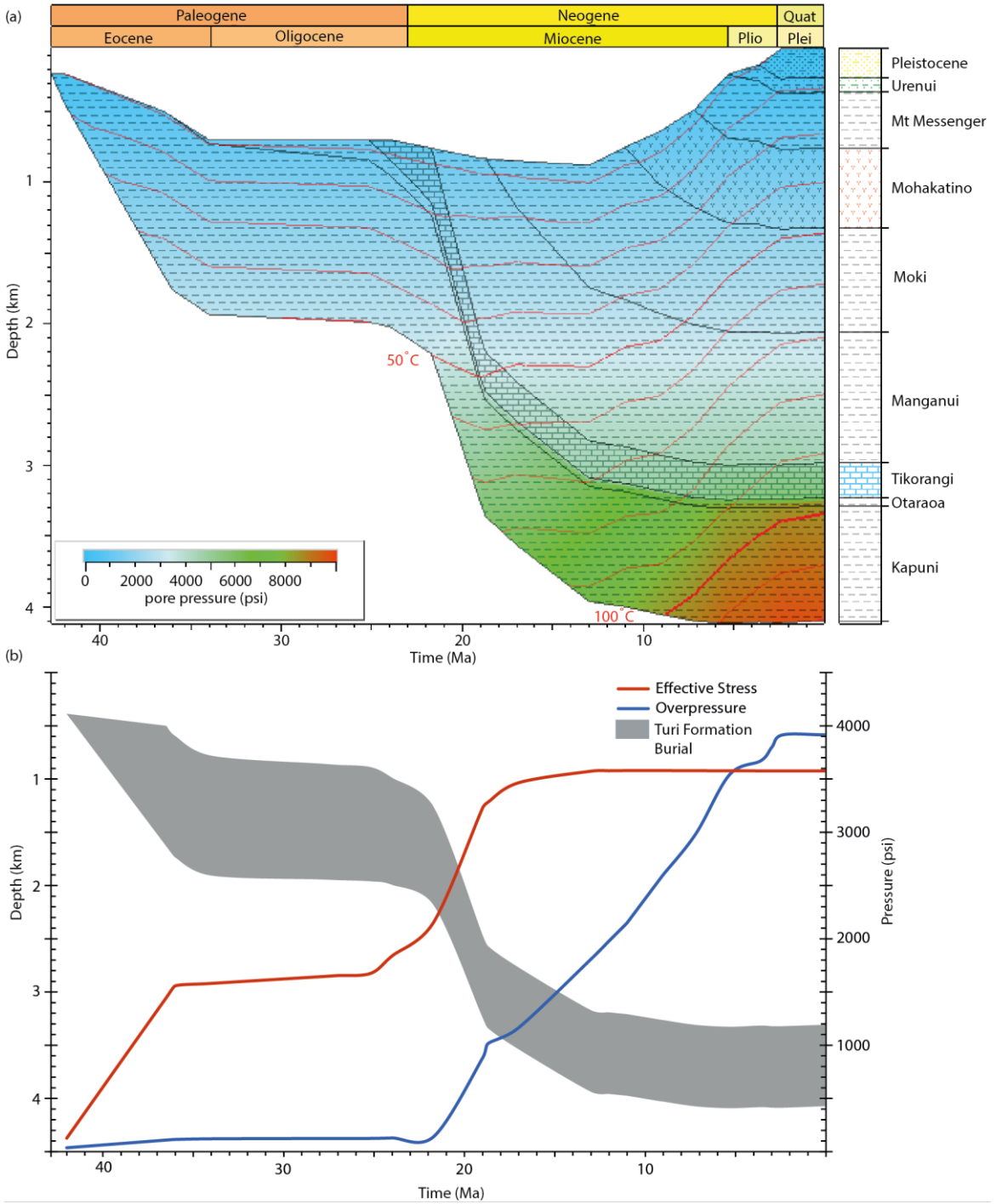

Figure 3.5. a) 1D burial history plot of Turi-1 (PetroMod). Red lines are isotherms and colour overlay denotes pore pressure; b) Plot displaying the evolution of overpressure and effective stress with burial since the deposition of the farewell Formation.

Waimanu-1 (Fig. 2.4b) was recently drilled (2011) to a depth of 5544 mTVDgl intercepting a number of pressure transition zones, most notably a 1400 psi pressure differential across the Omata Member, between the Mangahewa and Kaimiro formations (Appendix I.2). Both the sonic and resistivity logs indicate a porosity anomaly and undercompaction within the Omata Member, and shale pressure calculations show overpressure generation. The basin model for Waimanu-1 (Fig. I.1a) shows that the accumulation of the Manganui Formation loaded the already deeply buried Omata Member, leading to an onset of overpressure at the same time as within the Turi Formation at Turi-1 (Fig. I.1b).

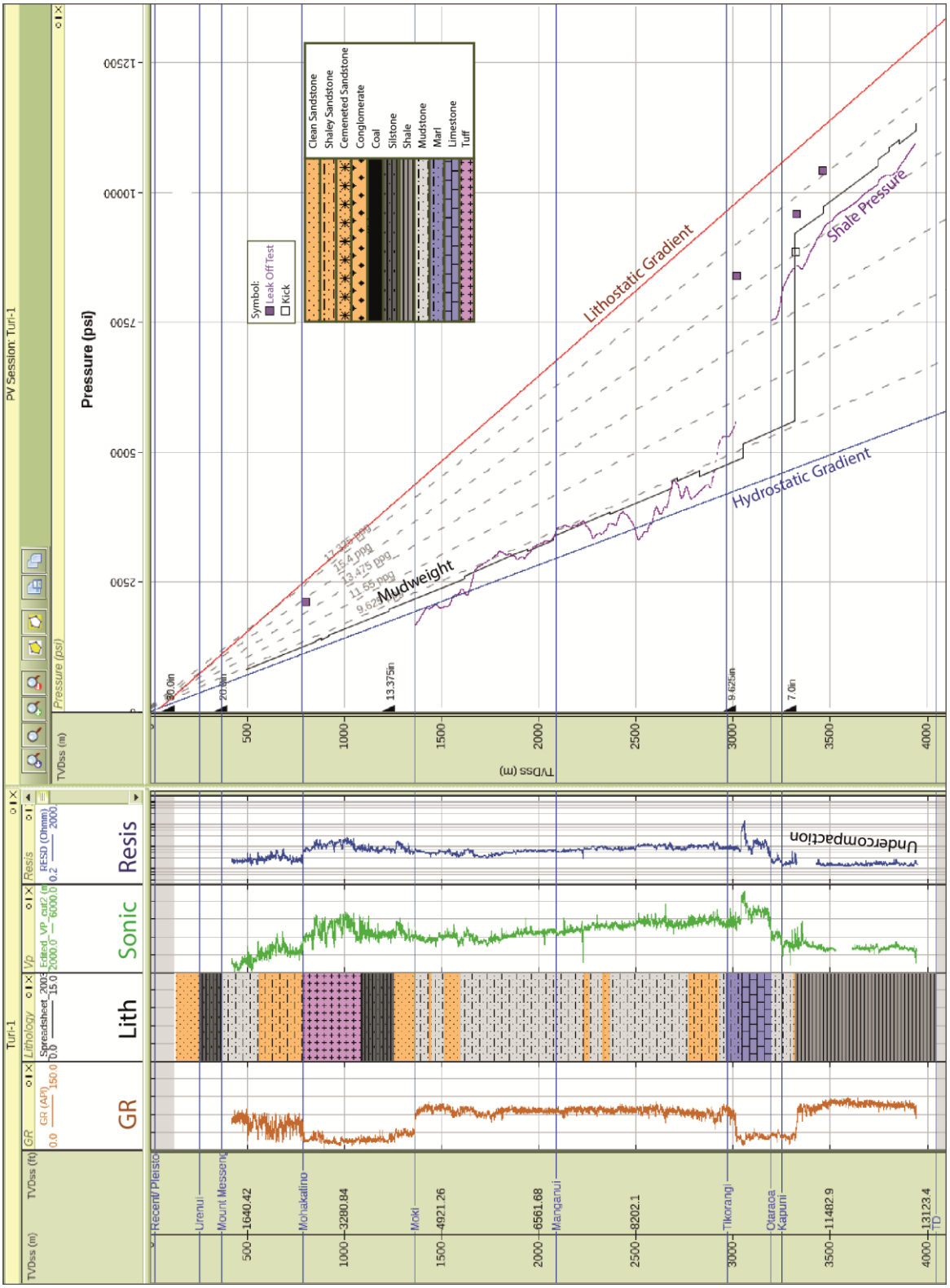

Figure 3.6. Turi-1 pressure depth plot with the suite of wireline measurements (Gamma Ray, sonic (interval transit time [ITT]), resistivity and density, a summary lithologic column, kick [white square], leak-off pressure [purple squares], mud-weight profile [black], shale pressure [purple]).

3.3.1.2. Mid-Miocene (Tawa B-1)

Tawa-B1 is located 10 km west of the Taranaki Fault in the Patea-Whanganui Coast sub-basin (Fig. 2.4a), and penetrated 5 km of predominately fine-grained Neogene sediments before entering sandstone beds of the Eocene Mangahewa Formation (Fig. I.4a). The well intercepted overpressures of 3297 psi in thin interbedded sandstone stringers within the

Otaraoa Formation. The Otaraoa Formation underwent initial rapid burial during the Late Oligocene (from ~30 Ma), which gradually decreased during the latest Oligocene and into the Early Miocene when Manganui Formation accumulated. From the late-Early Miocene (~16 Ma) the rate of sediment accumulation increased due to north-westward progradation of a basin-shelf-slope wedge including bathyal mudrocks, Moki Formation fans and muddy slope and shelf deposits (Fig. I.3a). Although the Otaraoa Formation experienced initial rapid subsidence, the fine-grained (low permeability) nature of this formation allowed for limited dewatering, leading to a porosity anomaly and the generation of overpressure during the late-Early Miocene onwards (~16 Ma; Fig. I.3b).

A further phase of subsidence, sediment accumulation and loading took place during the Late Miocene to Pliocene with accumulation of slope mudrocks of the Urenui Formation and overlying shelfal Matemateaonga Formation, which led to a further increase in pore pressure at ~6 Ma (Fig. I.3b). The isolated nature of sandstone stringers within the Oligocene Otaraoa Formation would restrict lateral drainage, meaning that the measured pore pressure should be consistent with the calculated shale pressure. The shale pressures plot higher than the measured pressure from the kick, but follow the same pattern (Fig. I.4). Kick calculations are not as reliable as wireline formation testers, as the ultimate pressure depends on the well shut-in time, which may not be long enough for build-up to the true formation pressure (Lee et al., in press).

3.3.1.3. Late Miocene (Maui-1, Takapou-1, Waimanu-1)

During the Late Miocene, very thick accumulation of Manganui Formation mudrocks and Mount Messenger Formation interpreted as deep water mudrock and turbiditic sandstone prograded across central and eastern parts of Taranaki Basin (King and Thrasher 1996; Kamp et al., 2004). During the early Tongaporutuan (from 11 Ma) the Mount Messenger Formation accumulated off the palaeoshelf, broadly following the shape of the modern day coastline of northern Taranaki Peninsula from west to northeast (see Strogen, 2011). This deposition loaded the underlying Oligocene succession, generating overpressure at ~10 Ma across the area of deposition encompassing three of the modelled wells: Maui-1 (Figs. 2.4c & 5.8b), Takapou-1 (Fig. 2.4c & 3.7b) and Waimanu-1 (Fig. 2.4b & I.1b).

Loading by the Mount Messenger Formation occurred during broadly the same time interval at all three wells, but the thickness of the underlying Eocene to Oligocene overpressured mudrocks varies dramatically (Fig. 2.4c), and consequently so does the magnitude of abnormal pressure generated. The Late Cretaceous to Oligocene stratigraphy in the Maui Field is predominantly sandstone, overlain by thin mudrocks of the Turi and Otaraoa formation's, which form the hydrocarbon seal. The coarse-grained nature and significant connectivity of the Eocene beds has inhibited the generation of significant overpressure, with basin modelling results showing ~500 psi (Fig. 5.8b), which is supported by calculated shale

pressures (Fig. 5.7). Direct wireline formation pressures from the entire field plot onto a hydrostatic gradient, meaning any overpressure that was present has laterally drained through highly permeable connected geobodies.

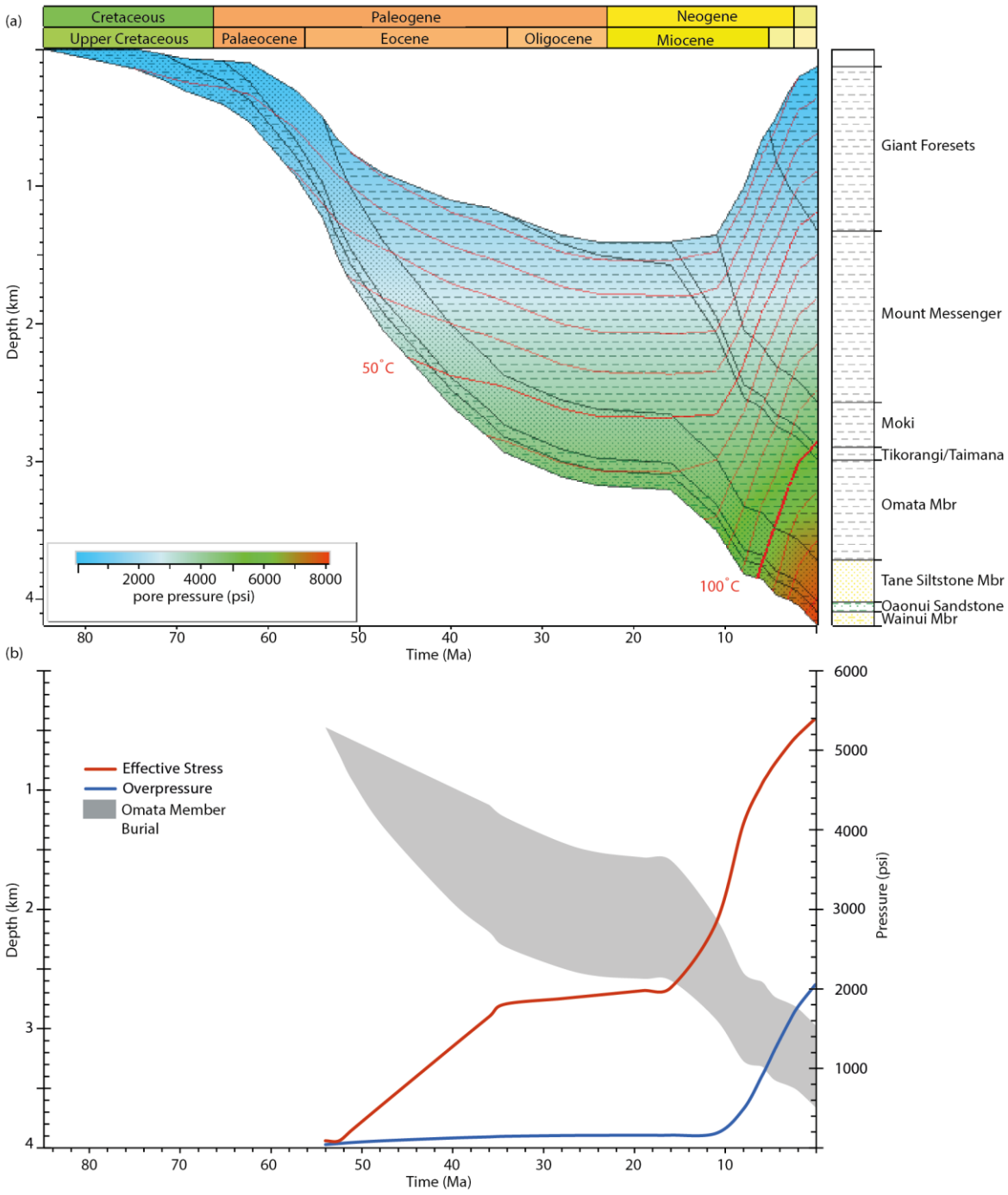

Figure 3.7. a) 1D burial history plot of Takapou-1 (PetroMod). Red lines are isotherms and colour overlay denotes pore pressure. b) Plot displaying the evolution of overpressure and effective stress with burial since the accumulation of the Omata Member.

Takapou-1 on the western Platform intercepted a significant thickness (734 m) of Turi Formation/Omata Member mudrocks. Model and shale derived pressures show this section to be ~2000 psi overpressured (Fig. I.5), but the underlying Palaeocene Tane Member and Cretaceous Wainui Member (Enclosure 1) are hydrostatic and ~500 psi overpressured, respectively (Fig. 2.4c). This pattern is indicative of lateral drainage that has been identified

at Tane-1 by Webster et al. (2011) in the same reservoir and shale interval. The increase of overpressure with depth in the Cretaceous section may be sourced from postulated underlying shales, which have been suggested as contributors to excess pressure at depth in Taranaki Basin (Webster et al., 2011).

3.3.1.4. Pliocene (Manaia Anticline {Kupe South-1 & Kapuni Deep-1)

Southern Taranaki Basin in the vicinity of the Kupe South Field (Enclosure I) experienced a significant hiatus in deposition after the Palaeocene, as sediments by passed the area and were deposited on the SW to NE trending Eocene palaeo-shoreline as the Kaimiro and Mangahewa formations (Martin et al., 1994). Water depth increased during the latest Eocene due to increased subsidence, leading to the accumulation of the Otaraoa Formation (Fig. I.6a). The onset of a limited amount of overpressure (~300 psi) began at ~20 Ma, due to loading by the Manganui Formation, but uplift and erosion in the Miocene led to some bleed-off of pressure (Fig. I.6b). The Toru Trough and Manaia Graben experienced a significant increase in subsidence during the Late Miocene to Early Pliocene when Urenui, Kiore and Matemateaonga formations accumulated as slope and shelfal deposits (Fig. 3.12d) (Kamp et al., 2004), leading to a second phase of increase in overpressure in the Otaraoa Formation from ~6 Ma (Fig. I.6b).

Model derived and calculated shale pressures show the Otaraoa Formation to be ~2000 psi overpressured, but the measured formation pressures are ~1000 psi (Fig. I.7). These pressure differences reflect lateral drainage across the Kupe South Field and the Manaia Anticline Palaeocene fairway (O'Neill et al., 2018, see Chapter IV).

3.3.1.5. Pleistocene (Tangaroa-1)

The Northern Taranaki Bight section of the Western Platform (Fig. 2.4d), has remained relatively quiescent since the Late Cretaceous aside from subsidence and accumulation of hemipelagic and a progradational succession onto it during the Pliocene and Pleistocene (King and Thrasher, 1996). The stratigraphic units are comprised of fine-grained facies, which enclose a Late Eocene redeposited sandstone succession (Tangaroa Formation; Gresko et al., 1990). Tangaroa-1 was drilled into a structural high to test the Tangaroa Formation, which was found to be 1642 psi overpressured (Fig. 2.4d).

Basin modelling results show a rapid increase in water depth from the Late Palaeocene to the Early Eocene in the vicinity of Tangaroa-1 with accumulation of bathyal marine mudrocks of the Turi Formation (Fig. 3.8a) (King and Thrasher, 1996). Sedimentation rates matched subsidence rates until the Manganui and Moki formations accumulated, which filled some of the accommodation space (Fig. 3.8a). Sedimentation rates steadily increased until the latest Miocene, when the marls of the Ariki Formation accumulated as a condensed section (Hansen and Kamp, 2004). During the Late Pliocene and Early Pleistocene, the Giant Foresets Formation prograded across the vicinity of Tangaroa-1 as a shelf-slope wedge, accumulating

~2000 m of mudrock at Tangaroa-1 (Baur et al., 2014), which rapidly loaded the undercompacted Turi Formation, leading to the generation of significant overpressure within the Turi Formation (Fig. 3.8b).

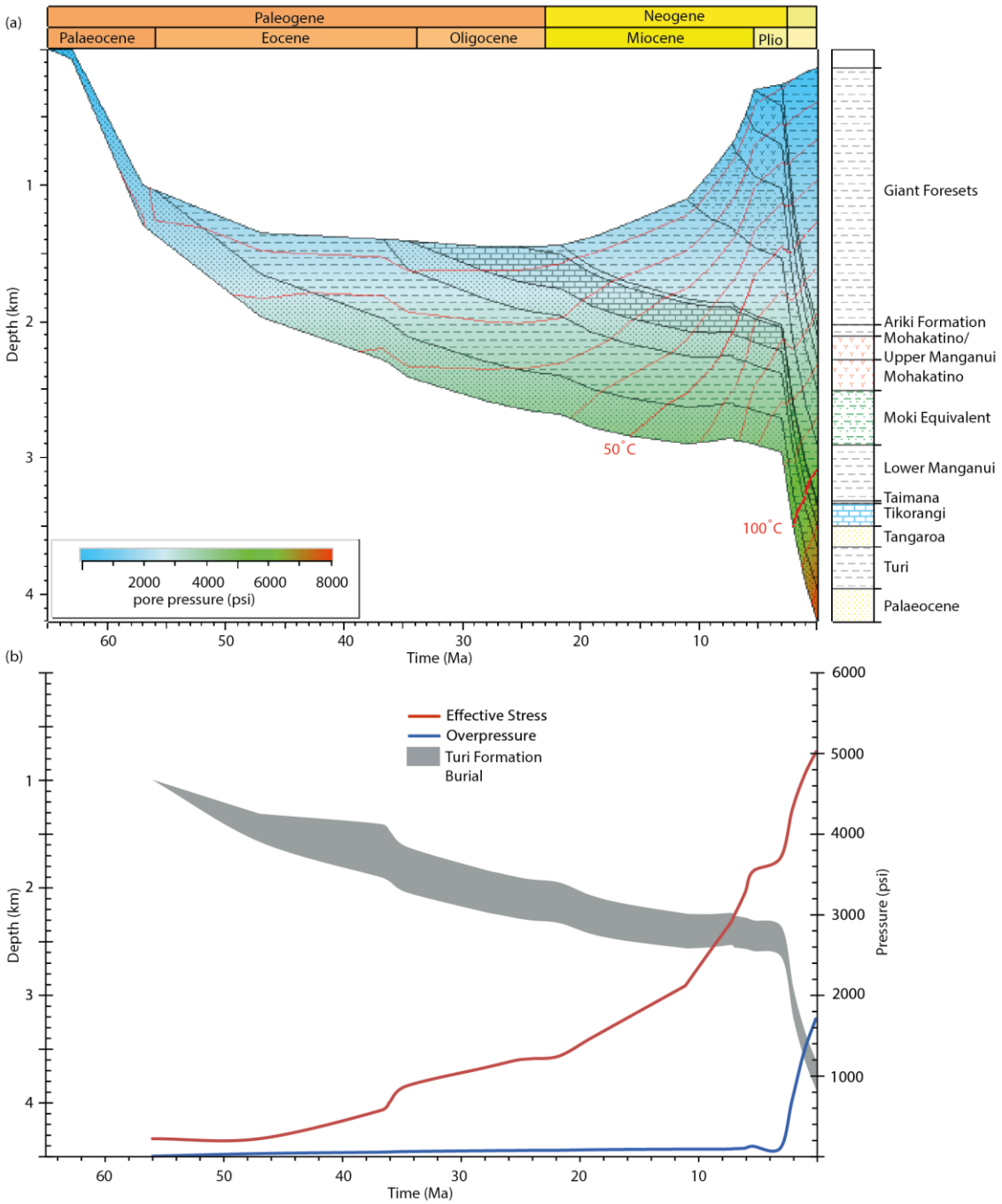

Figure 3.8. a) 1D burial history plot of Tangaroa-1(PetroMod). Red lines are isotherms and colour overlay denotes pore pressure. b) Plot displaying the evolution of overpressure and effective stress with burial since the deposition of the Farewell Formation.

Calculated shale pressures for the Turi Formation overestimate the measured pore pressure in the overlying Tangaroa Formation, but the overpressure increases up dip to 2122 psi in the Kora Field to the south-east. This trend is indicative of lateral transfer of pore pressure which can lead to elevated crestal pressure in dipping confined reservoirs (Yardley and Swarbrick, 2000). As previously discussed, this process has been identified in the Mangahewa Formation between Beluga-1 well and the McKee Field in the Tarata Thrust Zone (Fig. 2.15).

3.3.2. VERTICAL EFFECTIVE STRESS AND POROSITY

A basin-wide plot of average measured porosity per formation against maximum VES displays no clear relationships (Fig. 3.9a). Both high (20%) and low porosity (<10%) are present in reservoirs that have experienced high and low VES. The plot also displays no clear relationship between depth and average porosity or overpressure (Fig. 3.9b). Thin-section analysis has previously shown that reservoir quality is highly variable across the Taranaki Basin and that facies, grain size and burial history are the key control on porosity preservation at depth (Higgs et al., 2017, 2013, 2012; Martin et al., 1994; Smale et al., 1999; see also Chapter IV & V).

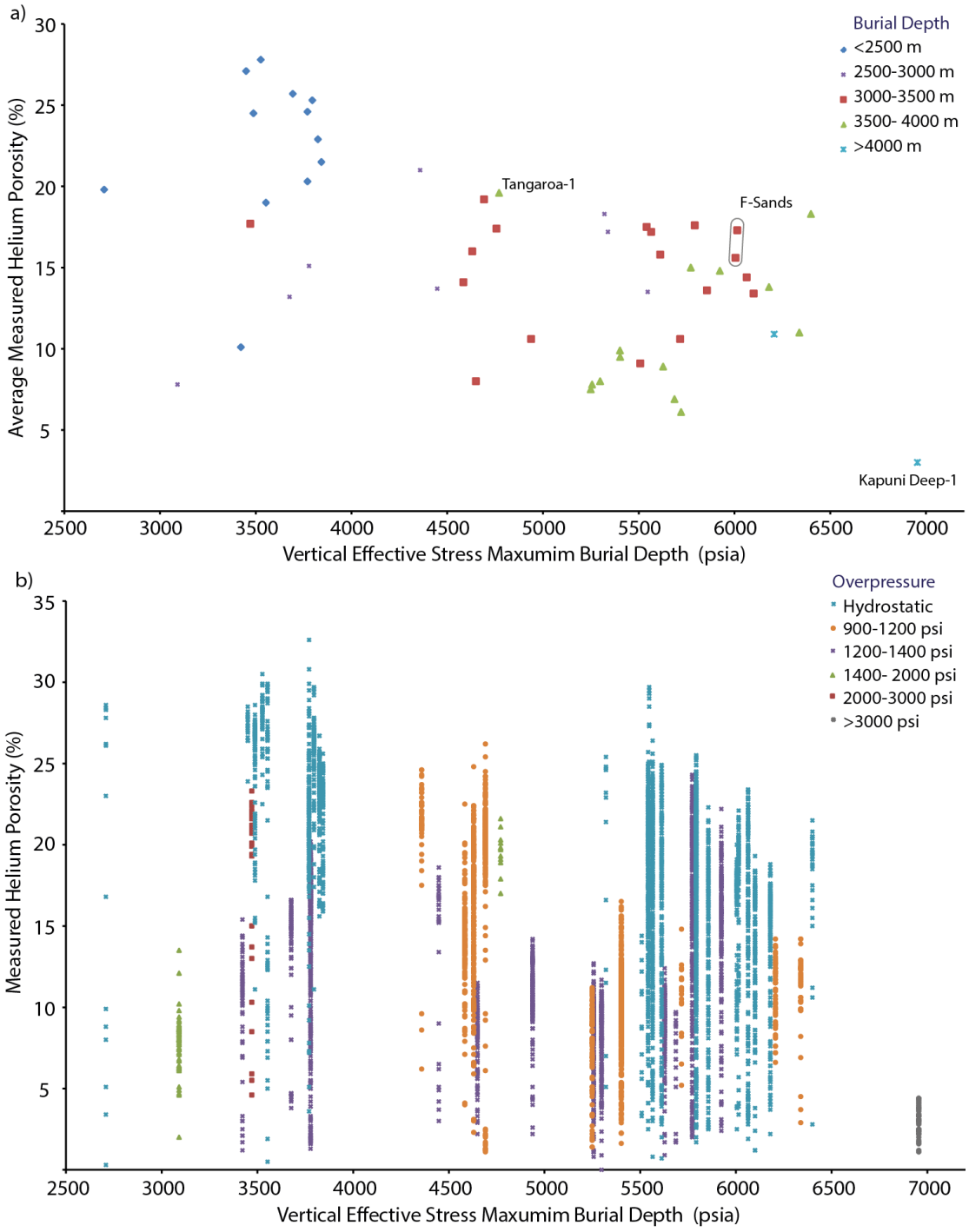

Figure 3.9. a) plot of average measured helium core porosity against vertical effective stress at maximum burial depth, coloured by depth; b) plot of helium core porosity against vertical effective stress at maximum burial depth, coloured by overpressure.

The one notable exception is the Late Eocene to Oligocene basin floor sandstone of the Tangaroa Formation, which shows a relatively elevated average porosity of 19.6 % when compared with their burial depth of ~4000 m. This high porosity is witnessed across the submarine fan sandstone from cores in both Tangaroa-1 well and the shallower Kora-4 well. Pleistocene to Miocene reservoirs are normally pressured across Taranaki Basin and in general have excellent reservoir quality due to limited compaction and relatively shallow burial (2500 mTVD) before the onset of chemical compaction (Smale et al., 1999). The exceptionally low porosity in Farewell Formation at Kapuni Deep-1 and the reservoir quality of the F-Sands in the Maui Field (Fig. 3.9a) will be discussed in chapters IV & V respectively.

3.4. DISCUSSION

3.4.1. TECTONOSTRATIGRAPHIC FORCING ON OVERPRESSURE EVOLUTION

The tectonostratigraphic evolution of a sedimentary basin plays a first order control on the initiation and development of abnormal pore pressures. Pore pressure evolution and distribution in the polyphase Pannonion Basin on the Great Hungarian Plain, has been explained through late-stage uplift and subsidence occurring coevally in different parts of the basin (Horváth, 1995). Rapid uplift and associated erosion of fractured basement plays during the Quaternary led to abnormal pressure at higher elevations, which have been maintained due to limited time for pore pressure re-equilibrium and through the presence of competent top seal (Horváth, 1995). In comparison, the Beaufort-Mackenzie Basin displays a history with initial high clastic input and rapid subsidence driving overpressure generation through disequilibrium compaction. Subsequent basin-wide contractional tectonics led to uplift/erosion, pore pressure re-equilibrium and the migration of depocentres and overpressure generation (Chen et al., 2010).

Differing overpressure generating mechanisms can operate during distinct periods of basin evolution, as shown in the Western Sichuan Basin: disequilibrium compaction (Late Triassic-end Jurassic), hydrocarbon generation (Early Jurassic-Neogene) and tectonic compression (since the Cretaceous) (Guo et al., 2012). The progradation of a sedimentary system in a basin-ward direction is coeval with the migration of the location of highest sedimentation rate and this generates overpressure through disequilibrium compaction (Tingay et al., 2005; Van Balen and Cloetingh, 1994; Zoccarato et al., 2018). Numerical modelling undertaken by Mello and Karner (1996) suggests that significant overpressures have been generated (and dissipated) at various times within the Gulf Of Mexico Basin during the Miocene–Quaternary, a consequence of rapid sediment deposition sourced from the Mississippi delta system.

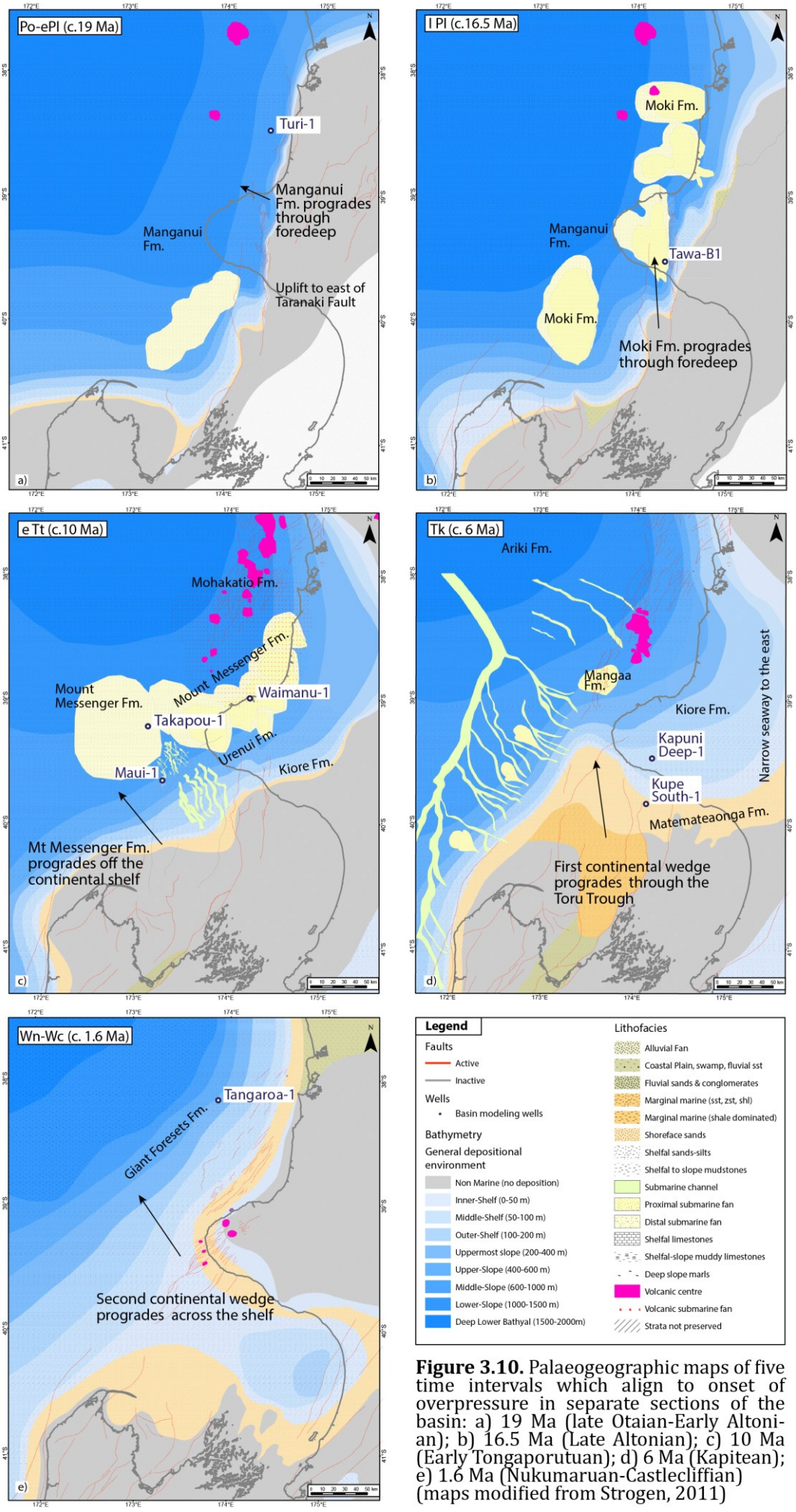

Figure 3.10. Palaeogeographic maps of five time intervals which align to onset of overpressure in separate sections of the basin: a) 19 Ma (late Otaian-Early Altonian); b) 16.5 Ma (Late Altonian); c) 10 Ma (Early Tongaporutuan); d) 6 Ma (Kapitean); e) 1.6 Ma (Nukumaruan-Castlecliffian) (maps modified from Strogen, 2011)

Crustal shortening focussed on Taranaki Fault during early phases in the development of the Australia-Pacific plate boundary through the eastern North Island's Hikurangi Margin (Kamp, 1986), led to the development of Taranaki Basin as a foreland basin during the Late Oligocene and Miocene (Holt and Stern, 1994; Stern and Davey, 1990). The overthrusting of basement wedges into eastern Taranaki Basin and uplift in the hinterland resulted in high rates of sediment input and deposition of a thick Neogene wedge that filled the foredeep during the Miocene (Fig. 3.2; Holt and Stern, 1994; King and Thrasher, 1992). The sedimentary system then progressively prograded in distinct phases northwest across the shelf during the Miocene and Plio-Pleistocene (Fig. 3.10 & 3.11; Kamp et al., 2004). These phases of basin development contributed significantly to the development of abnormal pressures across the basin (Fig. 3.4).

Early Miocene over-thrusting and displacement on Taranaki Fault was accompanied by a change from predominantly calcareous to terrigenous sedimentation across the basin and significant thickening of the Early Miocene stratigraphy adjacent to the fault by up to 200% (Fig. 3.2; King and Thrasher, 1996). During the Early Miocene on the modern-day Manganui Platform (Fig. 3.1) to the north of the basin, thrusting elevated the Herangi High, loading the underlying stratigraphy and generating accommodation space by subsidence. Subsequently, the bathyal terrigenous siltstone of the Manganui Formation accumulated within the foredeep (Fig. 3.10a) infilling some of the accommodation space (Kamp et al., 2014). The burial history of Turi-1 (Fig. 3.5a) displays the rapid Early Miocene loading of the underlying Turi Formation, leading to the earliest phase of overpressure generation in Taranaki Basin and of importance for stalling mechanical compaction and porosity loss.

The northern tip of the active section of the Taranaki Fault migrated southward during the Miocene (Stagpoole and Nicol, 2008), due to rotation of the plate boundary, which is consistent with the episodic migration southwards of younger depocentres in the hanging wall of the fault (Fig. 3.11; Kamp and Furlong, 2006; Stern et al., 2006, 1993). This southward migration of depocentres is also consistent with the southward migration of the onset of overpressure within the foredeep. By the mid-Miocene the focus of crustal shortening across Taranaki Fault and therefore generation of accommodation space had migrated to the modern-day southern Taranaki Peninsula, and that space was filled by progradation of the Manganui Formation through the foredeep, generating the abnormal pressures observed at Tawa-B1 well at 16 Ma (Fig. 3.10b & 3.11).

Stagpoole and Nicol (2008) argue that the main phases of basin development and deposition along strike in the fault hanging wall is linked to the episodic 'death' of the fault, as shown by the stepped decrease in the age of the sediments overlying the upper fault tip. They also suggest that fault displacement either produced uplift or significantly reduced subsidence, but when displacement terminated a period of subsidence and basin development began in

the hanging wall (Stagpoole and Nicol, 2008). This first occurs in the north and then moved progressively southward in Taranaki Basin (Fig. 3.11).

The cessation of Taranaki Fault displacement at ~20 Ma in the vicinity of Awakino township (Stagpoole and Nicol, 2008), onshore form Turi-1 well, coincides with accumulation of Manganui Formation and the onset of overpressure in the Turi Formation. As Taranaki Fault switched off southwards, this pattern is repeated, including continuing subsidence and sediment accumulation at 16 Ma in the vicinity of Hawera, coincides with overpressure generation at Tawa-B1 well (Fig. 3.11).

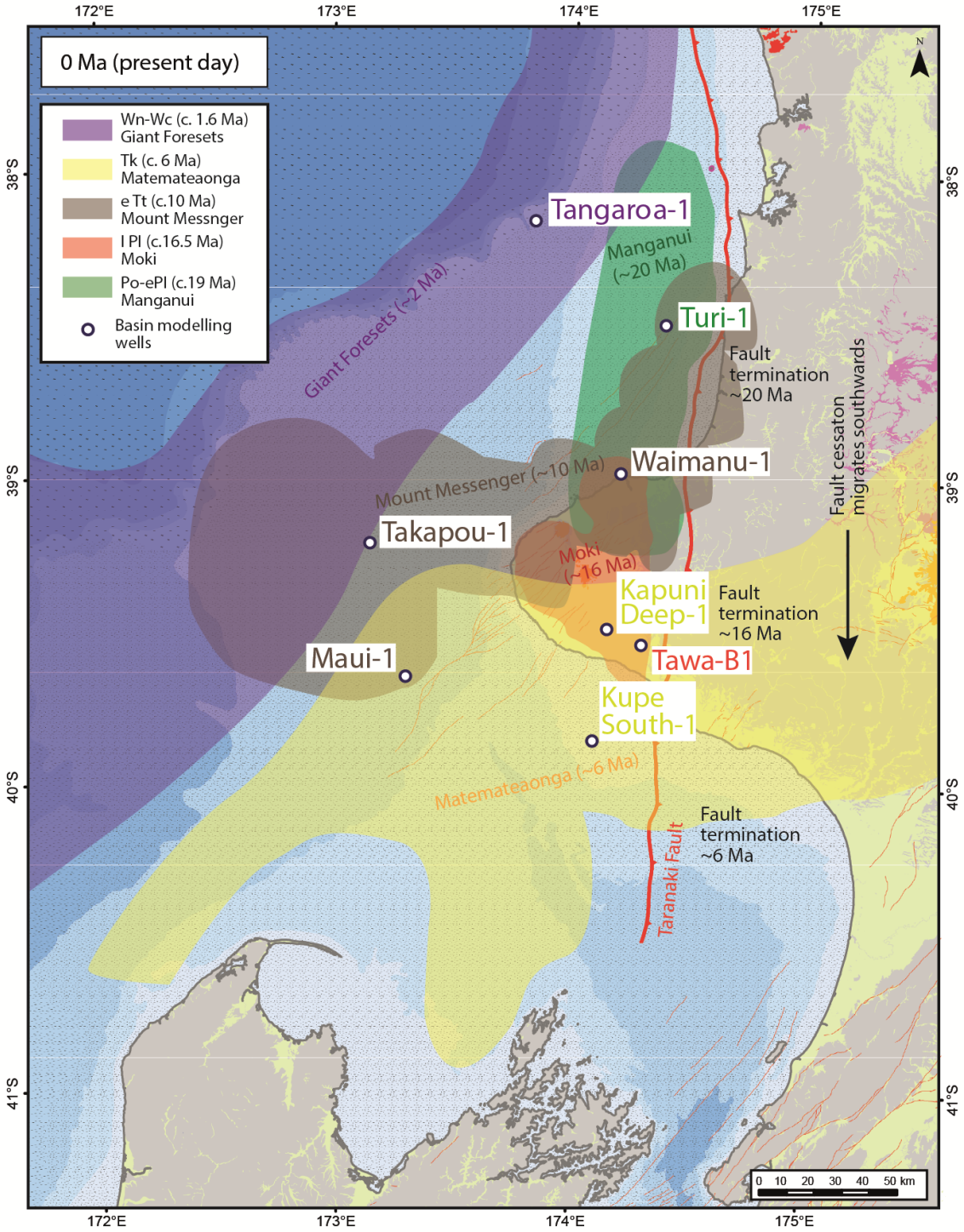

Figure 3.11. Compilation map of Taranaki Basin displaying basin modelling wells and zones covered by each phase of overpressure generation (map modified from Strogen, 2011)

Between 18-12 Ma subsidence continued and bathyal (>1000 m) environments persisted across central and northern parts of Taranaki Basin as it was undersupplied with sediment. This changed at ~12 Ma when inversion started in Southern Taranaki Basin and uplift and erosion of the Southern Alps started, substantially increasing from then onwards the supply of sediment to Taranaki Basin (Bull et al., 2018; Kamp et al., 2004). This resulted in north-westward progradation of a shelf-slope wedge within the basin involving Mount Messenger, Urenui, Kiore, and Matemateaonga formations (Fig. 3.10c) (Bull et al., 2018; Kamp et al., 2004). This sediment was sourced from the erosion of Torlesse Terrane and Alpine Schist in the Southern Alps (Kamp and Tippett, 1993), and was fed via northward-flowing rivers across basement topography (Kamp et al., 2004). This continental wedge loaded the Oligocene and underlying succession, generating a third phase of overpressure at ~10 Ma.

During late stages in the inversion of Southern Taranaki Basin, the extent of uplift reached as far north as the Maui Field. Urenui and Kiore formations accumulated as a shelf-slope wedge across the Taranaki Basin and farther to the west and onto parts of the Western Platform (Bull et al., 2018; Kamp et al., 2004). At the end of the intra-basin southern inversion (~6 Ma), the rate of sediment supply markedly reduced, leaving Northern Taranaki Basin starved of terrigenous sediment, leading to accumulation of condensed facies (Ariki Formation marl) (Hansen and Kamp, 2004). Takapou-1 well (Fig. I.5) on the Western Platform was well located to receive the thick wedge of Urenui and Kiore formations, which also accumulated south of southern Taranaki Peninsula in the Kupe Field and across the Peninsula including the Kapuni Field. The loading of this latest Miocene succession generated the fourth phase of overpressure in Otaraoa Formation in the Kupe South and Kapuni Fields at ~6 Ma.

The Northern Graben, which subsided under extension during the latest Miocene and Early Pliocene, acted as a local sink for sediment accumulation during the Middle Pliocene and early Pleistocene, particularly from 3 to 1 Ma (Manganapian and Nukumaruan stages). During this period terrigenous sedimentation rates exceeded subsidence rates in Northern Taranaki Bight, including the Northern Graben, causing the prograding shelf-slope wedge to spill over onto the Western Stable Platform (Hansen and Kamp, 2004). This system prograded north-westward (Fig. 3.10e & 3.11) resulting in a 2 km thick sequence of clinoforms and top sets (shelf sediments) in Tangaroa-1 (Fig. I.8) and in isopach maps from Baur et al. (2014). This significant loading led to the latest onset of overpressure in the basin at ~2 Ma at Tangaroa-1 well.

3.4.2. LATERAL DRAINAGE

Lateral drainage of fluid pressure is a well-established phenomenon in the Taranaki Basin but has only been identified through post drill analysis. The prediction of lateral drainage ahead of the bit is incredibly useful as mudweights can be adjusted accordingly to avoid invasion that can destroy the reservoir and to reduce well costs. A number of wells on the western platform have been drilled significantly overbalanced (Tane-1, Takapou-1 & Terrace-1), which could have been avoided with proper analysis of offset well data.

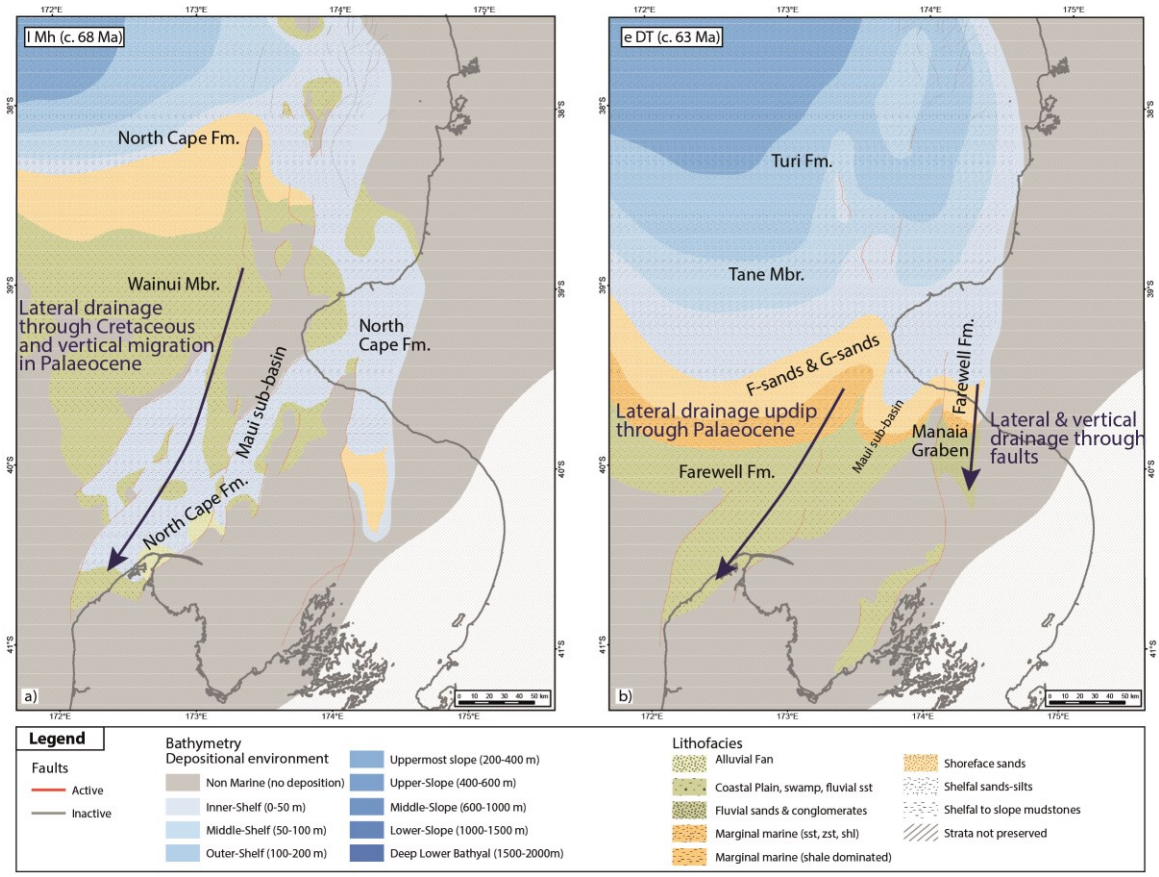

Figure 3.12. Palaeogeographic maps showing lateral drainage pathways in the Cretaceous and Palaeocene: a) 68 Ma (Late Haumurian) & b) 63 Ma (early Teurian) (maps modified from Strogen, 2011)

Palaeogeographic maps by Strogen (2011) display extensive Cretaceous and Palaeocene sandstone extending from wells drilled on the Western Platform to outcrops on the sea floor and the northern tip of the South Island (Fig. 3.12). Two wells that have intercepted the basement on the Western Platform, Kopuwai-1 and Taranga-1 (Enclosure I), both displayed oil bearing fractures which if connected could act as further pathways for lateral fluid flow. Gas chimneys associated vertical fluid flow in predominantly late stage (~3.6 Ma) normal faults, identified by Ilg et al. (2012) in the Southern Taranaki Basin, will also act as conduits for lateral drainage of pressure. Connected stratigraphy together with open faults combine to form high permeability pathways draining any excess pressure up-dip towards the south and southwest, producing the hydrostatic conditions intercepted by wells across the Southern Taranaki Inversion Zone and Western Platform. Lateral drainage and the subsequent

maintenance of overpressure in reservoirs of the Manaia Anticline will be discussed and illustrated in section 5.4.1.

3.4.3. VES DEVELOPMENT AND RESERVOIR QUALITY

Porosity preservation by pore fluid overpressure has been the subject of several studies (e.g., (Gluyas and Cade, 1997; Jeans, 1994; Ramm and Bjørlykke, 1994), however the development and maintenance of overpressure and the evolution of vertical effective stress throughout burial history have not been considered (Stricker, 2016). If VES is to act in arresting porosity loss through mechanical compaction, dewatering must be inhibited and excess pore pressure must develop at shallow depth and ideally early in the burial history and be maintained continuously throughout burial (e.g. Stricker et al., 2016; Sathar & Jones 2016; Oye et al., 2018). Late development of overpressure at greater depth by fluid transfer or hydrocarbon charge cannot be associated with a reduction in mechanical compaction (Swarbrick and Osborne, 1998).

The coarse nature and thus high permeability of the Cretaceous-Eocene proven hydrocarbon reservoirs in the south and east of the basin, promotes normal compaction and dewatering, inhibiting the formation of low VES conditions. High effective stress conditions prevail throughout burial and are maintained at depth across most reservoirs in the Taranaki Basin, destroying porosity at shallow depths through mechanical compaction. The potential for gas generation at depth and lateral transfer in tilted reservoirs, as discussed in sections 2.4.4 and 2.4.3.1, could not aid in the lessening of mechanical compaction. These findings highlight the need to include stress histories when making predictions of diagenesis and reservoir quality of clastic reservoirs, which will be discussed using a case study of the Farewell Formation at Kapuni Deep-1 in the following chapter.

Sandstone bodies with high primary porosities encased within undercompacted mudrocks have a restricted ability to dewater; which when coupled with a shallow onset of overpressure can maintain anomalously high porosity to depth. This configuration is present in the Northern Taranaki Bight where the basin floor fans of the Oligocene Tangaroa Formation are sealed within the Otaraoa and Turi formations (Gresko et al., 1990). Abnormal pressures did not develop in Northern Taranaki Bight until the Pleistocene (~2 Ma), though as discussed, depth of onset is far more crucial. The Tangaroa Formation subsided very slowly in bathyal water depths experiencing relatively low VES (<2000 psi) conditions for the first 33 M.y. of burial (Fig. 3.8b), allowing for limited porosity loss through mechanical compaction. The onset of overpressure occurred at ~2000 m, above the chemical compaction window, so the onset and subsequent development of overpressure/low VES could act in arresting porosity loss. These observations could explain why the average measured porosity for the Tangaroa sandstone beds are anomalously high when compared with other reservoirs at the same depth of burial.

The Turi Fault Zone is characterised by rapidly subsided narrow fault-bounded grabens, where low VES conditions can develop at shallow depth (<2000 m) and be maintained through burial, as shown in Turi-1 (Fig. 3.5b). These conditions are very conducive to porosity preservation, though the limiting factors in this region are the presence of a thick enough reservoir sequence and restricted migration pathways for hydrocarbon charging. If further deep-water sandstone beds are discovered on the Western Platform, Manganui Platform or in the Northern Taranaki Bight, charged with hydrocarbons then they could be attractive prospects.

3.5. CONCLUSIONS

1. The initial onset of overpressure in the Taranaki Basin occurred at ~22 Ma, driven by formation and initial filling of a foreland basin in the north-eastern parts of Taranaki Basin. The foredeep progressively migrated southwards, which is consistent with the southward migration of overpressure generation within the foredeep during the early to mid-Miocene.
2. Three subsequent phases of overpressure generation are triggered due to loading from a series of sedimentary sequences that prograde across the continental shelf during Late Miocene to Pleistocene.
3. No clear relationship between vertical effective stress and porosity in reservoir sandstone has been identified in the Taranaki Basin.
4. The comparison of calculated shale pressure and basin modelling derived pressure has highlighted the presence of lateral drainage in the Western Platform, Southern Taranaki Inversion and Manaia Anticline. Lateral fluid flow is controlled by compartmentalisation by faults acting as barriers and or conduits.
5. Sandstone bodies with high primary porosities encased within undercompacted mudrocks grade lithologies that have a shallow onset of overpressure can maintain anomalously high porosity to depth.

CHAPTER IV:

PORE PRESSURE AND RESERVOIR QUALITY EVOLUTION IN THE DEEP TARANAKI BASIN

This chapter has been published in the journal *Marine and Petroleum Geology:*

O'Neill, S.R., Jones, S.J., Kamp, P.J.J., Swarbrick, R.E., Gluyas, J.G., 2018. Pore pressure and reservoir quality evolution in the deep Taranaki Basin, New Zealand. Mar. Pet. Geol. 98, 815–835. doi:10.1016/J.MARPETGEO.2018.08.038

4.1. INTRODUCTION

Eocene clastic reservoirs within the Manaia Graben of Taranaki Basin, New Zealand (Fig. 4.1), display enhanced reservoir quality through local preservation of secondary porosity, generated by feldspar dissolution due to migration of large volumes of CO_2 rich fluids through permeable beds (Higgs et al., 2013). The Kapuni gas condensate field (Fig. 4.1 & 4.2) in the Manaia Anticline sub-basin produces natural gas (methane) and CO_2 from two Eocene reservoirs. In 1983 an exploration well, Kapuni Deep-1, was drilled in an attempt to increase the field's reserves by testing the reservoir potential of the deeply buried and overpressured (>5000 m, >3000 psi) Palaeocene Farewell Formation (Enclosure 2). As the CO_2 content is partly sourced from underlying Cretaceous strata (Enclosure 2 & Fig. 4.2), it could be expected that the Farewell Formation would display similar enhanced reservoir quality due to the up-dip migration of CO_2 towards the crest of the Kapuni structure.

Kapuni Deep-1 encountered sandstone beds in the Farewell Formation with extremely poor reservoir quality, exhibiting a measured porosity of between 1-4.5% (Fig. 4.3d) and a permeability of 0.1-0.25 mD. Measured helium core plug porosity data for Farewell Formation reservoirs from across the Taranaki Basin (Higgs et al., 2012b) and the associated compaction curves for varying ductile grain contents (Worden et al., 1997) are shown in Figure 4.3d. Since the Farewell Formation at Kapuni Deep-1 is comprised of 5% ductile grains, measured porosity data are significantly off trend, and display anomalously low porosity for its current burial depth. The compaction curves do not account for the impact of diagenetic cements or effective stress history; these aspects and others will be discussed when investigating mechanisms for the exceptionally low reservoir quality of the sandstone beds in the Farewell Formation.

Hydrocarbon producing basins that display shallow onset and the maintenance of high pore fluid pressure (i.e. low vertical effective stress (VES)) have been shown to preserve anomalously high porosity (>30%) at significant depth (>5000 m) by lessening the impact of mechanical compaction (Grant et al., 2014; Nguyen et al., 2013; Sathar and Jones, 2016; Stricker et al., 2016). In this chapter a one dimensional basin model has been constructed to investigate the onset and subsequent development of overpressure, compaction and the increase of temperature through burial. Pressure data reported for Kapuni Deep-1 are used to investigate vertical pressure distribution in the section encountered by the well and to calibrate the basin modelling parameters. A combination of approaches are used to resolve the diagenetic paragenesis of the Farewell Formation for improved understanding of porosity development in the deeper parts (>4500 mTVD) of the underexplored areas within the Taranaki Basin. More generally this work aims to contribute to improved understanding of the relationship between overpressure and reservoir quality in mature polyphase deformational basins and potential indicators of reservoir quality within them.

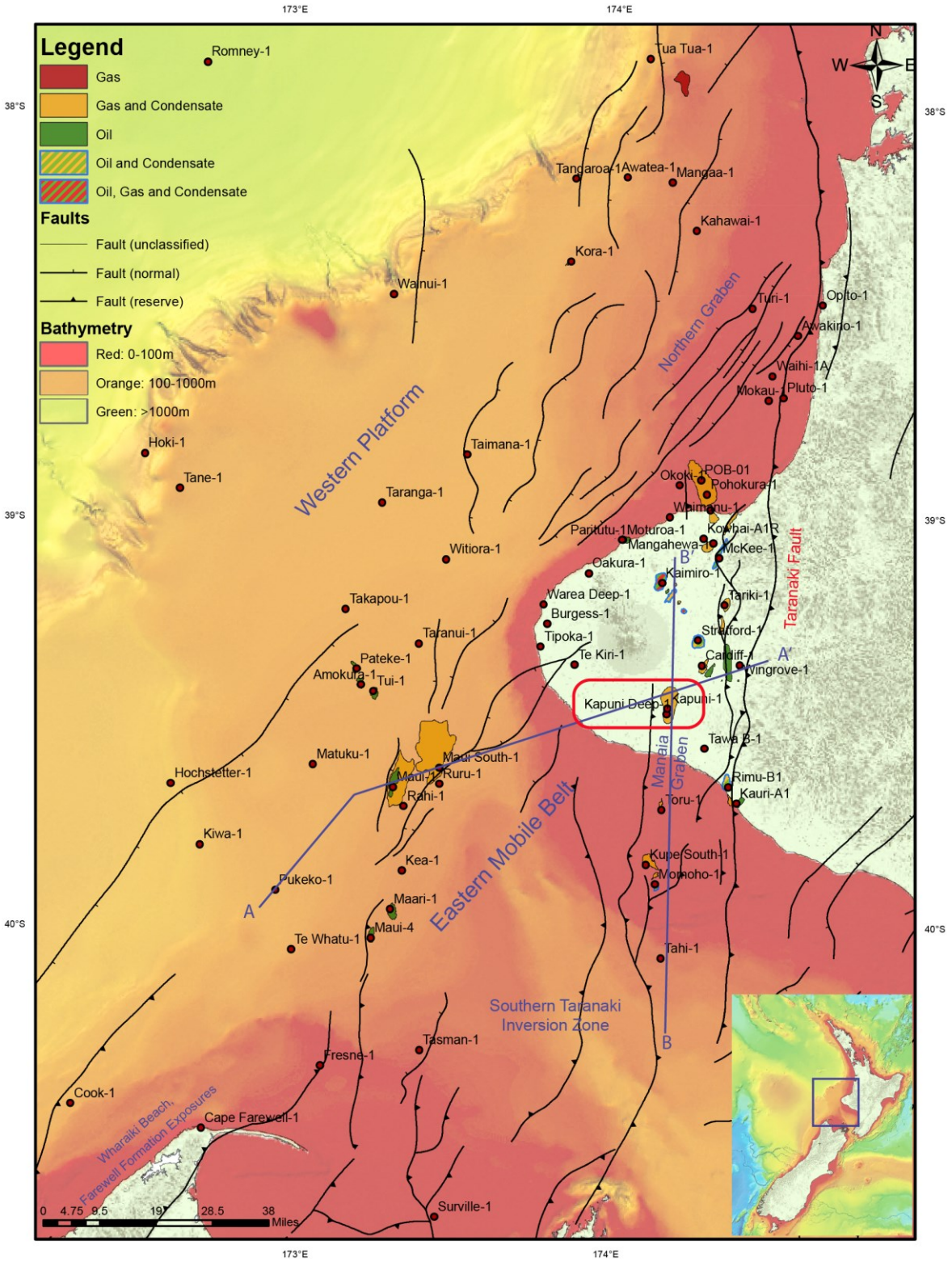

Figure 4.1. Map of Taranaki Basin displaying key wells, producing fields, structure and bathymetry. For location of line A-A' see Fig. 4.2 and line B-B' see Fig. 4.13. Red Box – location of Kapuni Field and Kapuni Deep-1 (bathymetry after Mitchell et al. 2012).

4.1.1. Geological setting of Kapuni Field

The Kapuni Field is situated in the Eastern Mobile Belt which contains significant shortening structures such as Taranaki Fault, and the Manaia Anticline, where Kapuni Deep-1 was drilled (Fig. 4.2). The Late Miocene inversion structures formed parallel to the major basin bounding Taranaki Fault, producing several anticlines that trap hydrocarbons in the Eocene Kapuni Group, which is comprised of a transgressive sequence of alternating sandstone, shale and

coal beds, deposited under fluvial and fluvio-estuarine conditions (Voggenreiter, 1993). Thickening of strata against the Manaia fault (Fig. 1 & 3) identified by Stagpoole & Nicol (2008) suggests that displacement may have started during the Late Eocene, but certainly by the Early Miocene (Kamp et al., 2014; King and Thrasher, 1996; Nelson et al., 1994). These inversion structures, which plunge to the north, formed through reactivation of Late Cretaceous-Palaeocene normal faults (Crowhurst et al., 2002).

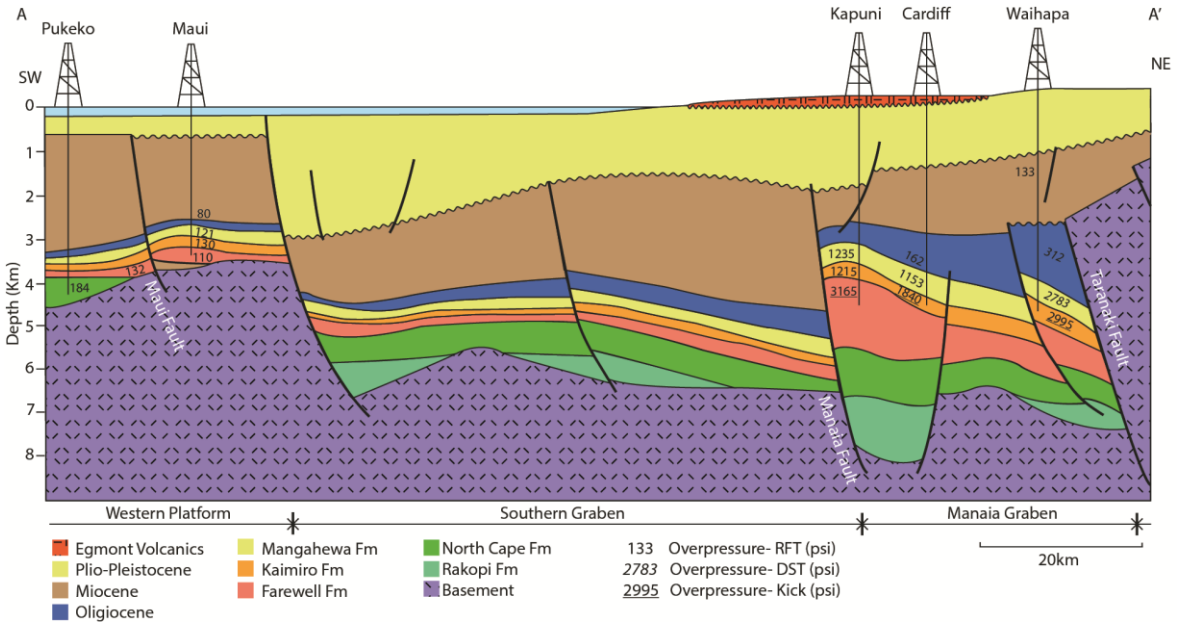

Figure 4.2. Cross section (line A-A', Fig. 4.1) displays lateral and vertical pressure variations (Modified from (King and Thrasher, 1996)

Farewell Formation crops out at Wharaiki Beach and the surrounding ridge in north-western South Island as a result of inversion on one of these types of faults (Fig. 4.1). The eastern margin of North Taranaki Basin has been uplifted and eroded since the Early Pliocene as a result of doming of central North Island, preceding the 1.6 Ma outbreak of andesitic and silicic volcanism in Taupo Volcanic Zone (Armstrong and Chapman, 1999; Kamp et al., 2004). There has been ~300-400 m of exhumation of Late Pliocene section over the Kapuni Field during the past ~1 M.y. (Kamp et al., 2004).

4.1.2. The Farewell Formation

The Farewell Formation is a Palaeocene fluvial sandstone, extending NE-SW across central parts of Taranaki Basin (Strogen, 2011; 2017). It was sourced from erosion of crystalline basement in north western South Island and structural highs within what is now Taranaki Basin, including granite batholiths of Cretaceous and Devonian age and Palaeozoic schists, quartzites and volcanics (Rattenbury et al., 1998). Farewell Formation has been interpreted as chiefly being deposited in fluvial, coastal plain and shore face to inner shelf environments (Strogen, 2011). To the north (down depositional dip) the formation inter-fingers with neritic to bathyal mudrock facies of Turi Formation, while to the north east it grades into shoreface facies deposited in a marginal marine environment, designated as F-sands (Strogen, 2011).

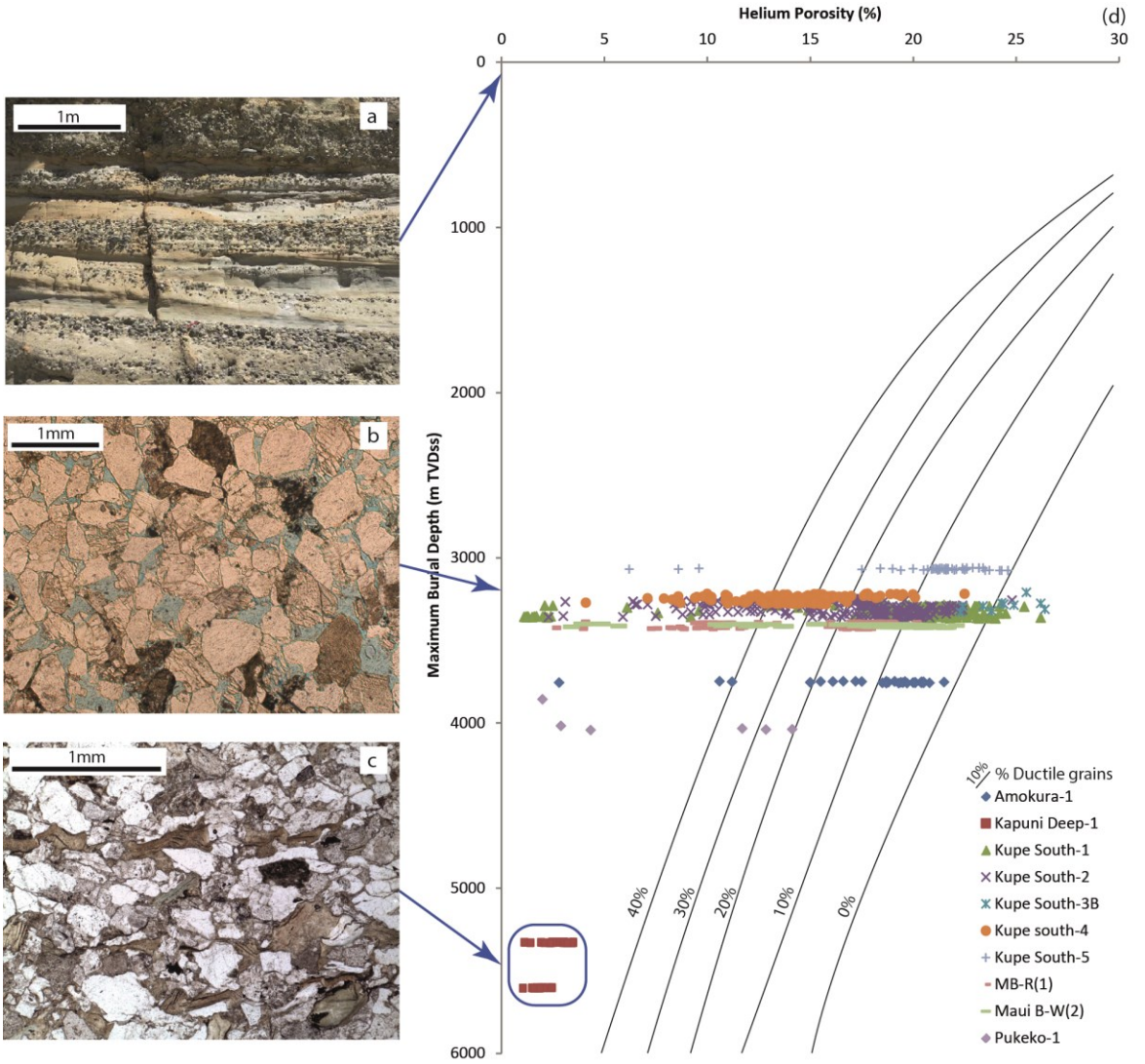

Figure 4.3. a) Gravel conglomerate beds in Farewell Formation at Whariki Beach, Kahurangi National Park, Northwest Nelson (see Fig. 4.1 for location). b) Thin section micrograph of Farewell Formation at Kupe South-1 well displaying >30% porosity (3100 mTVDss PPL). c) Thin section micrograph of Farewell Formation at Kapuni Deep-1 well displaying <5 % porosity (5335 mTVDss). d) Measured helium core plug porosity depth plot of Farewell Formation reservoirs (Compaction curves plotted for sandstones with varying ductile grain contents [0%, 10%, 20%, 30%, 40% from right to left]). Porosity-depth plot (after Trevena and Clark, 1986) compared to modelled trends. Porosity loss with depth has been modelled as a function of ductile sand content (after Atkinson and Bransby, 1978). No account has been taken of the effects of overpressure or the growth of mineral cements.

Exposures of Farewell Formation (Fig. 4.1) in coastal sections in Kahurangi National Park (NW Nelson) display multi-stacked multilateral sand bodies with abundant pebble-cobble grade beds (Fig. 4.3a) and coal seams of up to 2 m thick. These coal seams and others of Late Cretaceous age are postulated to be the source of oil and gas in productive fields within Taranaki Basin (Killops et al., 1998; King and Thrasher, 1996).

4.1.2.1. RESERVOIR STRATIGRAPHY

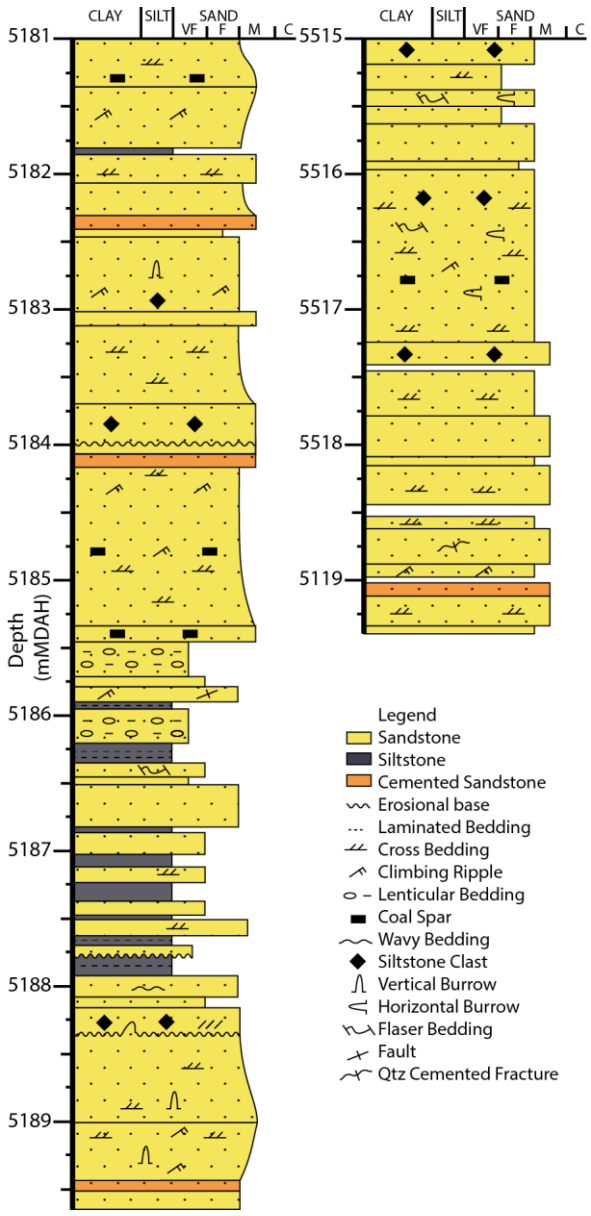

Farewell Formation forms the primary reservoir for the Kupe South Field in southern Taranaki Basin and its diagenetic history has previously been investigated by Martin et al., (1994). Farewell Formation at Kupe South has been subdivided into four seismically defined (A-D sands) intervals by Schmidt & Robinson (1989). The lower two of these (A and B sands) are hydrocarbon-bearing and have been further classified into upper and lower sands by Martin et al., (1994) based on petrological differences. The lower/B sand porosity and permeability is controlled predominantly by grain size and the presence of chlorite/smectite, whereas the upper/A sand is controlled by kaolinite content.

Figure 4.4. Sedimentary log through both of the Farewell Formation cores from Kapuni Deep- (Burn et al., 1995; STOS, 1984).

The Farewell Formation in Kupe Field is close to 90% net:gross, while mud log cuttings collected from the Farewell interval at Kapuni Deep-1 indicate a lower net:gross of ~80%, though some cored sections display higher values (Fig. 4.4). The lack of core collected in the Farewell Formation on the Taranaki Peninsula does not allow for the identification of specific units noted in the Kupe Field. Oil shows were encountered between 5446–5520 m in Kapuni Deep-1, and fractures in core at this depth display good yellow-green fluorescence and dark brown oil staining (STOS, 1984). Core analysis results showed the reservoir to be tight (0.1 mD), which together with dipmeter data from the cored interval suggests that shows are associated with fractures. Oil charged micro-fractures have apertures of up to 1.5 mm. Source rock intervals in Kapuni Deep-1 are confined to interbedded coals within the Farewell Formation, which are vitrinite rich and gas prone, but modelling has shown them to be mature for oil since ~2 Ma (Higgs et al., 2013).

4.2. METHODOLOGY

4.2.1. SAMPLING

In Kapuni Deep-1, approximately 1700 m of Farewell Formation was encountered and two conventional cores (Fig. 4.4) were cut at 5181-89 & 5515-19.4 mMDAH (measured depth along hole). Seventeen core samples were collected from sandstone beds in the upper (11) and lower core (6) of Kapuni Deep-1. The samples were predominantly taken from sections of clean sandstone with a lack of mudrock or coal laminae. Thin sections of these were produced for transmitted light microscopy, SEM and QEMSCAN (Quantitative Evaluation of Minerals by SCANning electron microscopy) analysis; as well as fluid inclusion wafers and rock chips for x-ray diffraction analysis. Twelve polished thin sections were obtained from the New Zealand Petroleum & Minerals collection. Petrophysical wireline data acquired over the cored intervals are representative of the Farewell Formation below 5000 mTVDgl (Total Vertical Depth below ground level).

4.2.2. PETROGRAPHIC ANALYSIS

Samples were analysed using transmitted-light microscopy on impregnated thin sections and modal analysis was undertaken on all samples to ascertain mineralogy (300 counts per section). The resulting data were used to calculate intergranular volume (IGV) (Paxton et al., 2002), porosity loss through mechanical compaction (COPL) and porosity loss by cementation (CEPL) (Lundegard, 1992):

$$COPL = P_i - \left(\frac{(100 - P_i)P_{mc}}{100 - P_{mc}}\right)$$

$$CEPL = (P_i - COPL)\left(\frac{C}{P_{mc}}\right)$$

where Pi is the initial or depositional porosity and Pmc is the intergranular volume or minus-cement porosity calculated by subtracting the total cement volume (C) from the total optical primary porosity (Po). The calculated COPL and CEPL are accurate if three conditions are met. First, the assumed initial porosity (Pi) must be correct. Second, the amount of cement derived by local grain dissolution must be negligible or known. And third, the amount of framework mass exported by grain dissolution must be negligible or known (Lundegard, 1992). The initial or depositional porosity of Farewell Formation has been estimated as 42% (Pryor, 1973).

All thin sections were highly polished to 30 μm and coated with 30 nm of carbon before analysis by a Hitachi SU-70 field emission scanning electron microscope (SEM) equipped with an energy-dispersive detector (EDS). Backscatter scanning electron microscopy of thin sections was conducted at acceleration voltages of 15 kV with a beam current of 0.6 nA. The SEM-EDS assembly was used for rapid identification of chemical species and their orientation in the sample. Scanning electron microscopy was undertaken on selected samples, providing

additional information on the pore-system geometry, authigenic mineralogy, and paragenetic relationships. The analysis was undertaken on gold palladium coated, freshly broken samples glued onto aluminium stubs with silver paint. Cathodoluminescence analysis was undertaken on selected thin sections with visible macro quartz overgrowths using a Gata MonoCL system with a panchromatic imaging mode operated at 15 kV. QEMSCAN data were collected on one representative sample depth (5518.1 mMDAH) from the lower core to supplement XRD (x-ray diffraction), scanning electron microscopy and modal analysis. QEMSCAN analyses measures and identifies minerals within a defined sample area, using a scanning electron microscope (SEM) fitted with four light element x-ray energy dispersive spectrometer detectors, allowing for fast, quantitative, and repeatable mineralogical and rock texture analyses (Higgs et al., 2015).

Microthermometry was conducted on doubly polished detached wafers to determine the conditions of cementation and evidence for formation water salinity. Fragments were cut from doubly polished rock wafers. The wafers were firstly checked under incident UV on a petrographic microscope to determine which ones contained petroleum inclusions, as well as under transmitted light to determine the distribution of both aqueous and non-aqueous fluid inclusions for subsequent analyses. The fluid inclusion and x-ray diffraction analyses were undertaken following the methodology as outlined in Stricker et al. (2018).

4.2.3. ONE-DIMENSIONAL BURIAL HISTORY MODELLING

Pore pressure evolution within the stratigraphy intersected by Kapuni Deep-1 was modelled in one dimension using Schlumberger's PetroMod (V. 2015) software. The burial model uses present-day well stratigraphy provided by the Kapuni Field operator, Shell Todd Oilfield Services and lithologies created from mud log cuttings data in the well completion report (STOS, 1984). The model was calibrated against corrected bottom hole data for the Kapuni Field (Rob Funnel pers. comm. 2017), measured formation pressures and helium porosity (Figs. 4.5c & 4.6b) (STOS, 1984). Further information on methodology for one-dimensional modelling can be found in Chapter III, section 3.2.1.

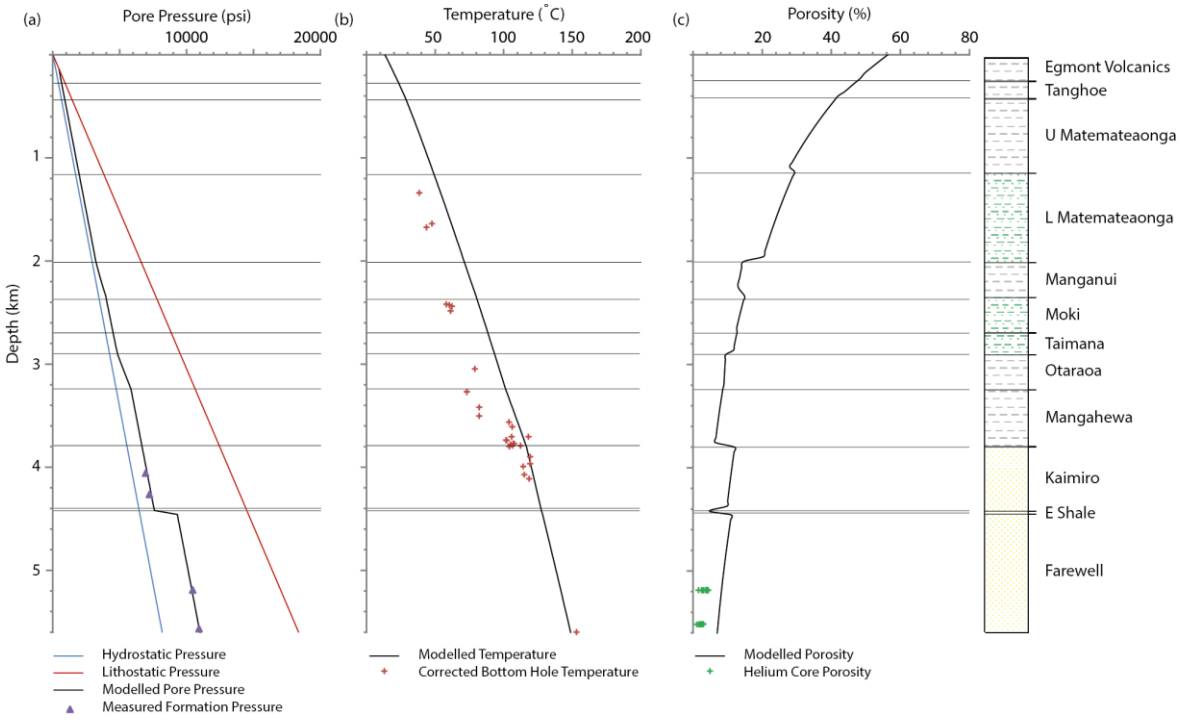

Figure 4.5. Calibration data for 1D basin model for Kapuni Deep-1 well. a) Plot of modelled and measured formation pressure gradient against depth. b) Plot of modelled formation temperature and corrected bottom hole temperature against depth. c) Plot of modelled porosity and measured helium core porosity from the Farewell Formation.

4.3. RESULTS

4.3.1. FAREWELL SANDSTONE COMPOSITION

The Farewell Formation at Kapuni Deep can be characterised as a sub-arkosic arenite (Fig. 4.6a & 4.7d) with abundant quartz (av. 47%) and feldspar (av. 21%); rock fragments of granite, schist, arenite and volcanics, make up av. 5% of the grains (Table 4.1). The detrital grains range in size from very fine to fine sand and are predominately angular to sub-angular, with minor intervals comprised of medium sand. There are calcite cemented zones up to 10 cm thick (Fig. 4.4) and primary pore filling authigenic clay minerals that form between 3-10% of the rock (Table 4.1). Detrital micas are present in most sections varying between 1-6% in abundance (Table 4.1), with high percentages occurring in mudrock rich sections (Fig. 4.7c). Micas can vary between being undeformed to heavily deformed. Detrital mud clasts are most prevalent in mudrock rich samples forming up to 8% abundance (Table 4.1). QEMSCAN (Fig. 4.7c & 4.7d) and SEM-EDS analyses identified the presence of detrital titanium oxide (1-3%). Significant replacement of detrital grains by clay and carbonate cement occurs in all samples. Rare hydrocarbon streaks are present within primary porosity.

Core logs (Fig. 4.4) and thin sections demonstrate that sandstone beds are interbedded with thin siltstone, mudstone and coal beds at millimetre to tens of centimetre scale, possibly representing a marsh or floodplain within a palaeo braided river system (Strogen, 2011). Siltstone clasts up to 5cm in diameter are common within sandstone beds; as are sandstone lenticles within mudrock horizons. Many of the mudrock horizons have convolute bedding,

which could be attributed to sediment loading, slumping, liquefaction or disruption by plant roots.

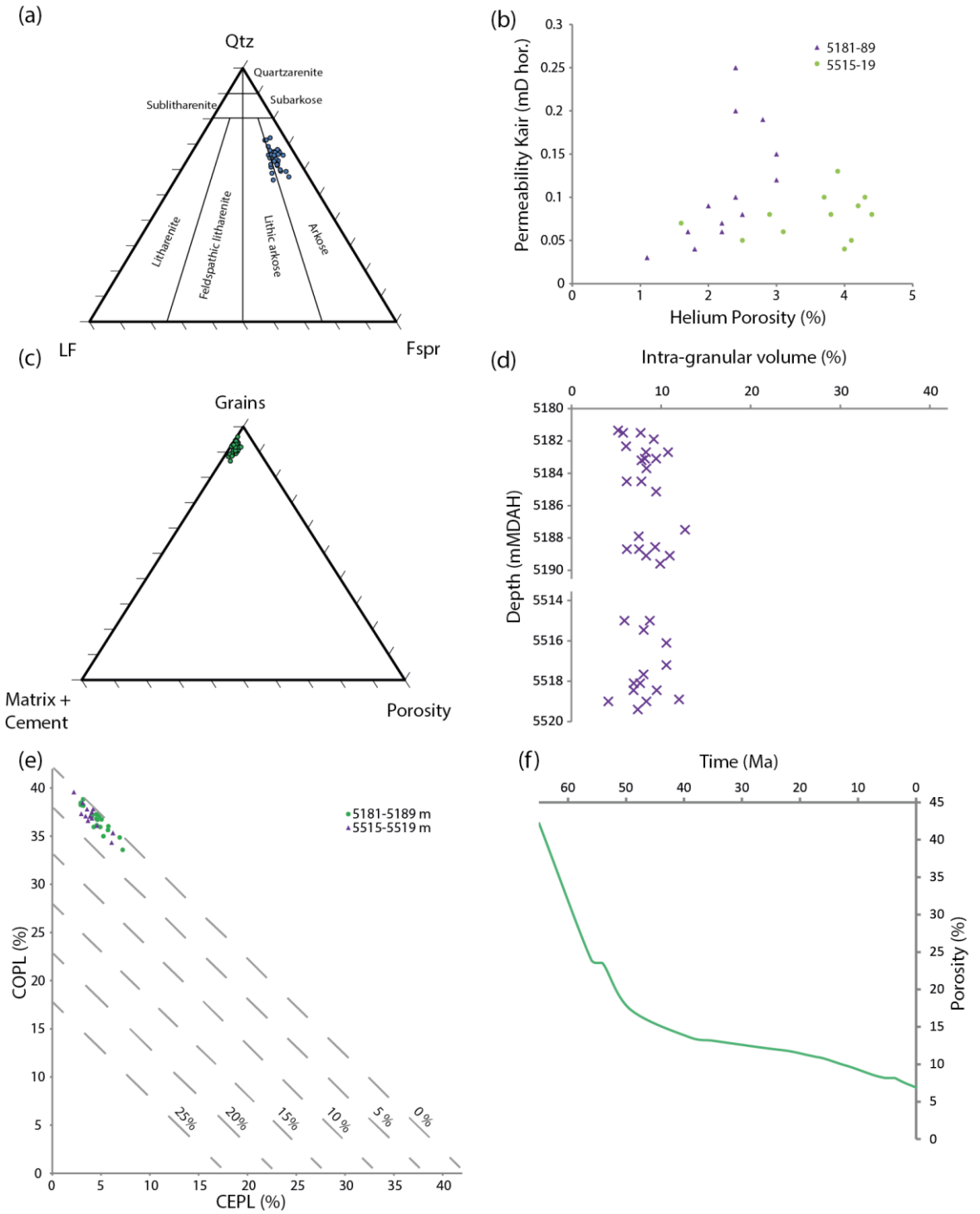

Figure 4.6. a) Ternary plot of present day composition of the Farewell Formation at Kapuni Deep-1 from point count data (Table 4.1). b) Measured porosity permeability cross-plot from core analysis data of the Farewell Formation at Kapuni Deep-1 [green circles 5181-5189 mMDAH and purple triangles 5515-5519 mMDAH] (STOS, 1984). c) Ternary plot displaying grains: matrix: porosity ratio of Farewell Formation data at Kapuni Deep-1 from point count measurements. d) Plot of inter granular volume variation with depth in the Farewell Formation at Kapuni Deep-1. e) Compactional (COPL) and cementational (CEPL) porosity loss for Kapuni Deep-1 [green circles 5181-5189 mMDAH and purple triangles 5515-5519 mMDAH] with remaining sample porosity (dashed lines). COPL and CEPL calculated after (Lundegard, 1992). f) Plot of modelled porosity of the lower core (~5500 mTVDgl) of the Farewell Formation at Kapuni Deep-1 against time.

Table 4.1: Modal point counting summary

Depth		Point Count (300)														
(mMDAH)	(mTVDgl)	Quartz (%)	Lithics (%)	Feldspar (%)	Fracture Porosity (%)	Primary carbonate cement (%)	Replaced carbonate cement (%)	Unknown carbonate cement (%)	Mud clasts (%)	Hydrocarbon streak (%)	Mica (%)	Primary clay cement (%)	Replacement Clay cement (%)	Unkonwn Clay cement (%)	Secondary porosity (%)	IGV (%)
5181.35	5161.04	53.3	3.7	22.3			0.3		1.3		0.3	5.0	10.0	3.3	0.3	5.2
5181.50	5161.19	54.3	5.0	21.7			0.3		0.7		1.3	7.7	8.3	0.7		7.7
5181.50	5161.19	52.3	4.0	22.0			1.0		1.7	1.0	1.0	4.7	10.7	1.7		5.8
5181.90	5161.59	47.3	8.0	22.3	1.0				1.3	1.0		7.0	10.0	1.3	0.7	9.2
5182.33	5162.01	52.3	7.0	20.3		0.3	1.7	0.3	1.3	1.3	1.3	4.3	8.7	0.7	0.3	6.1
5182.70	5162.38	49.0	5.3	22.7		0.3		0.3	0.7	1.0	0.3	6.7	10.3	2.3	1.0	8.3
5182.70	5162.38	54.3	5.3	16.3	0.7	0.3	2.0		2.0	2.0		7.7	8.3	1.0		10.8
5183.10	5162.78	52.7	3.7	22.7					2.3	1.0	1.3	7.0	7.0	2.0	0.3	8.2
5183.10	5162.78	49.0	3.0	22.7					3.3	2.7	0.7	6.3	7.7	4.3	0.3	9.4
5183.20	5162.88	50.3	5.3	23.7					2.0	1.3	1.0	6.3	8.0	2.0		7.8
5183.70	5163.38	47.0	5.0	20.0	0.3		0.3		1.7	0.7	1.3	7.0	12.3	4.3		8.4
5184.50	5164.17	48.3	6.0	23.3		0.7	1.0	0.3	2.7	1.0	0.3	4.3	9.7	1.3	1.0	6.2
5184.50	5164.17	44.3	5.0	28.3		1.0	1.0		2.3	1.3	1.0	5.3	8.7	1.0	0.7	7.8
5185.14	5164.81	49.3	5.0	19.7	1.0		1.3		2.3	0.7	1.0	7.3	7.7	3.3	1.3	9.4
5187.50	5167.16	40.3	3.7	12.3					5.0	1.7	5.7	10.0	13.3	7.0	1.0	12.7
5187.90	5167.56	52.0	3.7	21.0			1.3	0.3	3.0		1.3	7.3	8.0	1.7	0.3	7.5
5188.56	5168.22	46.0	6.3	19.0			0.3		2.7	0.3	0.7	8.7	12.3	1.7	2.0	9.3
5188.70	5168.36	50.7	6.0	20.3		0.7	0.3		2.0	0.3	0.3	6.3	10.3	0.3	2.3	7.5
5188.70	5168.36	50.7	4.7	20.7	0.7	0.3	1.0		4.3	0.3	0.7	4.7	9.0	2.3	0.7	6.2
5189.10	5168.76	41.0	5.0	20.0					8.0	0.3	3.7	10.3	9.0	1.7	1.0	11.0
5189.10	5168.76	38.3	8.3	22.0					3.7	0.3	3.7	7.7	12.0	2.7	1.3	8.3
5189.60	5169.25	44.7	6.0	24.7			2.0		1.3	1.0	0.3	8.7	9.0	1.7	0.7	9.9
5515.00	5492.78	46.3	6.0	23.0	2.3	0.3	2.7		3.3	0.3		5.3	8.3	1.7	0.3	8.5
5515.00	5492.78	47.0	9.0	24.3			2.0	0.3	3.3	0.7		5.0	7.0	1.3		5.8
5515.46	5493.23	45.7	6.0	24.7			1.3		3.0	1.7	1.0	6.0	8.3	1.0	1.3	7.8
5516.10	5493.87	41.7	5.3	20.3		2.0	3.3	0.3	3.3	0.7	0.7	7.3	12.3	2.0	0.7	10.3
5517.20	5494.96	47.0	5.0	19.7		2.7	3.7	0.3	3.0	0.7	0.7	6.7	8.0	2.0	0.7	10.3
5517.66	5495.42	44.0	7.0	20.0	0.7				6.0	1.7	2.0	5.3	11.3	1.7	0.3	7.8
5518.10	5495.85	48.3	5.0	16.7	0.3	0.1	1.7		3.7	0.7	1.0	4.7	15.7	1.0	0.3	6.8
5518.10	5495.85	45.7	5.0	17.0			1.7		2.0	2.7	0.7	4.7	19.0	1.0	0.7	7.5
5518.45	5496.20	44.0	4.7	25.7		1.0	3.3		3.3		1.0	5.7	10.3	0.7	0.3	6.7
5518.45	5496.20	42.3	5.3	19.0		1.7	7.0	0.7	2.7	2.0	1.0	5.3	11.0	1.7	0.3	9.2
5518.90	5496.65	29.7	3.3	13.3	1.0		34.0	3.0	4.3	1.3	1.0	1.3				11.7
5519.00	5496.75	50.0	3.3	15.7	7.7		4.7		4.0	1.7	2.0	6.3	10.7	1.7		8.1
5519.00	5496.75	47.7	4.0	20.7		0.3	4.7		4.0	0.3	2.3	3.3	12.3	0.3		4.0
5519.40	5497.14	39.0	5.0	17.7		2.0	16.7	1.3	1.7	0.7	1.0	4.3	9.3	1.3		7.2

4.3.1.1. COMPACTION

Concavo-convex and quartz-to-quartz long grain contacts are common in all sections, which are indicative of significant mechanical compaction. The COPL-CEPL results, shown in Figure 4.6e, indicate that mechanical compaction is the driver of porosity loss in both cored sections, leading to minimal primary porosity (Fig. 4.3c, 4.6c & 4.7a) and low IGVs (Fig. 4.6d).

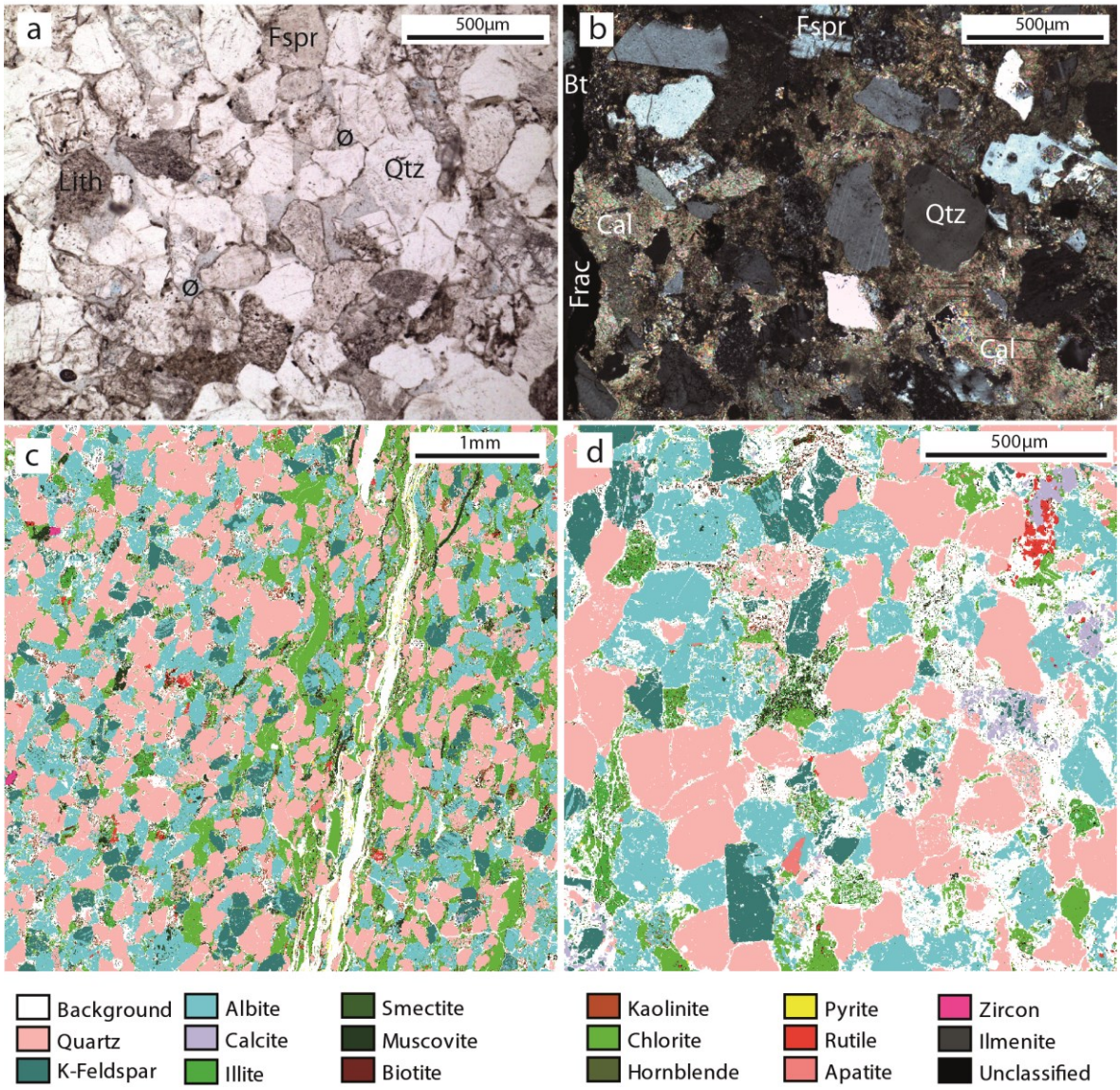

Figure 4.7. a) Thin section micrograph (5189.1 mMDAH): limited visible inter-granular porosity, texturally immaturity and concavo-convex sutured grain contacts. b) Thin section micrograph (5518.9 mMDAH): early calcite cement has created grain framework reducing grain-grain contacts (Lith= lithic fragments; Fspr= feldspar; Qtz=quartz; Frac= fracture; Bt= bitumen; cal= calcite). c) QEMSCAN image (5518.1 mMADAH): bitumen filled fracture with clay smear and mica grains. d) QEMSCAN image (5518.1 mMADAH): higher resolution scan displaying sporadic carbonate cement, degraded feldspar grains and pore filling clay cement: primarily kaolinite, mixed layer Illite smectite and chlorite.

4.3.1.2. AUTHIGENIC CLAY MINERALS

Authigenic kaolinite occurs as variably sized plates and books, filling pores and replacing partially or fully dissolved detrital grains (Fig. 4.8a), and forms aggregates up to the size of detrital grains (Fig. 4.8c). The micro-porosity within pore filling clay aggregates, predominantly kaolinite, is often stained black due to hydrocarbons.

Table 4.2: Bulk rock XRD summary

Depth (TVDgl)	Illite/Smectite (%)	Illite + Mica (%)	Kaolinite (%)	Chlorite (%)	Quartz (%)	K Feldspar (%)	Plagioclase (%)	Calcite (%)	Pyrite (%)
5161.19	1.63	2.62	2.44	1.64	61.63	8.21	21.82	TR	0
5162.38	1.73	3.37	2.13	2.16	63.00	7.89	19.72	TR	0
5162.88	1.05	2.59	4.35	2.14	60.93	9.81	19.14	0	0
5163.38	1.20	6.18	11.97	5.10	47.39	9.91	16.95	0	1.29
5164.17	1.51	2.62	4.25	1.93	62.69	7.78	18.33	0	0.88
5167.16	1.32	9.83	7.86	8.66	47.72	6.59	18.03	0	0.00
5167.56	1.48	3.07	1.17	2.76	65.09	6.86	18.57	1.00	0
5168.36	1.60	3.52	3.44	3.68	54.84	10.29	21.21	0	1.42
5168.76	1.20	9.98	5.00	5.14	49.92	9.17	19.59	0	0
5169.25	1.36	2.79	2.11	3.01	59.37	8.53	22.83	0	0
5492.78	1.63	3.05	2.13	3.80	61.46	6.40	20.16	1.37	0
5493.87	1.31	2.52	2.70	3.06	58.68	7.82	21.71	2.20	0
5494.96	1.23	6.26	1.64	2.51	59.00	6.60	19.06	3.70	0
5495.85	1.72	8.27	4.14	4.12	59.41	5.61	16.74	0	0
5496.65	TR	6.74	2.42	1.84	28.18	4.92	13.07	32.82	10.02
5496.75	1.56	9.01	3.21	2.96	53.22	6.61	21.03	2.40	0

Clay coatings could not be distinguished in reflected light, but SEM, SEM-EDS and QEMSCAN analyses identified sporadic thin chlorite alongside mixed layer Illite/smectite coats (Table 4.3). Illite bridges open pores and secondary porosity in dissolved calcite cement cavities (Fig. 4.8b). Sanidine (sourced from volcanic fragments) is the feldspar most susceptible to dissolution, but all feldspars have been affected (Smale et al., 1999). X-ray diffraction data show there to be an inverse relationship between Kaolinite and feldspar abundance (Table 4.2).

Table 4.3: Clay Fraction (<2µm) XRD summary

Depth	Wt. %	Illite/smectite			Illite				Kaolinite			Chlorite			Quartz		Calcite	
(TVDgl)	< 2µm	% A	% B	Order	% Illite	% A	% B	Crys	% A	% B	Crys	% A	% B	Crys	% A	% B	% A	% B
5161.19	3.2	50.5	1.6	RI/O	50–60	7.9	0.2	P	29.5	0.9	M	10.3	0.3	P	1.8	0.1	0	0
5162.38	3.1	56.8	1.7	RI/O	50–60	8.4	0.3	P	19.2	0.6	M	12.2	0.4	P	3.5	0.1	0	0
5162.88	2.5	40.6	1.0	RI/O	50–60	9.4	0.2	P	36.0	0.9	M	11.6	0.3	P	2.4	0.1	0	0
5163.38	3.7	33.3	1.2	O	60–80	17.0	0.6	P	34.2	1.3	M	13.9	0.5	P	1.7	0.1	0	0
5164.17	3.0	48.1	1.5	RI/O	50–60	7.7	0.2	P	28.7	0.9	M	14.3	0.4	P	1.3	0.0	0	0
5167.16	4.4	28.6	1.3	O	60–80	23.2	1.0	P	22.6	1.0	M	23.1	1.0	P	2.6	0.1	0	0
5167.56	2.7	55.1	1.5	O	60–80	9.8	0.3	P	12.9	0.3	P	19.9	0.5	P	2.3	0.1	0	0
5168.36	3.1	50.7	1.6	O	60–80	11.1	0.3	P	17.4	0.5	P	18.9	0.6	P	2.0	0.1	0	0
5168.76	2.8	43.5	1.2	O	60–80	13.5	0.4	P	21.2	0.6	P	19.9	0.6	P	1.8	0.1	0	0
5169.25	2.5	55.6	1.4	O	60–80	14.0	0.4	P	12.1	0.3	P	15.4	0.4	P	3.0	0.1	0	0
5492.78	3.1	51.3	1.6	RI/O	50–60	11.4	0.4	P	13.0	0.4	P	21.0	0.7	P	3.2	0.1	0	0
5493.87	2.8	47.0	1.3	RI/O	50–60	16.1	0.5	P	18.2	0.5	P	16.8	0.5	P	2.0	0.1	0	0
5494.96	3.1	39.4	1.2	RI/O	50–60	16.5	0.5	P	20.2	0.6	P	21.6	0.7	P	2.3	0.1	0	0
5495.85	3.8	44.3	1.7	RI/O	50–60	11.7	0.4	P	23.5	0.9	P	18.0	0.7	P	2.6	0.1	0	0
5496.65	3.0	TR	TR	RI/O	50–60	0.0	0.0	P	59.3	1.8	P	29.7	0.9	P	1.1	0.0	9.9	0.3
5496.75	3.7	43.9	1.6	RI/O	50–60	11.6	0.4	P	23.3	0.9	P	19.7	0.7	P	1.5	0.1	0	0

A = Weight % relevant size fraction
B = Weight % bulk sample

Mixed-layer Ordering:
R I = Randomly Interstratified (R0)
O = Ordered Interstratification (R1)

Crystallinity:
M = Moderately Crystallised
P = Poorly Crystallised

4.3.1.3. CARBONATE CEMENT

Calcite cement is confined to thin sporadic intervals, as shown in the core log for Kapuni Deep-1 (Fig. 4.4) and bulk rock XRD results (Table 4.2). Thin section (Fig. 4.7b) observations show the cement to be coarsely crystalline sparite, that can enclose all forms of authigenic clay and fill secondary grain dissolution and fracture porosity (Fig. 4.8b). QEMSCAN analyses (Fig. 4.7c & 4.7d) have shown the calcite cement to be sporadically developed even within these carbonate rich zones.

Modal analysis from a single thin section has shown calcite can contribute up to 40% of the rock (Table 4.1) found in primary pores and replacing both dissolved quartz (Fig. 4.8b) and feldspars. XRD analysis from a single carbonate cemented sample shows calcite to form 33% of the bulk rock (Table 4.2). The upper Kapuni Deep-1 core displays significantly less calcite

cement with an average abundance of 0.9% compared with 7.0% in the lower core (Table 4.1), which could be explained through the presence of corrosion surfaces on euhedral quartz grains (Collen, 1988), which is indicative of carbonate dissolution. Carbonate cement in Farewell Formation in the Kupe South Field incompletely replaces feldspars, rock fragments and micas, ranging from 10% to 55% of the bulk rock (Martin et al., 1994).

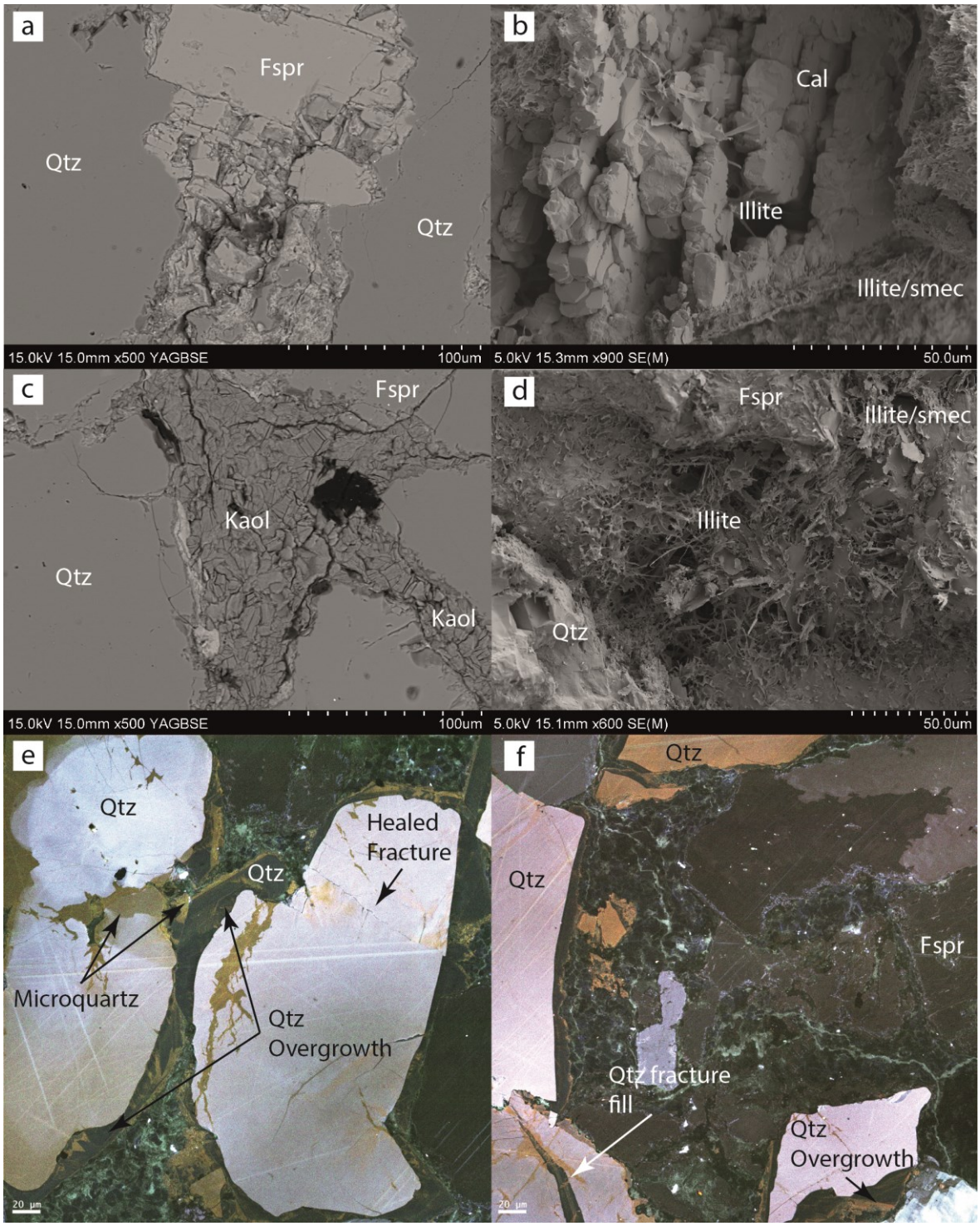

Figure 4.8. a) BSEM image (5518.1 mMDAH): heavily degraded feldspar grain and sutured contacts. b) SEM image (5187.9 mMDAH): calcite crystal that has been partially dissolved and bridged by Illite. c) BSEM image (5518.1 mMDAH): undercompacted pore filling kaolinite books. d) SEM image (5518.9 mMDAH): a pore lined by mixed layer illite/smectite and bridged by illite crystals; e) SEM-CL panchromatic false colour image (5183.7 mMDAH): displaying quartz overgrowths, micro-quartz and a healed fracture. f) SEM-CL false colour image (5183.7 mMDAH): minor quartz overgrowths and a quartz filled fracture within detrital quartz grain (Qtz= quartz; Fspr= feldspar; Cal= calcite; Kaol= kaolinite; smec= smectite).

Carbon isotope analysis of carbonate cements sampled from overlying Kapuni Group reservoirs, display enrichment in isotopically light carbon (Higgs et al., 2013), which is sourced through thermal maturation of organic material (Franks & Forester 1984), meaning that the carbonate precipitated from organic CO_2 via the breakdown of hydrocarbons.

4.3.1.4. QUARTZ CEMENTATION

Pressure dissolution and stylolitisation of quartz grains has been identified in reflected light microscopy (Fig. 4.7a) and in backscatter SEM images (Fig. 4.8a & 4.8c), prompting analysis by cathodoluminescence of selected samples to investigate the extent of silica cementation. Rare poorly developed and often interlocking anhedral quartz overgrowths (Fig. 4.8e & 4.8f) and very rare feldspar overgrowths are present. Macro-quartz that fills fractures in quartz grains (Fig. 4.8e) displays similar fluorescence to the overgrowths, which is suggestive of equivalence. Diagenetic micro-quartz is also present as rims on detrital quartz grains and as overgrowths (Fig. 4.8e & 4.8f).

4.3.1.5. POROSITY

Core analysis results (Fig. 4.6c) show helium reservoir porosities range between 1-4.5%. Very limited intra-granular porosity can be identified in reflected light (Fig. 4.7a). The low intergranular volumes are supported by the measured porosity values, as helium techniques measure total porosity, which includes micro-porosity within clay cement. The final present day basin modelling derived porosity of ~8% (Fig. 4.5c & 4.6f) is slightly higher than the measured helium porosities, the further loss could attributed to pervasive authigenic clays and calcite filling pores. Locally, secondary porosity is associated with dissolution of feldspars, quartz and of calcite cement.

4.3.1.6. FLUID INCLUSIONS

Very few definitively diagenetic pore-occluding quartz overgrowths were identified and of these only a small proportion display fluid inclusions. Oil inclusions that are present possess semi-opaque to opaque backgrounds in transmitted light, which prevents microthermometry and hence no other aqueous inclusions could be located in conclusively diagenetic phases, limiting analyses to both aqueous and mixed hydrocarbon aqueous phase inclusions in quartz micro-fracture fills (Table 4.4). The sediments are first cycle derived from granitic and metamorphic basement in the North West Nelson area, meaning that oil and micro-fracturing must be related to the present basin fill (as opposed to inherited from a previous sedimentary sequence that was sourced to the basin).

Table 4.4: Fluid inclusion microthermometry summary

Depth (mMDAH)	5183.7		5518.1	
Host	Detrital quartz grain, fracture fill	Detrital quartz grain, fracture fill	Detrital quartz grain, fracture fill	Detrital quartz grain, fracture fill
Type	secondary, oil assoc	secondary	secondary, oil assoc	secondary
Contents	aqueous	oil	aqueous	oil
Average Hom Temp (°C)	113.4	70.7	116.6	68.6
Min Hom Temp (°C)	106.1	69.0	114.1	41.2
Max Hom Temp (°C)	121.7	73.3	119.6	76.0
n	5.0	7.0	3.0	16.0
Standard Deviation	6.0	1.4	2.8	10.6

Results from samples prepared from both of the Kapuni Deep-1 cores display virtually identical fluid inclusion properties, suggesting the presence of an undersaturated oil (hence the disparity between aqueous and oil homogeneity temperatures) trapped at 105-125°C (av. 110°C), in waters of brackish salinity (Table 4.4). Temperatures from burial history modelling suggests that inclusions where trapped between 6-4 Ma. The oil inclusions identified in macro-quartz overgrowths display a reasonably consistent fluorescence colour throughout (Table 4.5), indicating little liquid compositional variation, as reflected in the relatively narrow spread of spectrometric API gravity estimates of 30 ± 5° C ('moderate'). They are, however, in low abundance, which, if drawn from the same petroleum column, suggests low permeability or poor generation at the time of trapping.

Table 4.5: Petroleum inclusion fluorescence summary

Depth (mMDAH)	n	Flourence Colour	Av. API
5185.7	39	blue-green	29.3
5189.1	3	blue-green	33.1
5516.1	8	blue-green	35.2
5518.1	28	blue-green	25.9
5519.0	5	blue-green	32.7

4.3.2. VERTICAL PRESSURE DISTRIBUTION

Figure 2.5b shows the entire Early Miocene to Pliocene to be normally pressured within the Taranaki Basin, which suggests that this stratigraphic section in Kapuni Deep-1 is very likely to be near to, or at, hydrostatic pressure. The wireline signatures of the sonic, density and resistivity logs display clear regressions from top Moki Formation downwards, which is an indication of undercompaction and the existence of overpressure (Fig. 4.9), primarily within the Oligocene Otaraoa Formation.

Shale pressures were calculated using the equivalent depth method (Hottmann and Johnson, 1965), and also suggest that the Otaraoa Formation is overpressured (Fig. 4.9). The mud log through the Oligocene to Mid-Miocene section indicates close to 100% fine-grained lithology and therefore low permeability; inhibiting the inflow of pore water into the borehole, so any overpressure in the mudrocks is therefore not reflected in the mudweight.

RFT measurements collected at Kapuni Deep-1 in the Middle Eocene Kaimiro Formation gave an average pore pressure of 6939 psi (1443 psi overpressure), which is consistent with the virgin pressure of the K3E reservoir interval recorded elsewhere in the Kapuni Field. The lack of influence from production within the Kaimiro Formation implies that there is no pressure communication, indicating lateral compartmentalisation on a production timescale. This overpressure is also in line with measurements taken in the overlying Mangahewa Formation recorded elsewhere in the field, indicating that the intervening Omata Member of Turi Formation is not acting as a vertical seal at Kapuni Deep-1 (Webster et al., 2011).

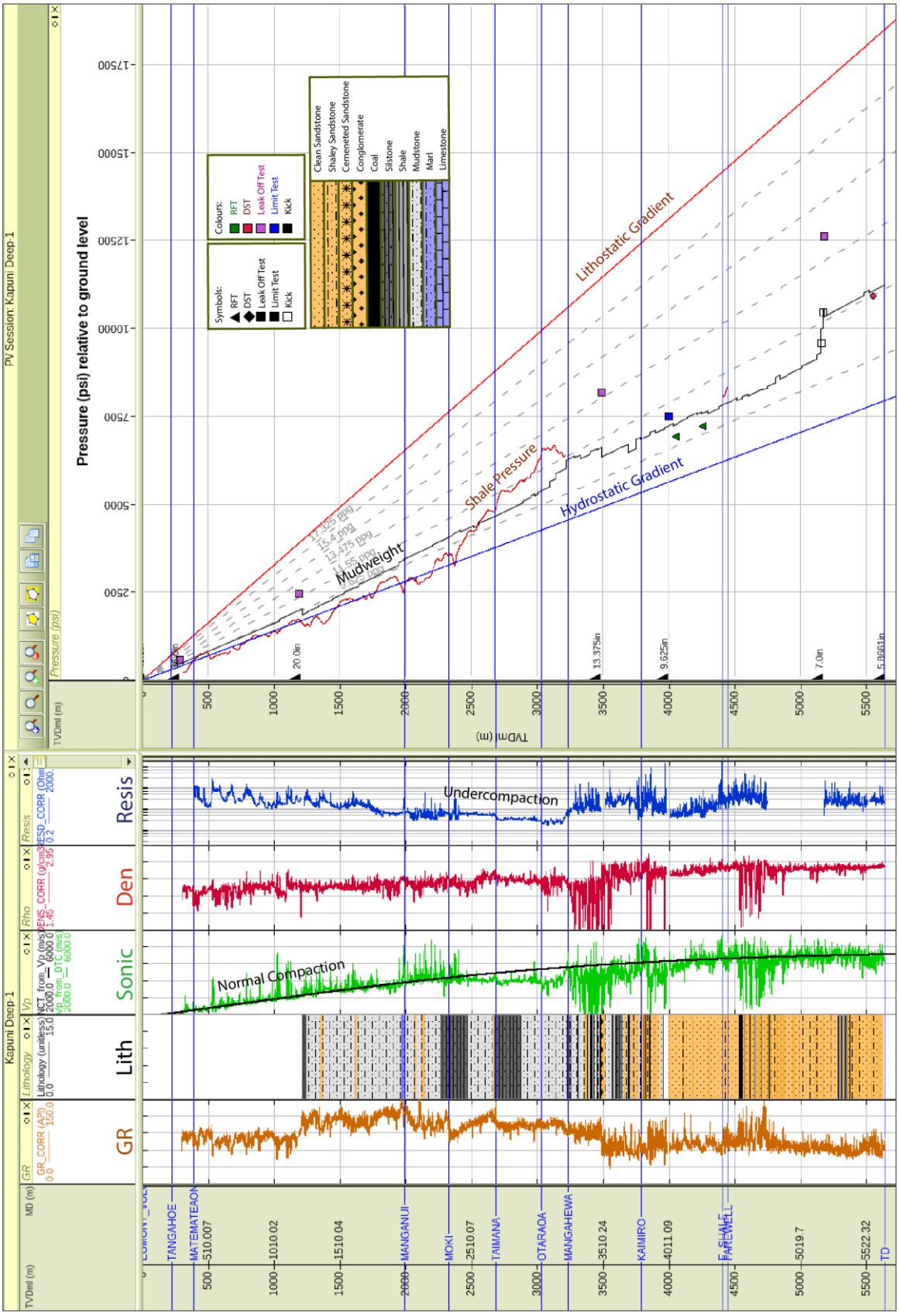

Figure 4.9. Kapuni Deep-1 pressure depth plot with the suite of wireline measurements (Gamma Ray, sonic (interval transit time [ITT]), resistivity, and density, a summary lithologic column, normal compaction trend [NCT], RFT pressure measurements [green triangles], Drill stem tests [red triangle], kicks [white square], leak-off pressure [purple squares], limit tests [blue squares], mud-weight profile [black], shale pressure [red]).

In Kapuni Deep-1 a constant mudweight of 10.4 ppg/1,246.2 kgm^2 was maintained through the Eocene and into the Palaeocene, until two drilling breaks occurred at 5155 and 5171

mTVDgl, which both resulted in water influxes. Drill mudweight and shut-in drill pipe pressures were used to calculate a reservoir overpressure of 3393 psi from the second deeper kick, indicating that the well was drilled 1513 psi underbalance.

4.3.3. BURIAL HISTORY MODELLING AND PORE PRESSURE EVOLUTION

Deposition of the Farewell Formation began during the Early Palaeocene on a coastal plain as indicated by the presence of coal, coarse grained sandstones and pebble conglomerates of fluvial origin (Fig. 4.3a). These deposits were rapidly buried (150 m/M.y.) during the Palaeocene to Early Eocene during waning basin extension (Fig. 4.10a). Mud log cuttings indicate that the ~3 km thick Palaeocene to Middle Eocene succession in Kapuni Deep-1 is almost entirely comprised of very fine to medium sandstone. The formation of overpressure is dependent on the presence of fine-grained lithologies where excess pressure is generated through disequilibrium compaction, as well as to act as seal to the pressure that has been transferred into reservoir/more permeable units. The 1D basin modelling shows that these sand rich sediments allowed vertical dewatering, leading to maintenance of close to hydrostatic conditions (Fig. 4.10b).

The rate of subsidence and sediment accumulation reduced during the Middle Eocene to Early Oligocene interval during post-extension thermal contraction. Slow rates of burial did not lead to the generation of any significant overpressure. Water depths across the whole of Taranaki Basin increased during the Oligocene, leading to the deposition of the 200 m thick Otoraoa Formation as a bathyal marine calcareous mudrock. The Otoraoa Formation is considered to have undergone limited initial compaction due to slow subsidence rates, but was subsequently buried by several km of terrigenous Miocene mudrocks (e.g. Manganui Formation). This allowed for limited dewatering, leading to the onset and generation of small amounts (c 400 psi) of overpressure through disequilibrium compaction from the Miocene onwards (Fig. 4.10b).

By the Late Miocene (~10 Ma) the rate of burial, particularly in southern and central parts of Taranaki Basin slowed and was followed by changes in the sense of displacement on prior normal faults, the associated development of anticlinal inversion structures and widespread uplift of southern Taranaki Basin (Crowhurst et al., 2002; Kamp and Green, 1990). Manaia Anticline in southern Taranaki Peninsula, which carries the Kapuni Field (Higgs et al., 2013), also developed at this time with ~300 m of erosion of Late Miocene section along the axis of the anticline (Armstrong et al., 1998). Horizontal stress enforced through the shortening may have led to increase in pore pressure as seen in the New Zealand's East Coast Basin (Burgreen-Chan et al., 2016). Though due to the limitations of 1D basin model this cannot be tested, though by the Pliocene, movement on the Taranaki fault had ceased, meaning any excess pore pressure generated by horizontal stress would have started to dissipate, during

the current extensional phase of the Taranaki Basin (Rajabi et al., 2016). Also, the erosion over the Kapuni Field will have enabled some pressure dissipation (Fig. 4.10b).

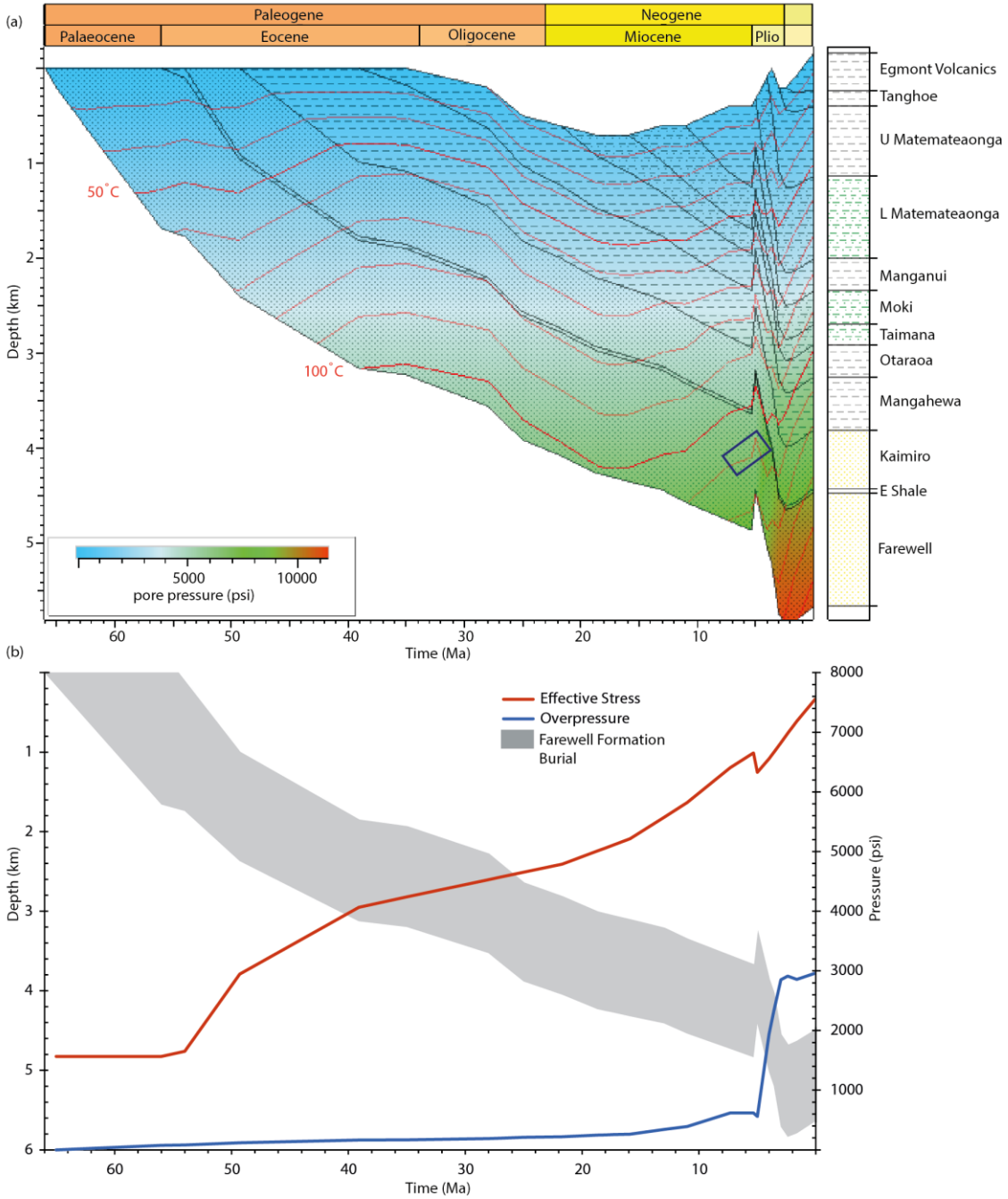

Figure 4.10. a) 1D burial history plot of Kapuni Deep-1 (Petromod). Red lines are isotherms and colour overlay denotes pore pressure. Blue rectangle= aqueous fluid inclusions within quartz filled fractures, where microthermometry suggests trapping temperatures of 105-125°C (av. 110°C); b) Plot displaying the evolution of overpressure and effective stress with burial since the deposition of the farewell Formation.

There was renewed subsidence and high sedimentation rates (620 m/M.y.) across southern Taranaki Peninsula and offshore immediately to the south during the Pliocene. This involved Kiore Formation and Matemateaonga Formation, which accumulated in shelfal environments in Taranaki Peninsula, followed by accumulation of mid Pliocene Tangahoe mudrock in upper bathyal environments and Late Pliocene Whenuakura Subgroup in shelfal environments (Kamp et al., 2004). The driving mechanism for the development of late overpressure in Palaeogene section below Oligocene Otaraoa Formation seal is considered to be the rapid

phase of Late Miocene and Pliocene burial in central to southern parts of the Taranaki Peninsula parts of Taranaki Basin, as also demonstrated in the Kupe South Field (Fig. I.6b).

4.3.4. DIAGENETIC PARAGENESIS

Diagenesis will have initiated during shallow burial with pore-filling carbonate cementation, supported by the lack of grain-grain point contacts in heavily cemented sections (Fig. 4.7b). Calcite cement in Farewell Formation at Kapuni-14 (4309 mTVDgl) has a $\delta^{18}O$ value of -2.6‰, corresponding to precipitation from seawater at 28^0C (Smale et al., 1999). Dolomite sampled in the same horizon interval precipitated at 60^0C ($\delta^{18}O$ -6.0 ‰) and calcite from the deeper cored section of Kapuni Deep-1 produced an $\delta^{18}O$ value of -15.3 ‰, corresponding to precipitation from sea water at approximately 121°C (Smale et al., 1999). Although there are few oxygen isotope analyses, these data suggest that carbonate cementation occurred over an extended interval through the Miocene and Pliocene during burial of Farewell Formation.

The onset of feldspar and mica degradation will have occurred during burial, contemporaneously with precipitation of authigenic chlorite, smectite and kaolinite, which is shown by clay mineral pore infilling and overgrowth of dissolution cavities in degraded feldspar grains (Fig. 4.8a). BSEM analysis displays pervasive filling of pores with kaolinite (Fig. 4.8c), and is dramatically increased where the highest feldspar degradation occurs (Table 4.3). Large kaolinite filled pores, which are often the same size as former detrital grains, indicates shallow, early diagenesis, leading to the formation of a grain framework.

Fluid inclusion data collected by Higgs et al. (2013) suggests that quartz cementation initiated at approximately 90°C in the Kapuni Field, with the main phase occurring between 100°C and 130°C. The temperature history shows that the relatively minor amount of quartz cement in Farewell Formation formed from the Mid-Eocene to the present-day with most precipitation occurring during the last 20 My. This major phase will have occurred at depths below 3500 m, after significant porosity reduction by mechanical compaction.

Limited amounts of micro and macro-quartz were precipitated in the Farewell Formation and, sourced from sutured grains (Fig. 4.7a & 4.8c) and feldspar dissolution reactions. The current formation temperatures of >130°C and lack of grain coating clays provides the perfect environment for nucleation and growth of pervasive quartz cement, but only limited overgrowths have been identified. The general lack of quartz cementation at these elevated temperatures could be explained through the early destruction of porosity and permeability in sandstone beds, limiting the rate of diffusion of dissolved solutes and restricted space for the growth of macro-quartz. The feldspar degradation reactions and subsequent clay reactions will have liberated silica, which would have led to the observed limited quartz cementation.

The illite:smectite ratio is as high as 60% in certain samples (Table 4.3). By burial heating to 120°C it can be expected that the vast majority of smectite would have transformed into Illite. The high K-feldspar content (Table 4.2) of the bulk rock excludes potassium availability as a limiting factor, but the exceptionally low porosity and permeability could have restricted flow and caused slow diffusion, further inhibited by hydrocarbon charging. The majority of the Illite/smectite is randomly interstratified with only a few ordered interstratified occurrences, which infers that the process is on-going (Table 4.3).

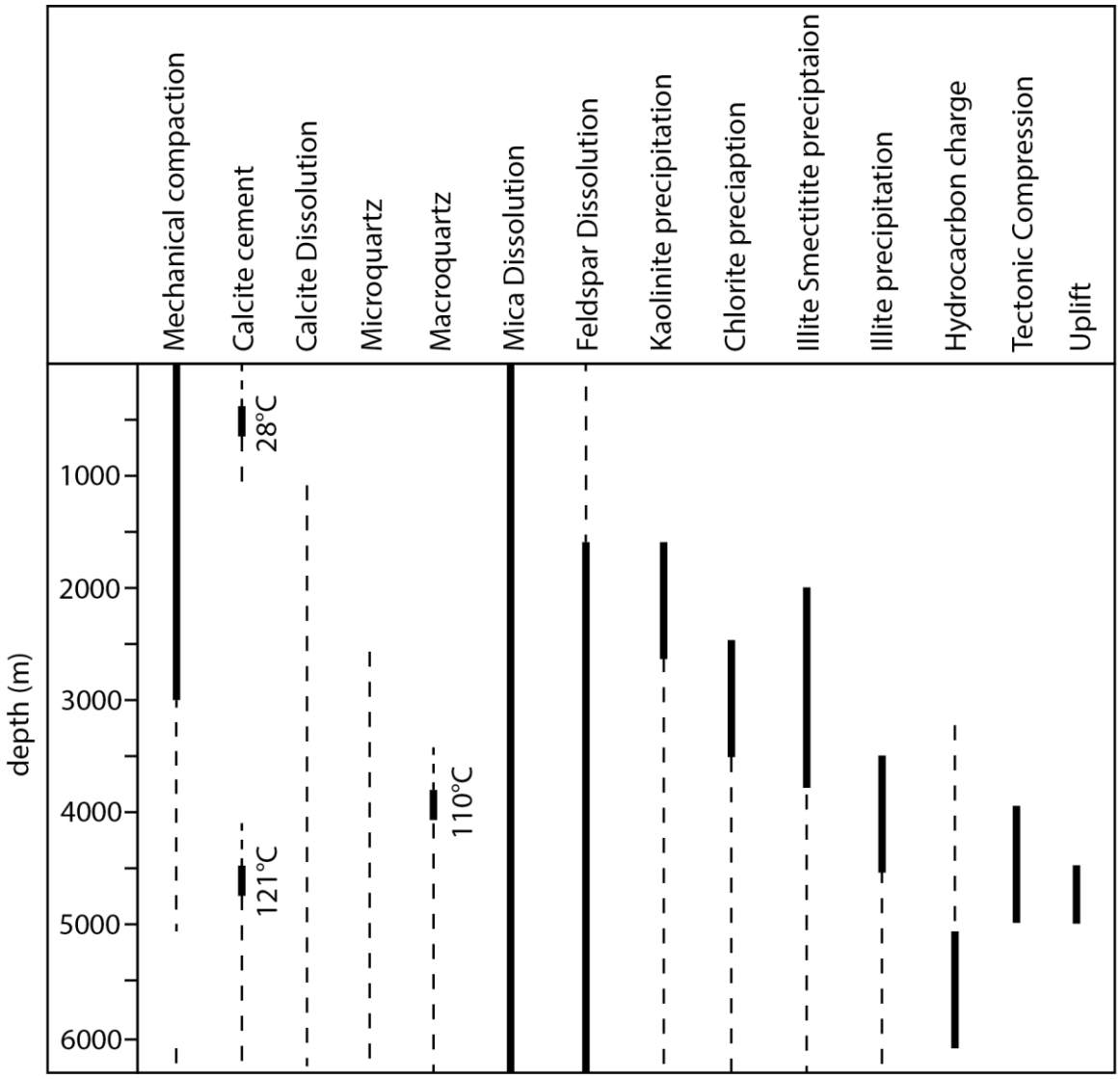

Figure 4.11. Diagenetic Paragenesis for Farewell Formation sandstone beds in Kapuni Deep-1.

The occurrence of Kaolinite in secondary dissolution pore space often displays an undercompacted form and associated micro porosity can be filled with hydrocarbons during the later stage of burial. A similar form of kaolinite has also been identified in the Mangahewa Formation at Cardiff-1 (Higgs et al., 2007). Additional evidence for continued feldspar dissolution and kaolinite precipitation comes from the pattern of oil staining observed in some kaolinite in thin-sections. Both stained and unstained kaolin are observed within a single thin-section, a feature identified in deep arkosic sediments in the central North Sea where variable staining is indicative of growth after charging, on-going dissolution, and low reservoir quality (Wilkinson et al., 2014).

Kaolinite becomes unstable with increasing formation temperature and is rarely preserved above 100°C (Bjørkum and Gjelsvik, 1988), suggesting that there is an anomalously high content based on measured formation temperatures for the Farewell Formation in this study. The supply of potassium is commonly ascribed as a limiting factor in the conversion of kaolinite to illite and usually sourced from k-feldspar dissolution (e.g. Bjørkum and Gjelsvik, 1988). The abundance of kaolinite in the Farewell formation reservoirs of the Kapuni deep-1 well is attributed to effect of recent and rapid burial with insufficient time at current formation temperatures for diagenetic reactions to have equilibrated and allow illitization of kaolinite.

The low abundance of hydrocarbon inclusions within the already rare quartz overgrowths in both of the Kapuni Deep-1 cores suggests that the reservoir quality was very poor during charging. Most clays are poorly crystalline with only a small number of kaolinite samples being moderately crystalline, which indicates very little space for growth. The low abundance and anhedral nature of quartz overgrowths, coupled with the lack of fluid inclusions and poorly crystalline clays, supports evidence for low porosity and permeability.

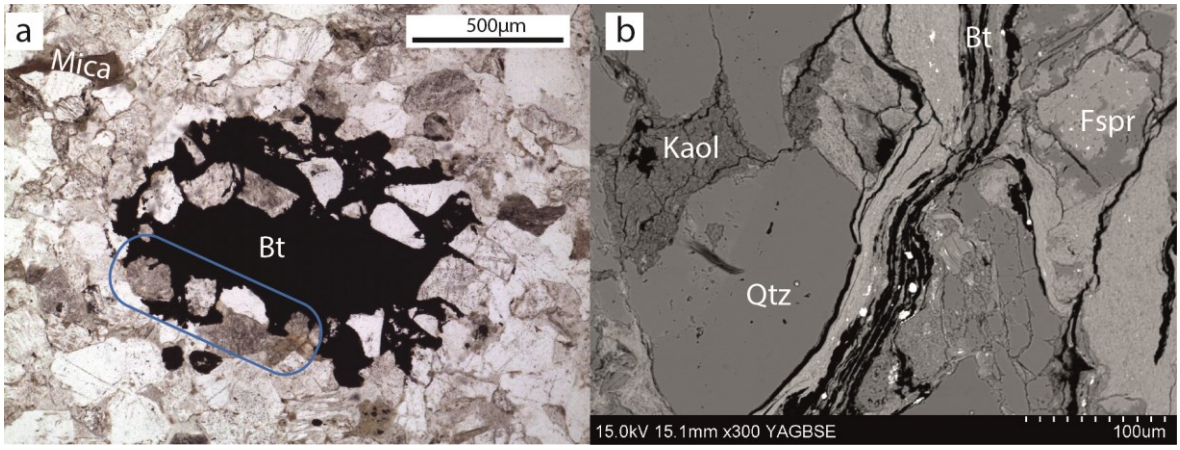

Figure 4.12. a) Thin section micrograph (5183.7 mMDAH): cross section through a fracture filled with bitumen displaying edged grains around the rim (blue rectangle); (b) BSEM image (5518.1 mMDAH): bitumen filled fractures, clay smear and pore filling kaolinite (Bt= bitumen; Kaol= kaolinite; Qtz= quartz; Fspr= feldspar).

The aqueous inclusions measured from quartz-filled fractures give an average homogenisation temperature of 110°C (Table 4.4), which when compared with the burial history will have been trapped between 6-4 Ma. Higgs et al., (2013) suggested that Palaeogene coals matured for oil during the past 2 M.y. and are therefore are a likely source for oil in the Farewell Formation. This is supported by a range in API gravities that indicate moderate maturities, which is indicative of late generation and charging. The presence of bitumen in fractures (Fig. 4.12a & b) suggests that they formed in the past 2 M.y. associated with the expulsion of oil from interbedded coals (Higgs et al., 2013), which was subsequently thermally cracked due to increasing temperatures during rapid Pliocene burial (Kukla et al., 2011; Schoenherr et al., 2007).

The present-day reservoir quality of the Farewell Formation is a cumulative product of depositional attributes, mechanical compaction and diagenesis during early and later stages of burial (Fig. 4.11). Compaction and the growth of authigenic clay and carbonate cement are the most significant diagenetic processes occurring in the Farewell Formation at Kapuni Deep-1. The COPL-CEPL analyses, grain fracturing, very low helium porosities and IGVs shows that mechanical compaction was the key driving mechanism for porosity reduction during the first 3500 m of burial through the steady increase of vertical effect stress, which has been demonstrated by basin modelling (Fig. 4.6f).

4.4. DISCUSSION

Measured porosity in the Farewell Formation at Kapuni Deep-1 are anomalously low for the current depth of burial and require explanation. Such low porosity is consistent with high vertical effective stress, partly explained by vertically and laterally expelled fluids prior to ~6 Ma such that no overpressure was maintained. Only after this period was overpressure retained.

4.4.1. OVERPRESSURE MAINTENANCE

The Farewell Formation has been allowed to dewater during continued burial, via vertical fluid escape and lateral drainage through high permeability pathways in the Cretaceous and Palaeocene (Fig. 4.13), which has inhibited the generation of overpressure. Lateral drainage has been identified across the Kupe South Field, where reservoir overpressures are less than intra-reservoir mudrocks, caused by fluid pressure loss through interbedded sands of Cretaceous Puponga Member (Webster et al., 2011; Chaper III, section 3.4.2). This signature has also been identified in the Kapuni Field. Figure 4.13 displays the decrease in reservoir overpressure in the Palaeocene towards the south from Kapuni Deep-1 through to Momoho-1. The Cretaceous and Palaeocene represent a continuous connected pathway for pressure dissipation until they outcrop on the sea floor and on the South Island (Figs.4.1 & 4.13). Since ~6 Ma the Farewell Formation has been able to maintain excess pressure, which has been generated through rapid Pliocene burial.

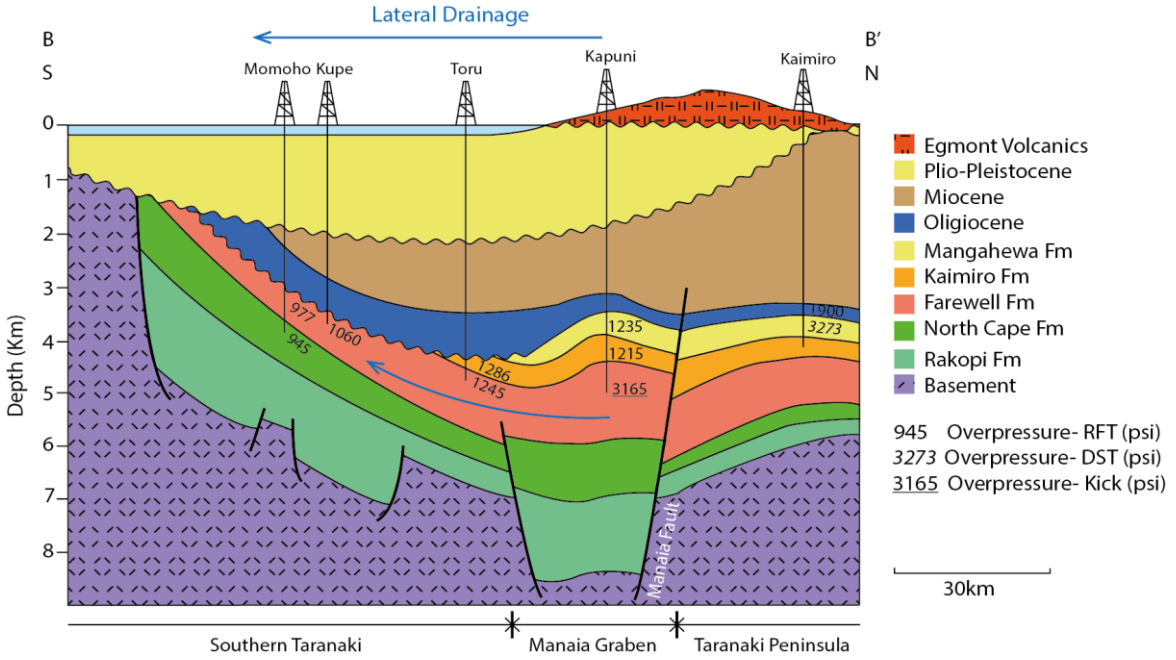

Figure 4.13. Cross section (line B-B', Fig. 4.1) displays lateral drainage in the Southern Taranaki (Modified from King and Thrasher (1996).

The exceptionally low permeability of the Farwell Formation will slow the transfer of pressure up dip, which would place the reservoir pressure in closer equilibrium with the shale pressure and explain the continued maintenance. The lateral drainage of pressure would also be inhibited through the compartmentalisation. The current Kapuni Field seismic reflection data is of very poor quality, but dipmeter data, albeit only acquired over short intervals, indicates some structural disturbance between 4612-5287 mTVDgl, and it is possible that there is a significant sealing fault cutting the section in the data gap at ~5160 mTVDgl. The presence of sealing faults in the region is supported by comparison of virgin pore pressures from Cardiff-1 and the Kapuni Field. The K3E reservoir pressure at Cardiff-1 is significantly higher there than in Kapuni Field (Webster et al., 2011), so there must be a lateral hydraulic barrier between them or the system is not in equilibrium. However, this structural configuration would still require a top seal to be effective.

4.4.2. Vertical effective stress and reservoir quality

Paxton et al., (2002) suggest that for overpressure/low VES to arrest mechanical compaction in reservoirs, abnormal pressures must develop at depths shallower than 2500 m, or within the depth window that mechanical compaction is active. As previously discussed the onset of overpressure occurred below 3500 mTVDgl in Farewell Formation during 6-2 Ma after significant mechanical compaction.

The Magnolia Field, Gulf of Mexico (Sathar & Jones, 2016) and the Kessog Structure in the North Sea (Grant et al., 2014) are at equivalent depths, and display very similar immature reservoir composition to the Farewell Formation, but have markedly lower VES and excellent reservoir quality. Magnolia reservoirs have a vertical effective stress range between ~700 – 3500 psi, and Kessog has ~2000 psi, whereas the Farewell Formation at Kapuni Deep-1 has

~6500 psi (lithostatic gradient 3.281 psi/m). The deep and late onset of abnormal pressure only allowed the formation of limited amounts of overpressure, which is not at a significant enough magnitude to arrest any further mechanical compaction and occurred after the Farewell Formation sandstones entered the chemical compaction window.

4.4.3. INTERGRANULAR VOLUME

Mechanical compaction is characterized by the reorientation and repacking of competent (brittle) grains by local fracture or cleavage of brittle grains, and by plastic deformation of ductile grains (Houseknecht, 1987). Mechanical compaction alone has the potential to reduce intergranular volume to a minimum of 26%, assuming moderately to well sorted, well rounded and fairly spherical grains (Paxton et al., 2002). The overlying Mangahewa Formation at Cardiff-1 (Fig. 4.1) displays IGVs of av. 15%, but this further reduction has been attributed to chemical compaction (Higgs et al., 2007).

Intergranular volumes of between 6-11% in the Farewell Formation at Kapuni Deep-1 are significantly lower than 26%. The presence of detrital mud clasts, mica and lithic fragments would reduce the initial porosity of the sandstone beds. These ductile grains combined with the poorly sorted nature of the sandstone beds allows for grain reorientation and sliding resulting in more efficient packing, and plastic deformation during burial further reduces the IGV (Worden et al., 2000).

The relatively deep onset and restricted nature of quartz cementation in Farewell Formation, would allow mechanical compaction to continue at high stress further reducing the intergranular volume (Chuhan et al., 2002). Although grain crushing is not common in very fine to fine grained sandstones, the poorly sorted angular nature of the grains led to increased stress at sharp contacts, increasing the potential for grain fracturing and a reduction in intergranular volume. This is supported by the presence of healed fractures observed in false colour cathodoluminescence images (Fig. 4.8f).

Basin modelling carried out on the Kapuni Field by (Higgs et al., 2013) suggests that thermal maturation of thick organic rich coaly source rocks within Farewell and Rapoki formations (Enclosure II) led to the generation and expulsion of large volumes of acidic fluids from ~60 Ma, thus enabling the dissolution of grain rims during shallow burial, weakening the grain framework and aiding in mechanical compaction. The onset of chemical compaction greatly reduces mechanical compaction (Chuhan et al., 2003), but the continued flushing of CO_2 rich fluids will be on-going, stimulating grain rim dissolution, which will reduce the strength of the grain framework and lead to further mechanical compaction.

4.4.4. CO_2 AND SECONDARY POROSITY

The flow of acidic rich fluids will have been an important mechanism in driving dissolution of carbonate cements and the generation of secondary porosity in the Kapuni Field (Higgs et al., 2013), producing oversized pores in some Taranaki reservoirs (Collen and Newman, 1991). Local patches of etched carbonate cement have been identified (Collen, 1988) along bitumen-filled fractures (Fig. 4.12a & b) and in the upper core, as observed in Figure 4.7b, implying that more extensive patches may have existed. The dissolved CO_2 in the pore fluids will also have driven feldspar dissolution, producing secondary porosity, but also have provided ions for precipitation of authigenic clays and quartz cements filling pore space elsewhere. This would lead to further compartmentalisation by formation diagenetic barriers to flow and aid in the maintenance of abnormal pressure.

4.4.5. FAREWELL FORMATION DEEP PRESSURE TRANSITION

The origin of the pressure transition zone within the Farewell Formation is not clear, as there is no obvious change in the wireline signature, indicating a subtle change in reservoir properties below the resolution and sensitivity of the wireline tools.

Webster et al., (2011) suggested kerogen cracking as a secondary overpressure mechanism, which could account for increased pressure below 5000 m. Swarbrick et al., (2002) show that kerogen transformation/gas generation has the potential to produce overpressures of 70–6000 psi, at equivalent maturity expected in the Cretaceous of Taranaki Basin. Kukla et al., (2011) showed that a self-charging interbedded source rock reservoir system, similar to the Farewell Formation, contributed 435 psi of overpressure to a Neoproterozoic system in Oman. However the Farewell Formation was only mature for oil during the past 2 Ma, but the low reservoir permeability would inhibit the contribution to the overpressure.

Furthermore the transition could be attributed to an effective vertical pressure seal, as even thin mudrock intervals can support a significant pressure differential, demonstrated by a 1595 psi increase in pore pressure in less than 50m in two fields of the Baram Delta (Tingay et al., 2009). Wireline signatures suggest that Palaeogene mudrocks in Farewell Formation are poorly developed to act as effective seals. However one potential unit, the 135 m thick E Shale (Fig. 4.9), is a transgressive interval found at the base of the Kaimiro Formation, comprised of sandy, light to moderate grey calcareous siltstone, which passes up into dark brown calcareous shale (STOS, 1984). Increases in density and velocity and reduction in gamma ray of the E Shale are all indicative of a fine grain size lithology.

4.4.5.1. SECONDARY COMPACTION

The Farewell Formation pressure transition zone occurs in a thick sandstone package, which under normal circumstances would not act as a pressure seal (Swarbrick and Osborne, 1996)., However, Weedman et al., (1992) proposed a model whereby early cementation allows loosely packed sandstones to subside to significant depths (equivalent to the Farewell

Formation at Kapuni Deep-1) followed by dissolution of these early carbonate cements. The ensuing compaction of sandstones creates zones of extremely low permeability, which act with interbedded mudrocks to form a pressure seal (Weedman et al., 1992).

The study of Weedman et al., (1992) was undertaken in the Upper Cretaceous Tuscaloosa Formation of onshore Louisiana, USA, which displays similar reservoir characteristics of interbedded sandstone and mudrocks and sandstone connectivity to the Farewell Formation. There are multiple sources of pressure generation attributed to deep basin overpressure (e.g. Osborne and Swarbrick, 1997; Swarbrick et al., 2002), but an effective barrier to vertical migration out of the Farewell Formation is needed to explain the present overpressure transition (1900 psi) between the measured pressures in the Kaimiro and Farewell formations (Fig. 4.9). In the absence of a laterally extensive thick mudrock to act as a vertical sealing mechanism, it is proposed that migration of acidic CO_2-rich pore fluids, already identified as an important dissolution process in the Kapuni Field (Higgs et al., 2013), could have created a pressure transition zone. Precipitation of early carbonate cements have been recognised in the Farewell Formation and are likely sites for secondary porosity generation through dissolution with subsequent extreme secondary compaction and corresponding permeability reduction (e.g. Weedman et al., 1996, 1992).

4.4.6. IMPLICATIONS FOR DEEPLY BURIED SANDSTONE RESERVOIRS

Early pore filling and late precipitation of calcite cement in partially or fully dissolved quartz and feldspars grains has produced secondary intergranular volumes of up to 42%, which has the potential to produce substantial secondary porosity. Higgs et al., (2013) suggested that in the Kaimiro and Mangahewa formations, which overlie Farewell Formation, these CO_2 rich fluids preferentially flow through vertically stacked, coarse sandstone facies, resulting in the generation of significant secondary porosity. Less feldspar reaction occurred in fine sandstone from heterolithic intervals, yet overall, more secondary minerals have precipitated. This implies that there has been a net redistribution of ions from coarse cleaner beds to fine heterolithic beds, and that this diagenetic redistribution has led to enhanced vertical reservoir heterogeneity (Higgs et al., 2013).

The cored sections of Farewell Formation sandstone at Kapuni Deep-1 are very fine to fine-grained with poor sorting and abundant labile grains and detrital clay. Ions from reactions could have migrated in pore fluids from coarser units and then precipitated as secondary minerals within the low permeability beds, further reducing reservoir quality. Conversely, it could be expected that coarser units of enhanced reservoir quality could exist at depth in the Farewell Formation, producing alternating cemented zones and enhanced porosity intervals.

Mapping out and predicting the diagenetic paragenesis of deep sandstone reservoirs poses many issues, which are further complicated by the flow of aggressive reactive pore fluids.

Furthermore, common bitumen-filled fractures (Fig. 4.12a & b) along with natural fractures identified in reservoirs deeper than 4000 m elsewhere in the Taranaki Basin (Webster and et al., 2011) hold the potential to further enhance permeability or conversely increase compartmentalisation (Schoenherr et al., 2007).

4.5. CONCLUSIONS

1) Mechanical compaction driven by initial rapid subsidence has been the key mechanism for porosity reduction in the Farewell Formation during the first 3000 m of burial. The low IGV, concavo-convex and quartz-to-quartz long grain contacts, anhedral nature of quartz overgrowths, general lack of fluid inclusions, and poor crystalline clay mineral content indicate that reservoir quality was markedly reduced by early burial compaction processes.
2) The absence of significant intervals of low permeability fine-grained strata within Palaeocene and Eocene section has allowed the reservoirs to dewater during burial inhibiting the preservation of any overpressures, documenting a history involving high vertical effective stress.
3) High sedimentation rates and associated rapid burial in the Pliocene generated late overpressure through disequilibrium compaction in the Oligocene to early Miocene sections during this period, but had little or no impact on reservoir quality of the Farewell Formation. The retention of the late overpressure is attributed to the severe reduction of permeability during cement dissolution and secondary compaction.
4) Late and rapid burial has not allowed sufficient time for clay mineral transformation to take place, with Farewell Formation displaying anomalously high kaolinite content and high Illite:smectite ratios relative to the present day formation temperatures.
5) Continued compaction of Farewell Formation sandstones after dissolution of early carbonate cements creates zones of extremely low permeability, which has the potential to act with interbedded mudrocks to form a pressure seal as seen in the deep section of the Kapuni Field.
6) Depositional facies and early diagenetic cements within the Farewell Formation play an important role in defining the pore pressure and must be included when predicting the geopressure regime in the deeper sections of the Taranaki Basin.
7) The resolution of a diagenetic paragenesis for the Farewell Formation has important implications for hydrocarbon exploration and prospect development in deep parts (>4500 mTVD) of the underexplored areas in Taranaki Basin.

CHAPTER V:

CONTROLS ON RESERVOIR QUALITY IN THE SHALLOW PALAEOCENE STRATIGRAPHY OF THE TARANAKI BASIN

5.1. INTRODUCTION

The previous two chapters have shown that vertical effective stress (VES) has had limited, to no influence on reservoir quality of sandstones in the Taranaki Basin. The fluvial to marginal marine Palaeocene Farewell Formation sandstones as discussed in Chapter IV and lateral equivalent shoreface greensands (F-Sands; Enclosure 2), display excellent reservoir quality (Killops et al., 2009; STOS, 1993a, 1993b; Strogen, 2011). The F-Sands are a major oil reservoir in the Maui Field (Fig. 5.1 & 5.2) and other smaller accumulations on the Western Platform (Tui, Amokura & Pateke; Fig. 5.1). The F-Sands and Farewell Formation are of a similar composition and textural maturity, but the former has markedly higher porosity and permeability (av. 16.2% & 419 mD) when compared with the Farewell Formation at Kapuni Deep-1 (av. 3% & 0.01 mD).

As discussed in Chapter IV the Palaeocene reservoirs of the Taranaki Basin are an important petroleum hydrocarbon producing interval (Martin et al., 1994) and are a focus for renewed exploration within the offshore Taranaki Basin. The reservoir quality of the Farewell Formation/F-Sand sandstones within the Taranaki Basin are controlled mostly by grain size and the presence of chlorite/smectite, but this can vary with the presence of kaolinite often cited as the single most important cause of poor reservoir quality (Killops et al., 2009; Martin et al., 1994; Pollock et al., 2003; Smale et al., 1999). The Farewell Formation sandstones at the Kupe South Field and other marginal marine shoreface sandstones within the Taranaki Basin (e.g. Kaimiro Formation; Higgs et al., 2013) contain a diagenetic mineral assemblage that documents major shifts in pore-water chemistry during the burial history of the basin (Martin et al., 1994). Early calcite precipitated from meteoric depositional pore waters during shallow period, whereas later chlorite/smectite records the downward flow of marine pore waters into the sandstones from overlying, marine mudrocks prior to significant sandstone compaction during the late Miocene-Pliocene (Martin et al., 1994; O'Neill et al., 2018b).

Dissolution of detrital grains and early carbonate cement, due to the flow of CO_2 rich fluids has generated secondary porosity in Palaeocene and Eocene reservoirs of the Taranaki Peninsula (Higgs et al., 2013; O'Neill et al., 2018b). The link between CO_2 and the generation of secondary porosity has been recognised for a long time (Schmidt and Mcdonald, 1979; Seewald, 2003; Higgs et al., 2013 and references therein), and occurs in both clastic (Franks and Forester, 1984; Higgs et al., 2013; Lundegard and Land, 1986; Yuan et al., 2015a) and carbonate reservoirs (Esteban and Taberner, 2003; Mazzullo and Harris, 1992). The dissolution of feldspars and the generation of significant secondary porosity in the F-sands will be discussed in the context of hydrocarbon maturation and the flow of aggressive CO_2 rich fluids. The balance between feldspar dissolution and authigenic clay precipitation will be discussed in the context of whether the F-Sands are geochemically open (Day-Stirrat et al.,

2010; van de Kamp, 2008) or closed (Bjørlykke, 2014; Bjørlykke and Jahren, 2012; Ehrenberg, 1993; Xi et al., 2019) system, which is a subject of much debate.

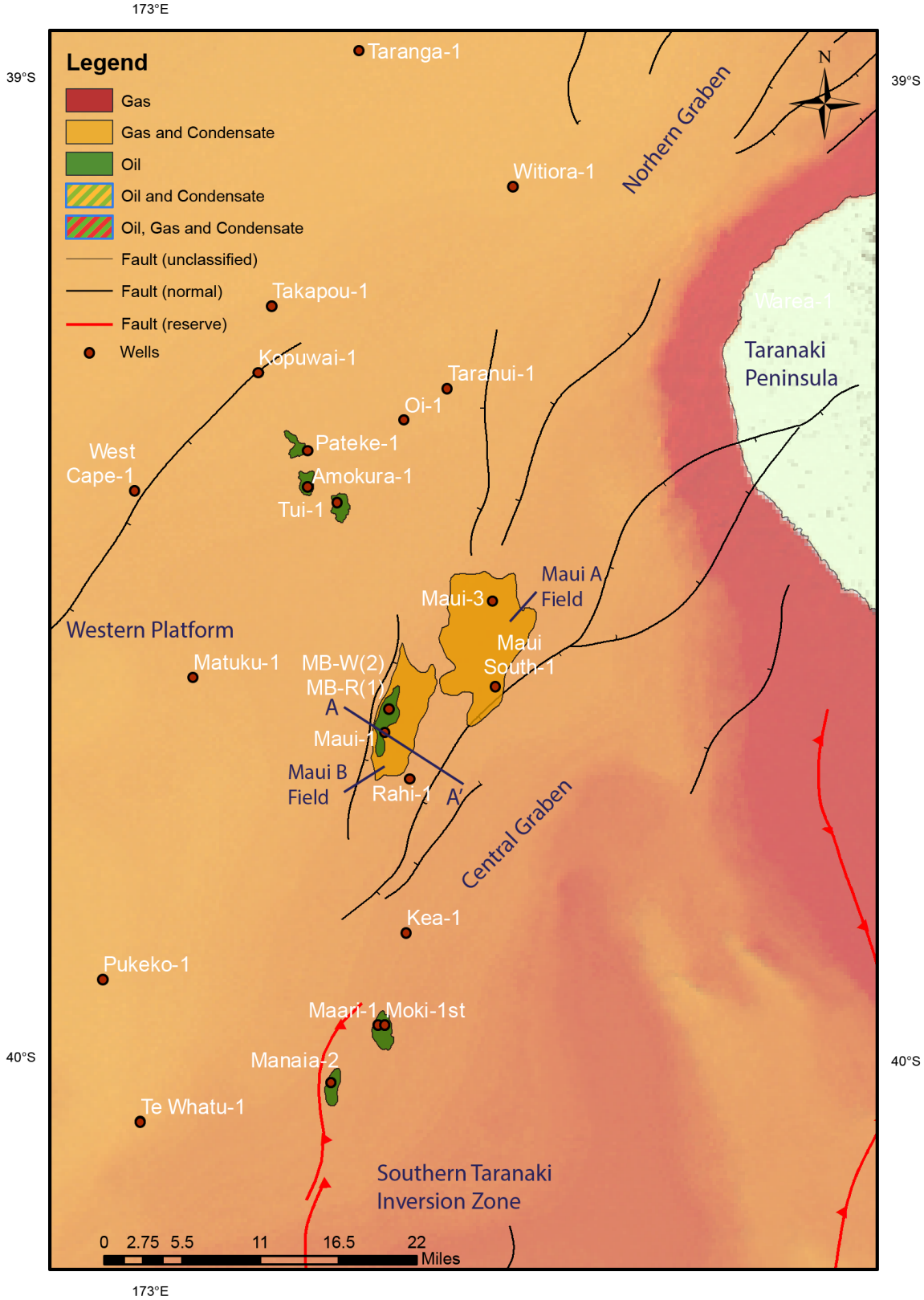

Figure 5.1. Map of Taranaki Basin showing the Maui Field and cross section for Fig. 5.2.

Greensand reservoirs, like the F-Sands, are particularly significant in siliciclastic shoreline systems, and are restricted almost exclusively to the rising limb of a relative sea-level curve , and usually associated with estuarine, barrier bar and shoreface environments (Dyson, 1998). These three depositional environments are often targets in hydrocarbon exploration

(Dyson, 1998), as they often display excellent reservoir quality and act as petroleum reservoirs worldwide (Çağatay et al., 1996; Slot-Petersen et al., 1998; Winn, 1994). The specific depositional environments allow for the placing of greensands within a sequence stratigraphic framework for regional exploration analyses. The relative deformity of glauconite grains can provide a good indication of the extent of mechanical compaction and thus can be used as a proxy for reservoir quality in real time during drilling, and furthermore can be an effective method for complementing measurement-while-drilling (MWD) controlled geosteering (Schulz-Rojahn et al., 2003).

This chapter will present new data and combine a number of approaches to resolve the diagenetic paragenesis of the F-Sands for improved understanding of the mechanisms involved in the generation of secondary porosity and precipitation of silica and clay cement.

5.1.1. The Maui Field

The Maui Field is comprised of two anticlinal closures, bounded to the SE by the normal Cape Egmont Fault and to the SW by the reverse Whitiki Fault (Fig. 5.2; King and Thrasher, 1996). Petroleum accumulations occur in the Palaeocene F-Sands (Farewell Formation equivalent see Enclosure II), Eocene C and D-Sands (Mangahewa & Kaimiro Formation), and Miocene B-Sands (Moki Formation), each of which is capped by a transgressive mudrock (Killops et al., 2009; Enclsoure 2). The reservoirs produce mainly gas, but oil rims are present in the C & D-Sands and in the F-Sands on the Maui B structure (Seybold et al., 1996). The F-Sands are draped over a structural high on the Maui B structure (Fig. 5.2), thinning towards the north-east, and did produce oil until the reservoir was abandoned.

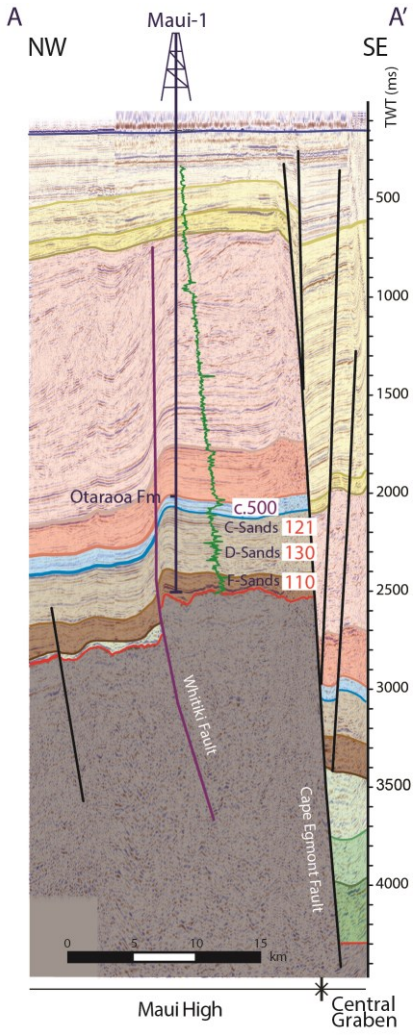

Figure 5.2. Interpreted seismic line through the Maui B Field, display Maui-1 well and associated reservoirs and formation overpressures. A-A' section can be seen in Fig. 5.2 and legend in Fig. 2.4. (modified from Line OTS-2, Strogen et al., 2014a)

5.1.2. The F-Sands

The F-Sands were deposited on a mature continental margin, extending from the NE-SW across the central part of the Taranaki Basin (Fig. 2.16), and show a progressive transition from a coastal plain facies in Maui-1 well in the south to upper and lower shoreface

environment in Tui-1 to the north-west (Fig. 5.1; Higgs et al., 2012; Pollock et al., 2003; Pollock and Crouch, 2005; Strogen, 2011; Strogen et al., 2014). Maui-1 well displays a low percentage of dinocyst (<3%) and numerous coal horizons, which are both indicative of coastal plain environment (Higgs et al., 2012a; Pollock and Crouch, 2005; Shiers et al., 2017). MB-R(1) and MB-W(2) drilled to the north-east from the Maui B platform display significant amounts of glauconite. Glauconite, an iron potassium phyllosilicate minerals is an authigenic mineral that forms exclusively in marine settings and commonly associated with low-oxygen conditions (Odin, 1988; Odin and Matter, 1981). Normally glauconite is considered a diagnostic of shallow marine shelfal environments with slow rates of sedimentation, but has been shown to precipitate in an dolomitic lagoonal sediment and marl-limestone alternation deposited in a brackish water estuary (El Albani et al., 2005). The F-Sands and Farewell Formation are sourced from erosion of crystalline basement in northwestern South Island and structural highs within what is now The Taranaki Basin, including granite batholiths of Cretaceous and Devonian age and Palaeozoic schists, quartzites and volcanics (Rattenbury et al., 1998).

5.1.2.1. Reservoir stratigraphy

The F-Sands are 95 mTVD thick at MB-R(1) and contain with 30m oil column (STOS, 1993a). Reservoir sandstones are interbedded with siltstone beds of up to 1.5m thick, are often heavily bioturbated. Net-to-gross across all then cored intervals is consistently in excess of 90%. The F-sands are split in the F1 & F0 sands, but both these intervals characterised by coastal plain to shoreface deposits in MB-R(1) and MB-W(2) (Pollock and Crouch, 2005).

5.2. Methodology

5.2.1. Sampling

Cores from the F-Sands in the Maui Field, have been cut in two development wells MB-R(1) (54 m) and MB-W(2) (28 m) from Maui B Platform (Fig. 5.1 & 5.2). Sixteen core samples were collected from sandstone beds across both wells from sections that were predominantly clean sandstone with a lack of shale or silt laminae. Thin sections of these were produced for transmitted light microscopy, SEM and QEMSCAN (Quantitative Evaluation of Minerals by SCANning electron microscopy) analysis. Eleven polished thin sections were obtained from Shell Taranaki Ltd. Petrophysical wireline data acquired over the cored intervals are representative of the F-sands across the Maui Field.

5.2.2. Petrographic analysis

Samples were analysed using transmitted-light microscopy on impregnated thin sections and modal analysis was undertaken on all samples to ascertain mineralogy (300 counts per section). The resulting data were used to calculate intergranular volume (IGV) (Paxton et al., 2002), porosity loss through mechanical compaction (COPL) and porosity loss by cementation (CEPL) (Lundegard, 1992), see Chapter IV, section 4.2.2 for methodology.

Scanning electron microscopy was undertaken on selected samples, providing additional information on the pore-system geometry, authigenic mineralogy, and paragenetic relationships. QEMSCAN data were collected from polished and carbon coated thin sections at two representative sample depths (3229.16 TVDss; MB-R(1) & 3238.7 TVDss; MB-W(2)) to supplement scanning electron microscopy and modal analysis. QEMSCAN analyses measures and identifies minerals within a defined sample area, using a scanning electron microscope (SEM) fitted with four light element x-ray energy dispersive spectrometer detectors, allowing for fast, quantitative, and repeatable mineralogical and rock texture analyses (Higgs et al., 2015).

5.2.3. One-dimensional burial history modelling

Pore pressure evolution within the stratigraphy intersected by MB-R(1) in the Maui Field was modelled in one dimension using Schlumberger's PetroMod (V. 2015) software. The burial model uses present-day well stratigraphy provided by the current Kapuni Field operator, Shell Todd Oilfield Services and lithologies created from mud log cuttings data in the well completion report (STOS, 1993a). The model was calibrated against corrected bottom hole data for the Kapuni Field (Rob Funnel pers. comm. 2017), measured formation pressures and helium porosity (Figs. 6c & 7b) (STOS, 1993a, 1993b). Further information on methodology for one-dimensional modelling can be found in Chapter III, section 3.2.1.

5.3. Results

5.3.1. F-Sands sandstone composition

The F-Sands in the Maui Field can be characterised as arkosic arenites (Fig. 5.3a) with abundant quartz (av. 47%) and feldspar (av. 24%); rock fragments of granite, schist, arenite and volcanics, make up av. 4% of the grains (Fig. 5.3b; Table 5.1). The rock is moderately sorted, medium to coarse-grained and mineralogically immature (Fig. 5.4a & b). The detrital grains range in size from very fine to very coarse sand and are predominately sub-angular to sub-rounded (STOS, 1993b, 1993a)(5.3a & b). Very rare preserved carbonate grains are present in one-third of the samples. Rare primary pore filling authigenic clay minerals that form between 0-10% of the rock (Fig. 5.5f; Table 5.1). Detrital micas are present in most sections varying between 0-3% in abundance (Table 5.1), with high percentages occurring in mudrock rich sections. Micas can vary between being undeformed to heavily deformed, both broken and bent as seen in Figure 5.6e. Detrital mud clasts are most prevalent in mudrock rich samples forming up to 6% abundance (Table 5.1). QEMSCAN (Fig. 5.4a & b) analyses identified the presence of detrital titanium oxide (1-3%). Hydrocarbon streaks are present within primary intra-granular porosity and very rarely fracture porosity (Fig. 5.6c).

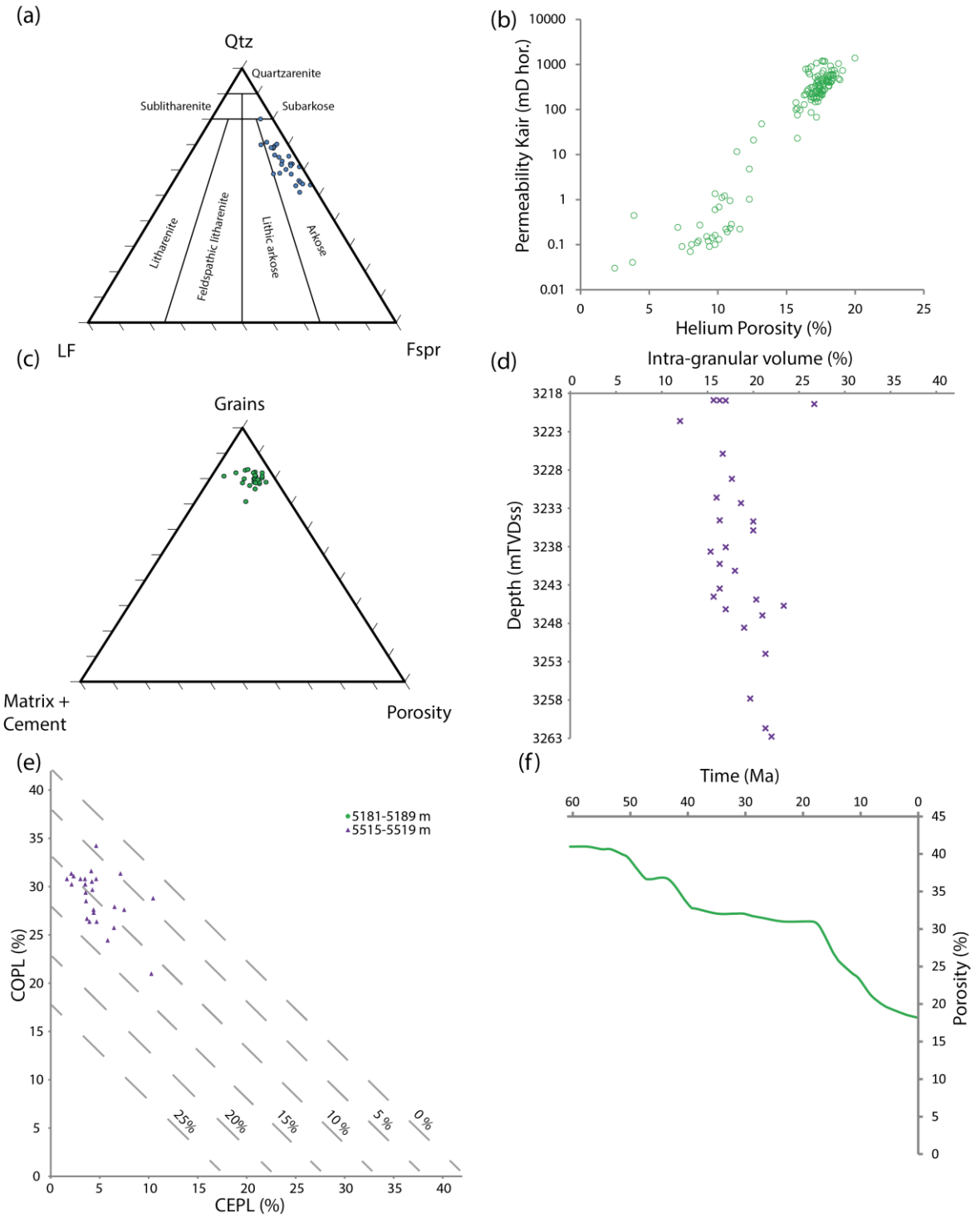

Figure 5.3. a) Ternary plot of present day composition of the F-Sands at MB-R(1) & MB-W(2) from modal point count data (Table: 5.1). b) Measured porosity permeability cross-plot from core analysis data of the F-Sands at MB-R(1) & MB-W(2) (STOS, 1993a, 1993b). c) Ternary plot displaying grains: matrix: porosity ratio of F-Sands at MB-R(1) & MB-W(2) from modal point count measurements. d) Plot of inter-granular volume variation with depth in the F-Sands at MB-R(1) & MB-W(2). e) Compactional (COPL) and cementational (CEPL) porosity loss for the F-Sands at MB-R(1) & MB-W(2) with remaining sample porosity (dashed lines). COPL and CEPL calculated after (Lundegard, 1992). f) Plot of modelled porosity development of F-Sands at MB-R(1) & MB-W(2) Kapuni Deep-1 against time.

Grains of yellow to bright green glauconite are present in every sample (Fig. 5.4, 5.5b & 5.6b), many of which are deformed and degraded. Both orthoclase and plagioclase feldspars are present and display various stages of alteration from fresh to highly corroded (Fig. 5.5a, 5.6a & 5.4), and often display overgrowths. In addition, there are rare titanium oxides (Fig. 5.4a).

Table 5.1: Model point count summary for the F-Sands at the Maui Field (IGV= intergranular volume; COPL= porosity loss due to mechanical compaction; CEPL= porosity loss due to chemical compaction).

Depth		Quartz	Lithics	Feldspar	Carbonate grain	Carbonate cement	Carbonate replacement cement	Heavy mineral	Mud clast	Hydrocarbon	Mica	Clay cement	Quartz overgrowth	Intergranular porosity	Secondary porosity	Glauconite	Feldspar Overgrowth	IGV	COPL	CEPL
[m] MDAH	[m] TVDss	[%]	[%]	[%]	[%]	[%]	[%]	[%]	[%]	[%]	[%]	[%]	[%]	[%]	[%]	[%]	[%]	[%]	[%]	[%]
3516.38	3218.90	54.3	5.3	17.3		0.3		1.0	0.3	0.3			2.7	12.3	5.3	0.7		15.7	31.2	2.1
3516.40	3218.95	60.0	3.3	12.0		1.3	0.3	1.0	0.7		3.0	2.3	1.0	12.0	1.7	1.3		17.0	30.1	3.5
3517.93	3218.92	50.0	3.7	18.7			0.0	1.0	1.0		1.7	2.0	4.3	9.7	4.7	3.0	0.3	16.3	30.7	4.6
3518.30	3219.40	45.0	6.0	13.7		0.3		1.7	1.3	0.7	1.3	4.0	6.3	13.0	2.0	2.3	2.3	26.7	20.9	10.3
3520.91	3221.62	48.0	2.3	27.0	0.3			0.7	4.3	0.7	0.7	5.0	1.7	4.3	4.3	0.3	0.3	12.0	34.1	4.6
3525.50	3225.88	43.3	4.0	27.3		0.3		0.3	0.3	0.3	2.0	2.7	2.7	10.3	3.0	3.0	0.3	16.7	30.4	4.2
3529.20	3229.16	50.7	5.3	21.3	0.3		0.3	0.3			0.3	2.0	3.0	11.7	2.0	2.0	0.7	17.7	29.6	4.2
3531.94	3231.60	48.0	4.3	23.7		0.3		0.3	0.3		1.3	0.3	2.0	12.7	3.3	2.7	0.7	16.0	31.0	2.3
3535.20	3234.57	53.0	4.7	20.0	0.3	0.3	0.3		0.3	1.0	0.7	2.0	1.3	11.0	0.7	4.0	0.3	16.3	30.7	3.0
3539.20	3238.07	54.3	4.7	20.3	0.7			0.7	0.3			2.0	2.3	12.0	1.3	0.7	0.7	17.0	30.1	3.5
3545.20	3243.47	50.7	4.7	23.0	0.3	0.3	1.3	0.7	0.3		0.3	0.3	2.3	11.3	1.0	2.7	0.7	16.3	30.7	3.5
3548.41	3246.17	51.7	3.0	19.3		1.7		0.3	1.7	1.0	1.3		1.0	13.0	1.7	4.0	0.3	17.0	30.1	2.1
3560.90	3257.82	50.3	2.0	25.0	0.3	3.0	1.7	1.0				1.7	2.0	10.7		1.7	0.7	19.7	27.8	6.5
3565.25	3261.69	44.0	8.3	23.3		2.0		0.3		0.3		2.3	1.0	15.7	0.3	2.3	0.0	21.3	26.3	3.9
3569.90	3262.77	52.0	5.0	19.0		1.0	0.3			0.7	0.7	6.3	0.7	12.7	0.3	1.0	0.3	22.0	25.6	6.4
4111.20	3232.33	40.3	2.3	22.3		3.0	1.3	0.3	0.3	0.7	5.0	10.0	0.3	3.3		10.7		18.7	28.7	10.5
4113.88	3234.71	35.7	4.3	30.0				0.7	0.3	0.3	1.0	8.7	1.7	9.3	1.3	6.7		20.0	27.5	7.5
4115.20	3235.89	40.3	3.0	29.3		3.0	0.3	0.3	1.3	0.7	1.0	1.7	0.7	13.3		4.7	0.3	20.0	27.5	4.4
4118.30	3238.65	42.0	1.0	35.0					1.3		1.0	2.3	3.0	9.3	0.7	3.7	0.7	15.3	31.5	4.1
4120.10	3240.26	48.3	1.0	30.0		0.7		0.3	0.7	0.7	0.7		1.3	13.3	1.0	1.7	0.3	16.3	30.7	1.6
4121.10	3241.15	41.3	3.0	31.0	0.3	0.3		1.3	1.0		1.0	2.0	2.0	13.0	0.3	2.7	0.7	18.0	29.3	3.5
4124.88	3244.53	44.3	4.7	22.7				0.3	2.0	1.0	1.0	6.3	3.3	4.3	1.7	7.7	0.7	15.7	31.2	7.1
4125.30	3244.91	44.0	6.7	24.7		1.3		0.3	0.3		0.3	1.0	3.0	14.3	0.3	3.0	0.7	20.3	27.2	4.4
4126.20	3245.71	42.3	4.3	24.0		0.7		0.7	1.0	0.7	0.7	4.3	1.3	15.0	0.3	3.3	1.3	23.3	24.3	5.8
4127.60	3246.96	40.7	2.7	31.7	0.3	1.0	0.3		0.3	0.3		1.0	2.0	15.7		3.3	0.7	21.0	26.6	3.7
4129.40	3248.58	42.3	2.7	24.0				0.7	5.7	3.3	1.3	2.0	2.3	10.7	1.0	3.3	0.7	19.0	28.4	3.6
4133.20	3251.98	40.7	4.7	30.7	0.3	0.3			0.3	0.3	0.3	2.7	2.3	14.7		1.7	1.0	21.3	26.3	4.7

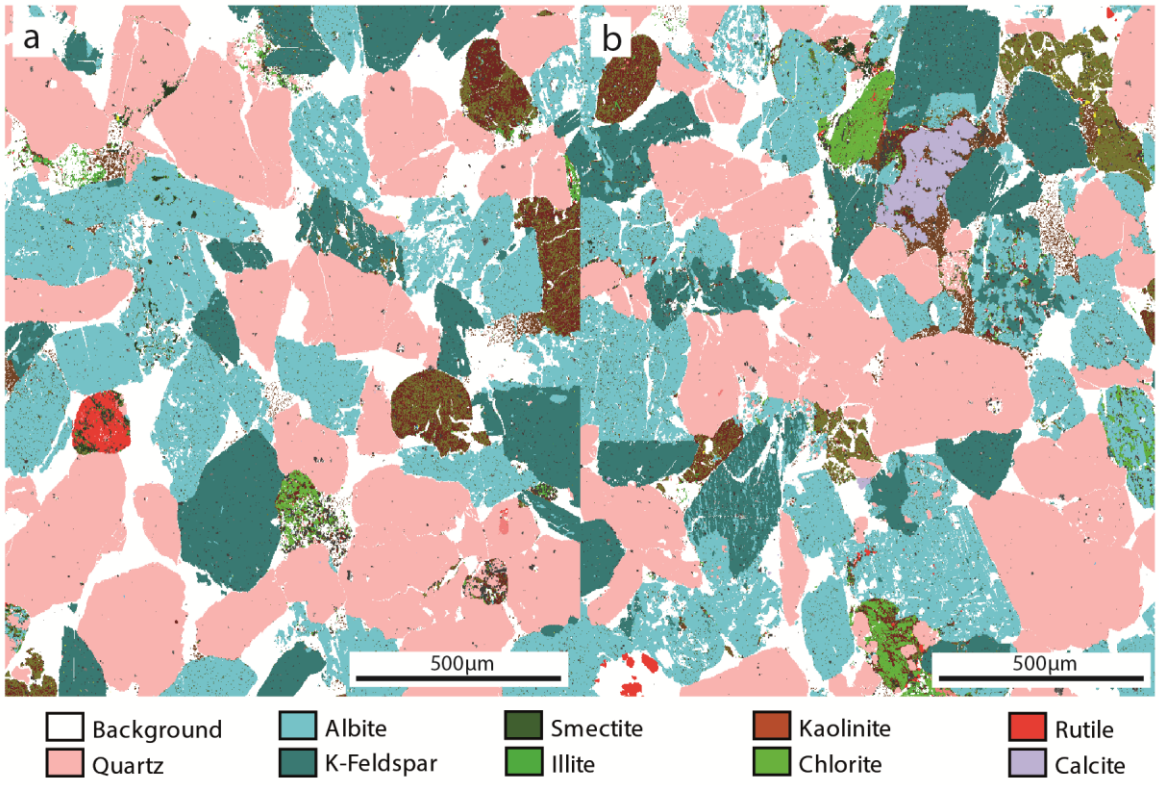

Figure 5.4. a) QEMSCAN image (3229.16 TVDss; MB-R(1)): degraded feldspar grains, heavy mineral and connected inter-granular porosity. b) QEMSCAN image (3238.7 TVDss; MB-W(2)): late carbonate cement, degraded glauconite, minor pore filling kaolinite and pressure solution.

5.3.1.1. Mechanical compaction

Maui F-Sand samples display features of mechanical compaction with soft grains, such as deformed lithic clay grains, kinked mica grains and chemical compaction features such as concavo-convex grain contacts at detrital quartz grain boundaries are common (Fig. 5.6a). Mechanical compaction led to fracturing of both feldspar and quartz grains, and the bending and breaking of micas (Fig. 5.6e). The average values for porosity loss due to compaction (28%) and cementation (5%), from Figure 5.2e (Lundegard, 1992), identifies that the main driver of porosity loss in the Maui F-Sands is due to mechanical compaction rather than cementation.

5.3.1.2. Authigenic clay minerals

Authigenic clay minerals are not common in any section under reflected light, rarely filling pore space (Fig. 5.5f) and never rimming grains whole grains. SEM, SEM-EDS and QEMSCAN analyses identified sporadic thin chlorite coating alongside mixed layer Illite/smectite coats, which are in places impeding the nucleation and growth of quartz overgrowths (Fig. 5.5d). Kaolinite booklets rarely fill intergranular porosity and can bridge pore (Fig. 5.5f), and can coat grains where individual booklets project out from the surface. Heavily degraded glauconite grains can be seen in both reflected light and SEM, which are altering progressively to kaolinite and chlorite (Fig 5.5b).

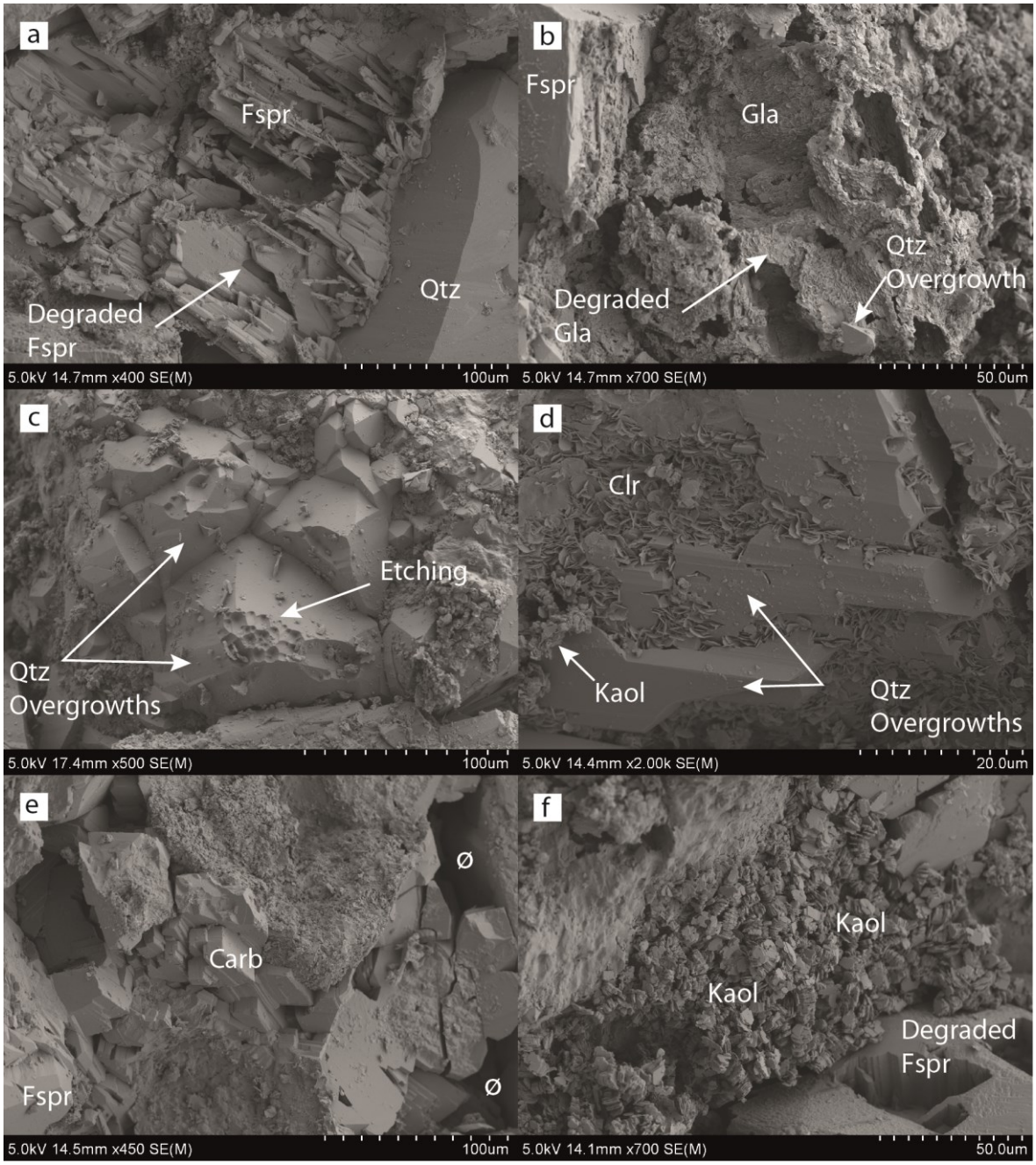

Figure 5.5. a) SEM image (3244.90 mTVDss; MB-W(2)): heavily degraded feldspar grain displaying honeycomb porosity. b) SEM image (3261.69 mTVDss; MB-R(1)): heavily degraded glauconite grain. c) BSEM image (3244.90 mTVDss; MB-W(2)): macro-quartz overgrowths with etched crests d) SEM image (3261.69 mTVDss; MB-R(1)): quartz overgrowths and grain coating chlorite. e) SEM image (3244.90 mTVDss; MB-W(2)): pore filling carbonate cement and open inter-granular porosity. f) SEM image (3244.90 mTVDss; MB-W(2)): degraded feldspars and pore filling kaolinite. (Fspr= feldspar; Qtz= quartz; Gla= glauconite; Ø= porosity; Clr= chlorite; Kaol= kaolinite; carb= carbonate cement; Clr/smectite-mixed layer chlorite/smectite).

5.3.1.3. CARBONATE CEMENT

Carbonate cements are localised throughout the F-Sands and within isolated patches they tend to be euhedral sparitic calcite cement fills (Fig. 5.5e) and partially or fully replacive of feldspar and quartz grains (Fig. 5.4b). Carbonate cementation can also be found between cleavage planes of mica grains (Fig. 5.6f). QEMSCAN analyses (Fig. 5.4b) supports the hypothesis that calcite cement to be sporadically developed and only fills secondary porosity. Modal analysis from all thin sections has shown calcite to contribute up to 5% of the rock.

The euhedral nature of calcite cement indicates that there has been limited subsequent dissolution (Liu et al., 2018; STOS, 1993a; Xi et al., 2019), which suggests that they formed at a late stage.

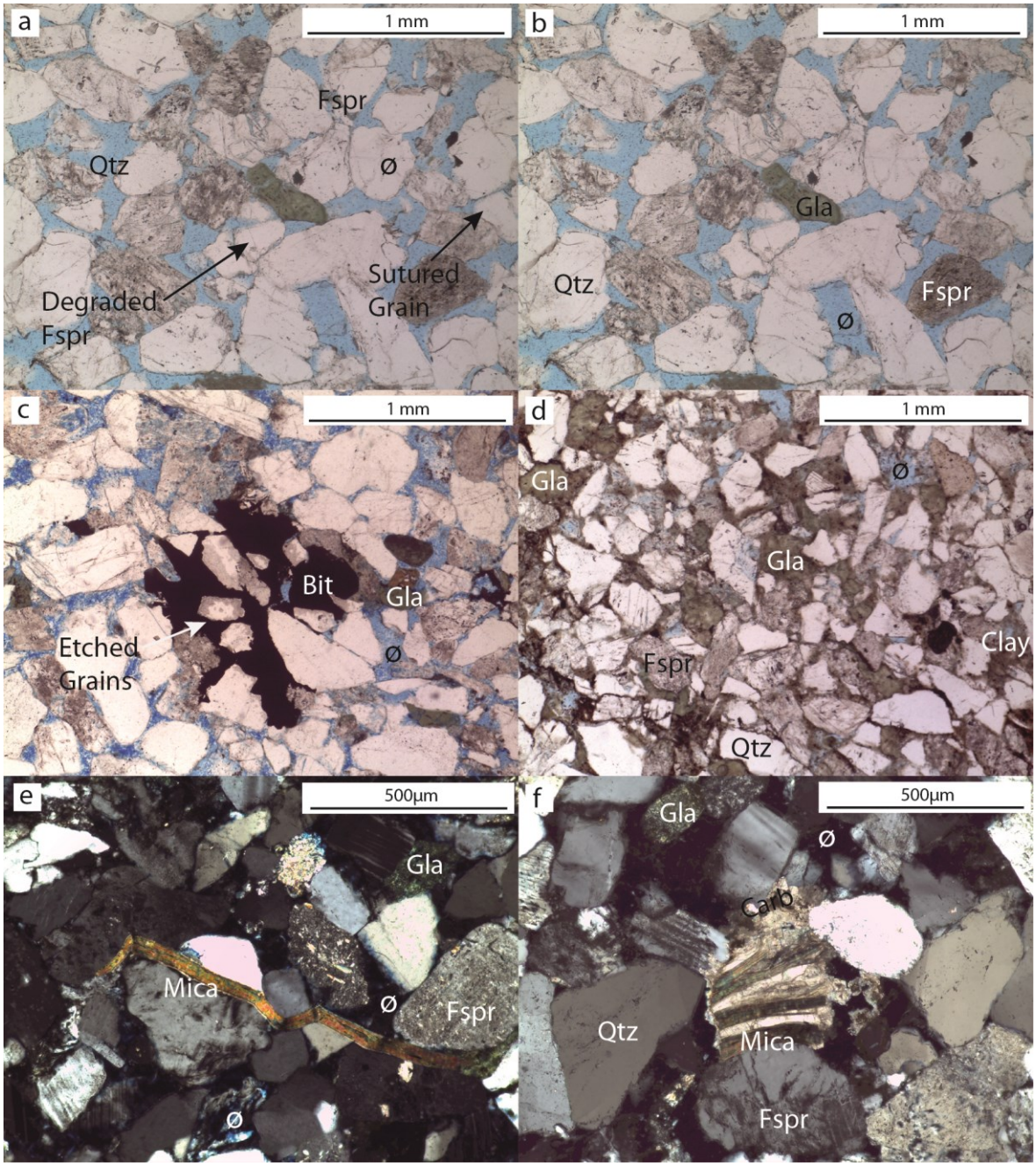

Figure 5.6. a) Thin section micrograph (3219.0 mTVDss; MB-R(1)): open inter-granular porosity, sutured grain contacts and degraded feldspar. b) Thin section micrograph (3251.82 mTVDss; MB-R(1)): connected intergranular porosity and glauconite. c) Thin section micrograph (3240.20 mTVDss; MB-W(2)): bitumen filled fracture displaying etched grains. d) Thin section micrograph (3234.70 mTVDss; MB-W(2)): very-fine grained sandstones displaying abundant glauconite and clay cement, and limited visible inter-granular porosity. e) Thin section micrograph (3238.70 mTVDss; MB-W(2)): deformed mica and glauconite grain. f) Thin section micrograph (3244.90 mTVDss; MB-W(2)): carbonate cement growing between cleavage planes in a mica grain. (Fspr= feldspar; Qtz= quartz; Gla= glauconite; Ø= porosity; Bt= bitumen; carb= carbonate cement).

5.3.1.4. Quartz cementation & fluid inclusions

Pressure dissolution and stylolitisation of quartz grains has been identified in reflected light microscopy (Fig. 5.6a) and in backscatter SEM images (Fig. 5.7a). Quartz cements are

recognised in all samples used in this study, and dominated by blocky and thick macro-quartz overgrowths, present on detrital quartz grain surfaces and especially non-coated grain surfaces (Fig. 5.7a). The macro-quartz overgrowths are defined as syntaxial quartz overgrowth larger than 20 μm in optical continuity with the detrital quartz grain. They are well developed euhedral overgrowths, with abundant fluid inclusions in dust rims and pitted crests (Fig 5.5c). Minor overgrowths have been identified on degraded glauconite grains (Fig. 5.5b). Although quartz cement is common amongst the samples in this study, but usually only contributes 2% of the bulk rock and can exceed this in single samples.

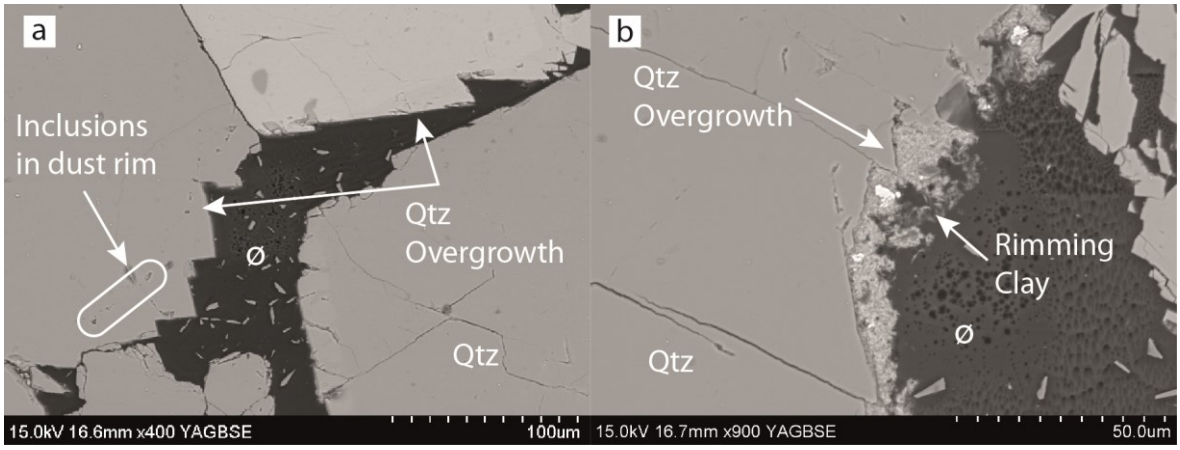

Figure 5.7. a) BSEM image (3238.07 mTVDss; MB-R(1)): fluid inclusions trapped in the dust rim of macro-quartz overgrowths. b) BSEM image (3238.07 mTVDss; MB-R(1)): mixed clay coating on surface of quartz overgrowth. (Ø= porosity)

Growth of quartz overgrowths may have been inhibited by the presence of chlorite coating on grains (Fig. 5.5d). Killops et al. (2009) identified appreciably more aqueous inclusions than oil inclusions, with the majority of the oil inclusions being found in dust rims between overgrowths, which document multiple phases of hydrocarbon charge. Homogenisation temperatures of quartz aqueous inclusions are between 93°C to 127°C (Killops et al., 2009).

5.3.1.5. POROSITY

Core analysis results (Fig. 5.3b) show helium reservoir porosities range between 3-22 % (av. 16.2%) (STOS, 1993b, 1993a). Porosity is a combination of primary intergranular (Fig. 5.6b), secondary dissolution (Fig. 5.6a) and very minor fracture porosity (av. <1%). Primary intergranular and secondary dissolution pores are often interconnected, aided through minor fracturing of feldspars grains. Secondary pores are formed through corrosion of feldspars, producing honeycomb textures (STOS, 1993a) (Fig. 5.5a & 5.6a). The final present day basin modelling derived porosity of c. 18% (Fig. 5.3f) matches the average helium porosity when fine grained intervals are excluded. Rare grain sized pores are evidence for total dissolution (Fig. 5.6a), though there is a possibility that these are artefacts of sample preparation. The limited amount of authigenic pore filling or pore throat blocking clay cement types will have assisted in maintaining the high permeabilities (av. 419 mD; Fig. 5.3a).

5.3.2. VERTICAL PRESSURE DISTRIBUTION

As previously discussed all reservoirs on the Western Platform and Southern Taranaki Inversion are hydrostatically pressured from the Cretaceous to Pliocene, with no difference in the Maui Field (Fig. 5.8). Thin interbedded transgressive marine mudrocks act as vertical pressures seals, producing the minor pore pressure variations between the C, D and F Sands in the Maui Field (see Figs. 5.2 & .5.8).

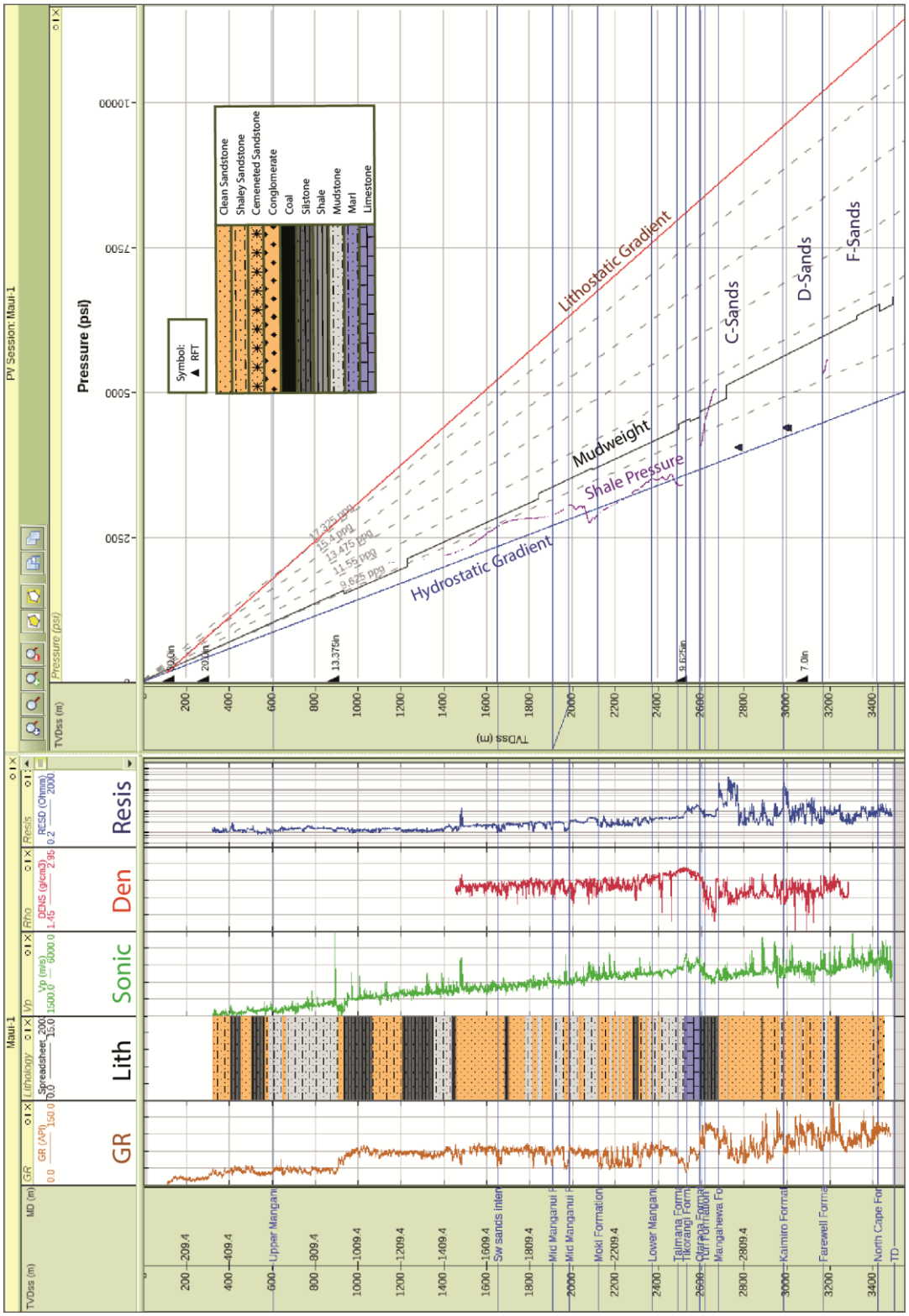

Figure 5.8. Maui-1 pressure depth plot with associated suite of wireline measurements (gamma ray [brown], Vp [green), resistivity [blue], density [red], lithology column, RFT [black triangle], mudweight [black] and shale pressure [purple])

5.3.3. BURIAL HISTORY MODELLING AND PORE PRESSURE EVOLUTION

Deposition of the F-Sands began during the Early Palaeocene on a mature continental margin (Fig. 2.17) in shoreface to inner shelf setting as indicated by the high net-to-gross, presence of glauconite and poorly developed thin shale horizons. These deposits experienced markedly reduced initial subsidence of 32 m/M.y. in comparison to the Farwell Formation at Kapuni Deep-1 (150 m/M.y.). During the early Eocene the basin was starved of sediment and subsidence rapidly increased (Kamp et al., 2004; King and Thrasher, 1996; Strogen et al., 2014b), which led to a significant increase in water depth to bathyal levels (Fig 5.9a). One-dimensional basin modelling shows that the sand rich Palaeocene to Eocene sediments allowed for vertical dewatering, leading to maintenance of close to hydrostatic conditions throughout this period (Fig. 5.9a).

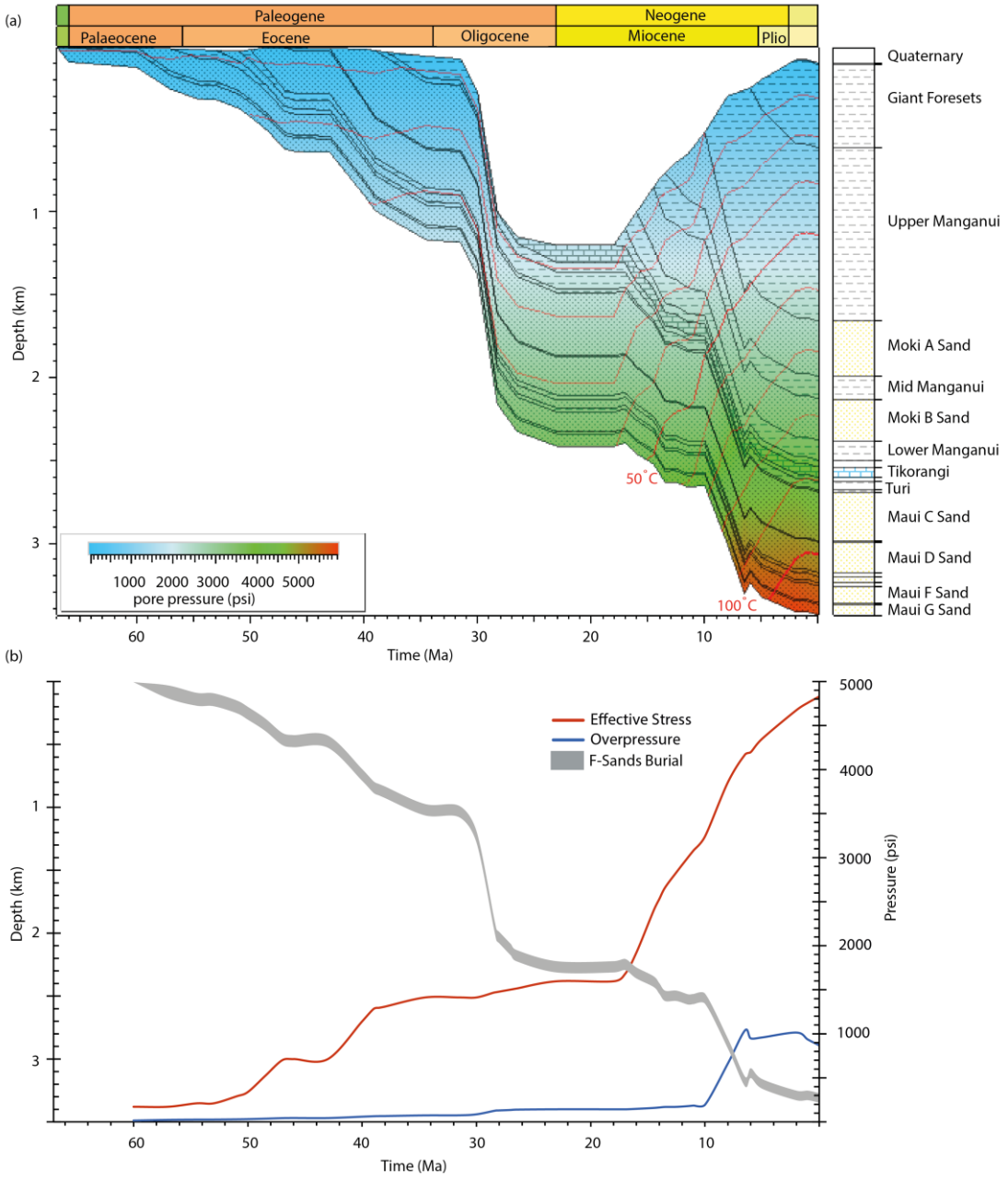

Figure 5.9. a) 1D burial history plot of MB-R(1) (Petromod). Red lines are isotherms and colour overlay denotes pore pressure. b) Plot displaying the evolution of overpressure and effective stress with burial since the deposition of the Turi Formation.

Sedimentation rates increased to 330 m/M.y. during the early Miocene leading to the onset of overpressure at c.10 Ma due to the deposition and loading of the previously mentioned continental sedimentary wedge (Fig. 5.9b). By the Late Miocene (~6 Ma) the rate of burial, particularly in southern and central parts of Taranaki Basin slowed and was followed by changes in the sense of displacement on prior normal faults, the associated development of anticlinal inversion structures and widespread uplift of southern Taranaki Basin (Crowhurst et al., 2002; Kamp and Green, 1990).

The structural development of the Maui trap occurred during this period, at ~6 Ma (Funnell et al., 2004; King and Thrasher, 1996), which coincided with the initial hydrocarbon charge into the Maui Field (Killops et al., 2009). The trapping temperature (av. 103°C) inferred from the homogenisation of aqueous inclusions was reached 7-7.5 Ma, towards the end of the deposition of the Manganui Formation (Killops et al., 2009). The burial history (Fig. 5.9a) shows that trapping occurred close to maximum burial depth, after which passive subsidence prevailed until the present.

5.3.4. DIAGENETIC PARAGENESIS

Mechanical compaction will have begun during shallow burial demonstrated by the deformation of liable grains (micas and glauconite) and the formation of concavo-convex and long grain contacts. The minor grain fracturing observed will have formed throughout burial occurred due to pressure at grain point contacts (Chuhan et al., 2003, 2002). Carbonate cementation will have also initiated at shallow depths with initial pore-filling calcite cement, supported by the lack of grain-grain point contacts in some sections. Although no oxygen isotope analyses are available, it can be assumed that carbonate cementation occurred over an extended interval throughout the Eocene to Pliocene during burial of F-Sands.

The onset of feldspar and mica degradation will have occurred during shallow burial, contemporaneously with precipitation of kaolinite (Bjorlykke, 1998; Lanson et al., 2002) (Fig. 5.10). Detrital glauconite grains can be heavily deformed and will have begun to dissolve towards maximum burial in temperatures above 100-110°C (Hansley and Nuccio, 1992; Ivanovskaya et al., 2003). Iron released during the degradation of glauconite has shown to re-precipitate as chlorite, as demonstrated in the Shannon Sandstones of Wyoming (Hansley and Nuccio, 1992), which could account for chlorite rims on detrital grains in the F-Sands. Fluid inclusion data collected by Killops et al. (2009) suggests that quartz cementation initiated at approximately 93°C in the F-Sands in the Maui Field, with a main phase occurring between 97 °C and 107°C. The in situ temperature inferred by homogenization of aqueous inclusions was reached 7.0–7.5 Ma ago, towards the end of the deposition of the Manganui Formation (Killops et al., 2009). The liberation of silica from the feldspar degradation and subsequent clay reactions will also aid in the nucleation and growth of quartz overgrowths.

Minor quantities of Illite have been identified, which may have transformed from kaolinite and/smectite at temperatures in excess of 70°C below 3 km of burial (Worden and Morad, 2009). Oil charging will have begun it c.6 Ma (Funnell et al., 2004; King and Thrasher, 1996) associated with the flushing of aggressive acidic fluids, which has been demonstrated in the Kapuni Field (Higgs et al., 2013; O'Neill et al., 2018b). This would lead to enhanced dissolution of framework grains, early carbonate cement and etching on quartz overgrowths. Carbonate cement precipitation is also still occurring at a late stage shown by pervasive filling of secondary porosity.

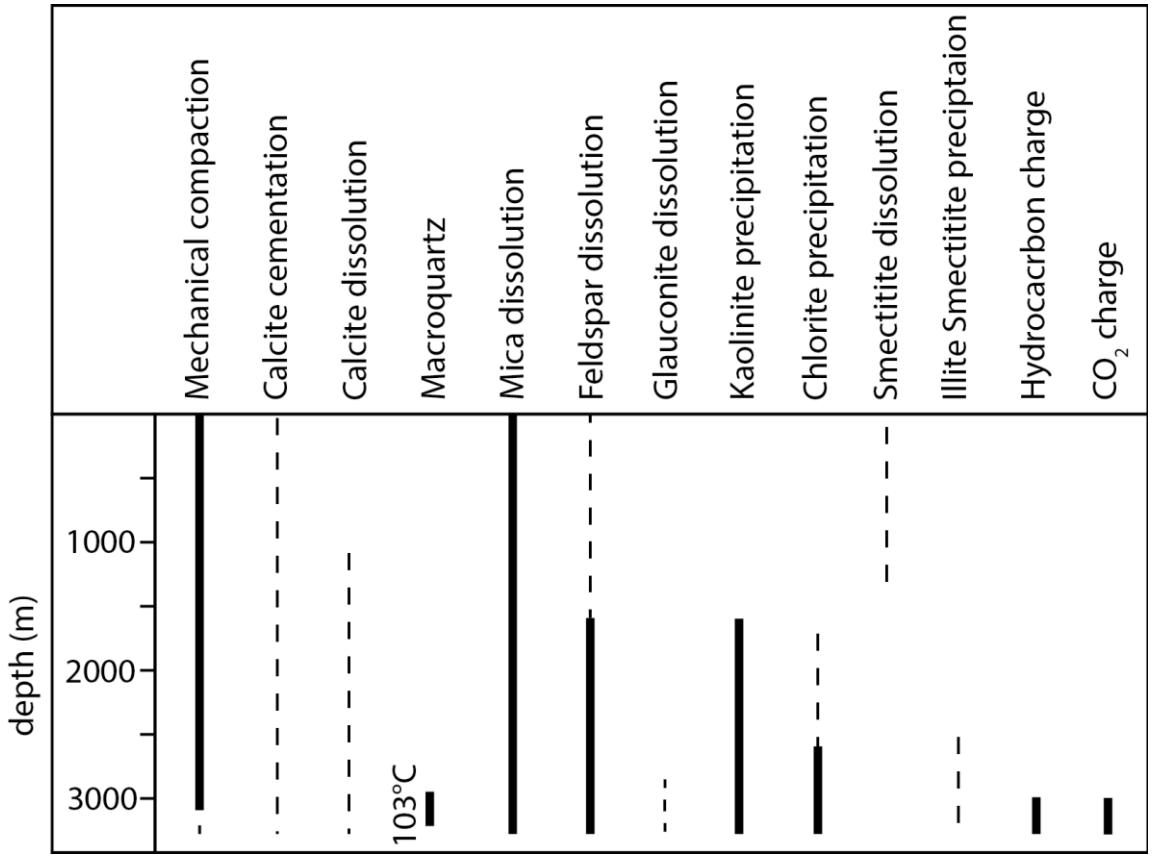

Figure 5.10. Diagenetic Paragenesis for F-Sands sandstone beds in Kapuni Deep-1 (fluid inclusion microthermometry after (Killops et al., 2009)

The present-day reservoir quality of the Farewell Formation is a cumulative product of depositional attributes (facies and grain size), mechanical compaction and diagenesis during early and later stages of burial (Fig. 5.10). Mechanical compaction and late generation of secondary porosity are the most significant diagenetic processes occurring in the F-Sands at Kapuni Deep-1. The COPL-CEPL analyses, minor grain fracturing, and grain deformation all suggest that mechanical compaction was the key driving mechanism for porosity reduction during the first 2500 m of burial through the steady increase of vertical effect stress, which has been demonstrated by basin modelling (Fig. 5.9b).

5.4. DISCUSSION

The excellent reservoir quality of the F-Sands reservoir at the Maui Field is due to a three key factors, namely: the relatively shallow depth of burial, limited amount of both authigenic silica and clay cements and the formation and preservation of secondary porosity. The high net-to-gross and significant connectivity of associated reservoirs is facilitated the lateral drainage of any generated overpressure. The F-Sands could be characterised as a geochemically closed system, where dissolved solutes are redistributed within the reservoir.

5.4.1. RESERVOIR QUALITY

Although some primary inter-granular porosity has been lost through mechanical compaction, the effective stress conditions of the reservoir are still relatively low (Fig 5.9b; 4800 psi), especially when compared with Kapuni Deep-1 (Fig. 4.10b; 7600 psi). The onset of the precipitation of silica cement can occur in a range between 70-100°C (Bjorlykke and Egeberg, 1993), but the start of significant silica cementation typically occurs between 90-100°C (Giles et al., 2009). The F-Sands have experienced a maximum temperature of 105°C (Fig. 5.9a), suggesting that pervasive silica cement could be present, but this is not the case. The limited quartz cementation could be due to the F-Sands only entering the chemical compaction window (>2500 m) in the past 10 Ma and the 'significant' quartz cementation realm 7 M.y ago. Also, in places chlorite grain coatings have shown to limit the nucleation and growth of quartz overgrowths (Fig. 5.5d; e.g. Ehrenberg, 1993; Stricker and Jones, 2016; Stricker et al., 2016).

The limited volume of pore filling clay cement has left pore throats open, allowing for excellent permeability and thus connectivity within the reservoir, which is enhanced through significant secondary dissolution porosity (Table 5.1) and some minor fracturing (Chuhan et al., 2002). The limited ductile grain content combined with the moderately well sorted nature of the sandstone beds, has allowed for less efficient packing grains, enhancing porosity and permeability (Paxton et al., 2002), which is suggestive of a facies control on reservoir quality, which has been demonstrated in marine shelfal facies worldwide (Ambrose et al., 2017; Haile et al., 2018; Mansurbeg et al., 2008; Porter et al., 2018). The ductile nature of glauconite grains (Ranganathan and Tye, 1986) allows for non-elastic deformation of greensand (Hossain et al., 2009), which would affect reservoir quality by potentially blocking pore throats.

5.4.2. CO_2 AND SECONDARY POROSITY

CO_2 rich fluids have been shown to contribute towards feldspar dissolution in clastic reservoirs (Cao et al., 2014; Hansley and Nuccio, 1992; Higgs et al., 2013; Lundegard and Land, 1986; Yuan et al., 2015b), supported by both experimental work (Wang et al., 2017) and numerical modelling (Barclay and Worden, 2000; Xu et al., 2005). The flow of acidic CO_2

rich fluids has been shown to be an important mechanism in driving dissolution of carbonate cements and detrital grains, generating secondary porosity in the Kapuni Field (Higgs et al., 2013; O'Neill et al., 2018b), and producing oversized pores in some Taranaki reservoirs (Collen and Newman, 1991). Dissolved CO_2 in the pore fluids within the F-Sands could have driven feldspar dissolution, producing the previously mentioned honeycomb texture secondary porosity.

The source of the oil, and therefore CO_2, in the Maui Field is enigmatic, but a discrete Late Cretaceous coaly source with a marine contribution is thought to be responsible (Killops, 1996). The Late Cretaceous Rakopi Formation (Enclosure 2) is immature in the vicinity of the Maui Field, and oils of that age are rare in the Taranaki Basin as most were expelled >20 Ma, prior to trap development and so lost from the petroleum system (Armstrong et al., 1994; S. D. Killops et al., 1994). More recent work has suggest numerous phases of hydrocarbon charge from a number of potential source areas, with long migration pathways (Funnell et al., 2004, 2001; Killops et al., 2009). As these acidic fluids migrate over large distances, it could be expected that they would reach equilibrium with pore waters, but that is not case in the Maui Field, as we see significant etching and degradation of detrital grain in the F-Sands. Bitumen filled fractures (Fig. 5.6c) with etched grains (Fig. 5.5c) identified in the F-Sands could act as high permeability pathways of enhanced fluid flow, transporting the aggressive fluids over long distances relatively quickly.

Basin modelling of the Kapuni Field carried out by Higgs et al. (2013) suggests that the Cretaceous source rocks within the Manaia Graben were only mature for CO_2 expulsion below 4000 mTVD. If this holds true for source kitchens in the Southern Taranaki Inversion and Western Platform, which reached those depths only recently (c.10 Ma), then acidic fluids will have been expelling relatively recently towards maximum burial of the F-Sands. The associated dissolution will have weakened the grain framework, but limited subsequent burial reduces the potential for secondary compaction, leading to the preservation of secondary porosity in the F-Sands.

5.4.3. CONNECTIVITY & OVERPRESSURE MAINTENANCE

At a certain depth within the burial of the Farewell Formation sandstones at Kapuni Deep-1, the reservoir permeability reduced to a point where lateral and vertical fluid migrated was restricted, leading to the onset of abnormal pressure. The very high net-to-gross of the F-sands, often in excess of 95% (STOS, 1993a), and therefore connectivity of the reservoir would allow for dissipation of abnormal reservoir pressure (Harrison and Summa, 1991). High permeabilities are maintained throughout burial of the F-Sands, allowing for continued pressure bleed off, which is supported by the presence of lateral drainage on the Western Platform and Southern Taranaki Inversion (O'Neill et al., 2018b; Webster et al., 2011).

5.4.4. CEMENT DISTRIBUTION

It could be assumed that the significant degradation of detrital feldspars within the F-Sands would have led to the precipitation of pervasive clay cement, but analyses using both reflect light and SEM petrography have shown this not to be the case. This suggests that the F-sands may be part of a geochemically open system; a topic of much debate within the field of diagenesis within sedimentary basins. It has been suggested that deep sandstones reservoirs (>2 km) are geochemically closed system, such that diagenetic reactions can be written as balanced equations, due to the fact that the precipitation of cement equals dissolution at a local scale (Bjørlykke, 2014; Bjørlykke and Jahren, 2012; Ehrenberg, 1993; Higgs et al., 2007). The open-system model is characterised by large-scale import and export of solids in solution, which has been supported by the work on mudrocks where diagenetic reactions within the mudrocks can be the source of silica to surrounding sandstones (van de Kamp, 2008), while also absorbing kaolinite for use in clay transformation reactions (Day-Stirrat et al., 2010)

Open geochemical systems within sandstones are postulated to occur in the presence of low-salinity meteorically sourced pore waters, which can be associated with flushing of solutes derived from feldspar dissolution (Yuan et al., 2017, 2015a). Through flow of meteoric water within shallow marine sandstones often occurs post deposition, driven by the head of groundwater table in adjacent land areas (Bjørlykke, 2014). The hydraulic head, created by the presence of Mount Taranaki (Allis et al., 1997) and Cretaceous to Palaeocene outcrops across the north coast of the South island (Browne et al., 2008), could be providing a flow of meteoric water. However, this seems unlikely given the significant depth, low water-flow rates and low concentration gradients for diffusion (Bjørlykke and Jahren, 2012). The F-Sands represent a hydraulically open system receptive to lateral fluid flow, but this does not translate to an open geochemical system where the potential to transport solutes at low concentration is limited (Bjørlykke and Jahren, 2012).

Significant leaching could have occurred during shallow burial, leading to a loss of the dissolved solutes form the system, but subsequent rapid loading from 10-6 Ma (Fig. 5.9a) would have rapidly increased the effective stress and destroyed secondary porosity.

The F-Sands acting as geochemically closed system could be a more plausible option. Higgs et al. (2013) suggest that a greater percentage of secondary minerals have been precipitated in fine grained heterolithic beds than associated coarser well sorted intervals in the Mangahewa and Kaimiro formations of the Kapuni Field. This implies a net redistribution of ions from coarse cleaner beds to fine heterolithic beds, a mechanism which could be invoked in the F-Sands where siltstone beds contain a significantly higher percentage of clay cement (Fig. 5.6d) compare with associated high permeability reservoir facies (Fig. 5.6b).

5.4.5. VERTICAL EFFECTIVE STRESS AND RESERVOIR QUALITY

The very limited amount of generated overpressure and the constant high permeabilities throughout burial, leading to constant pressure bleed off; means that the F-Sands did not experience a significant deviation away from hydrostatic pressure, so vertical effective stress could have no impact on porosity preservation.

5.5. CONCLUSIONS

1) Mechanical compaction is the key mechanism for porosity reduction in the F-Sands of the Maui Field during the first 2500 m of burial, shown by grain fracturing, concavo-convex and quartz-to-quartz long grain contacts, and deformed liable grains has reduced reservoir quality by early burial compaction processes.
2) The high net-to-gross reservoir intervals and absence of significant intervals of low permeability fine-grained strata within Palaeocene and Eocene sections has allowed the reservoirs to dewater during burial inhibiting the preservation of any shallow or early overpressures and low-VES.
3) Dissolved CO_2 in the pore fluids within the F-Sands are likely to have driven feldspar dissolution and enhancing secondary porosity within the F-sands of the Maui Field.
4) The limited amount of quartz cement could be due to the fact that the F-Sands only entered the chemical compaction window (>2500 m) in the past 10 Ma and the 'significant' quartz cementation realm 7 M.y ago.
5) The F-Sands could be characterised as a geochemically closed system, where dissolved solutes are being preferentially precipitated in fine grained heterolithic siltstone beds, leaving open pore throats and maintaining primary inter-granular porosity.

CHAPTER VI:

DISCUSSION, CONCLUSIONS, AND FUTURE WORK

6.1. OVERPRESSURE AND FACIES DISTRIBUTION: WIDER IMPLICATIONS

As hydrocarbon exploration moves into ultra-deep water (>2000 m) (Vear, 2005; Weimer and Pettingill, 2007), and more complex geological environments, in both frontier and mature basins, the need to be predictive with respect to formation pressures is essential if issues like the McKee-13 blowout are to be prevented (O'Neill and others, 2018a). As demonstrated in this study, the inclusion of tectonostratigraphic information in polyphase basins can aid the prediction and magnitude of abnormal pore fluid pressures and potential pathways for lateral fluid flow (Chen and others, 2010; Drews and others, 2018; Guo and others, 2012; Horváth, 1995; O'Connor and Swarbrick, 2008) .

This work has tested the Webster et al. (2011) model of discrete depth-based pressure intervals through the analysis of a more comprehensive set of pressure data for wells that are now open file (Fig. 2.5b & 2.6a). A key outcome of this research is the introduction of a novel sub-basin approach in analysis and interpretation of pore pressure data available for the basin. This approach is considered to have applicability to other basins globally exhibiting fluid overpressure and having a complex polyphaser tectonostratigraphic history.

The current model of discrete depth-based pressure distribution, outlined by Webster et al. (2011), does not capture the complexity and nuances of the pore pressure system within Taranaki Basin. Each new sub-basin defined in this study displays its own pore pressure regime, nevertheless linked through a shared stratigraphy and regional fluid flow pathways; placing the spatial variation of overpressure in a tectonic context (Chen and others, 2010). Variations in net-to-gross and thickness of Late Eocene-Oligocene mudrocks have been shown to provide a first-order control on the magnitude, distribution and maintenance of overpressure across the Taranaki Basin, which has been demonstrated in other polyphase basins worldwide (Drews and others, 2018; Harrison and Summa, 1991; Yan and others, 2002).

This relationship is most clearly highlighted in the Eocene Mangahewa Formation, which towards the centre of the onshore Taranaki Peninsula is characterised by high net-to-gross coal-rich terrestrial coastal plain facies (Higgs and others, 2012a) with limited overpressure (~700 psi). The overpressure magnitude within the Mangahewa Formation sequentially increases in basinward direction, culminating at Turi-1 (Fig. 3.6; >4000 psi), which intersects bathyal mudrocks deposited off the palaeoshelf displaying very low net-to-gross (<5%). Overpressure has been shown to increase in a basinward direction in other basins (e.g. Javanshir et al., 2015; Tingay et al., 2005; Van Balen and Cloetingh, 1994; Zoccarato et al., 2018), due to a gradual reduction in net-to-gross, resulting in decreasing hydraulic connectivity and permeability (Harrison and Summa, 1991) and a greater ability for associated permeable beds to maintain overpressure.

The effectiveness of mudrocks in the maintenance of overpressure also controls the nature of pressure transition zones. Disequilibrium compaction induced transition zones are characterised by relatively abrupt deviations from hydrostatic gradient, as demonstrated in wells on the Manganui Platform (Fig. 2.16), and highlighted in numerous rapidly subsiding Tertiary Basins (Badri et al., 2000; Bilotti and Shaw, 2005; Dickinson, 1953; Swarbrick and Osborne, 1996).

The pore pressure depth profiles of wells within each discrete sub-basin (apart from Tarata Thrust Zone and Patea Whanganui Coast) display a similar trend. These general trends can be utilised when developing a pore pressure prediction and for well engineering design within a sub-basin, as most wells will have similar casing points and mudweight profiles. This research is one of the first appraisals of pore pressure distributions across a complex polyphase basin, demonstrating the potential advantages of dividing pore pressure data by sub-basin, which could be applied to many sedimentary basins worldwide.

Australia's North West Shelf would be an excellent region to implement a tectonic sub-basin approach to pore pressure distribution, as it is comprised of a network of long-lived sedimentary basins (Harrowfield and Keep, 2005). The basins are often structurally complex and comprised of several Palaeozoic and Mesozoic sub-basins and platformal areas as seen in the Bonaparte Basin (Frankowicz and McClay, 2010). Various studies have been carried out on overpressure generation mechanisms across the margin (Bekele and others, 2001; van Ruth and others, 2004; Swarbrick and Hillis, 1999), and pore pressure distribution within specific sub-basins (He and Middleton, 2002), but no studies of the entire NW Shelf margin has not been carried out. The findings of this research demonstrate the importance of variations in lithofacies, thickness of sedimentary sequences and the interactions between tectonics and stratigraphic successions in complex sedimentary basins.

6.2. BASIN MODELLING APPROACHES

The application of basin modelling in the prediction of pore pressure for hydrocarbon well drilling is becoming increasingly common (Duppenbecker and others, 1999; Ghosh and others, 2015; Helset and others, 2009; Kundu and Basu, 2008; Yu and Cole, 2003), but limited work has been undertaken focusing on pore pressure evolution and distribution at a regional scale (Burgreen-Chan and others, 2016; Yardley and Swarbrick, 2000). The generation and dissipation of pore pressure in sedimentary basins is a 3D process, which is not wholly captured in a 1D system. Overpressure distributions are strongly influenced by long-range pressure interactions caused by horizontal water flows along highly permeable layers (Hantschel and Kauerauf, 2009), which is an active process in the south and west of Taranaki Basin (O'Neill and others, 2018b; Webster and others, 2011). One-dimensional models simplify the pore pressure system, but still can be used to discuss fundamental processes of overpressure formation and compaction (Hantschel and Kauerauf, 2009).

An alternative to 3D modelling is presented in this study, where results from numerous 1D models are combined with the knowledge of basin plumbing gained through the interpretation of pressure data from an established and expanded basin-wide pore pressure database. Modelling derived pore pressures are calibrated to wireline shale pressures, and compared with measured pressure data, to enable the identification of 3D processes like lateral fluid flow.

One-dimensional pore pressure modelling only considers mechanical compaction when describing the interactions between overburden due to sedimentation and overpressure formation (Hantschel and Kauerauf, 2009). Overpressures within the Taranaki Basin are primarily generated through disequilibrium compaction, implying that, although assumptions are made in one dimension, it can provide a relatively accurate representation of the pore pressure history for the region. Combining numerous 1D models can deliver an estimation of the variation in the onset of abnormal pressures and provide a broad understanding of the development of pore pressure at a basin scale. Importantly, it requires significantly less time than 3D modelling and can render reliable results even in complex multiphase basins such as in this study.

6.3. OVERPRESSURE PRESERVATION, MAINTENANCE AND DISSIPATION

Overpressure is not static; rather, it is a transient phenomenon (e.g. Tingay et al., 2009), which has a tendency to dissipate over time unless renewed by active generation mechanisms (Robertson, 2013). Overpressure is caused by the inability of fluids within a rock matrix to escape, which in the case of disequilibrium compaction (the principle mechanism in the Taranaki Basin), occurs when permeability has reduced to a point where water cannot be sufficiently expelled or dewatered and the pore pressure assumes some of the load. For overpressure to be maintained in reservoirs, requires the presence of an effective top seal and lateral barriers to flow, either stratigraphic or structural, or a combination.

Eocene and Oligocene mudstones on the Western Platform are significantly overpressured, but the surrounding reservoirs have high net-to-gross and no lateral seal, so abnormal pressures present have been allowed to dissipate. In stark contrast, basin floor fans of the Oligocene Tangaroa Formation have been encased in very low permeability mudrocks from shallow burial, leading to the maintenance of significant overpressures (>2000 psi). The Palaeocene Farewell Formation at Kapuni Deep-1 displays an intermediary, where dewatering continued to deep burial, but since ~6 Ma the permeability was reduced to the point where excess pressure was maintained. Overpressure loss through seal failure by overpressure-driven hydraulic fracturing is unlikely to be active across much of the basin (Darby, 2002), through episodic fault plane leakage, pockmarks and gas chimneys have been identified which could all contribute towards overpressure dissipation (Chenrai and Huuse, 2017; Ilg and others, 2012; Webster and others, 2011). The variations in the preservation of

abnormal pressures within the Taranaki Basin has shown to be controlled by a combination of fault permeability, lithofacies variations and mechanical compaction (permeability).

6.4. RESERVOIR QUALITY

Porosity preservation by pore fluid overpressure has been the subject of several studies (e.g., (Gluyas and Cade, 1997; Jeans, 1994; Ramm and Bjørlykke, 1994), however the development of and maintenance of overpressure and the evolution of vertical effective stress throughout the burial history have not been widely considered (Stricker, 2016). If VES is to act upon arresting porosity loss through mechanical compaction, dewatering must be inhibited and excess pore pressure needs to be maintained (e.g. Stricker et al., 2016; Sathar & Jones 2016; Oye et al., 2018). The high net-to-gross of Cretaceous to Eocene stratigraphy within the Taranaki Basin enabled the preservation of high effective stress conditions throughout burial which are maintained at depth across most reservoirs, promoting dewatering and destroying primary porosity at shallow depths through mechanical compaction. However, the strong compartmentalisation across the entirety of the Taranaki Basin resulting from the complex tectonostratigraphic evolution could still preserve significant early pore fluid overpressures and help arrest mechanical compaction, resulting in anomalously porous sandstones at significant burial depths in undrilled deeper parts of the Taranaki Basin.

Although the Palaeocene represents an important hydrocarbon reservoir within the Taranaki Basin, a limited amount of reservoir quality studies have been carried out (Martin and others, 1994; Pollock and others, 2003; Smale and others, 1999). The Palaeocene Farewell Formation at Kapuni Deep-1 and the F-sands at the Maui Field, are two end members with respect to reservoir quality; their depositional compositions are not dissimilar (Fig. 6.1a & b), but the resulting rocks at maximum burial are substantially different (Fig. 6.1g & h). Modelling derived porosity data (Fig. 6.1e & f) demonstrates that initial rapid burial reduced the porosity of the F-sands by ~27% during the first 15 Ma, while F-Sands experienced very little porosity loss (~6%), due to slow background subsidence. The detrital grains of the Farewell Formation are poorly sorted ranging in size from very fine to fine-grained sandstone and are predominately angular to sub-angular. Combined with ductile detrital mud clasts, micas and lithic fragments would allow for grain reorientation and sliding resulting in more efficient packing, and plastic deformation during burial providing the very low porosities (e.g.Worden et al., 2000).

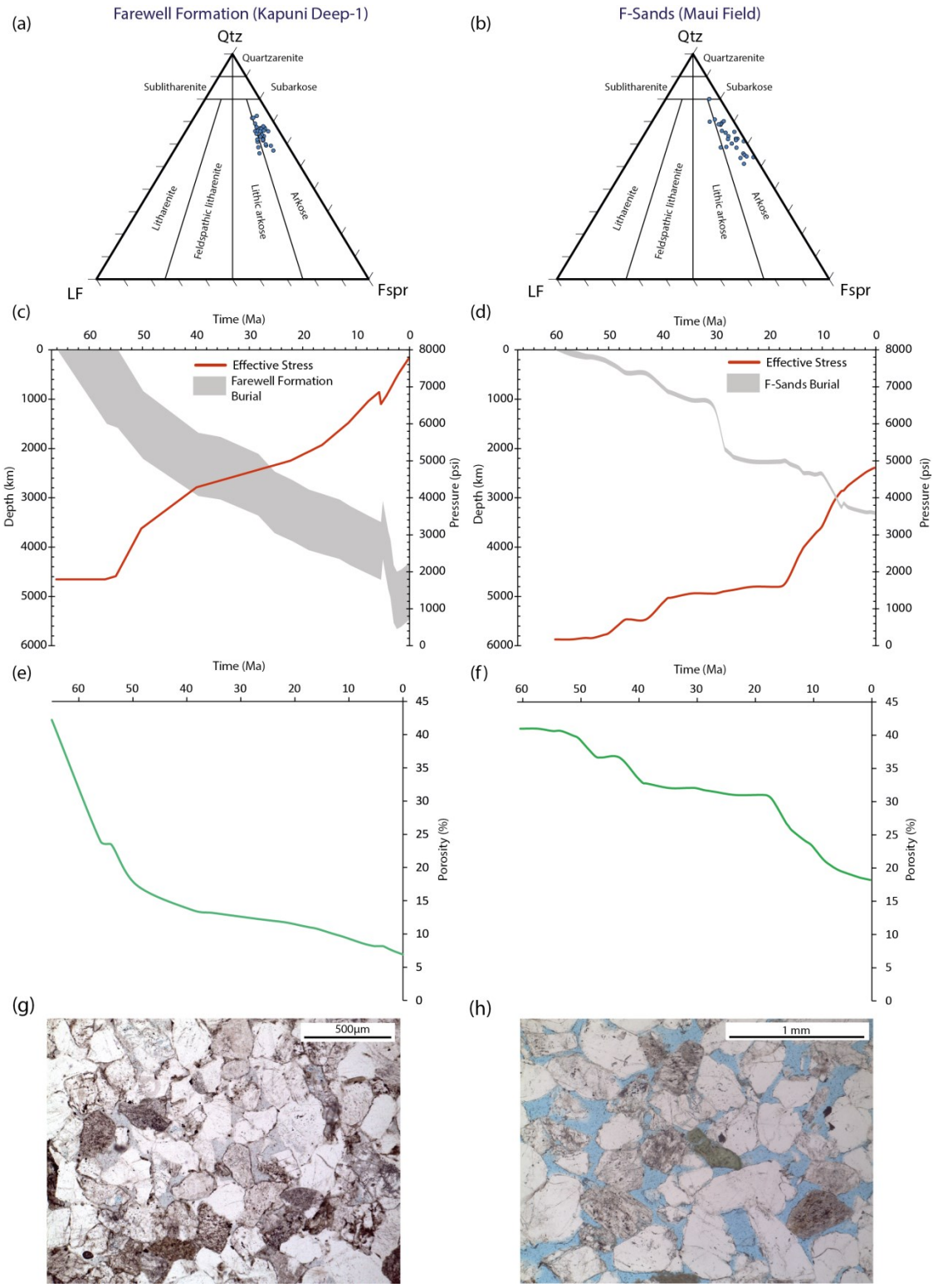

Figure 6.1. a) Ternary plot of present-day composition of the Farewell Formation at Kapuni Deep-1 from point count data (Table: 5.1). b) Ternary plot of present-day composition of the F-Sands at the Maui Field. c) Plot displaying the evolution of vertical effective stress with burial since the deposition of the Farewell Formation at Kapuni Deep-1. d) Plot displaying the evolution of vertical effective stress with burial since the deposition of the F-Sands at the Maui Field. e) Plot of modelled porosity evolution of the lower core (c. 5500 mTVDgl) of the Farewell Formation at Kapuni Deep-1 against time. f) Plot of modelled porosity evolution of the F-Sands at the Maui Field against time. g) Thin section micrograph (5189.1 mMDAH; Kapuni Deep-1): limited visible inter-granular porosity, texturally immaturity and concavo-convex sutured grain contacts. h) Thin section micrograph (3251.82 mTVDss; MB-R(1)): limited mechanical compaction and connected intergranular porosity.

Reservoir sandstones with high porosity (10-30%) and overpressures are encountered at >2 km depths in many sedimentary basins (Bloch and others, 2002; Cao and others, 2014; Javanshir and others, 2015; Sathar and Jones, 2016; Stricker and others, 2016b; Weedman and others, 1992). This investigation has demonstrated that this is not always the case, being dependent on the stress history and stratigraphic stacking of the basin fill. The Farewell Formation at Kapuni Deep-1 has experienced a continued increase in VES during burial which drove porosity loss through mechanical compaction. Consequently, the late and deep onset of abnormal pressures at Kapuni Deep-1 has meant that the pore pressure regime is, in part, controlled by the diagenetic evolution of the reservoirs. In comparison, the F-Sands at the Maui Field experienced relatively low-VES throughout burial but were still subjected to porosity loss via mechanical compaction (Fig. 6.1a & b).

CO_2 rich fluids have been shown to partially or fully dissolve detrital grains in both the Farewell Formation and laterally equivalent F-Sands, generating secondary porosity (Higgs and others, 2013; O'Neill and others, 2018b). The naturally occurring CO_2 is produced along with gas/condensate in many of the hydrocarbon fields (e.g. Kapuni field) of the onshore Taranaki Basin and as such presents an excellent natural laboratory for understanding the effect of high CO_2 partial pressures on host rocks. The CO_2 in the reservoirs is thought to have been sourced from intra-formational coals within the Cretaceous and Palaeocene, which has subsequent migrated up-dip through many of the structures.

The degree of CO_2-related reactions observed within this study appears dependent upon grain size, lithofacies and stratigraphic position in the reservoir. Coarse-grained, high-energy facies have undergone the most feldspar dissolution, coupled with formation and local preservation of secondary porosity. A reduced amount of feldspar degradation and increased amount of clay cement has been identified in finer heterolithic beds, suggesting a redistribution of ions within geochemically closed system. It has been demonstrated in several studies that in the presence of acidic pore fluids feldspars will react to form kaolinite, bicarbonate, cations ($K^+/Na^+/Ca^{2+}$) and silica (eg. Higgs et al., 2013; Watson et al., 2004; Worden, 2006). QEMSCAN and XRD data from Kapuni and Maui fields in this study has identified a greater percentile of plagioclase to K-feldspar content. As silica is only a product of K-feldspar reactions and not plagioclase reactions (eg. Watson et al., 2004; Worden, 2006), the relatively low volumes of authigenic quartz in Farewell Formation sandstones could be evidence for more advanced plagioclase than K-feldspar reaction driven by acidic pore fluids.

The CO_2 is transported through zones of focused fluid flow of potentially increased porosity and permeability, which could act as 'valves' that are at risk from local collapse during secondary compaction, producing diagenetic pressure barriers as postulated for the Farewell Formation pressure transition zone (O'Neill and others, 2018b). By analogy with observations from the Moore-Sams Field, Tuscaloosa Trend, USA reported by Weedman et al.

(1992) the Farewell Formation may have developed internal pressure barriers, which could have led to the current distribution of overpressure beneath a pressure transition zone. The mechanism for a fluid barrier is "secondary" compaction caused by dissolution of cement. Results from this research demonstrate how potentially CO_2-related reactions can significantly impact the vertical heterogeneity of a reservoir leading to increased compartmentalization leading to tight beds from compaction effects, which can pose a major problem for drilling safety due to the unpredictable and potentially abrupt pressure transitions.

6.5. SUMMARY

1) The pore pressure distributions within Taranaki Basin is redefined using eight sub-basin areas and structural zones, each displaying individual pore pressure trends defined by their stratigraphic architecture and structural development.
2) Variations in the thickness and facies of Eocene-Oligocene stratigraphy provide a first-order control on the magnitude, distribution and maintenance of overpressure across the Taranaki Basin. Fluid pressure compartmentalisation through sealing faults and stratigraphic architecture has been identified across the basin.
3) The origin of deep pressure transitions in the basin has been shown to be sealed by diagenetic, structural and stratigraphic mechanisms and generated by an increase in mudrock volume (reduced permeability) or gas generation.
4) The initial onset of overpressure in the Taranaki Basin occurred at ~22 Ma, driven by formation and initial filling of a foreland basin in the north-eastern parts of the basin. The subsequent development of the plate boundary during the Early Miocene to the Pleistocene, involved the episodic north-westward progression of a further series sedimentary sequences across the continental shelf. This resulted in continued phases of overpressure generation from 10 Ma to the present day.
5) No clear relationship between vertical effective stress and porosity preservation in reservoir sandstones has been identified in the Taranaki Basin, due to the late and deep onset of overpressure.
6) Mechanical compaction has been shown to be the principle porosity reducing mechanism in both the Palaeocene Farewell Formation and the F-Sands during the first 3000 m of burial, and compaction of secondary porosity within the Farewell Formation has further reduced porosity towards maximum burial.
7) Dissolved CO_2 in the pore fluids within the F-Sands and Farewell Formation are likely to have driven the dissolution of detrital grains, generating secondary porosity and enhancing permeability.
8) The F-Sands and Farewell Formation could be characterised as geochemically closed systems, where dissolved solutes are being preferentially precipitated in fine-grained heterolithic siltstone beds

6.6. SUGGESTIONS FOR FURTHER WORK

6.6.1. SEISMIC PORE PRESSURE PREDICTION

The Northern and Central grabens of the Taranaki Basin have not been a focus for exploration so have no well control, which poses an issue for pore pressure prediction and well planning. They display a differing tectonic history and stratigraphic stacking to other areas of the basin, so the application of offset well pore pressure data is not possible. In poorly explored frontier regions pore pressure can be estimated by extracting elastic wave velocities from seismic reflection surveys, and calculated using a velocity to pore pressure transforms, like the equivalent depth method (Hottmann and Johnson, 1965; Sayers and others, 2002). A pilot study using seismic velocities from the Taranaki Basin successfully predicted pore pressure which validates the use of this methodology for the Northern and Central grabens (Humphris and Ravens, 2000). Further to this, previously interpreted seismic horizons from Strogen et al. (2014) could be extracted, depth converted and used in one-dimensional basin modelling to investigate the pore pressure evolution in the Northern and Central grabens.

6.6.2. EVOLUTION OF PORES PRESSURE AND PREDICTION OF RESERVOIR QUALITY IN THRUST TECTONIC/COMPRESSIONAL REGIMES.

The preservation of porosity within clastic reservoirs in the mechanical compaction regime is an accepted theory, but studies have only been carried out in basins where the maximum stress is vertical and the ratio of vertical to horizontal stress is relatively constant (Oye and others, 2018; Sathar and Jones, 2016; Stricker and others, 2016b). In comparison, few studies have tested the models in compressional settings, where horizontal stress is prevalent. Mechanical compaction is based on total effective stress, which is a combination of both vertical and horizontal stress; therefore it is essential that both are included when investigating the development of pore pressure and reservoir quality through time.

Porosity preservation through horizontal stress has been suggested to be acting in New Zealand's East Coast Basin, where less mechanical compaction has been observed than would be predicted at maximum burial in the Middle Miocene Whakataki Formation from Titihaoa-1 well (Hathon, 1995). Burgreen-Chan et al., (2016) carried out two-dimensional basin modelling to investigate the pore pressure evolution of the East Coast Basin, which could be extended to investigate porosity preservation.

6.6.3. MODELLING LATERAL FLUID FLOW WITHIN THE TARANAKI BASIN USING TWO- DIMENSIONAL BASIN MODELLING

It has been suggested that both lateral transfer (O'Neill and others, 2018a) and later drainage are active processes within the Taranaki Basin. These concepts could be tested through the application of two-dimensional basin modelling in both the Tarata Thrust Zone (lateral transfer) and Southern Taranaki Inversion (lateral drainage), a methodology which has been

applied in basins worldwide (Bredehoeft and others, 1988; Leduc and others, 2013; Obradors-Prats and others, 2017; Yardley and Swarbrick, 2000). These models can be calibrated using shale pressure calculations as demonstrated in Chapter III.

6.6.4. Implementation of sub-basin and one-dimensional basin modelling to investigate pore pressure evolution and distribution in basins worldwide

The sub-basin approach to pore pressure distribution can be applied to complex multi-compartment basin worldwide, for example: Nova Scotian continental margin (Williamson, 1995); Faeroe-Shetland Basin (Iliffe and others, 1999); Bohai Bay Basin, China (Liu and others, 2019); Cauvery Basin, India (Dasgupta and others, 2016) and West Siberian Basin, Russia (Matusevich and others, 1997).

The one-dimensional basin modelling approach could also be applied to polyphase tectonostratigraphically complex basins worldwide, for example: Vienna Basin, Austria (Lee and Wagreich, 2017), Qamar basin, Eastern Yemen (Brannan and others, 1997); Baram-Balabac Basin, NW Borneo (Cullen, 2010) and the South China Sea (Ye and others, 2018).

REFERENCES

Adams, M., Kelly, C., and Khasi, K., 1989, Mckee-8 well completion report. PML38086: Ministry of Economic Development Unpublished Petroleum Report 1458.:

El Albani, A., Meunier, A., and Fürsich, F., 2005, Unusual occurrence of glauconite in a shallow lagoonal environment (Lower Cretaceous, northern Aquitaine Basin, SW France): Terra Nova, v. 17, no. 6, p. 537–544.

Allis, R.G., Zhan, X., Evans, C., and Kroopnick, P., 1997, Groundwater flow beneath Mt Taranaki , New Zealand , and implications for oil and gas migration: New Zealand Journal of Geology and Geophysics, v. 40, no. 2, p. 137–149.

Ambrose, W.A., Dutton, S.P., and Loucks, R.G., 2017, Depositional Systems, Facies Variability, and their Relationship to Reservoir Quality in the Jurassic Cotton Valley Group, Texas, Louisiana, and Mississippi Onshore Gulf Coast: Gulf Coast Association of Geological Societies Journal, v. 6, p. 21–46.

Armstrong, P.A., Allis, R.G., Funnell, R.H., and Chapman, D.S., 1998, Late Neogene exhumation patterns in Taranaki Basin (New Zealand): Evidence from offset porosity-depth trends: Journal of Geophysical Research-Solid Earth, v. 103, no. B12, p. 30269–30282.

Armstrong, P.A., and Chapman, D.S., 1999, Combining Tectonics and Thermal Fields in Taranaki Basin, New Zealand, *in* Förster, A. and Merriam, D.F. eds., Geothermics in Basin Analysis: Springer US, Boston, MA, p. 151–176.

Armstrong, P.A., Chapman, D.S., Funnell, R.H., Allis, R.G., and Kamp, P.J.., 1994, Thermal state, thermal modelling and hydrocarbon generation in the Taranaki Basin., *in* New Zealand Petroleum Conference Proceedings:, p. 289–307.

Armstrong, P.A., Chapman, D.S., Funnell, R.H., Allis, R.G., and Kamp, P.J.J., 1996, Thermal modeling and hydrocarbon generation in an active-margin basin; Taranaki Basin, New Zealand: AAPG Bulletin, v. 80, no. 8, p. 1216–1241.

Athy, L.F., 1930, Density, Porosity, and Compaction of Sedimentary Rocks: AAPG Bulletin, v. 14, no. 1, p. 1–24.

Atkinson, J.H., and Bransby, P.L., 1978, The Mechanics of Soils: An Introduction to Critical State Soil Mechanics: McGraw-Hill, 375 p.

Badri, M., Sayers, C., Awad, R., and Graziano, A., 2000, A feasibility study for pore-pressure prediction using seismic velocities in the offshore Nile Delta, Egypt: The Leading Edge, v. 19, no. 10, p. 1103–1108.

Van Balen, R., and Cloetingh, S., 1994, Tectonic control of the sedimentary record and stress-induced fluid flow: constraints from basin modelling: Geological Society, London, Special Publications, v. 78, no. 1, p. 9–26.

Barclay, S.A., and Worden, R.H., 2000, Geochemical modelling of diagenetic reactions in a sub-arkosic sandstone: Clay Minerals, v. 35, no. 1, p. 57–67.

Baur, J., Sutherland, R., and Stern, T., 2014, Anomalous passive subsidence of deep-water sedimentary basins: A prearc basin example, southern New Caledonia Trough and Taranaki Basin, New Zealand: Basin Research, v. 26, no. 2, p. 242–268.

Bekele, E.B., Johnson, M.D., and Higgs, W.G., 2001, Numerical modelling of overpressure generation in the barrow sub-basin, Northwest Australia: The APPEA Journal, v. 41, no. 1, p. 595–608.

Bilotti, F., and Shaw, J.H., 2005, Deep-water Niger Delta fold and thrust belt modeled as a critical-taper wedge: The influence of elevated basal fluid pressure on structural styles:

AAPG Bulletin, v. 89, no. 11, p. 1475–1491.

Bjørkum, P.A., and Gjelsvik, N., 1988, An Isochemical Model for Formation of Authigenic Kaolinite, K-Feldspar and Illite in Sediments: Journal of Sedimentary Petrology, v. 58, no. 3, p. 506–511.

Bjorlykke, K., 1998, Clay mineral diagenesis in sedimentary basins; a key to the prediction of rock properties; examples from the North Sea Basin: Clay Minerals, v. 33, no. 1, p. 15–34.

Bjørlykke, K., 2014, Relationships between depositional environments, burial history and rock properties. Some principal aspects of diagenetic process in sedimentary basins: Sedimentary Geology, v. 301, p. 1–14.

Bjorlykke, K., and Egeberg, P.K., 1993, Quartz cementation in sedimentary basins: AAPG bulletin, v. 77, no. 9, p. 1538–1548.

Bjørlykke, K., and Jahren, J., 2012, Open or closed geochemical systems during diagenesis in sedimentary basins: Constraints on mass transfer during diagenesis and the prediction of porosity in sandstone and carbonate reservoirs: AAPG Bulletin, v. 96, no. 12, p. 2193–2214.

Bloch, S., 1991, Empirical Prediction of Porosity and Permeability in Sandstones: Aapg Bulletin-American Association of Petroleum Geologists, v. 75, no. 7, p. 1145–1160.

Bloch, S., 1994, Case Histories – Offshore Mid-Norway/Taranaki Basin, New Zealand/San Emigdio Area, California, *in* Wilson, M.D. ed., Reservoir Quality Assessment and Prediction in Clastic Rocks: SEPM Society for Sedimentary Geology.

Bloch, S., Lander, R.H., and Bonnell, L., 2002, Anomalously high porosity and permeability in deeply buried sandstone reservoirs: Origin and predictability: AAPG Bulletin, v. 86, no. 2, p. 301–328.

de Bock, J.F., Palmer, J.A., and Lock, R.G., 1990, Tariki Sandstone – early Oligocene hydrocarbon reservoir, eastern Taranaki, New Zealand., *in* New Zealand Petroleum Conference:, p. 214–224.

Bowers, G.L., 2001, Determining an Appropriate Pore-Pressure Estimation Strategy, *in* Offshore Technology Conference: Offshore Technology Conference, Houston, Texas, p. 1–14.

Brannan, J., Gerdes, K., and Newth, I., 1997, Tectono-stratigraphic development of the Qamar basin, Eastern Yemen: Marine and Petroleum Geology, v. 14, no. 6, p. 701–730.

Bredehoeft, J.D., Djevanshir, R.D., and Belitz, K.R., 1988, Lateral fluid flow in a compacting sand-shale sequence: South Caspian basin.: American Association of Petroleum Geologists Bulletin, v. 72, no. 4, p. 416–424.

Browne, G.H., Kennedy, E.M., Constable, R.M., Raine, J.I., Crouch, E.M., and Sykes, R., 2008, An outcrop-based study of the economically significant Late Cretaceous Rakopi Formation, northwest Nelson, Taranaki Basin, New Zealand: New Zealand Journal of Geology and Geophysics, v. 51, no. 4, p. 295–315.

Bull, S., Nicol, A., Strogen, D., Kroeger, K.F., and Seebeck, H.S., 2018, Tectonic controls on Miocene sedimentation in the Southern Taranaki Basin and implications for New Zealand plate boundary deformation: Basin Research, p. 0–3.

Burgreen-Chan, B., Meisling, K.E., and Graham, S., 2016, Basin and petroleum system modelling of the East Coast Basin, New Zealand: a test of overpressure scenarios in a convergent margin: Basin Research, v. 28, no. 4, p. 536–567.

Burn, M., Crookbain, R., and Bourke, A., 1995, Kapuni Group Core Description and digital

Logging, Onshore Taranaki Basin. Unpublished Petrocorp Report Number 0684.:

Çağatay, M.N., Saner, S., Al-Saiyed, I., and Carrigan, W.J., 1996, Diagenesis of the Safaniya Sandstone Member (mid-Cretaceous) in Saudi Arabia: Sedimentary Geology, v. 105, no. 3–4, p. 221–239.

Cao, Y., Yuan, G., Li, X., Wang, Y., Xi, K., Wang, X., Jia, Z., and Yang, T., 2014, Characteristics and origin of abnormally high porosity zones in buried Paleogene clastic reservoirs in the Shengtuo area, Dongying Sag, East China: Petroleum Science, v. 11, no. 3, p. 346–362.

Chapman, R.E., 1980, Mechanical versus thermal cause of abnormally high pore pressures in shales.: American Association of Petroleum Geologists Bulletin, v. 64, no. 12, p. 2179–2183.

Chen, Z., Osadetz, K.G., Issler, D.R., and Grasby, S.E., 2010, Pore pressure patterns in Tertiary successions and hydrodynamic implications, Beaufort-Mackenzie Basin, Canada: Bulletin of Canadian Petroleum Geology, v. 58, no. 1, p. 3–16.

Chenrai, P., and Huuse, M., 2017, Pockmark formation by porewater expulsion during rapid progradation in the offshore Taranaki Basin, New Zealand: Marine and Petroleum Geology, v. 82, p. 399–413.

Chuhan, F.A., Kjeldstad, A., Bjørlykke, K., and Høeg, K., 2003, Experimental compression of loose sands : relevance to porosity reduction during burial in sedimentary basins: Canadian Geotechnical Journal, v. 1011, p. 995–1011.

Chuhan, F.A., Kjeldstad, A., Bjùrlykke, K., and Hùeg, K., 2002, Porosity loss in sand by grain crushing - experimental evidence and relevance to reservoir quality: Marine and Petroleum Geology, v. 19, no. 1, p. 39–53.

Cobbold, P.R., Mourgues, R., and Boyd, K., 2004, Mechanism of thin-skinned detachment in the Amazon Fan: Assessing the importance of fluid overpressure and hydrocarbon generation: Marine and Petroleum Geology, v. 21, no. 8, p. 1013–1025.

Collen, J.D., 1988, Diagenetic Control of Porosity and Permeability in Pakawau and Kapuni Group Sandstones, Taranaki Basin, New Zealand: Energy Exploration & Exploitation, v. 6, no. 3, p. 263–280.

Collen, J.D., and Newman, R.H., 1991, Porosity development in deep sandstones, Taranaki Basin, New Zealand: Journal of Southeast Asian Earth Sciences, v. 5, no. 1–4, p. 449–452.

Crowhurst, P. V., Green, P.F., and Kamp, P.J.J., 2002, Appraisal of (U-Th)/He apatite thermochronology as a thermal history tool for hydrocarbon exploration: An example from the Taranaki Basin, New Zealand: AAPG Bulletin, v. 86, no. 10, p. 1801–1819.

Cullen, A.B., 2010, Transverse segmentation of the Baram-Balabac Basin, NW Borneo: refining the model of Borneo's tectonic evolution: Petroleum Geoscience, v. 16, no. 1, p. 3–29.

Darby, D., 2002, Seal properties , overpressure and stress in the Taranaki and East Coast Basins , New Zealand, *in* 2002 New Zealand Petroleum Conference Proceedings:, p. 1–10.

Darby, D., and Ellis, S., 2003, Contrasting pressure regimes in sedimentary basins associated with a plate boundary, New Zealand: Journal of Geochemical Exploration, v. 78–79, p. 149–152.

Darby, D., and Funnell, R.H., 2001, Overpressure associated with a convergent plate margin: East Coast Basin, New Zealand: Petroleum Geoscience, v. 7, no. 3, p. 291–299.

Darby, D., Haszeldine, R.S., and Couples, G.D., 1996, Pressure cells and pressure seals in the UK Central Graben: Marine and Petroleum Geology, v. 13, no. 8, p. 865–878.

Dasgupta, S., Chatterjee, R., and Mohanty, S.P., 2016, Prediction of pore pressure and fracture

pressure in Cauvery and Krishna-Godavari basins, India: Marine and Petroleum Geology, v. 78, p. 493–506.

Day-Stirrat, R.J., Milliken, K.L., Dutton, S.P., Loucks, R.G., Hillier, S., Aplin, A.C., and Schleicher, A.M., 2010, Open-system chemical behavior in deep Wilcox Group mudstones, Texas Gulf Coast, USA: Marine and Petroleum Geology, v. 27, no. 9, p. 1804–1818.

Dickey, P.A., 1976, Abnormal Formation Pressure: DISCUSSION: AAPG Bulletin, v. 60, no. 7, p. 1124–1128.

Dickinson, G., 1953, Geological Aspects of Abnormal Reservoir Pressures in Gulf Coast Louisiana: AAPG Bulletin, v. 37, no. 2, p. 410–432.

Drews, M.C., Bauer, W., Caracciolo, L., and Stollhofen, H., 2018, Disequilibrium compaction overpressure in shales of the Bavarian Foreland Molasse Basin: Results and geographical distribution from velocity-based analyses: Marine and Petroleum Geology, v. 92, p. 37–50.

Duppenbecker, S.J., Osborne, M.J., Bunney, J.R., and Duncan, R.A.B., 1999, Pre-Drill Pressure Prediction provided by multi-dimensional Basin Modelling technique, *in* AAPG International Conference and Exhibition, Birmingham, England.:

Dyson, I.A., 1998, Greensand reservoirs in siliciclastic shoreline systems: facies models for hydrocarbon exploration: The APPEA Journal, v. 38, no. 2, p. 132–144.

Ehrenberg, S.N., 1993, Preservation of anomalously high porosity in deeply buried sandstones by grain-coating chlorite: examples from the Norwegian continental shelf: AAPG Bulletin, v. 77, no. 7, p. 1260–1286.

England, W.A., Mackenzie, A.S., Mann, D.M., and Qqigley, T.M., 1987, The movement and entrapment of petroleum fluids in the subsurface: Journal of the Geological Society, v. 144, no. 2, p. 327–347.

Esteban, M., and Taberner, C., 2003, Secondary porosity development during late burial in carbonate reservoirs as a result of mixing and/or cooling of brines: Journal of Geochemical Exploration, v. 78–79, p. 355–359.

Flemings, P.B., and Lupa, J.A., 2004, Pressure prediction in the Bullwinkle Basin through petrophysics and flow modeling (Green Canyon 65, Gulf of Mexico): Marine and Petroleum Geology, v. 21, no. 10, p. 1311–1322.

Frankowicz, E., and McClay, K.R., 2010, Extensional fault segmentation and linkages, Bonaparte Basin, outer North West Shelf, Australia: AAPG Bulletin, v. 94, no. 7, p. 977–1010.

Franks, S.G., and Forester, R.W., 1984, Relationships Among Secondary Porosity , Pore-Fluid Chemistry and Carbon Dioxide , Texas Gulf Coast, *in* Mcdonald, D.A. and Surdam, R.C. eds., Clastic Diagenesis: American Association of Petroleum Geologists, p. 63–79.

Funnell, R., Chapman, D., Allis, R., and Armstrong, P., 1996, Thermal state of the Taranaki Basin, New Zealand: Journal of Geophysical Research, v. 101, p. 25197.

Funnell, R.H., Stagpoole, V.M., Nicol, A., Killops, S.D., Reyes, A.G., and Darby, D., 2001, Migration of Oil and Gas into the Maui Field, Taranaki Basin, New Zealand, *in* PESA Eastern Australasian Basins Symposium:, p. 121–128.

Funnell, R., Stagpoole, V.M., Nicol, A., McCormack, N., and Reyes, A.G., 2004, Petroleum generation and implications for migration - a Maui Field charge study, Taranaki Basin: New Zealand Petroleum Conference, p. 1–9.

Furlong, K.P., and Kamp, P.J.J., 2013, Changes in plate boundary kinematics: Punctuated or

smoothly varying - Evidence from the mid-Cenozoic transition from lithospheric extension to shortening in New Zealand: Tectonophysics, v. 608, p. 1328–1342.

Ghosh, D., Yusoff, W.I., and Satti, I., 2015, 3D Predrill Pore Pressure Prediction Using Basin Modeling Approach in a Field of Malay Basin: Asian Journal of Earth Sciences, v. 8, no. 1, p. 24–31.

Giba, M., Nicol, A., and Walsh, J.J., 2010, Evolution of faulting and volcanism in a back-arc basin and its implications for subduction processes: Tectonics, v. 29, no. 4, p. 1–18.

Giles, M.R., Indrelid, S.L., Beynon, G. V, and Amthor, J., 2009, The Origin of Large-Scale Quartz Cementation: Evidence from Large Data Sets and Coupled Heat–Fluid Mass Transport Modelling, *in* Quartz Cementation in Sandstones: John Wiley & Sons, Ltd, p. 21–38.

Gilham, R., and Hercus, C., 2005, Shearwater (UK Block 22/30b): managing changing uncertainties through field life: Geological Society of London, 663-673 p.

Gluyas, J., and Cade, C.A., 1997, Prediction of Porosity in Compacted Sands, *in* Kupscz, J.A., Gluyas, J., and Bloch, S. eds., AAPG Memoir 69: Reservoir Quality Prediction in Sandstones and Carbonates,:, p. 19–27.

Grant, N.T., Middleton, A.J., and Archer, S., 2014, Porosity trends in the Skagerrak Formation , Central Graben , United Kingdom Continental Shelf : The role of compaction and pore pressure history: AAPG Bulletin, v. 6, no. 6, p. 1111–1143.

Gresko, M.., Jordan, D.W., and Thompson, P.R., 1990, A Sequence Stratigraphic Study of the Tangaroa Sandstone, Taranaki Basin, New Zealand, *in* AAPG Annual Convention Conference Preceedings.:

Gunter, J.M., and Moore, C. V., 1987, Improved Use of Wireline Testers for Reservoir Evaluation: Journal of Petroleum Technology, v. 39, no. 6, p. 635–644.

Guo, Y., Pang, X., Chen, D., Leng, J., and Tian, J., 2012, Evolution of continental formation pressure in the middle part of the Western Sichuan Depression and its significance on hydrocarbon accumulation: Petroleum Exploration and Development, v. 39, no. 4, p. 457–465.

Haile, B.G., Klausen, T.G., Czarniecka, U., Xi, K., Jahren, J., and Hellevang, H., 2018, How are diagenesis and reservoir quality linked to depositional facies? A deltaic succession, Edgeøya, Svalbard: Marine and Petroleum Geology, v. 92, no. August 2017, p. 519–546.

Hansen, R.J., and Kamp, P.J.J., 2004, Late Miocene to early Pliocene stratigraphic record in northern Taranaki Basin: Condensed sedimentation ahead of Northern Graben extension and progradation of the modern continental margin: New Zealand Journal of Geology and Geophysics, v. 47, no. 4, p. 645–662.

Hansley, P.L., and Nuccio, V.F., 1992, Upper Cretaceous Shannon Sandstone Reservoirs, Powder River Basin, Wyoming: Evidence for Organic Acid Diagenesis? AAPG Bulletin, v. 76, no. 6, p. 781–791.

Hantschel, T., and Kauerauf, A.I., 2009, Fundamentals of basin and petroleum systems modeling: Springer-Verlag, Berlin, 1-476 p.

Harrison, W.J., and Summa, L.L., 1991, Paleohydrology of the Gulf of Mexico Basin: American Journal of Science, v. 291, no. 2, p. 109–176.

Harrold, T.W.D., Swarbrick, R.E., and Goulty, N.R., 1999, Pore Pressure Estimation from Mudrock Porosities in Tertiary Basins, Southeast Asia: AAPG Bulletin, v. 83, no. 7, p. 1057–1066.

Harrowfield, M., and Keep, M., 2005, Tectonic modification of the Australian north-west shelf:

Episodic rejuvenation of long-lived basin divisions: Basin Research, v. 17, no. 2, p. 225–239.

Hathon, L.A., 1995, Reservoir quality of the Middle Miocene Whakataki Formation Sandstones, Titihaoa #1 well, New Zealand. New Zealand Petroleum Report Series, PR 8081.:

He, S., and Middleton, M., 2002, Pressure seal and deep overpressure modelling in the Barrow Sub-basin, North West Shelf, Australia, *in* Proceedings of The Sedimentary Basins of Western Australia 3: Petroleum Exploration Society of Australia (PESA), p. 531–549.

Helset, H.M., Luthje, M., and Ojala, I., 2009, Improved pore pressure prediction by integrating basin modeling and seismic methods, *in* AAPG Hedberg Confernce: Basin and Petroleum System Modeling: New Horizons in Research and Applications.:

Higgs, K.E., Arnot, M.J., and Brindle, S., 2015, Advances in grain-size, mineral, and pore-scale characterization of lithic and clay-rich reservoirs: AAPG Bulletin, v. 99, no. 7, p. 1315–1348.

Higgs, K.E., Arnot, M.J., Browne, G.H., and Kennedy, E.M., 2010, Reservoir potential of Late Cretaceous terrestrial to shallow marine sandstones, Taranaki Basin, New Zealand: Marine and Petroleum Geology, v. 27, no. 9, p. 1849–1871.

Higgs, K., Crouch, E., and Raine, J.I., 2017, An interdisciplinary approach to reservoir characterisation; an example from the early to middle Eocene Kaimiro Formation, Taranaki Basin, New Zealand: Marine and Petroleum Geology, v. 86, p. 111–139.

Higgs, K.E., Funnell, R.H., and Reyes, A.G., 2013, Changes in reservoir heterogeneity and quality as a response to high partial pressures of CO2 in a gas reservoir, New Zealand: Marine and Petroleum Geology, v. 48, p. 293–322.

Higgs, K.E., and King, P.R., 2018, Sandstone provenance and sediment dispersal in a complex tectonic setting: Taranaki Basin, New Zealand: Sedimentary Geology, v. 372, p. 112–139.

Higgs, K.E., King, P.R., Raine, J.I., Sykes, R., Browne, G.H., Crouch, E.M., and Baur, J.R., 2012a, Sequence stratigraphy and controls on reservoir sandstone distribution in an Eocene marginal marine-coastal plain fairway, Taranaki Basin, New Zealand: Marine and Petroleum Geology, v. 32, no. 1, p. 110–137.

Higgs, K.E., Strogen, D.P., Griffin, A., Ilg, B.R., and Arnot, M.J., 2012b, Reservoirs of the Taranaki Basin, New Zealand. GNS Science Data Series No. 2012/13a.:

Higgs, K.E., Zwingmann, H., Reyes, A.G., and Funnell, R.H., 2007, Diagenesis, porosity evolution, and petroleum emplacement in tight gas reservoirs, Taranaki Basin, New Zealand: Journal of Sedimentary Research, v. 77, no. 12, p. 1003–1025.

Holt, W.E., and Stern, T.A., 1991, Sediment loading on the Western Platform of the New Zealand continent: Implications for the strength of a continental margin: Earth and Planetary Science Letters, v. 107, no. 3–4, p. 523–538.

Holt, W.E., and Stern, T.A., 1994, Subduction, platform subsidence, and foreland thrust loading: The late Tertiary development of Taranaki Basin, New Zealand, *in* Tectonics:, p. 1068–1092.

Hood, S.D., Nelson, C.S., and Kamp, P.J.J., 2003a, Lithostratigraphy and depositional episodes of the Oligocene carbonate-rich Tikorangi Formation, Taranaki Basin, New Zealand: New Zealand Journal of Geology and Geophysics, v. 46, no. 3, p. 363–386.

Hood, S.D., Nelson, C.S., and Kamp, P.J.J., 2003b, Modification of fracture porosity by multiphase vein mineralization in an Oligocene nontropical carbonate reservoir, Taranaki Basin, New Zealand: American Association of Petroleum Geologists Bulletin, v.

87, no. 10, p. 1575–1597.

Hood, S.D., Nelson, C.S., and Kamp, P.J.J., 2003c, Petrogenesis of diachronous mixed siliciclastic-carbonate megafacies in the cool-water Oligocene Tikorangi formation, Taranaki Basin, New Zealand: New Zealand Journal of Geology and Geophysics, v. 46, no. 3, p. 387–405.

Hood, S.D., Nelson, C.S., and Kamp, P.J.J., 2004, Burial dolomitisation in a non-tropical carbonate petroleum reservoir: The Oligocene Tikorangi Formation, Taranaki Basin, New Zealand: Sedimentary Geology, v. 172, no. 1–2, p. 117–138.

Horváth, F., 1995, Phases of compression during the evolution of the Pannonian Basin and its bearing on hydrocarbon exploration: Marine and Petroleum Geology, v. 12, no. 8, p. 837–844.

Hossain, Z., Fabricius, I.L., and Christensen, H.F., 2009, Elastic and nonelastic deformation of greensand: The Leading Edge, v. 28, no. 1, p. 86–88.

Hottmann, C.E., and Johnson, R.K., 1965, Estimation of Formation Pressures from Log-Derived Shale Properties: Journal of Petroleum Technology, v. 17, no. 6, p. 717–722.

Houseknecht, D.W., 1987, Assessing the Relative Importance of Compaction Processes and Cementation to Reduction of Porosity in Sandstones: AAPG Bulletin, v. 71, no. 6, p. 633–642.

Hovadik, J.M., and Larue, D.K., 2010, Stratigraphic and structural connectivity: Geological Society Special Publications, v. 347, no. 1, p. 219–242.

Hubbert, M.., and Rubey, W.W., 1959, Role of fluid pressure in mechanics of overthrust faulting: Bulletin of the Geological Society of America, v. 70, p. 115–166.

Humphris, D., and Ravens, J., 2000, A braver approach to seismic velocity analysis in the Taranaki Basin, New Zealand: Exploration Geophysics, v. 31, no. 2, p. 267.

Ilg, B.R., Hemmings-Sykes, S., Nicol, A., Baur, J., Fohrmann, M., Funnell, R., and Milner, M., 2012, Normal faults and gas migration in an active plate boundary, southern Taranaki Basin, offshore New Zealand: AAPG Bulletin, v. 96, no. 9, p. 1733–1756.

Iliffe, J.E., Robertson, a G., Ward, G.H.F., Wynn, C., Pead, S.D.M., and Cameron, N., 1999, The importance of fluid pressures and migration to the hydrocarbon prospectivity of the Faeroe-Shetland White Zone: Petroleum geology of Northwest Europe; proceedings of the 5th conference., v. 5, p. 600–611.

Ivanovskaya, T.A., Gor'kova, N. V, Karpova, G. V, Pokrovskaya, E. V, and Drits, V.A., 2003, Chloritization of Globular and Platy Phyllosilicates of the Glauconite Series in Terrigenous Rocks of the Upper Riphean Päräjarvi Formation (Srednii Peninsula): Lithology and Mineral Resources, v. 38, no. 6, p. 495–508.

Javanshir, R.J., Riley, G.W., Duppenbecker, S.J., and Abdullayev, N., 2015, Validation of lateral fluid flow in an overpressured sand-shale sequence during development of Azeri-Chirag-Gunashli oil field and Shah Deniz gas field: South Caspian Basin, Azerbaijan: Marine and Petroleum Geology, v. 59, p. 593–610.

Jeans, C. V, 1994, Clay diagenesis, overpressure and reservoir quality: an introduction: Clay Minerals, v. 29, no. 4, p. 415–423.

Jolley, S.J., Fisher, Q.J., and Ainsworth, R.B., 2010, Reservoir compartmentalization: an introduction: Geological Society, London, Special Publications, v. 347, no. 1, p. 1–8.

Kaeng, G.C., Sausan, S., and Satria, A., 2014, Geopressure Centroid as Pore Pressure Prediction Challenge in Deepwater South East Asia, *in* International Petroleum Technology

Conference: International Petroleum Technology Conference, Kuala Lumpur, Malaysia, p. 11.

Kamp, P.J.J., 1986, The mid-Cenozoic Challenger Rift System of western New Zealand and its implications for the age of Alpine fault inception: Geological Society of America Bulletin, v. 97, p. 255–281.

Kamp, P.J.J., and Furlong, K.P., 2006, Neogene plate tectonic reconstructions and geodynamics of North Island sedimentary basins : Implications for the petroleum systems, *in* 2006 New Zealand Petroleum Conference Proceedings:, p. 1–16.

Kamp, P.J.J., and Green, P.F., 1990, Thermal and tectonic history of selected Taranaki Basin (New Zealand) wells assessed by apatite fission track analysis: American Association of Petroleum Geologists Bulletin, v. 74, no. 9, p. 1401–1419.

Kamp, P.J.J., and Tippett, J.M., 1993, Dynamics of Pacific plate crust in the South Island (New Zealand) zone of oblique continent-continent convergence: Journal of Geophysical Research, v. 98, no. B9, p. 16,105-16,118.

Kamp, P.J.J., Tripathi, A.R.P., and Nelson, C.S., 2014, Paleogeography of Late Eocene to earliest Miocene Te Kuiti Group, central-western North Island, New Zealand: New Zealand Journal of Geology and Geophysics, v. 57, no. 2, p. 128–148.

van de Kamp, P.C., 2008, Smectite-illite-muscovite transformations, quartz dissolution, and silica release in shales: Clays and Clay Minerals, v. 56, no. 1, p. 66–81.

Kamp, P.J.J., Vonk, A.J., Bland, K.J., Hansen, R.J., Hendy, A.J.W., McIntyre, A.P., Ngatai, M., Cartwright, S.J., Hayton, S., and Nelson, C.S., 2004, Neogene stratigraphic architecture and tectonic evolution of wanganui, king country, and eastern taranaki basins, New Zealand: New Zealand Journal of Geology and Geophysics, v. 47, no. 4, p. 625–644.

Killops, S.D., 1996, A geochemical perspective of oil generation in New Zealand basins, *in* New Zealand Petroleum Conference Proceedings:, p. 179–187.

Killops, S.D., Allis, R.G., and Funnell, R.H., 1996, Carbon Dioxide Generation from Coals in Taranaki Basin, New Zealand: Implications for Petroleum Migration in Southeast Asian Tertiary Basins: AAPG Bulletin, v. 80, no. 4, p. 545–568.

Killops, S.D., Funnell, R.H., Suggate, R.P., Sykes, R., Peters, K.E., Walters, C., Woolhouse, A.D., Weston, R.J., and Boudou, J.-P., 1998, Predicting generation and expulsion of paraffinic oil from vitrinite-rich coals: Organic Geochemistry, v. 29, no. 1, p. 1–21.

Killops, S.D., Reyes, A., and Funnell, R.H., 2009, Filling history of the Maui B Field, New Zealand: new information from oil inclusions in authigenic minerals from the oil leg in the Maui-B1 well F Sands: Journal of Petroleum Geology, v. 32, no. 3, p. 271–286.

Killops, S.D., Woolhouse, A.D., Weston, R.J., and Cook, R.A., 1994a, A geochemical appraisal of oil generation in the Taranaki Basin, New Zealand: American Association of Petroleum Geologists Bulletin, v. 78, no. 10, p. 1560–1584.

Killops, S.D., Woolhouse, A.D., Weston, R.J., and Cook, R.A., 1994b, A Geochemical Appraisal of Oil Generation in the Taranaki Basin, New Zealand: AAPG Bulletin, v. 78, no. 10, p. 1560–1585.

King, P.R., Bland, K.J., and Lever, L., 2009, Opportunities for underground geological storage of CO2 in New Zealand - Report CCS -08 / 5 - Onshore Taranaki Basin overview Opportunities for underground geological storage of CO 2 in New Zealand - Report CCS-08 / 5 - Onshore Taranaki Basin overview.:

King, P.R., and Thrasher, G.P., 1992, Post-Eocene Development of the Taranaki Basin, New Zealand: Convergent Overprint of a Massive Margin, *in* Watkins, J.S., Zhiqiang, F., and

McMillen, K.J. eds., Geology and Geophysics of Continental Margins AAPG Memoir:, p. 93–118.

King, P.R., and Thrasher, G.P., 1996, Cretaceous-Cenozoic Geology and Petroleum Systems of the Taranaki Basin, New Zealand: New Zealand: Institute of Geological and Nuclear Sciences, Monograph 13, Ministry of Economic Development Petroleum Report 3224, 244 p.

Kukla, P.A., Reuning, L., Becker, S., Urai, J.L., and Schoenherr, J., 2011, Distribution and mechanisms of overpressure generation and deflation in the late Neoproterozoic to early Cambrian South Oman Salt Basin: Geofluids, v. 11, no. 4, p. 349–361.

Kundu, N., and Basu, S., 2008, Application of Stratigraphy Specific Shale Compaction Curves in Pore PressurePrediction: A Basin Modeling Approach, *in* GEO 2008 Middle East Conference and Exhibition. American Association of Petroleum Geologists, Manama, Bahrain.:

van de Lagemaat, S.H.A., Boschman, L.M., Kamp, P.J.J., Langereis, C.G., and van Hinsbergen, D.J.J., 2018, Post-remagnetisation vertical axis rotation and tilting of the Murihiku Terrane (North Island, New Zealand): New Zealand Journal of Geology and Geophysics, v. 61, no. 1, p. 9–25.

Lahann, R.W., and Swarbrick, R.E., 2011, Overpressure generation by load transfer following shale framework weakening due to smectite diagenesis: Geofluids, v. 11, no. 4, p. 362–375.

Lander, R.H., and Walderhaug, O., 1999, Predicting porosity through simulating sandstone compaction and quartz cementation: AAPG Bulletin (American Association of Petroleum Geologists), v. 83, no. 2–3, p. 433–449.

Lanson, B., Beaufort, D., Berger, G., Bauer, A., Cassagnabère, A., and Meunier, A., 2002, Authigenic kaolin and illitic minerals during burial diagenesis of sandstones: a review: Clay Minerals, v. 37, no. 1, p. 1–22.

Law, B.E., and Spencer, C.W., 1998, Abnormal pressure in hydrocarbon environments, *in* Law, B.E., Ulmishek, G.F., and Slavin, V.I. eds., Abnormal pressure in hydrocarbon environments: AAPG Memoir 70:, p. 1–11.

Leap Energy, 2014, Leap Energy's New Zealand ArcGIS Geodatabase:

Leduc, A.M., Davies, R.J., Swarbrick, R.E., and Imber, J., 2013, Fluid flow pipes triggered by lateral pressure transfer in the deepwater western Niger Delta: Marine and Petroleum Geology, v. 43, p. 423–433.

Lee, J.K., Swarbrick, R.E., and O'Connor, S.A. (in press) Kicks and their significance in pore pressure prediction: Operations Geology: A Specialist Discipline in Petroleum Geology

Lee, E.Y., and Wagreich, M., 2017, Polyphase tectonic subsidence evolution of the Vienna Basin inferred from quantitative subsidence analysis of the northern and central parts: International Journal of Earth Sciences, v. 106, no. 2, p. 687–705.

Lindberg, P., Riise, R., and Fertl, W.H., 1980, Occurrence And Distribution Of Overpressures In The Northern North Sea Area, *in* SPE Annual Technical Conference and Exhibition: Society of Petroleum Engineers, Dallas, Texas, p. 21.

Liu, M., Gluyas, J., Wang, W., Liu, Z., Liu, J., Tan, X., Zeng, W., and Xiong, Y., 2018, Tight oil sandstones in Upper Triassic Yanchang Formation, Ordos Basin, N. China: Reservoir quality destruction in a closed diagenetic system: Geological Journal, no. May, p. 1–18.

Liu, H., Yuan, F., Jiang, Y., Zhao, M., Chen, K., Guo, Z., and Wang, Y., 2019, Mechanisms for overpressure generated by the undercompaction of paleogene strata in the Baxian

Depression of Bohai Bay Basin, China: Marine and Petroleum Geology, v. 99, no. June 2018, p. 337–346.

Lodwick, G.R.M., 2018, What controls the reservoir quality of andesitic arc derived volcaniclastic sandstone reservoirs: An example from the Mohakatino Formation, Taranaki Basin, New Zealand:

Lundegard, P.D., 1992, Sandstone porosity loss--a "big picture" view of the importance of compaction: Journal of Sedimentary Petrology, v. 62, no. 2, p. 250–260.

Lundegard, P.D., and Land, L.S., 1986, Carbon dioxide and organic acids: their role in porosity enhancement and cementation, Paleogene of the Texas Gulf Coast: Roles of Organic Matter in Sediment Diagenesis, v. 38, p. 129–146.

Mansurbeg, H., Morad, S., Salem, A., Marfil, R., El-ghali, M.A.K., Nystuen, J.P., Caja, M.A., Amorosi, A., Garcia, D., and La Iglesia, A., 2008, Diagenesis and reservoir quality evolution of palaeocene deep-water, marine sandstones, the Shetland-Faroes Basin, British continental shelf: Marine and Petroleum Geology, v. 25, no. 6, p. 514–543.

Martin, K.R., Baker, J.C., Hamilton, P.J., and Thrasher, G.P., 1994, Diagenesis and reservoir quality of Palaeocene sandstones in the Kupe South Field, Taranaki Basin, New Zealand: AAPG Bulletin, v. 78, no. 4, p. 624–643.

Masalimova, L.U., Lowe, D.R., Sharman, G.R., King, P.R., and Arnot, M.J., 2016, Outcrop characterization of a submarine channel-lobe complex: The Lower Mount Messenger Formation, Taranaki Basin, New Zealand: Marine and Petroleum Geology, v. 71, p. 360–390.

Mattos, N.H., Alves, T.M., and Scully, A., 2018, Structural and depositional controls on Plio-Pleistocene submarine channel geometry (Taranaki Basin, New Zealand): Basin Research, v. 0, no. 0.

Matusevich, V.M., Myasnikova, G.P., Maximov, E.M., and Volkov, A.M., 1997, Abnormal formation pressures in the West Siberian Mega-basin , Russia: Petroleum Geoscience, v. 3, p. 269–283.

Mazzullo, S.J., and Harris, P.M., 1992, Mesogenetic dissolution: its role in porosity development in carbonate reservoirs: AAPG Bulletin, v. 76, no. 5, p. 607–620.

Mello, U.T., and Karner, G.D., 1996, Development of sediment overpressure and its effect on thermal maturation: Application to the Gulf of Mexico basin: AAPG Bulletin, v. 80, no. 9, p. 1367–1396.

Mitchell, J.S., Mackay, K.A., Neil, H.L., Mackay, E.J., Pallentin, A., and Notman, P., 2012, Undersea New Zealand, 1:5,000,000. NIWA Chart, Miscellaneous Series No. 92.:

Murray, D., 2000, Pohokura-1 well completion report. New Zealand Petroleum Report Series No. 2491.:

Nelson, C.S., Kamp, P.J.J., and Young, H.R., 1994, Sedimentology and petrography of mass-emplaced limestone (Orahiri Limestone) on a late Oligocene shelf, western North Island, and tectonic implications for eastern margin development of Taranaki Basin: New Zealand Journal of Geology and Geophysics, v. 37, no. 3, p. 269–285.

Nguyen, B.T.T., Jones, S.J., Goulty, N.R., Middleton, A.J., Grant, N., Ferguson, A., and Bowen, L., 2013, The role of fluid pressure and diagenetic cements for porosity preservation in Triassic fluvial reservoirs of the Central Graben, North Sea: AAPG Bulletin, v. 97, no. 8, p. 1273–1302.

NZP&M, 2018, New Zealand Petroleum Exploration Data Pack, at https://data.nzpam.govt.nz/GOLD/system/mainframe.asp.

O'Connor, S.A., and Swarbrick, R.E., 2008, Pressure regression, fluid drainage and a hydrodynamically controlled fluid contact in the North Sea, Lower Cretaceous, Britannia Sandstone Formation: Petroleum Geoscience, v. 14, no. 2, p. 115–126.

O'Neill, S.R., Jones, S.J., Gluyas, J.G., Kamp, P.J.J., and Crookbain, R., 2018a, Well Control Issues In A Mature Basin: A Case Study Of The Mckee-13 Blowout, Taranaki Basin, New Zealand, *in* AAPG Asia Pacific Region GTW, Pore Pressure & Geomechanics: From Exploration to Abandonment.:

O'Neill, S.R., Jones, S.J., Kamp, P.J.J., Swarbrick, R.E., and Gluyas, J.G., 2018b, Pore pressure and reservoir quality evolution in the deep Taranaki Basin, New Zealand: Marine and Petroleum Geology, v. 98, no. April, p. 815–835.

Obradors-Prats, J., Rouainia, M., Aplin, A.C., and Crook, A.J.L., 2017, Hydromechanical Modeling of Stress, Pore Pressure, and Porosity Evolution in Fold-and-Thrust Belt Systems: Journal of Geophysical Research: Solid Earth, v. 122, no. 11, p. 9383–9403.

Odin, G.S., 1988, Introduction to The Study of Green Marine Clays: Developments in Sedimentology, v. 45, p. 1–3.

Odin, G.S., and Matter, A., 1981, De glauconiarum origine: Sedimentology, v. 28, no. 5, p. 611–641.

Osborne, M.J., and Swarbrick, R.E., 1997, Mechanisms for generating overpressure in sedimentary basins: a reevaluation: American Association of Petroleum Geologists Bulletin, v. 81, no. 6, p. 1023–1041.

Oye, O., Aplin, A.C., Jones, S., Gluyas, J., Bowen, L., Orland, I., and Valley, J., 2018, Vertical effective stress as a control on quartz cementation in sandstones: Marine and Petroleum Geology, v. 98, p. 640–652.

Paxton, S., Szabo, J., Ajdukiewicz, J., and Klimentidis, R., 2002, Construction of an intergranular volume compaction curve for evaluating and predicting compaction and porosity loss in rigid-grain sandstone reservoirs: AAPG Bulletin, v. 86, no. 12, p. 2047–2067.

Pollock, R.M., and Crouch, E., 2005, Correlation of Paleocene to Eocene sediments between Tui-1 and the Maui Field, offshore Taranaki, New Zealand. New Zealand Petroleum Report Series, PR 3009.:

Pollock, R.M., Reyes, A.G., and Sykes, R., 2003, Petrographic and fluid inclusions analysis of Kapuni Group sandstones in Tui-1 well, Taranaki Basin. New Zealand Petroleum Report Series, PR2836.:

Porter, R.J., Rojas, A.M., and Schlüter, M., 2018, The impact of heterogeneity on waterflood developments in clastic inner shelf reservoirs: an example from the Holland Greensand Member, Rotterdam Field, The Netherlands, *in* Kilhams, B., Kukla, P.A., Mazur, S., McKie, T., Mijnlieff, H.F., and van Ojik, K. eds., Mesozoic Resource Potential in the Southern Permian Basin. Geological Society, London, Special Publications.:

Prada, M., Lavoué, F., Saqab, M.., O'Reilly, B.., Lebedev, S., Walsh, J.., and Childs, C., 2018, Across-axis variations in petrophysical properties of the North Porcupine Basin, offshore Ireland: new insights from long-streamer traveltime tomography: Basin Research, no. June, p. 1–18.

Pryor, W.A., 1973, Permeability-porosity patterns and variations in some Holocene sand bodies: AAPG Bulletin, v. 57, no. 1, p. 162–189.

Rajabi, M., Ziegler, M., Tingay, M., Heidbach, O., and Reynolds, S., 2016, Contemporary tectonic stress pattern of the Tarnaki Basin, New Zealand: Journal of Geophysical Research-Solid Earth, v. 121, p. 6053–6070.

Ramdhan, A.M., and Goulty, N.R., 2010, Overpressure-generating mechanisms in the Peciko Field, Lower Kutai Basin, Indonesia: Petroleum Geoscience, v. 16, no. 4, p. 367–376.

Ramm, M., and Bjørlykke, K., 1994, Porosity/depth trends in reservoir sandstones: assessing the quantitative effects of varying pore-pressure, temperature history and mineralogy, Norwegian Shelf data: Clay Minerals, v. 29, no. 4, p. 475–490.

Ranganathan, V., and Tye, R.S., 1986, Petrography, Diagenesis, and Facies Controls on Porosity in Shannon Sandstone, Hartzog Draw Field, Wyoming: American Association of Petroleum Geologists Bulletin, v. 70, no. 1, p. 56–69.

Rattenbury, M.S., Cooper, R.A., and Johnston, M.R., 1998, Geology of the Nelson area. Institute of Geological & Nuclear Sciences Limited 1:250,000 geological map 0: Institute of Geological & Nuclear Sciences Limited, Lower Hutt, New Zealand, 1 sheet +37p p.

Reilly, C., Nicol, A., Walsh, J.J., and Kroeger, K.F., 2016, Temporal changes of fault seal and early charge of the Maui Gas- condensate fi eld , Taranaki Basin , New Zealand: Marine and Petroleum Geology, v. 70, p. 237–250.

Reilly, C., Nicol, A., Walsh, J.J., and Seebeck, H., 2015, Evolution of faulting and plate boundary deformation in the Southern Taranaki Basin, New Zealand: Tectonophysics, v. 651, p. 1–18.

Richards, F.W., Vrolijk, P.J., Gordon, J.D., and Miller, B.R., 2010, Reservoir connectivity analysis of a complex combination trap: Terra Nova Field, Jeanne d'Arc Basin, Newfoundland, Canada: Geological Society, London, Special Publications, v. 347, no. 1, p. 333–355.

Robertson, J., 2013, Overpressure and Lateral Drainage in the Palaeogene Strata of the Central North Sea:

Robertson, J., Goulty, N.R., and Swarbrick, R.E., 2013, Overpressure distributions in Palaeogene reservoirs of the UK Central North Sea and implications for lateral and vertical fluid flow: Petroleum Geoscience, v. 19, no. 3, p. 223–236.

van Ruth, P., Hillis, R., and Tingate, P., 2004, The origin of overpressure in the Carnarvon Basin, Western Australia: implications for pore pressure prediction: Petroleum Geoscience, v. 10, no. 3, p. 247–257.

Salazar, M., Moscardelli, L., and Wood, L., 2018, Two-dimensional stratigraphic forward modeling, reconstructing high-relief clinoforms in the northern Taranaki Basin: AAPG Bulletin, v. 102, no. 12, p. 2409–2446.

Sathar, S., and Jones, S., 2016, Fluid overpressure as a control on sandstone reservoir quality in a mechanical compaction dominated setting : Magnolia Field , Gulf of Mexico: Terra Nova, v. 28, p. 155–162.

Sayers, C.M., Johnson, G.M., and Denyer, G., 2002, Predrill pore-pressure prediction using seismic data: Geophysics, v. 67, no. 4, p. 1286–1292.

Schmidt, V., and Mcdonald, D.A., 1979, The Role of Secondary Porosity in the Course of Sandstone Diagenesis, *in* Scholle, P.A. and Schluger, P.R. eds., Aspects of Diagenesis: SEPM Society for Sedimentary Geology, p. 175–207.

Schmidt, D.S., and Robinson, P.H., 1989, The structural setting and depositional history for the Kupe South Field, Taranaki Basin, *in* Ministry of Commerce 1989 New Zealand Oil Exploration Conference Proceedings:, p. 1347–1353.

Schoenherr, J., Littke, R., Urai, J.L., Kukla, P.A., and Rawahi, Z., 2007, Polyphase thermal evolution in the Infra-Cambrian Ara Group (South Oman Salt Basin) as deduced by maturity of solid reservoir bitumen: Organic Geochemistry, v. 38, no. 8, p. 1293–1318.

Schofield, J.K., 2016, Relationships between Observed Hydrocarbon Column Heights, Occurrence of Background Overpressure and Seal Capacity within North West Europe , Durham theses, Durham University.:

Schulz-Rojahn, J.P., Seeburger, D.A., and Beacher, G.J., 2003, Application of Glauconite Morphology in Geosteering and for on-Site Reservoir Quality Assessment in Very Fine-Grained Sandstones: Carnarvon Basin, Australia, *in* Worden, R.H. and Morad, S. eds., Clay Mineral Cements in Sandstones:, p. 473–488.

Scott, G.H., King, P.R., and Crundwell, M.P., 2004, Recognition and interpretation of depositional units in a late Neogene progradational shelf margin complex, Taranaki Basin, New Zealand: Foraminiferal data compared with seismic facies and wireline logs: Sedimentary Geology, v. 164, no. 1–2, p. 55–74.

Secor, D.T., 1965, Role of fluid pressure in jointing: American Journal of Science, v. 263, no. 8, p. 633–646.

Seewald, J.S., 2003, Organic–inorganic interactions in petroleum-producing sedimentary basins: Nature, v. 426, p. 327.

Seybold, O.M., Greenstreet, C.W., and Hawton, D.A., 1996, Reservoir management of the giant Maui gas/condensate field, *in* New Zealand petroleum exploration conference proceedings. Ministry of Economic Development, Wellington, New Zealand:, p. 125–132.

Sharman, G.R., Graham, S.A., Masalimova, L.U., Shumaker, L.E., and King, P.R., 2015, Spatial patterns of deformation and paleoslope estimation within the marginal and central portions of a basin-floor mass-transport deposit, Taranaki Basin, New Zealand: Geosphere, v. 11, no. 2, p. 266–306.

Shiers, M.N., Hodgson, D.M., and Mountney, N.P., 2017, Response of A Coal-Bearing Coastal-Plain Succession To Marine Transgression: Campanian Neslen Formation, Utah, U.S.A.: Journal of Sedimentary Research, v. 87, no. 2, p. 168–187.

Slot-Petersen, C., Eidesmo, T., White, J., and Rueslâtten, H.G., 1998, Nmr Formation Evaluation Applications In A Complex Low-Resistivity Hydrocarbon Reservoir, *in* SPWLA 39th Annual Logging Symposium: Society of Petrophysicists and Well-Log Analysts, Keystone, Colorado, p. 14.

Smale, D., Mauk, J.L., Palmer, J., Soong, R., and Blattner, P., 1999, Variations in sandstone diagenesis with depth, time, and space, onshore Taranaki wells, New Zealand: New Zealand Journal of Geology and Geophysics, v. 42, no. 2, p. 137–154.

Stagpoole, V., Funnell, R., and Nicol, A., 2004, Overview of the structure and associated petroleum prospectivity of the Taranaki Fault , New Zealand: PESA Eastern Australian Basins Symposium II, p. 197–206.

Stagpoole, V., and Nicol, A., 2008, Regional structure and kinematic history of a large subduction back thrust : Taranaki Fault, New Zealand: Journal of Geophysical Research, v. 113, no. B01403, p. 1–19.

Stern, T.A., and Davey, F.J., 1990, Deep seismic expression of a foreland basin: Taranaki Basin, New Zealand: Geology, v. 18, no. 10, p. 979–982.

Stern, T.A., Quinlan, G.M., and Holt, W.E., 1993, Crustal dynamics associated with the formation of Wanganui Basin, New Zealand, *in* Ballance, P.F. ed., Sedimentary Basins of the World, vol. 2, South Pacific Sedimentary Basins: Elsevier, Amsterdam, p. 213–223.

Stern, T.A., Stratford, W.R., and Salmon, M.L., 2006, Subduction Evolution and Mantle Dynamics At a Continental Margin : Central North Island , New Zealand: Review of Geophysics, v. 44, no. 2005, p. 1–36.

STOS, 1984, Geological Summary Kapuni Deep-1, Taranaki, New Zealand: unpublished New Zealand petroleum report 38839.:

STOS, 1993a, MB-R(1) Well Completion Report, Mau B Field, PML381012. Offshore Taranaki Basin. Petroleum Report Series No. 1912.:

STOS, 1993b, MB-W(2) Well Completion Report, Mau B Field, PML381012. Offshore Taranaki Basin. Petroleum Report Series No. 1932.:

Stricker, S., 2016, Influence of fluid pressure on the diagenesis of clastic sediments:

Stricker, S., and Jones, S.J., 2016, Enhanced porosity preservation by pore fluid overpressure and chlorite grain coatings in the Triassic Skagerrak, Central Graben, North Sea, UK: Geological Society, London, Special Publications, v. 435.

Stricker, S., Jones, S.J., and Grant, N.T., 2016a, Importance of vertical effective stress for reservoir quality in the Skagerrak Formation, Central Graben, North Sea: Marine and Petroleum Geology, v. 78, p. 895–909.

Stricker, S., Jones, S.J., Meadows, N., and Bowen, L., 2018, Reservoir quality of fluvial sandstone reservoirs in salt-walled mini-basins: an example from the Seagull field, Central Graben, North Sea, UK: Petroleum Science, v. 15, no. 1, p. 1–27.

Stricker, S., Jones, S.J., Sathar, S., Bowen, L., and Oxtoby, N., 2016b, Exceptional reservoir quality in HPHT reservoir settings : Examples from the Skagerrak Formation of the Heron Cluster , North Sea , UK: Marine and Petroleum Geology, v. 77, p. 198–215.

Strogen, D.P., 2011, Paleogeographic synthesis of the Taranaki Basin and surrounds. GNS Science Report, 2010/53.:

Strogen, D.P., Bland, K.J., Bull, S., Fohrmann, M.F., Scott, G.P.L., and Zhu, H., 2014a, Regional seismic transects of selected lines from Taranaki Basin. GNS Data Series 7b.:

Strogen, D.P., Bland, K.J., Nicol, A., and King, P.R., 2014b, Paleogeography of the Taranaki Basin region during the latest Eocene-Early Miocene and implications for the total drowning of Zealandia: New Zealand Journal of Geology and Geophysics, v. 57, no. 2, p. 110–127.

Strogen, D.P., Seebeck, H., Nicol, A., King, P.R., and Cret, E., 2017, Two-phase Cretaceous – Paleocene rifting in the Taranaki Basin region, New Zealand; implications for Gondwana break-up: Journal of the Geological Society, v. 174, p. 929–946.

Swarbrick, R.E., and Hillis, R.R., 1999, The origin and influence of overpressure with reference to the North West shelf, Australia: The APPEA Journal, v. 39, no. 1, p. 64–72.

Swarbrick, R.E., Lee, K., Lahann, R.W., Thomas, S., and Hardy, N., 2004, North Sea Central Graben Pressure Study. GeoPressure Technology and IHS Energy.:

Swarbrick, R.E., and Osborne, M.J., 1996, The nature and diversity of pressure transition zones: Petroleum Geoscience, v. 2, no. 2, p. 111–116.

Swarbrick, R.E., and Osborne, M.J., 1998, Mechanisms that Generate Abnormal Pressures: An Overview, *in* Law, B.E., Ulmishek, G.F., and Slavin, V.I. eds., Abnormal Pressures in Hydrocarbon Environments: American Association of Petroleum Geologists.

Swarbrick, R.E., Osborne, M.J., and Yardley, G.S., 2002, Comparison of Overpressure Magnitude Resulting from the Main Generating Mechanisms, *in* Huffman, A.R. and Bowers, G.L. eds., Pressure regimes in sedimentary basins and their prediction: AAPG Memoir 76,:, p. 1–12.

Sykes, R., 2001, Depositional and rank controls on the petroleum potential of coaly source rocks, *in* Eastern Australasian basins symposium:, p. 591–601.

Terzaghi, K., 1943, Theoretical Soil Mechanics: John Wiley & Sons, Inc., Hoboken, NJ, USA.

Thrasher, G.P., and Cahill, J.P., 1990, Subsurface maps of the Taranaki Basin region 1:50 000, New Zealand. New Zealand Geological Survey Report G-142.:

Tingay, M.R.P., Hillis, R.R., Morley, C.K., Swarbrick, R.E., and Drake, S.J., 2005, Present-day stress orientation in Brunei: a snapshot of 'prograding tectonics' in a Tertiary delta: Journal of the Geological Society, v. 162, no. 1, p. 39 LP-49.

Tingay, M.R.P., Hillis, R.R., Swarbrick, R.E., Morley, C.K., and Damit, A.R., 2007, 'Vertically transferred' overpressures in Brunei: Evidence for a new mechanism for the formation of high-magnitude overpressure: Geology, v. 35, no. 11, p. 1023.

Tingay, M.R.P., Hillis, R.R., Swarbrick, R.E., Morley, C.K., and Damit, A.R., 2009, Origin of overpressure and pore-pressure prediction in the Baram province, Brunei: AAPG Bulletin, v. 93, no. 1, p. 51–74.

Tingay, M.R.P., Morley, C.K., Laird, A., Limpornpipat, O., Krisadasima, K., Pabchanda, S., and Macintyre, H.R., 2013, Evidence for overpressure generation by kerogen-to-gas maturation in the northern Malay Basin: AAPG Bulletin, v. 97, no. 4, p. 639–672.

Townsend, D., Vonk, A., and Kamp, P., 2008, Geology of the Taranaki area. Institute of Geological & Nuclear Sciences 1:250,000 geological map 7.1 sheet: GNS Science, Lower Hutt, New Zealand, 77 p.

Traugott, M., 1997, Pore/fracture pressure determinations in deep water: 68-70 p.

Trevena, A.S., and Clark, R.A., 1986, Diagenesis of Miocene gas sands in Pattani Basin, Gulf of Thailand: AAPG Bulletin, v. 70, no. 3, p. 299–308.

Vear, A., 2005, Deep-water plays of the Mauritanian continental margin, *in* Petroleum Geology: North-West Europe and Global Perspectives—Proceedings of the 6th Petroleum Geology Conference:, p. 1217–1232.

Verweij, J.M., 1999, Application of fluid flow systems analysis to reconstruct the post-Carboniferous hydrogeohistory of the onshore and offshore Netherlands: Marine and Petroleum Geology, v. 16, no. 6, p. 561–579.

Voggenreiter, W.R., 1993, Structure and evolution of the Kapuni Anticline , Taranaki Basin , New Zealand : Evidence from the Kapuni 3D seismic survey: New Zealand Journal of Geology and Geophysics, v. 36, no. May, p. 77–94.

Vonk, A.J., and Kamp, P.J.J., 2004, Late Miocene-Early Pliocene Matemateaonga Formation in eastern Taranaki Peninsula: A new 1:50,000 geological map and stratigraphic framework, *in* New Zealand Petroleum Conference Proceedings: Ministry of Economic Development, Conference held at Auckland, p. 1–9.

Vonk, A.J., and Kamp, P.J.J., 2008, The Late Miocene Southern and Central Taranaki Inversion Phase (SCTIP) and related sequence stratigraphy and paleogeography: New Zealand Petroleum Conference Proceedings, no. 1996, p. 1–17.

Wang, X., Wang, X., Hu, W., Wan, Y., Cao, J., Lv, C., Wang, R., and Cui, M., 2017, Supercritical CO_2 -involved water–rock interactions at 85°C and partial pressures of 10–20 MPa: Sequestration and enhanced oil recovery: Energy Exploration & Exploitation, v. 35, no. 2, p. 237–258.

Watson, M.N., Boreham, C.J., and Tingate, P.R., 2004, Carbon dioxide and carbonate cements in the Otway Basin: implications for geological storage of carbon dioxide: The APPEA Journal, v. 44, no. 1, p. 703–720.

Webster, M., and Adams, S., 1996, Geopressures and Hydrocarbon Generation and Migration

Onshore Taranaki: Petroleum Exploration in New Zealand News, v. 47, no. August, p. 13–22.

Webster, M., O'Connor, S., Pindar, B., and Swarbrick, R., 2011, Overpressures in the Taranaki Basin: Distribution, causes, and implications for exploration: AAPG Bulletin, v. 95, no. 3, p. 339–370.

Weedman, S.D., Brantley, S.L., and Albrecht, W., 1992, Secondary compaction after secondary porosity: can it form a pressure seal? Geology, v. 20, no. 4, p. 303–306.

Weedman, S.D., Brantley, S.L., Shiraki, R., and Poulson, S.R., 1996, Diagenesis, compaction, and fluid chemistry modeling of a sandstone near a pressure seal: Lower Tuscaloosa Formation, Gulf Coast: AAPG Bulletin, v. 80, no. 7, p. 1045–1064.

Weimer, P., and Pettingill, H.S., 2007, Global Overview of Deep-water Exploration and Production, *in* Nilsen, T.H., Shew, R.D., Steffens, G.S., and Studlick, J.R.J. eds., Atlas of Deep-Water Outcrops. AAPG STUDIES IN GEOLOGY.:

Wilkinson, M., Haszeldine, R.S., Morton, A., Fallick, A.E., Road, C., Cv, B.C., Universities, S., and G, E.K., 2014, Deep burial dissolution of K-feldspars in a fluvial sandstone, Pentland Formation, UK Central North Sea: Journal of the Geological Society of London, v. 171, p. 635–647.

Williamson, M.A., 1995, Overpressures and hydrocarbon generation in the Sable sub-basin, offshore Nova Scotia: Basin Research, v. 7, no. 1, p. 21–34.

Winn, R.D., 1994, Shelf Sheet-Sand Reservoir of the Lower Cretaceous Greensand, North Celtic Sea Basin, Offshore Ireland: AAPG Bulletin, v. 78, no. 11, p. 1775–1789.

Wonham, J.P., Cyrot, M., Nguyen, T., Louhouamou, J., and Ruau, O., 2010, Integrated approach to geomodelling and dynamic simulation in a complex mixed siliciclastic-carbonate reservoir, N'Kossa field, Offshore Congo: Geological Society, London, Special Publications, v. 347, no. 1, p. 133–163.

Worden, R.H., 2006, Dawsonite cement in the Triassic Lam Formation, Shabwa Basin, Yemen: A natural analogue for a potential mineral product of subsurface CO2 storage for greenhouse gas reduction: Marine and Petroleum Geology, v. 23, no. 1, p. 61–77.

Worden, R.H., Mayall, M.J., and Evans, I.J., 1997, Predicting reservoir quality during exploration : lithic grains , porosity and permeability in Tertiary clastic rocks of the South China Sea basin, *in* Fraser, A.J., Matthews, S.J., and Murphy, R.. eds., Petroleum Geology of Southeast Asia, Geological Society Special Publication No. 126:, p. 107–115.

Worden, R.H., Mayall, M., and Evans, I.J., 2000, The effect of Ductile-Lithic sand grains and quartz cement on porosity and permeability in Oligocene and lower Miocene clastics, South China Sea: Prediction of reservoir quality: AAPG Bulletin, v. 84, no. 3, p. 345–359.

Worden, R.H., and Morad, S., 2009, Clay Minerals in Sandstones: Controls on Formation, Distribution and Evolution, *in* Worden, R.H. and Morad, S. eds., Clay Mineral Cements in Sandstones.:

Xi, K., Cao, Y., Liu, K., Wu, S., Yuan, G., Zhu, R., Kashif, M., and Zhao, Y., 2019, Diagenesis of tight sandstone reservoirs in the Upper Triassic Yanchang Formation, southwestern Ordos Basin, China: Marine and Petroleum Geology, v. 99, no. April 2018, p. 548–562.

Xu, T., Apps, J.A., and Pruess, K., 2005, Mineral sequestration of carbon dioxide in a sandstone-shale system: Chemical Geology, v. 217, no. 3–4 SPEC. ISS., p. 295–318.

Yan, S., Xinyu, X., Feng, H., Shengfei, Q., and Guoyou, F.U., 2002, Abnormal overpressure distribution and natural gas accumulation in foreland basins , Western China: Chinese Science Bulletin, v. 47, p. 71–77.

Yang, Y., and Aplin, A.C., 2007, Permeability and petrophysical properties of 30 natural mudstones: Journal of Geophysical Research: Solid Earth, v. 112, no. 3.

Yardley, G.S., and Swarbrick, R.E., 2000, Lateral transfer: A source of additional overpressure? Marine and Petroleum Geology, v. 17, no. 4, p. 523–537.

Ye, Q., Mei, L., Shi, H., Camanni, G., Shu, Y., Wu, J., Yu, L., Deng, P., and Li, G., 2018, The Late Cretaceous tectonic evolution of the South China Sea area: An overview, and new perspectives from 3D seismic reflection data: Earth-Science Reviews, v. 187, p. 186–204.

Yu, Z., and Cole, G., 2003, Application of 2D basin modeling for pre-drill pressure prediction in the Gulf of Mexico and offshore West Africa, *in* AAPG Hedberg Conference on Advances in Basin Modeling:, p. 362–363.

Yu, Z., and Lerche, I., 1996, Modelling abnormal pressure development in sandstone/shale basins: Marine and Petroleum Geology, v. 13, no. 2, p. 179–193.

Yuan, G., Cao, Y., Cluyas, J., Li, X., Xi, K., Wang, Y., Jia, Z., Sun, P., and Oxtoby, N.H., 2015a, Feldspar dissolution, authigenic clays, and quartz cements in open and closed sandstone geochemical systems during diagenesis: Typical examples from two sags in Bohai Bay Basin, East China: AAPG Bulletin, v. 99, no. 11, p. 2121–2154.

Yuan, G., Cao, Y., Gluyas, J., and Jia, Z., 2017, Reactive transport modeling of coupled feldspar dissolution and secondary mineral precipitation and its implication for diagenetic interaction in sandstones: Geochimica et Cosmochimica Acta, v. 207, p. 232–255.

Yuan, G., Cao, Y., Jia, Z., Gluyas, J., Yang, T., Wang, Y., and Xi, K., 2015b, Selective dissolution of feldspars in the presence of carbonates: The way to generate secondary pores in buried sandstones by organic CO2: Marine and Petroleum Geology, v. 60, p. 105–119.

Zoccarato, C., Minderhoud, P.S.J., and Teatini, P., 2018, The role of sedimentation and natural compaction in a prograding delta: insights from the mega Mekong delta, Vietnam: Scientific Reports, v. 8, no. 1, p. 1–12.

APPENDIX I:

BASIN MODELLING AND SINGLE WELL PRESSURE PLOTS

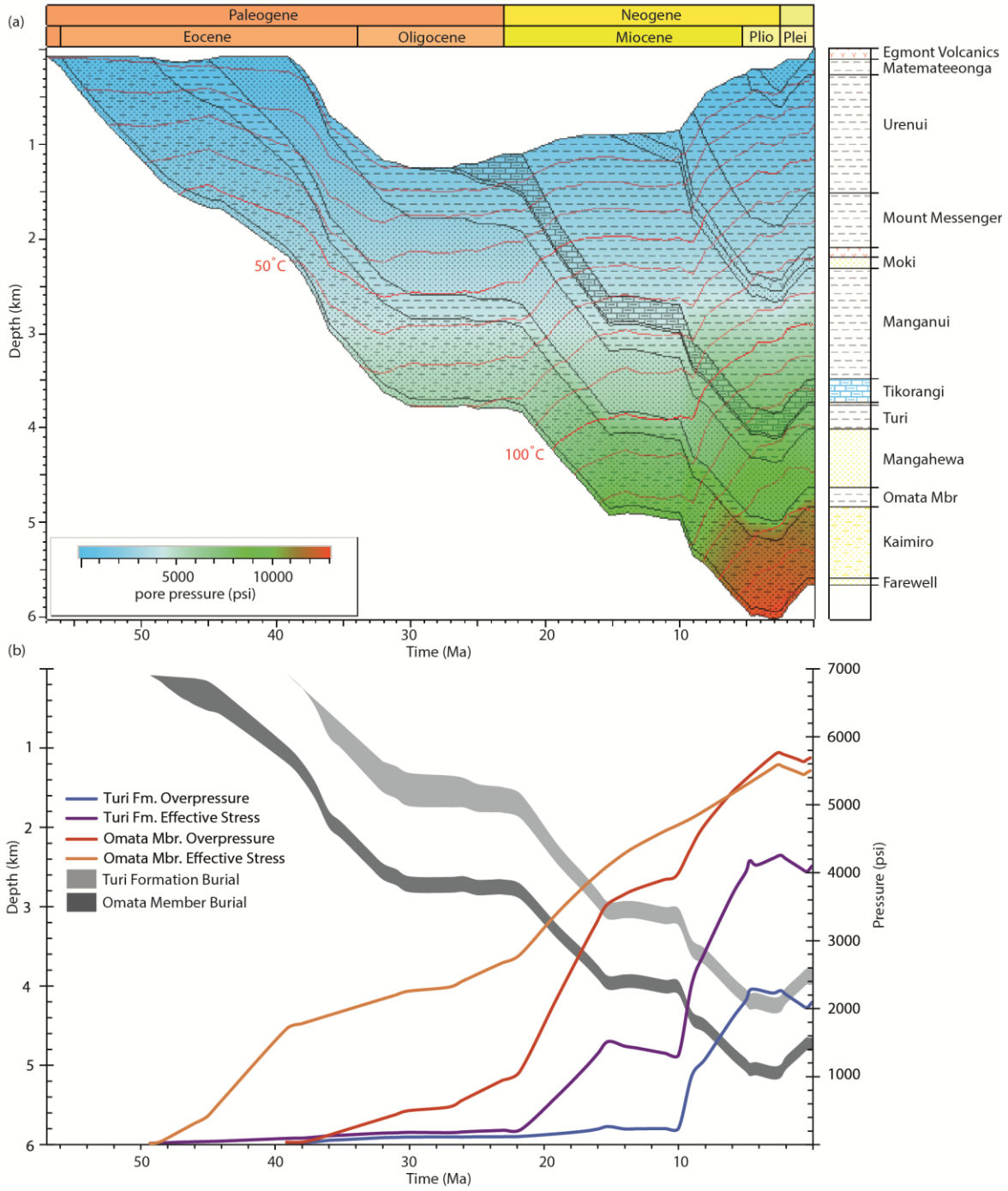

Figure I.1. a) 1D burial history plot of Waimanu-1 (Petromod). Red lines are isotherms and colour overlay denotes pore pressure. b) Plot displaying the evolution of overpressure and effective stress with burial since the deposition of the Turi Formation and Omata Member.

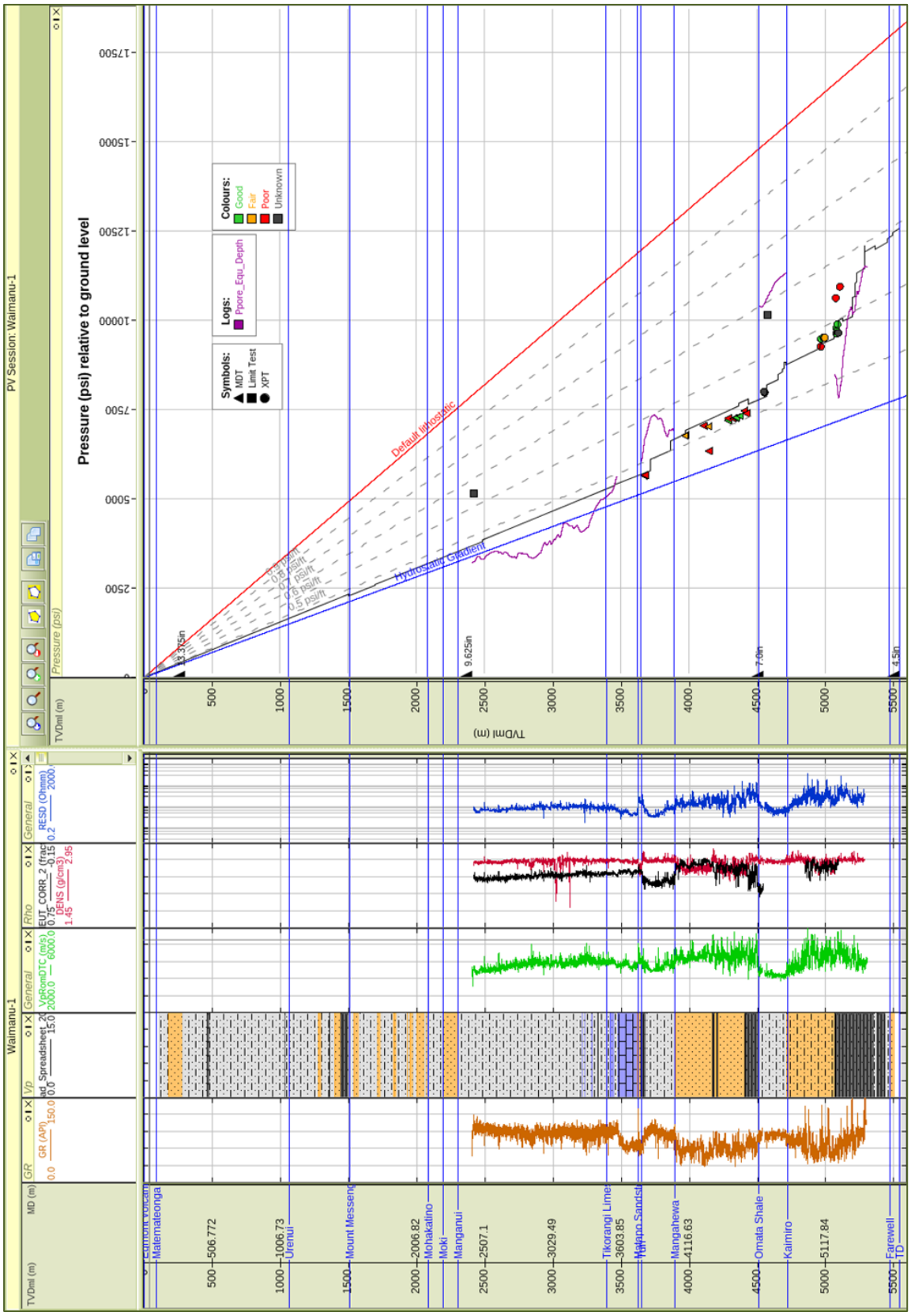

Figure I.2. Waimanu-1 pressure depth plot with associated suite of wireline measurements (gamma ray [brown], Vp [green), resistivity [blue], neutron [black], density [red], lithology column, RFT [triangles], XPT [circles), squares [limit test], mudweight [black] and shale pressure [purple]).

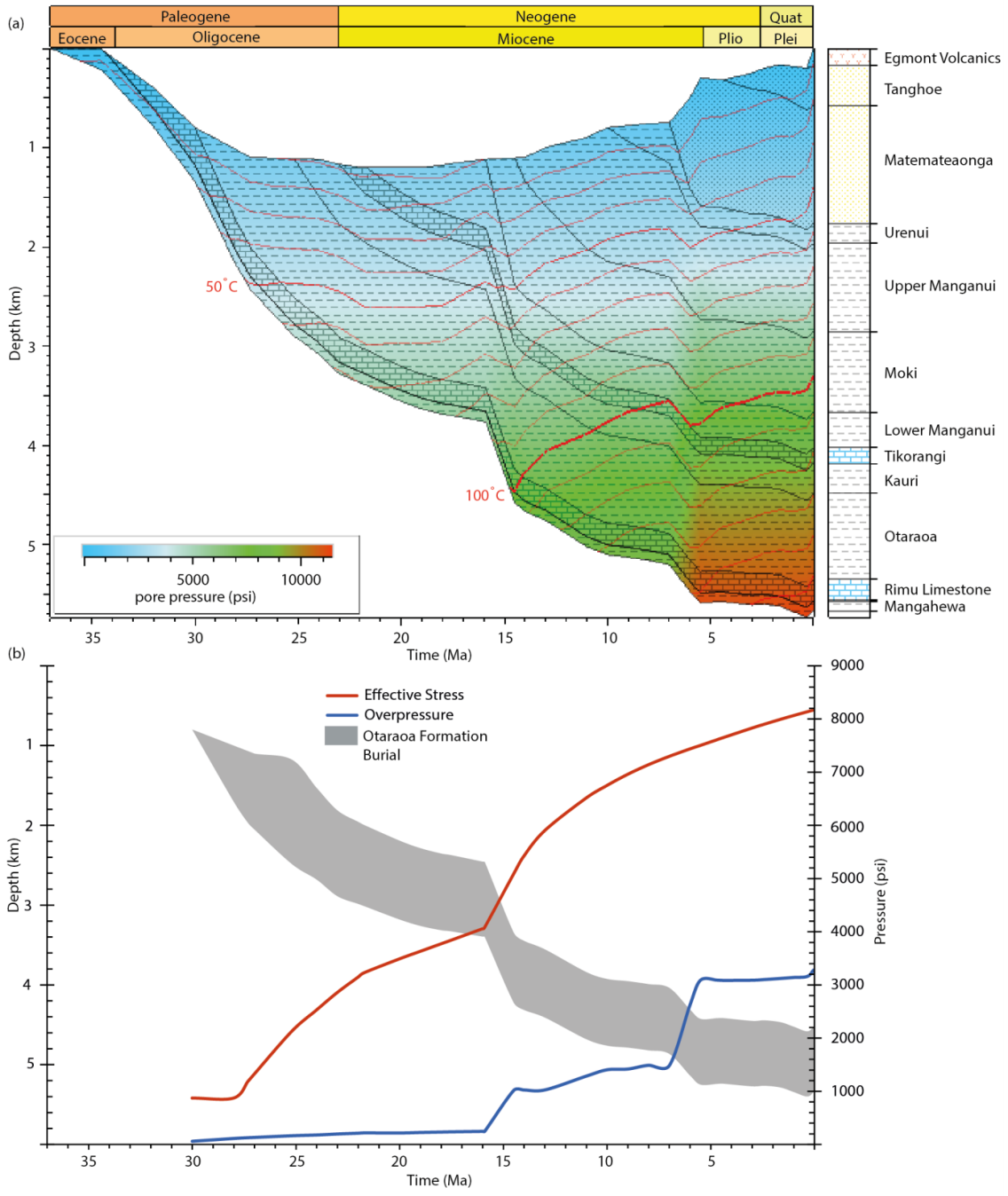

Figure I.3 a) 1D burial history plot of Tawa-B1 (Petromod). Red lines are isotherms and colour overlay denotes pore pressure. b) Plot displaying the evolution of overpressure and effective stress with burial since the deposition of the Otaraoa Formation

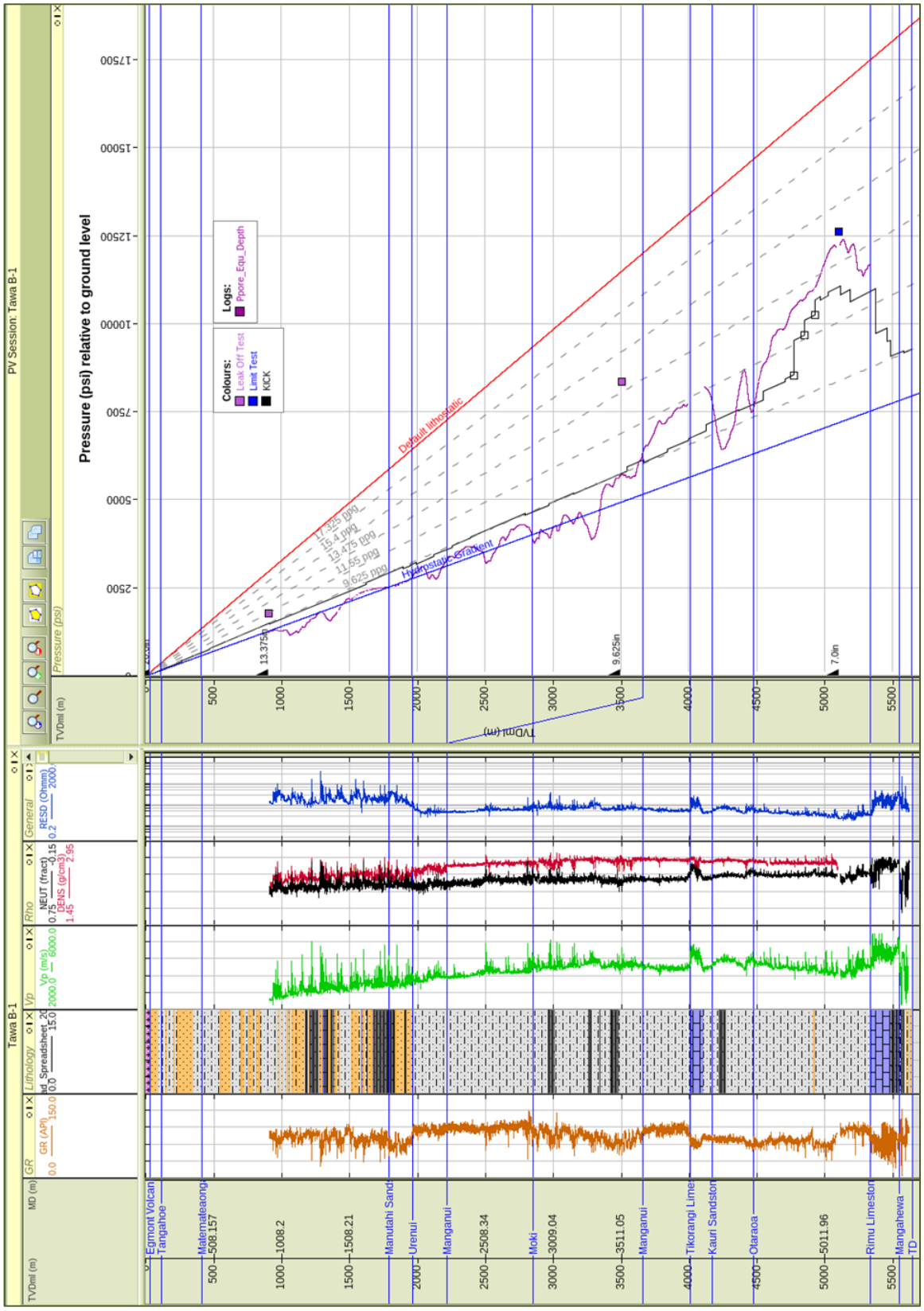

Figure I.4 Tawa B-1 pressure depth plot with associated suite of wireline measurements (gamma ray [brown], Vp [green], resistivity [blue], neutron [black], density [red], lithology column, kick [open squares], leak off test [purple squares], limit test [blue squares], mudweight [black] and shale pressure [purple]).

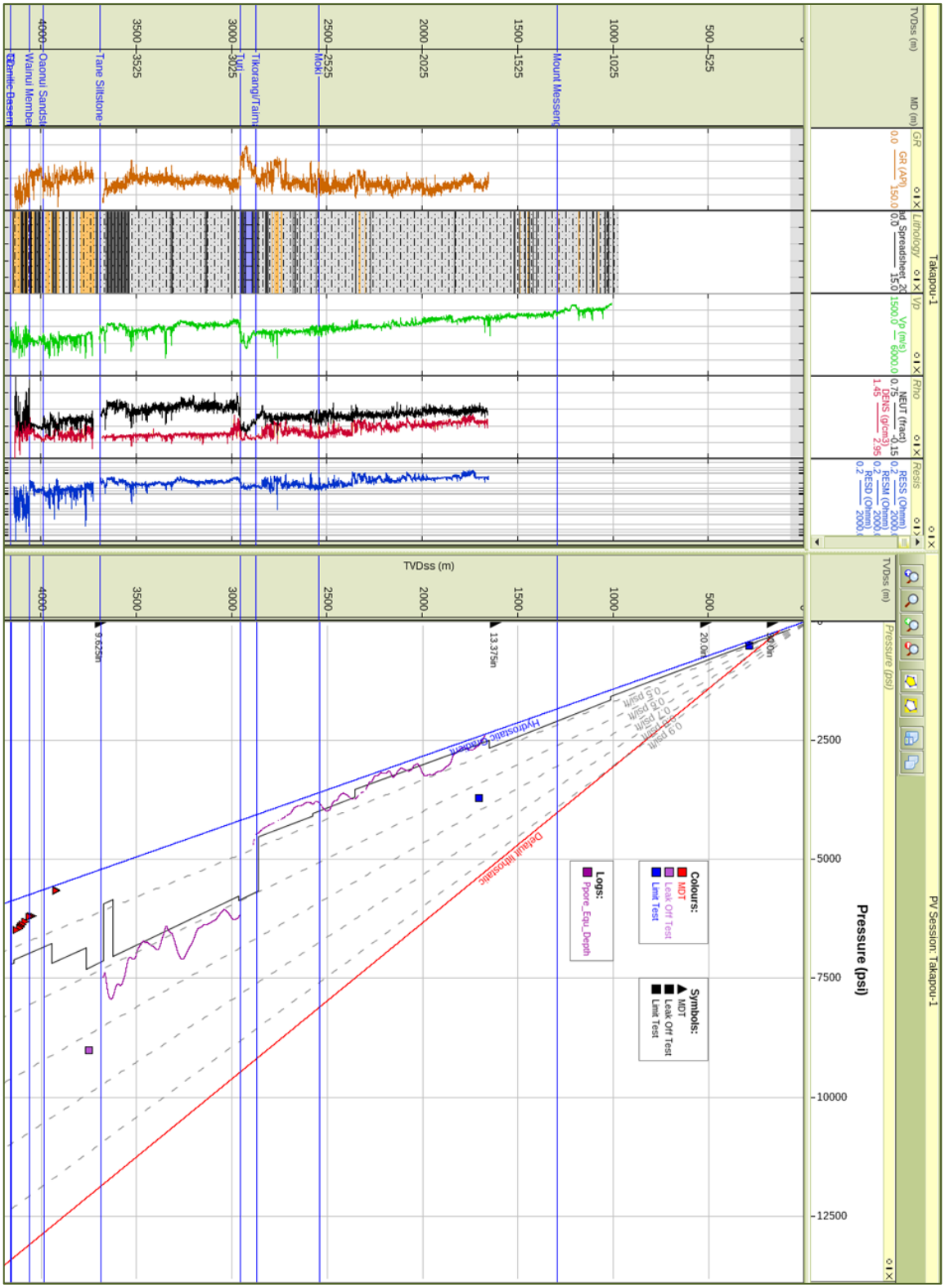

Figure I.5. Takapou-1 pressure depth plot with associated suite of wireline measurements (gamma ray [brown], Vp [green), resistivity [blue], neutron [black], density [red], lithology column, MDT [triangles], blue squares [limit test], purple squares [limit test], mudweight [black] and shale pressure [purple]).

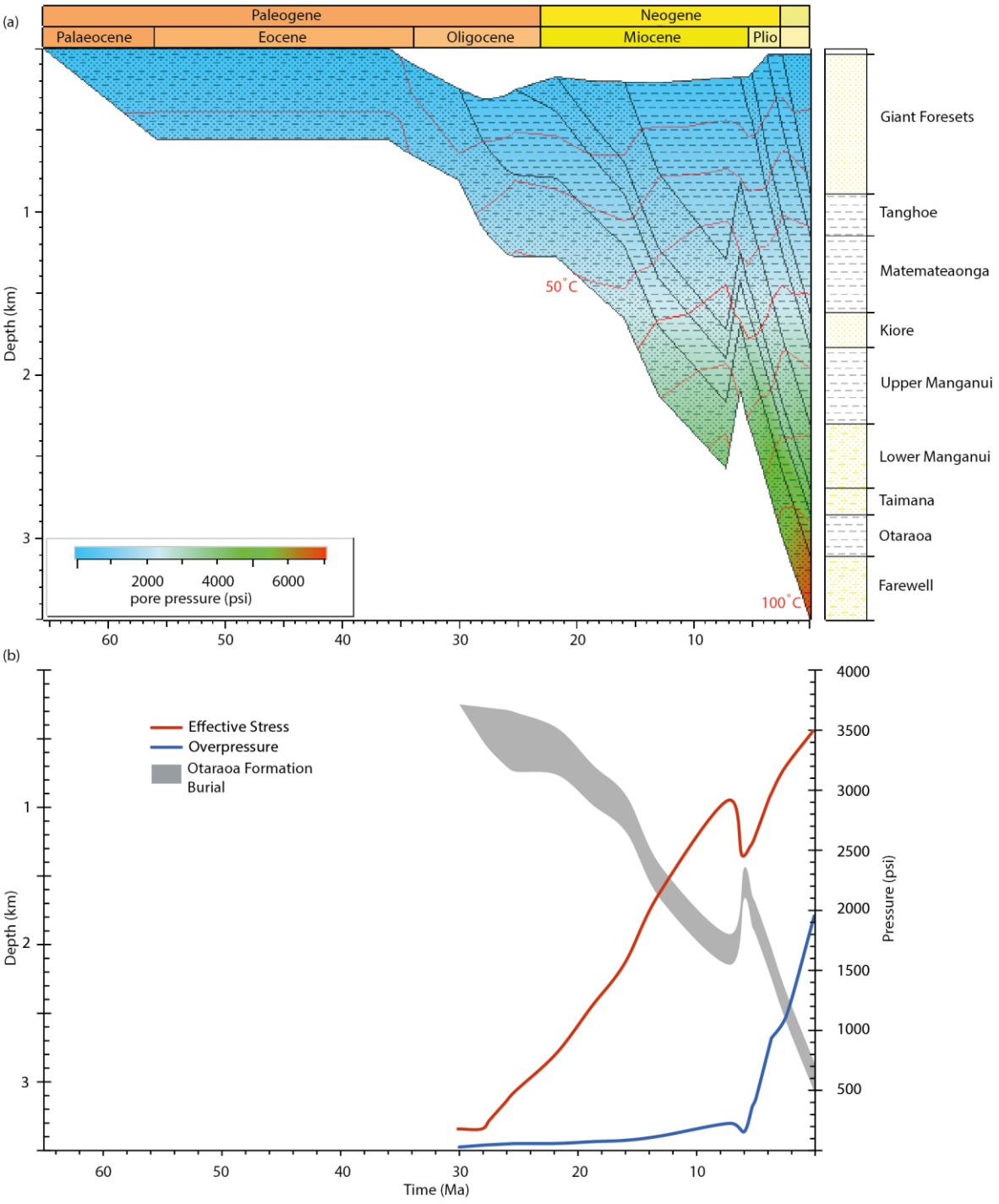

Figure I.6. a) 1D burial history plot of Kupe South-1 (Petromod). Red lines are isotherms and colour overlay denotes pore pressure. b) Plot displaying the evolution of overpressure and effective stress with burial since the deposition of the Otaraoa Formatio

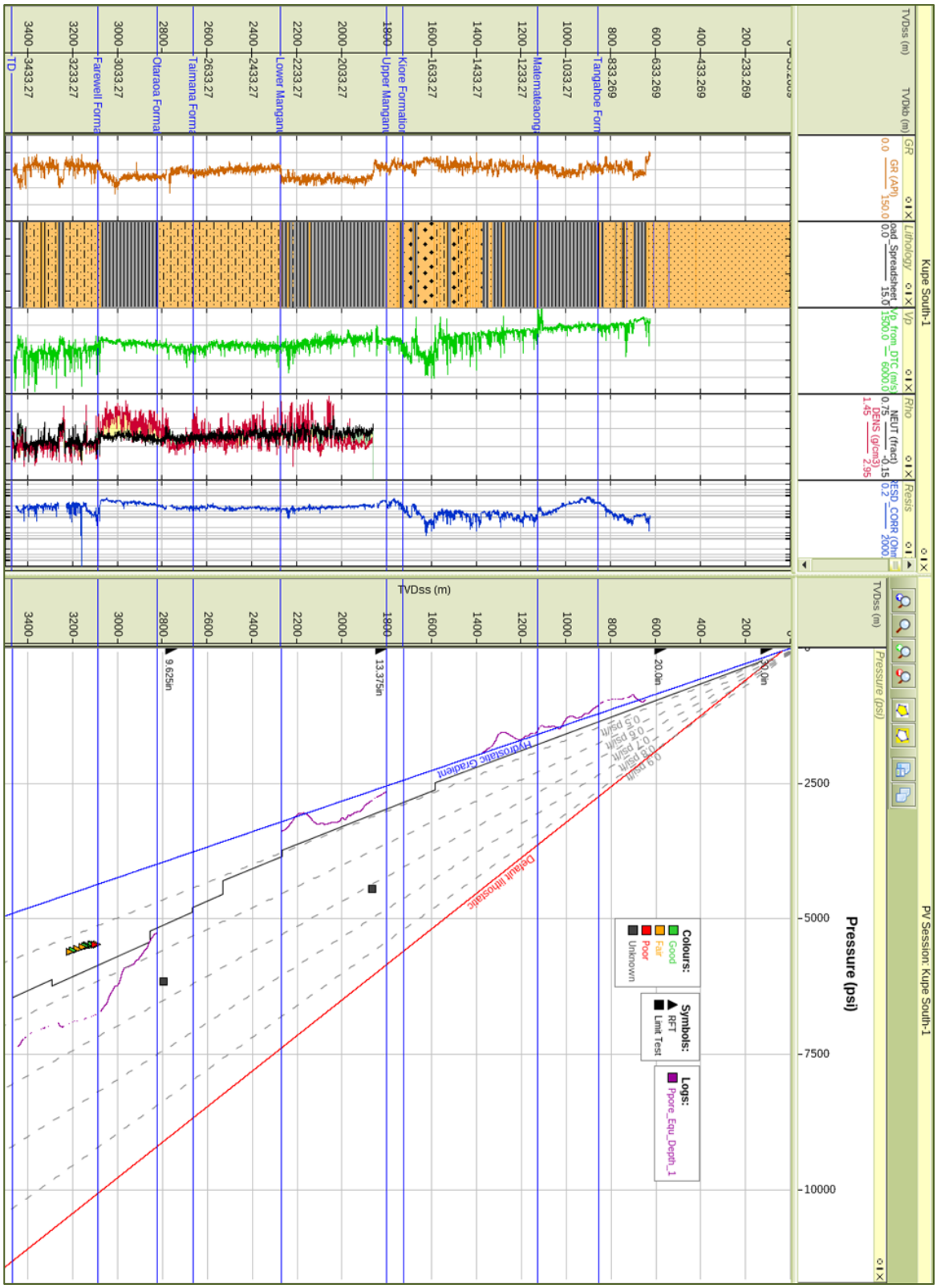

Figure I.7. Kupe South-1 pressure depth plot with associated suite of wireline measurements (gamma ray [brown], Vp [green], resistivity [blue], neutron [black], density [red], lithology column, RFT [triangles], squares [limit test], mudweight [black] and shale pressure [purple]).

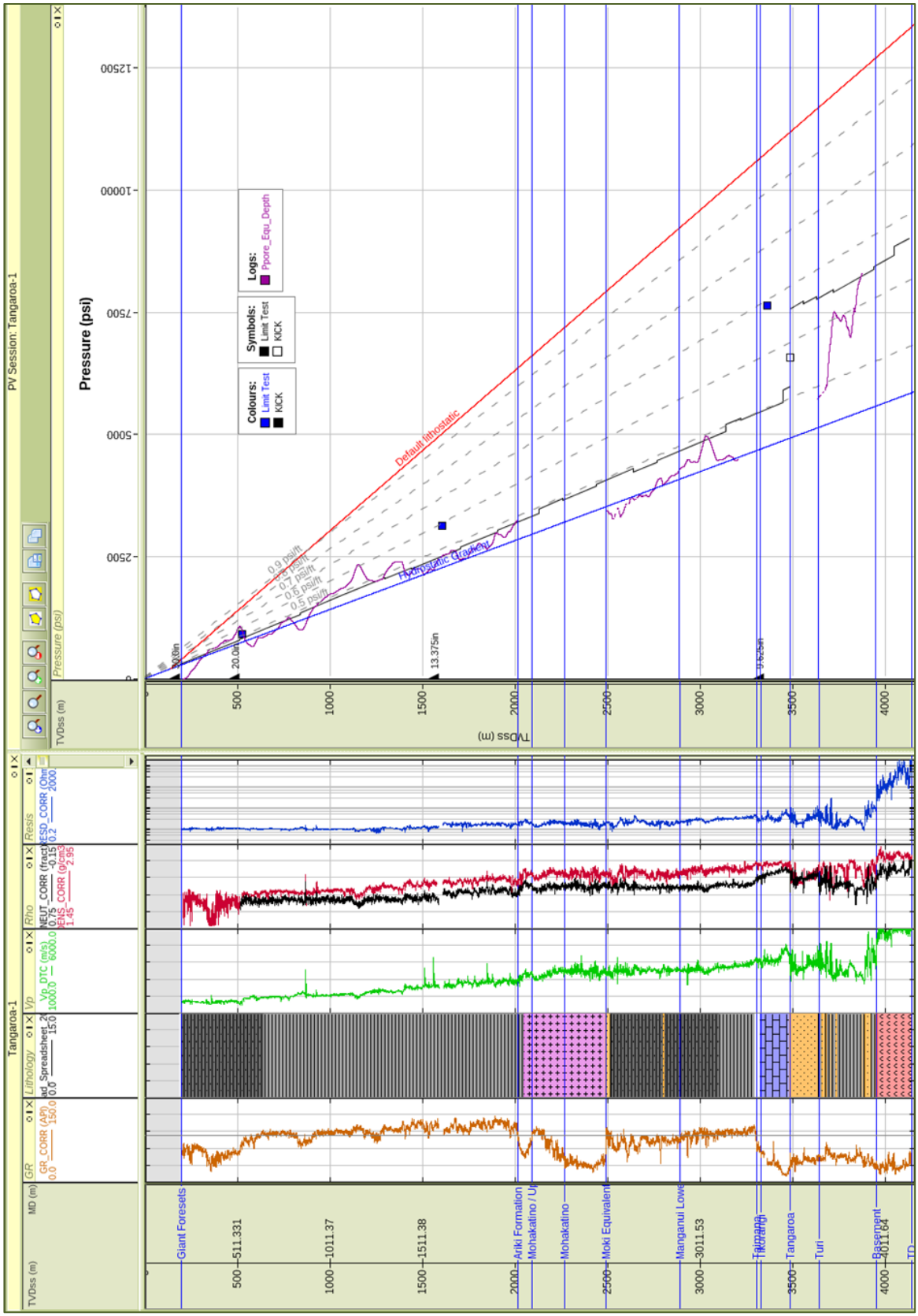

Figure I.8. Tangaroa-1 pressure depth plot with associated suite of wireline measurements (gamma ray [brown], Vp [green), resistivity [blue], neutron [black], density [red], lithology column, kick [open square], blue squares [limit test], mudweight [black] and shale pressure [purple]

Enclosure I: Map of Taranaki Basin displaying key wells, producing fields, structure and bathymetry

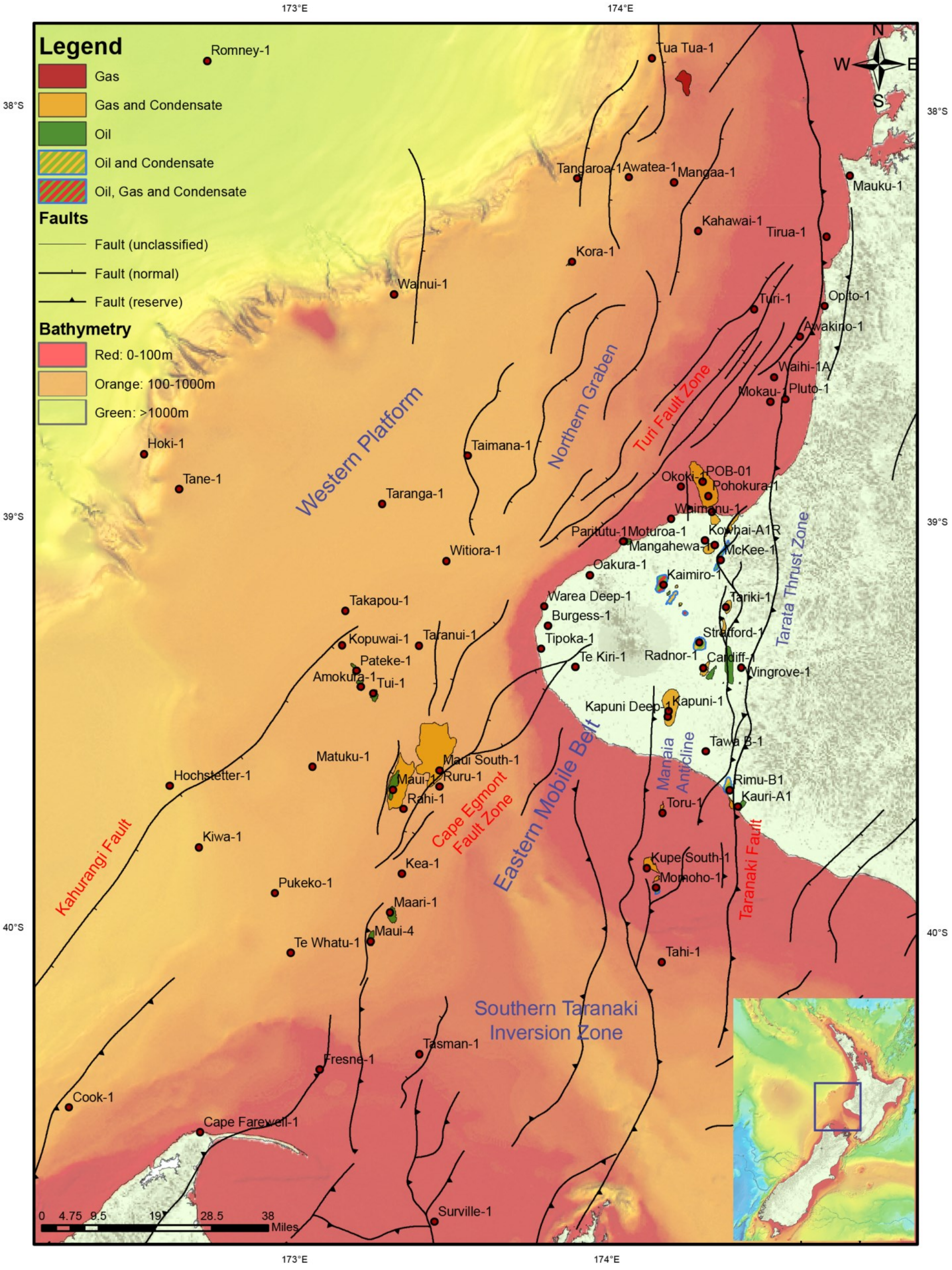

Enclosure II: Subsurface stratigraphy of Taranaki Basin from the Taranaki Peninsula across the Western Platform (modified from King and Thrasher, 1996).